PRELIMINARY VALIDATION OF HANDHELD X-RAY FLUORESCENCE (HHXRF) SPECTROMETRY: DISTINGUISHING OSSEOUS AND DENTAL TISSUE FROM NON-BONE MATERIAL OF SIMILAR CHEMICAL COMPOSITION

by

HEATHER ANN ZIMMERMAN
B.S. Florida Gulf Coast University, 2010

A thesis submitted in partial fulfillment of the requirements
for the degree of Master of Arts
in the Department of Anthropology
in the College of Science
at the University of Central Florida
Orlando, Florida

Summer Term
2013

ABSTRACT

Forensic anthropologists normally examine bone from a variety of medicolegal contexts. The skeletal remains may in some cases be highly fragmented or taphonomically modified, making it difficult to sort bone from non-bone material. In these cases, the forensic anthropologist may rely on microscopic or destructive chemical analyses to sort the material. However, these techniques are costly and time-intensive, prompting the use of nondestructive analytical methods in distinguishing bone and teeth from non-bone materials in a limited number of cases. The proposed analytical techniques are limited in that they rely on an examination of the major elements in the material, and do not sort out all materials with a similar chemical composition to bone/teeth. To date, no methods have been proposed for the use of handheld X-ray fluorescence (HHXRF) spectrometry in discriminating human and nonhuman bone/teeth from non-bone materials. The purpose of this research was to develop a method for the use of HHXRF spectrometry in forensic anthropology specifically related to distinguishing human and nonhuman bone and teeth from non-bone materials of a similar chemical composition using multivariate statistical analyses: principal components analysis (PCA), linear discriminant analysis (LDA), quadratic discriminant analysis (QDA), and hierarchical cluster analysis (HCA). This was accomplished in two phases. Phase 1 consisted of a Reliability Test and involved sampling a single human long bone in thirty locations. Multiple spectra were collected at each location to examine the reliability of the instrument in detecting the elements both within a single site and between multiple sites. The results of the Reliability Test indicated that HHXRF consistently detected the major and minor elements found on the surface of a human bone.

These results were used for Phase 2, designated the Accuracy Test, which involved analyzing a set of materials compiled from the literature to test the accuracy of the technique in discriminating bone (human and nonhuman) and non-bone samples (other biological and non-biological). The results of the Accuracy Test indicate that osseous and dental tissue can be distinguished from non-bone material of similar chemical composition with a high degree of accuracy (94%) when data is collected from several locations on a sample and analyzed separately during multivariate statistical analyses. Overall, it was not possible to discriminate rock apatite and synthetic hydroxyapatite (synthetic bone) from bone. However, this technique successfully discriminated other non-bone materials that are chemically similar to bone, such as ivory and octocoral, which previous methods focusing on only a comparison of Ca/P ratios were unable to distinguish from bone.

To Ben, for his endless encouragement, and to my parents, Ernie and Darby, for lovingly pushing me to pursue my dreams as long as I can remember.

And:

To myself, for all my hard work and dedication ☺

ACKNOWLEDGMENTS

"There has been an alarming increase in the number of things I know nothing about."

– Winnie the Pooh

Graduate school has been an exhausting and fulfilling journey; I have learned vast amounts on a variety of topics, yet realized there is still much more to be discovered. My journey has been steered by a number of guiding forces – mentors, professors, peers, friends – all whom have been influential in different ways.

First, I would like to thank my chair and advisor Dr. John Schultz for his guidance and instruction these past two years at UCF. I thank you for providing me every opportunity necessary to grow both as a student and professional by encouraging me to constantly expand my knowledge, attend conferences, get involved in community outreach and work to develop my Curriculum Vitae. I would also like to thank Dr. Michael Sigman for allowing me the opportunity to conduct this research at the National Center for Forensic Science. I also thank Dr. Sigman for his constant support and time-dedication throughout this research, especially in regards to helping develop the data analyses used in this study, and for providing me with necessary feedback to complete my thesis. Additionally, I would like to thank Dr. J. Marla Toyne for serving on my committee and providing me with feedback essential to the completion of my thesis.

I also would like to thank those individuals who have become part of my intellectual community at UCF during the past two years. I especially would like to thank Dr. Sandra

Wheeler for helping me grow as an educator, and Dr. Lana Williams for her constant advice and support. I also express thanks to my close friends Rachael Kangas and Katie Whitmore for their constant support and reassurance that the crazy will soon be over.

Finally, I would like to express my sincere gratitude to family, for giving me the opportunity to reach this goal, and to Ben, for his constant support during this journey.

TABLE OF CONTENTS

LIST OF FIGURES

LIST OF TABLES

LIST OF ABBREVIATIONS/ACRONYMS

Ca	Calcium
HCA	Hierarchical Cluster Analysis
HHXRF	Handheld X-Ray Fluorescence
LDA	Linear Discriminant Analysis
P	Phosphorus
PC	Principal Component
PCA	Principal Components Analysis
QDA	Quadratic Discriminant Analysis
XRF	X-Ray Fluorescence

CHAPTER ONE: INTRODUCTION

Forensic anthropologists examine bone in a variety of contexts. This can include examining skeletal material for law enforcement officials or the local medical examiner/coroner and/or identifying the fragmentary remains of individuals following cases of mass or natural disaster. In some cases, the skeletal remains encountered by forensic anthropologists may not always consist of easily identifiable material, and bone and dental tissue may not be discernible from other non-osseous material commingled with the skeletal remains. This is more common in cases where skeletal material has been taphonomically modified by any number of factors including burning/charring, weathering, and animal scavenging to produce fragmentary remains.

In these questionable cases, it may be necessary for the forensic anthropologist to rely on laboratory methods consisting of microscopic, (bio)chemical, and/or elemental analysis, in order to determine if the material is forensically significant. Common laboratory techniques for sorting bone and non-bone material include DNA analysis (biochemical) (Hagelberg et al., 1991; Cattaneo, 2007) and histological analysis (microscopic) (Mulhern and Ubelaker 2001; Mulhern and Ubelaker, 2012), but these techniques are costly, destructive, and time-intensive. Forensic anthropologists may also employ the use of an analytical method to sort the material into groups of bone/teeth and non-bone materials (Ubelaker et al., 2002; Christensen et al., 2012). Analytical methods are used to identify and quantitate the chemical components of materials, both natural and artificial, using wet chemistry (qualitative, gravimetric and volumetric analysis) and/or instrumental methods (spectroscopy, microscopy, electrochemistry, and chromatography) (Pietrzyk and Frank, 1979). Instrumental methods are used more often in forensic anthropology,

specifically those involving elemental analysis, in which samples are analyzed and distinguished according to their elemental composition, for example the amount of calcium and phosphorus (Ubelaker et al., 2002; Christensen et al., 2012). However, the analytical techniques that have been proposed for sorting bone from non-bone material are limited in that they rely on an examination of the major elements in the material, and thus do not discriminate between all materials with a similar chemical composition to bone/teeth. Additional methods (histological, protein, analytical) may be used to separate the human bone from all other materials including nonhuman bone (Lowenstein, 1980; Cattaneo et al., 1992a, 1992b, 1994, 1995; Ubelaker et al., 2004; Vass et al., 2005). If the remains consist of cremains, additional analytical techniques may be used to identify the remains as bone or non-bone (Kravchenko et al., 2001; Warren et al., 2002; Brooks et al., 2006) and possibly used for identification of the individual under certain circumstances (Schultz et al., 2008); however analysis of possible cremains currently falls outside the scope of this research.

While several techniques are available to forensic anthropologists for sorting bone and teeth from non-bone materials, such as histology, protein analysis and analytical methods, all of the currently used approaches have drawbacks. The techniques employing elemental analysis (Ubelaker et al., 2002; Christensen et al., 2012) show the most promise as they are less destructive. However, these methods lack standardization and are limited in their analysis of the materials as minor/trace elements are not examined; the analysis of major elements limits the technique from distinguishing materials with a similar chemical composition to bone. Additionally, these elemental analytical techniques are still costly and time intensive. Handheld or portable X-ray fluorescence (HHXRF) spectrometry represents a viable alternative to these

methods, as it allows for rapid data collection, requires minimal sample preparation, is nondestructive, and has the ability to be field portable or to provide stationary analysis of materials. The development of a protocol for the use of HHXRF for forensic anthropology would be beneficial in that it would allow unidentifiable fragments to be sorted quickly in the field as an initial method of identification, from which fragments identified as bone or teeth could then be further analyzed to determine if they are human using other methods.

The use of HHXRF is already prevalent in anthropology in a number of areas. In the field of archaeology, it is used in the sourcing of lithics (Williams-Thorpe, 1995; Williams-Thorpe et al., 1999; Pappalardo et al., 2003; De Francesco et al., 2007; Phillips and Speakman, 2009; Frahm et al., 2013), ceramics (Liritzis et al., 2002, 2007; Liritzis, 2005; Mantzourani and Liritzis, 2006; Papadopoulou et al., 2006; Papageorgiou and Liritzis, 2007) and metals (Ferretti et al., 1997; Ferretti and Moioli, 1998). Further use of HHXRF in bioarchaeology includes the study of ancient burial practices (Granite, 2012). Additionally, with the establishment of data collection protocols, HHXRF could be increasingly implemented into additional bioarchaeological projects examining diet and lifestyle, replacing expensive and destructive elemental analysis techniques that have already been proposed for studying ancient diet, burial practices and lifestyle (Samek et al., 2001; Kasem et al., 2011; Alvira et al., 2010; Djingova et al., 2004; Castro et al., 2010; Webb et al., 2005; Wessen et al., 1978; Mantler & Schreiner, 2000; Carvalho et al., 2004).

The research presented here attempts to establish a standard protocol for the collection of data using a HHXRF for use in forensic anthropology. There were three main goals for the research:

1. Develop a reliable technique for elemental data collection of bones and teeth using HHXRF spectrometry
2. Discriminate bone and teeth from non-bone materials of differing chemical composition
3. Discriminate bone and teeth from non-bone materials of similar chemical composition

The thesis will be structured systematically as follows: a brief background will be provided which will include information on the anatomy and chemical composition of bones and teeth and the chemical analysis of bone in forensic anthropology. Subsequently, the sampling materials and equipment will be presented, followed by a description of the methods used for data collection and data analysis in the study. The results of the research will then be presented, followed by a detailed discussion. Finally, conclusions will be drawn, and recommendations will be provided for future work.

CHAPTER TWO: BACKGROUND INFORMATION

The methods to be discussed in later chapters rely on a basic knowledge of bones and teeth at the chemical and anatomical level, prompting a review of these topics. Additionally, it is necessary to provide a detailed background of the laboratory techniques currently used in forensic anthropology to identify remains as (1) bone, and as (2) human or nonhuman bone, as this information typically determines if questionable skeletal material is actually skeletal material of forensic significance. Once skeletal material has been identified as human, biochemical analysis may be used for identification of the remains, although this does not usually involve the forensic anthropologist, but rather the medical examiner or forensic pathologist. This chemical analysis typically involves DNA analysis, which falls outside the scope of this research; however, recent studies suggest that elemental analysis combined with multivariate statistical analysis (Castro et al., 2010; Gonzalez-Rodriguez and Fowler, 2013) may be useful in the discrimination of individuals, which will be discussed.

Anatomy and Chemical Composition of Bones and Teeth

Dental and osseous tissues consist of both organic and inorganic components (Table 1). The organic component of bone consists of the bone cells (osteoblasts, osteoclasts, and osteocytes) and the osteoid, the organic part of the bone matrix. The osteoid consists of collagen, proteoglycans, and glycoproteins, all of which are secreted by osteoblasts, and makes up approximately one-third of the bony matrix. The organic component of bone, particularly collagen, gives bone its "flexibility and great tensile strength that allows [it] to resist stretch and

twisting" (Marieb and Hoehn, 2007:183). The inorganic component of bone, accounting for the remaining two-thirds of the bony matrix, consists of hydroxyapatites, or mineral calcium phosphates, with the structural formula, $Ca_5(PO_4)_3OH$. The hydroxyapatite gives bone its incredible strength, allowing it to resist compression (Marieb and Hoehn, 2007).

Table 1: Bone organic and inorganic components (Marieb and Hoehn, 2007)

Bone Composition			
Water (H_2O)	10-20% in living bone, but <1% in dry bone		
Organic Components	~ 33% (dry bone)		
	Main Component(s)	**Complete Breakdown**	**Function(s)**
	Bone cells	osteoblasts, osteoclasts, osteocytes	gives bone its flexibility and great tensile strength; allows bone to resist stretch and twisting
	Osteoid	collagen, proteoglycans, glycoproteins	
Inorganic Components	~ 66% (dry bone)		
	Main Component(s)	**Complete Breakdown**	**Function(s)**
	Hydroxyapatite	$Ca_5(PO_4)_3OH$ (mineral calcium phosphates)	give bone it's incredible strength; allowing bone to resist compression

Teeth consist of several structures, each of which has varying amounts of organic and inorganic components. Each tooth can be separated into three main sections; (1) crown, (2) neck, and (3) root (Figure 1). Teeth also have a chemical composition similar to bone (Table 2). An acellular material called enamel covers the crown. Enamel is the hardest substance in the body, with a chemical composition of 96% inorganic material (mostly hydroxyapatite), 1% organic material and 3% water (Marieb and Hoehn, 2007). The enamel protects the underlying dentin, which is a living, porous, bone-like material that forms the bulk of the tooth. Dentin is

harder than bone but softer than enamel, with a chemical composition of 70% inorganic material (mostly hydroxyapatite), and 30% inorganic material and water. A substance called cementum covers the outer surface of the root, attaching the tooth to the periodontal ligament and anchoring the tooth in the bony alveolus. The layer of cementum is thin and composed of 55% organic material and 45% inorganic material (mostly hydroxyapatite) (Marieb and Hoehn, 2007).

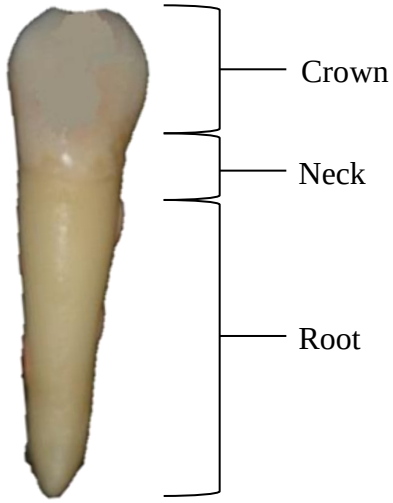

Figure 1: Basic tooth anatomy showing the crown, neck and root sections.

Table 2: Tooth organic and inorganic components (Marieb and Hoehn, 2007)

Tooth Composition			
Water (H_2O)	~ 3% in living tissue, <1% in dry tissue		
Organic Components	~ 1-55% (dry tissue) depending on enamel, dentin or cementum		
	Main Component(s)	**Complete Breakdown**	**Function(s)**
	Protein	amelogenins and enamelins in enamel; odontoblasts in dentin	Framework for the development of enamel/dentin
Inorganic Components	~ 45-96% (dry tissue) depending on enamel, dentin or cementum		
	Main Component(s)	**Complete Breakdown**	**Function(s)**
	Hydroxyapatite	$Ca_5(PO_4)_3OH$ (mineral calcium phosphates)	makes teeth strong and resistant to degradation; protects living portion of tooth

Chemical Analysis of Bone in Forensic Anthropology

The use of chemical analysis in forensic anthropology revolves around specific questions that researchers strive to answer about a set of possible human remains. The main questions in forensic anthropology include:

1. *How can we differentiate bone from non-bone?*

   This is usually only a problem when the remains are highly fragmented and/or taphonomically modified; researchers rely on elemental analysis to answer this question when necessary.

2. *How can we differentiate human from nonhuman bone?*

Several microscopic and analytical techniques have been proposed for differentiating human and nonhuman remains, but DNA, histology and protein analysis are the most common.

3. *Is it possible to determine identity or discriminate between individuals?*

   In instances of commingling and fragmentation in a medicolegal context, DNA is more traditionally used for individual identification.

In some cases, these questions may be easy to answer, as the morphology of whole bones or large fragments of bone will indicate quickly that the material is bone, and that it is or is not human. However, if the fragments are too small to show detail consistent with human bone or even detail consistent with bone, it may be necessary for the forensic anthropologist to refer to a laboratory method of some type for help with identification of the material. For this purpose, researchers have developed microscopic, chemical and analytical methods.

Bone versus Non-Bone

A limited number of techniques have been proposed for distinguishing bone and teeth from non-bone materials. The common technique is to determine the elemental composition of the material and compare the Ca/P ratio to those that have been determined by researchers as within the acceptable range for consistency with bone (Ubelaker et al., 2002; Christensen et al., 2012). Research has shown that dry bone should have a Ca/P atomic ratio within the range of 1.61 to 2.02 when a calibrated analytical method based on peak height is used (Braz, 2001; Ubelaker et al., 2002); however, additional research has shown that archaeological bone may have a ratio as high as 2.58 (Ubelaker et al., 2002). This is important to note since in some cases

the bone being examined by a forensic anthropologist may be from an archaeological, rather than a forensic context (Ubelaker et al., 2002).

One of the early applications of analytical chemistry techniques to the field of forensic anthropology consisted of Ubelaker and colleagues (2002) sorting fragmentary osseous and dental tissue from other materials of similar chemical composition. The researchers developed a method using scanning electron microscopy/energy dispersive X-ray spectroscopy (SEM/EDS). This technique, which is capable of detecting elements carbon through uranium, is commonly used to determine the structure and elemental composition of unknown/unidentified materials from the X-ray spectrum that is produced during the EDS portion of the analysis (Ubelaker et al., 2002).

Ubelaker et al. (2002) proposed the use of SEM/EDS to sort bone and non-bone material, which allowed the researchers to make presumptive identification of materials that were later corroborated with DNA testing. In this method, samples underwent elemental analysis, producing a spectrum, and then this spectrum was compared against a spectral library developed by the FBI called SLICE, or Spectral Library for Identification and Classification Explorer. The spectral library, SLICE, was demonstrated in the past by researchers as useful in identifying materials in a number of forensic contexts (Bush et al., 2008; Ward and Colby, 2008), however, the availability of the database following 2008 cannot be confirmed (by means of an internet search). This method is limited is several aspects, including: (1) the absolute identification of materials is not considered possible, restricting it to a presumptive test; (2) it is largely based on the relative proportion of Ca/P found in the bone, which prevents some non-bone materials from

being completely discriminated from bone and teeth, such as synthetic hydroxyapatite, mineral apatite, octocorals, and ivory; (3) it requires significant sample preparation; and (4) it can be destructive to the sample, as samples must be relatively small (approximately no larger than the size of a dime) or fragments must be removed from a larger sample in order for the specimen to fit in the instrument for analysis. Additionally, Ubelaker et al. (2002) recommend grinding all samples into powder form for analysis in order to optimize the homogeneity of each sample; however, this increases the destructivity of the technique.

Christensen et al. (2012) recently published a study similar to that of Ubelaker et al. (2002). In their study, Christensen and colleagues (2012) used X-ray fluorescence (XRF) to analyze the same samples from the SEM/EDS study by Ubelaker et al. (2002) (Table 3), in order to determine if XRF was an appropriate method for distinguishing bone/teeth from non-bone materials of similar chemical composition. X-ray fluorescence involves an X-ray photon, produced by either an X-ray tube or a photon emission source, which "creates a vacancy by knocking out an inner-shell electron" (Glascock, 2011:162). When the atom reconfigures in order to stabilize, it does so by filling the inner electron shell with one of its outer electrons. When this electron relaxation occurs, a new X-ray photon is emitted from the atom; this photon is known as a fluorescent X-ray. The energy given off by the fluorescent X-ray "corresponds exactly to the difference in energy between the two atomic energy levels and is unique for each element" (Glascock, 2011:162). X-ray fluorescence is capable of measuring all periodic elements, although this is not usually the case, as low-Z elements (those with low energy and a long wavelength) are usually too difficult to detect. Low-Z elements are those occurring below Ca (Migliori et al. 2011). The results from XRF are provided in spectral form, with elements

shown at predictable energies and varying in intensity depending on the sample. Quantification of the information can be achieved "by measuring the intensities of the X-rays observed in the spectrum" (Glascock, 2011:163). The benefits of XRF are that it requires little to no sample preparation, and can be nondestructive (as long as the sample preparation is nondestructive).

Table 3: Summary of materials analyzed in Christensen et al. (2012) using XRF; adapted from Ubelaker et al. (2002).

Material Types			**Alterations/Conditions**
Human bones and teeth	• Cranium • Humerus • Femur • Fibula • Foot phalanx	• Molars • Premolar • Canine • Dental plaque • Calculus	• Unaltered • Burned • Chemically altered (nitric acid) • Ancient (up to 9000 years) • Subadult (including newborn)
Nonhuman bones and teeth	• Pig • Cow • Turtle	• Dog • Rodent • Ungulate	• Unaltered, • Burned • Chemically altered (nitric acid and sodium hydroxide)
Other biologic materials	• Shell • Coral • Octocoral	• Sand dollar • Brachiopod shell • Beak	• Unaltered • Burned
Nonbiologic materials	• Various woods • Various plastics • Various minerals/ rocks • Ceramic • Lime	• Various metals • Glass • Garden hose • Carpet • Fabric	• Unaltered • Burned

The study by Christensen et al. (2012), modeled after Ubelaker et al. (2002), involved the analysis of a variety of materials, including human and non-human osseous and dental tissue; additional biological hard tissues that include shell, coral, horn and beak; and non-biological

materials including glass, plastic, metal, wood and minerals (Table 3). The materials were examined in a variety of states, such as burned/charred, weathered, antiquity, and exposure to erosive chemicals (Christensen et al., 2012). This technique, like that of Ubelaker et al. (2002), is largely based on the relative proportions of Ca/P found in the sample, which prevented some non-bone categories of specimens from being distinguished from osseous and dental tissue conclusively. These categories of specimens were: mineral apatite, octocoral, and brachiopod shells. There are some advantages associated with XRF, including: (1) it requires little to no sample preparation, and (2) is non-destructive to the sample, making it an appealing method for forensic anthropologists (Christensen et al., 2012). However, this method is limited when it is restricted to the analysis of only the Ca/P ratio of the materials, as certain non-bone materials have a similar or overlapping Ca/P ratio to bone, making them indistinguishable from bone. These materials include mineral apatite, octocoral, synthetic hydroxyapatite, and ivory (Christensen et al., 2012).

Human versus Nonhuman

Following the identification of questionable material as consistent with bone/tooth, the next step is determining whether the skeletal material is human or nonhuman. Differentiating human and nonhuman skeletal material is important because material identified as nonhuman may be excluded from subsequent analyses, as it is not of forensic significance. Researchers rely on two main methods for species differentiation: (1) histological examination (Mulhern and Ubelaker, 2001; Cattaneo et al., 2009; Mulhern and Ubelaker, 2012) and (2) protein analysis (Lowenstein, 1980; Ubelaker et al., 2004). These techniques are more established, and generally

accepted as being more reliable in discriminating human from nonhuman bone, despite their drawbacks including extensive sample preparation and destruction of the sample. A limited number of analytical chemistry techniques have also been proposed for use in differentiating human and nonhuman bone and teeth, and these include: near-infrared (NIR) Raman spectroscopy (McLaughlin and Lednev, 2012), Fourier transform (FT) Raman spectroscopy (Brody et al., 2001; Edwards et al., 2006), NIR-FT Raman spectroscopy (Shimoyama et al., 1997), and laser induced breakdown spectroscopy (LIBS) (Vass et al., 2005). However, compared to histology and protein analysis, the use of analytical techniques is limited. A summary of the techniques used to discriminate human and nonhuman skeletal material (to be discussed in this section) can be found in Table 4.

Table 4: Summary: laboratory methods used in the discrimination of human and nonhuman skeletal remains.

Method	Type	Advantages	Disadvantages	References
Histology	Microscopic	• Reliable/ established • High correct classification rates for H vs. NH and species differentiation	• Researchers must be highly trained • Significant sample preparation • Destructive	Chamberlain (1994); Ubelaker (1989); Mulhern and Ubelaker (2001); Cattaneo et al. (1999); Urbanova and Novotny (2005)
Protein analysis	Chemical	• Reliable/ established • Species specific	• Researchers must be highly trained • Significant sample preparation • Destructive	Lowenstein (1980); Cattaneo et al. (1992a, 1992b, 1994, 1995); Ubelaker et al. (2004)
Near-infrared (NIR) Raman spectroscopy	Analytical	• Nondestructive • Little to no sample preparation • Species-specific discrimination	• Advanced statistical analysis may require training • Small sample analyzed in study on fresh bone • Not standardized	McLaughlin and Lednev (2012)
Fourier transform (FT) Raman spectroscopy	Analytical	• Nondestructive • Little to no sample preparation • High correct classification rates • Species specific	• No forensic-specific application • Advanced statistical analysis may require training	Brody et al. (2001); Edwards et al. (2006)
NIR-FT Raman spectroscopy	Analytical	• Nondestructive • Little to no sample preparation • Sub-species specific discrimination	• No forensic-specific application • Advanced statistical analysis may require training	Shimoyama et al. (1997)
Laser induced breakdown spectroscopy (LIBS)	Analytical	• Relatively nondestructive • Little to no sample preparation	• Small sample • Incomplete results • Not standardized	Vass et al. (2005)

Histology

The microscopic examination of bone cross sections or histological analysis of bone is useful in forensic anthropology for identifying bone fragments of unknown origin to the species level (Chamberlain, 1994; Ubelaker, 1989; Mulhern and Ubelaker, 2001; Cattaneo et al., 1999; Urbanova and Novotny, 2005). This technique is also accepted by forensic anthropologists as a reliable and established method for use in court.

Chamberlain (1994) noted that human and nonhuman bone differ microscopically in terms of osteon organization, with human bone having evenly distributed osteons when viewed in cross-section and nonhuman bone having osteons that are organized into horizontal rows (in cross section). Mulhern and Ubelaker (2001) quantified previous notions that there were differences in human and nonhuman bone at the level of the Haversian system (Chamberlain, 1994) by statistically comparing the number of specimens with osteon banding in a mixed sample of human and nonhuman femora. The researchers found that nonhuman bone more often contained linear organization of osteons or osteon banding, and that this difference was significant at the 0.05 level (Mulhern and Ubelaker, 2001). Ubelaker (1989) notes the usefulness of osteon organization in identifying an isolated bone fragment as nonhuman in origin, thus determining it was not forensically significant. In the case described by Ubelaker (1989), a bone fragment with a surgical implant device (metal plate and screws) was determined to be nonhuman due to the presence of a linear pattern of osteons when cross sections of the bone were examined microscopically. Additional comparisons of the bone cross section with known species revealed that the bone was from a dog (Ubelaker, 1989).

Researchers have also demonstrated the utility of the size of the Haversian canal in discriminating between several species, including humans (Cattaneo et al., 1999; Urbanova and Novotny, 2005; Mulhern and Ubelaker, 2012). Mulhern and Ubelaker (2012:122) note that the size of the Haversian canal is "the most consistent distinguishing feature between human and nonhuman bone, with smaller Haversian canals in nonhuman taxa", especially when discriminant function analysis is also used. Cattaneo et al. (1999) developed a canonical discriminant function for the analysis of human and nonhuman bone that evaluated the minimum and maximum diameter of the Haversian canal along with the area. The predicted correct classification rate of the discriminant function was determined to be 79.3%, and initial testing by the researchers showed correct classification rates of 100% for both human and nonhuman samples (Cattaneo et al., 1999). However, subsequent testing of the method on a larger dataset that included neonate and juvenile remains showed high classification rates for nonhuman samples (95-100% depending on the species) but low classification rates for human samples (7-70% depending on age and bone type) (Cattaneo et al., 2009).

Urbanova and Novotny (2005) developed a set of two equations used for the discrimination of human and nonhuman bone samples that are based on the examination of several variables including the area of the Haversian canal as well as the cortical thickness of the midshaft of the femur. The researchers reported that the predicted correct classification rate of the first discriminant function was 94%, and that the predicted correct classification rate for the second was 100%, based on a sample of 53 human femora and tibiae, and bones from 10 nonhuman taxa (unspecified number) (Urbanova and Novotny, 2005).

Overall, while the microscopic or histological examination of bone has been shown to be useful in discriminating between human and nonhuman specimens, there are several drawbacks to the technique including significant sample preparation, destruction of the sample, and the necessity of highly trained individuals to perform the analysis (Mulhern and Ubelaker, 2012).

Protein Analysis

Protein studies in forensic anthropology, although relied on by researchers, are rather limited. Cattaneo et al. (1992a, 1992b, 1994, 1995) proposed a method for the detection of blood proteins, specifically albumin, in human bone. Albumin was chosen by the researchers due to its ability to outlast most other proteins and elements during long post-mortem intervals, since it becomes encapsulated "within the hydroxyapatite crystals of [the] bone" (Cattaneo et al., 1994:565) during this time. This method uses a specific enzyme-linked immunosorbent assay (ELISA), developed by the researchers, that employs monoclonal antibodies in its analysis (Cattaneo et al., 1994). The method can be used to analyze the amount of albumin left in the bones of an individual person or animal, thus providing information on species specificity, as well as information concerning additional methods that may be useful to the researcher (Cattaneo et al., 1994; Cattaneo et al., 1995). These additional methods can consist of blood group determination and human leukocyte antigen (HLA) typing, both of which can shed light on the genetic profile of an individual (Cattaneo et al., 1995).

The main protein analytical technique used by researchers is the one proposed by Ubelaker et al. (2004). This method is based on protein analysis, and uses the solid-phase radioimmunoassay technique (pRIA) developed by Lowenstein (1980). This assay provided

researchers with species-specific information in bones ranging from ancient to modern in origin. This method also relied on the extraction of albumin (as well as collagen) from the bone, but was then followed by exposure of the extract to rabbit serum that contained species-specific antibodies, which differed from Lowenstein (1980). Ubelaker et al. (2004) then exposed the material to a mixture of radioactively-labeled goat antibody and rabbit gamma globulin (GARGG), which allowed for a reaction between the radioactive material and the rabbit antibody, further deviating from Lowenstein (1980). Depending on the extent of binding that took place between the radioactive material and the rabbit antibody, as quantified by the level of radioactivity, the species was able to be determined with a high degree of certainty (Ubelaker et al., 2004). In a test of the method in discriminating human and nonhuman bone, Ubelaker et al. (2004) examined six samples, three human, one deer, one ungulate, and one dog, and compared them against one another as well as several standards. The method accurately discriminated the human from the nonhuman samples, and an "unknown" deer specimen was correctly classified as a deer, demonstrating that the method was effective in differentiating human and nonhuman bone (Ubelaker et al., 2004).

Overall, while protein analysis may be a reliable and established technique, minimal research has been conducted on this technique outside of its initial development, and specifically in its application to forensic anthropology. Additionally, despite the high correct classification rates of the technique, there are several drawbacks associated with protein analysis including significant sample preparation, destruction of the sample and advanced training of researchers.

Analytical Techniques

Several studies have suggested that the elemental composition of bones and teeth differ at the species level (Bratter et al., 1997; Biltz and Pellegrino, 1969; Aerssens et al., 1998; Rautray et al., 2007; Beckett et al., 2011). Most of the analytical techniques proposed for distinguishing human and nonhuman skeletal material in forensic anthropology have involved the use of Raman spectroscopy (Shimoyama et al., 1997; Brody et al., 2001; Edwards et al., 2006; McLaughlin and Lednev, 2012); however, limited research has also been proposed involving laser induced breakdown spectroscopy (Vass et al., 2005). These analytical techniques are advantageous in that they are nondestructive and require less sample preparation than histological and protein techniques, yet still provide species-specific information. However, these techniques are limited in that they are not standardized or well-established methods, which limit their credibility for use in court.

Several researchers have published work demonstrating the utility of different types of Raman spectroscopy in discriminating bone and tooth specimens at the species level (Shimoyama et al., 1997; Brody et al., 2001; Edwards et al., 2006; McLaughlin and Lednev, 2012). Raman spectroscopy is an analytical technique that involves the use of a laser, but is completely non-destructive (McLaughlin and Lednev, 2012), an added benefit for forensic anthropology. There are several types of Raman spectroscopy, including Fourier transform or FT Raman spectroscopy, dispersive near-infrared Raman, and micro-Raman spectroscopy, to name a few (Vij, 2006). Typical Raman spectroscopy, however, involves using a laser as an excitation source and then analyzing the scattered light with a spectrometer (Vij, 2006). Using this mechanism, the material to be analyzed will collide with the laser, resulting in inelastic

scattering of the photons. The energy change in the scattered photons is analyzed by the instrument to produce the Raman spectrum in the form of intensity versus energy (Vij, 2006). Inelastic scattering only occurs for vibrational modes where the vibration involves a change in polarizability (Vij, 2006). In addition to being a nondestructive technique, Raman spectroscopy also requires limited sample preparation and allows for rapid analysis (McLaughlin and Lednev, 2012).

Shimoyama and colleagues (1997) demonstrated the usefulness of near-infrared (NIR) Fourier transform (FT) Raman spectroscopy combined with chemometrics in discriminating between hard ivory, soft ivory (both from African elephant) and mammoth tusks. In their study, the researchers collected spectra from 10 hard ivory, 10 soft ivory and 5 mammoth ivory samples using a NIR FT-Raman spectrometer. The spectra were normalized to correct for differences in intensity and principal components analysis (PCA) was performed on the spectral data. The scores of the principal components were plotted and used to determine discrimination between the samples (Shimoyama et al., 1997). The researchers determined that all three types of ivory were distinct from one another in their scores plots, even when a leave-one-out classification method was used to test the "ruggedness" of the method (Shimoyama et al., 1997).

The combination of FT-Raman and chemometrics has also been shown by Brody et al. (2001) to be useful in discriminating ivory, bone and tooth samples from elephant, sperm whale, mammoth, bovine, walrus, ovine, hippopotamus, and porcine samples. In this study, 10 spectra were collected from each specimen, individually normalized to the dominant peak in the spectra, and then analyzed using PCA (Brody et al., 2001). Scatterplots of the scores from the first two

principal components showed overlap between several of the specimens, but results of the stepwise discriminant analysis, showed 90% correct classification or higher for all groups except the Asian elephant samples and the mammoth samples, both of which overlapped with the African elephant samples (Brody et al., 2001). A follow-up study conducted by Edwards et al. (2006) using infrared FT-Raman spectroscopy and the same method proposed by Brody et al. (2001), found better discrimination, with 98% of ivory specimens from six species classifying correctly.

McLaughlin and Lednev (2012) recently proposed the use of NIR Raman spectroscopy to differentiate bones from different species. In their study, the researchers examined chicken, turkey, cow and pig bone samples cut from freshly cleaned bone that was recently purchased from a meat market; no human bone was analyzed in the study (McLaughlin and Lednev, 2012). A total of 36 spectra were collected from each bone fragment, with one fragment representing each species (McLaughlin and Lednev, 2012). The researchers normalized the data to the dominant peak in the spectra and analyzed the data using partial least squares discriminant analysis (PLS-DA) (McLaughlin and Lednev, 2012). Partial least squares-DA reduces the dimensionality of the spectral data, as occurs in PCA, but extends the analysis to include the definition of specific classes and show the loading of the components in terms of the amount and type of variation contained in the component (McLaughlin and Lednev, 2012). The results of the PLS-DA were positive, showing discrimination between all four species, with only a small area of overlap when a 95% confidence interval ellipsoid was applied to the results scatterplot (McLaughlin and Lednev, 2012).

However, regarding the application of this technique to forensic anthropology, there are several limitations to this study, specifically in terms of the sample. The sample chosen for the study was small in terms of the number of species represented. Additionally, while 36 spectra were collected from each species, the area where the spectra were collected from was only approximately 75 square micrometers, rather than representative of the entire bone. The bones were also all fresh, which may sometimes occur in a forensic case, but dry bone should also be included for comparison purposes.

Another method was proposed by Vass et al. (2005) that used laser induced breakdown spectroscopy (LIBS) to sort human and nonhuman skeletal material, but the only available data is preliminary and rather incomplete. Laser induced breakdown spectroscopy is an analytical technique that "allows for the determination of a sample's elemental composition" (Sigman, 2010:5). The technique consists of laser ablation, followed by atomic, ionic, and molecular emission analysis of the plasma produced by the laser interacting with the sample. This process produces atomic emission lines, which are observed in the form of a spectrum. The intensities of the atomic emission lines can then be used to infer the concentrations of the elements present in the sample if appropriate standards are available (Sigman, 2010). In the study by Vass et al. (2005), eight adult human femora were compared with the tibiae and femora of 14 species of animals, all fully matured at the time of analysis. Cortical bone was chosen for the site of analysis since it is less variable than cancellous bone, and remodels in a predictable pattern throughout life (Vass et al., 2005). It was noted by researchers that preliminary spectral data indicated "sufficiently significant elemental differences among humans and between humans and

animal bones" (Vass et al., 2005:308). However, more research is necessary in this area, in addition to more specific information as to how the researchers performed their analyses.

There are several advantages and disadvantages to using LIBS in forensic anthropology analyses. The advantages include that it is a relatively nondestructive technique, as the laser produces a small (approximately 200-μm) impact crater in which a very low amount of mass is removed from the sample (a few micrograms). Other positive characteristics of LIBS include its rapid analysis time, and its requirement of minimal to no sample processing (Sigman, 2010; Kasem et al., 2011; Kaiser et al., 2009). The main disadvantage cited in the literature was a problem with reproducibility (Bridge et al., 2007). However, the main limiting factor associated with LIBS in forensic anthropology is the lack of research using the method in this field.

Individual Identification

Although not the focus of this research, recent research has indicated that elemental analysis may be useful in identifying individuals (Castro et al., 2010). Castro et al. (2010) uses laser ablation (LA-ICP-SF-MS) to discriminate bone and teeth samples of individuals based on elemental analysis for trace metals. Laser ablation, or laser ablation-sector field-inductively coupled plasma mass spectrometry (LA-ICP-SF-MS), is a combination of several methods (Castro et al., 2010). Inductively coupled plasma mass spectrometry (ICP-MS) is an analytical technique that provides highly sensitive elemental analysis using plasma as the ionization source, with a mass spectrometer to analyze the ions produced by the plasma (Jarvis et al, 1992). This allows for the measurement of nearly all elements found on a periodic table and makes ICP-MS capable of trace element analysis down to the parts-per-trillion (ppt) level. In LA-ICP-SF-MS,

the ICP-MS is upgraded to a double focusing (electric and magnetic) technique, also called Sector Field (SF) focusing, making it better able to detect trace and ultra-trace elements. Coupling this method with laser ablation (LA) reduces the sample preparation needed for analysis, as solid samples can be used, and reduces/eliminates the need for comparison or calibration with a reference standard, as non-matrix matched internal calibration standards are available for use within the instrument software (Castro et al., 2010). Additionally, laser ablation allows for the evaluation of elemental composition changes in the matrix, as determined by spatial resolution analysis at the micrometer level (Castro et al., 2010).

The study by Castro et al. (2010) used bone reference standards to develop the method, and was then applied to real bone samples in a study examining 12 individuals. The researchers found that the individuals were best discriminated when just the femur or humerus were considered separately, with 42.7% correct classification with all elements versus 75.2% and 63.1% for femoral and humeral bones, respectively. Individuals were also discriminated based on elemental composition of whole teeth samples. The elements used for discrimination purposes were: Al, Ba, Cu, Fe, Mg, Mn, Pb, Sr and Rb. The study used PCA as a data dimensionality reduction method, as well as a variety of statistical methods for discrimination, including ANOVA and linear discriminant analysis (LDA). With correct classification rates ranging from 43-75%, this method is not currently useful for forensic anthropology as this indicates that commingled skeletal material could be incorrectly associated as high as 57% of the time. However, with further refinement this technique may be applicable to forensic anthropology, particularly in the sorting process of commingled human remains (Castro et al. 2010).

Another study using handheld XRF recently reported higher correct classification rates for discriminating between individuals when using a small sample (Gonzalez-Rodriquez and Fowler, 2013). In this study, the researchers examined five individuals excavated from a medieval period cemetery in Lincoln, United Kingdom, and analyzed 23 bones from each skeleton. The researchers analyzed each element three times, and averaged the spectra, to obtain a single measurement for each bone sampled (Gonzalez-Rodriquez and Fowler, 2013). The researchers selected specific elements relating to diet and metabolism for use in discrimination (Ca, Fe, K, Pb, Sr and Zn), quantitated the amounts of these elements present in each bone using the XRF software, and then performed PCA on the quantitated data for these elements only (Gonzalez-Rodriquez and Fowler, 2013). Using LDA for classification, the researchers obtained 96-100% correct classification when discriminating between three individuals.

In a follow-up analysis (within the same study), the researchers used elemental ratios for discrimination (Pb/Ca, Zn/F and Sr/Pb), which were determined using the PCA factor loadings (Gonzalez-Rodriquez and Fowler, 2013). The factor loadings provide information on which elements are contributing most to the variation in a principal component, and in this case, the bone/element the PC is describing. Using these elemental ratios as data for PCA and LDA, the researchers obtained 83-96% correct classification when discriminating between four individuals, but only 53-96% correct classification when discriminating between five individuals (Gonzalez-Rodriquez and Fowler, 2013). While the researchers obtained high classification rates in some cases, their study is limited in that the greater the number of individuals being discriminated, the lower the correct classification percentage during LDA. This is specifically problematic since the number of individuals being discriminated in forensic commingling events

such as airplane crashes, mass disasters (i.e., World Trade Center attack), and natural disasters (i.e., Hurricane Katrina), typically involve much larger numbers of individuals.

Summary

Specific laboratory techniques are used in forensic anthropology to identify questionable and fragmentary remains as (1) bone, and as (2) human or nonhuman bone, in order to determine if possible skeletal material is forensically significant skeletal material. In identifying bone/teeth from non-bone material, elemental analysis using either SEM/EDS (Ubelaker et al., 2002) or XRF (Christensen et al., 2002) examining the ratio of Ca/P are relied on by forensic anthropologists. There are three main types of laboratory techniques used for distinguishing human bone/teeth from nonhuman skeletal material: (1) histology (Chamberlain, 1994; Ubelaker, 1989; Mulhern and Ubelaker, 2001; Cattaneo et al., 1999; Urbanova and Novotny, 2005), (2) protein analysis (Lowenstein, 1980); Cattaneo et al., 1992a, 1992b, 1994, 1995; Ubelaker et al., 2004), and (3) analytical techniques (McLaughlin and Lednev, 2012; Brody et al., 2001; Edwards et al., 2006; Shimoyama et al., 1997; Vass et al., 2005).

Overall, the proposed analytical techniques using Raman spectroscopy (Shimoyama et al., 1997; Brody et al., 2001; Edwards et al., 2006; McLaughlin and Lednev, 2012) appear valuable in distinguishing human and nonhuman skeletal material. The methods proposed demonstrate high classification rates, especially when advanced statistical analyses are used. These techniques are beneficial in several ways: (1) they are nondestructive (2) require little to no sample preparation, and (3) they provide species-specific information. However, compared to histology and protein analysis, the use of analytical techniques is limited and has not been

accepted as an industry standard. Standardization is necessary for these techniques in order for them to meet the Daubert standard for use in court (*Daubert v. Merrell Dow Pharmaceuticals*, 1993; Grivas and Komar, 2008; Christensen and Crowder, 2009).

The research discussed in the following proposed methods, attempts to address the lack of standardization concerning the use of elemental analysis in forensic anthropology by utilizing a robust statistical analysis for fragment discrimination. At the same time, while not the goal of this thesis, this method may meet the needs of the Daubert standard by utilizing a statistical analysis that includes correct classification percentages, which can be used to calculate error rates. In this research, a method is proposed and tested for sorting bone/teeth from non-bone material using a simple analytical technique (handheld or portable X-ray fluorescence spectrometry) and statistical analysis for discrimination, which provides a major and trace element analysis of the materials.

CHAPTER THREE: BACKGROUND ON STATISTICAL TESTS

Several statistical analyses will be discussed throughout the remaining sections necessitating a prerequisite knowledge of each, to be established in this chapter. The statistical methods that will be discussed include PCA, LDA, QDA and cluster analysis.

Principal Components Analysis

Principal components analysis is generally used as a data reduction tool in most applications, as the method works to analyze the variability or variance in a dataset and represent this information in the smallest number of principal components (PCs) possible (Varmuza and Filzmoser, 2009). This technique is often used for exploratory analysis of data (i.e. to find underlying similarities or differences in the dataset), and, as such, is considered an unsupervised method. Following PCA, a dataset (in the form of a matrix, *X*) consists of a combination of scores (*T*), eigenvectors or component loadings (P^T), and residual error (*E*) as explained by the following equation (Varmuza and Filzmoser, 2009):

$$X = T \cdot P^T + E \quad (1)$$

Principal components, also called eigenvectors or linear latent variables (*E* in Equation 1), represent the data in terms variance, as determined based on the relative distances between the objects "in high dimensional variable space" when the entire dataset is considered (Varmuza and Filzmoser, 2009:59). The PCs obtained from PCA are organized in order of decreasing variance, with PC1 representing the maximum variance in the dataset, PC2 representing the

second highest variance in the dataset (but the maximum amount of the remaining variance), and so on (Varmuza and Filzmoser, 2009). Scores (*T* in Equation 1) obtained from the PCs are uncorrelated (versus the correlated data they represent) and can be used in subsequent analyses such as visual examination by scatterplots or used in other statistical analyses (Varmuza and Filzmoser, 2009). The residual error (*E* in Equation 1) fluctuates depending on the number of PCs used in subsequent analyses; if all PCs were used (equal to the number of original variables), then the residual error would be zero. However, in most cases, only a few PCs are retained for subsequent analyses. Before subsequent testing is performed on the data, the optimum number of PCs to retain must be determined (Varmuza and Filzmoser, 2009).

A common method for determining the optimum number of PCs is by plotting the PCA eigenvalues, which correspond to the PC variances, versus the PC number to obtain a scree plot (Figure 2) (Cattell, 1966; Varmuza and Filzmoser, 2009). The eigenvalues represent the amount of total variance of a principal component (Bryant and Yarnold, 2010; Varmuza and Filzmoser, 2009). According to Cattell (1966), breaks or drops in the scree plot indicate components that should be used in subsequent analyses, as they indicate components representing a significant amount of variance in the data. The flat region in the graph represents components with a small amount of variance, which are not optimum for subsequent analyses, and thus should not be retained (Varmuza and Filzmoser, 2009).

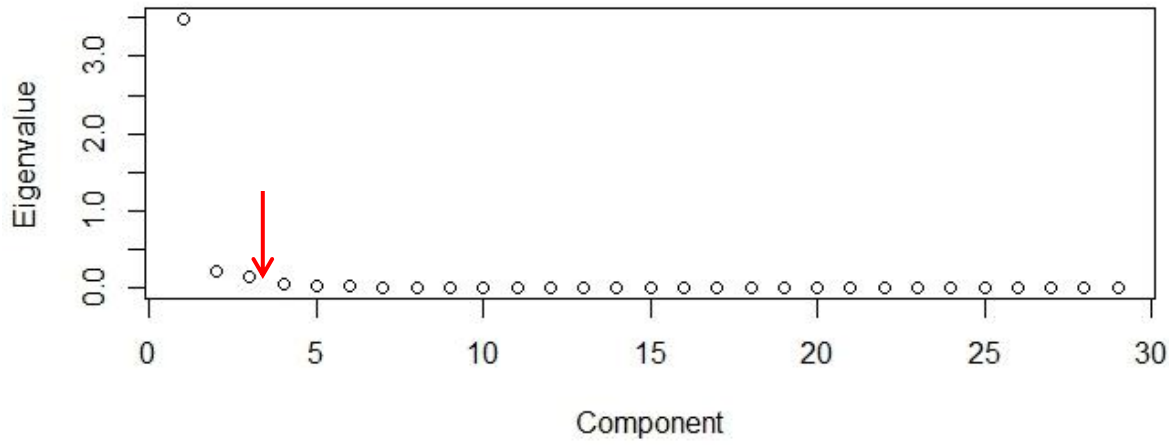

Figure 2: Example of a scree plot showing the number of principal components that should be used in subsequent analyses; in this case, the graph indicates 3 PCs should be retained (arrow).

Linear and Quadratic Discriminant Analysis

Linear discriminant analysis utilizes a classification function that assigns samples to a specific category using a linear surface as the separating mechanism between the groups (Silva and Stam, 1995). Linear discriminant analysis requires that data be normally distributed and have variance-covariances that are equal across the groups that are being analyzed. There are two types of LDA, Bayesian and Fisher; only Fisher's LDA will be discussed, as this was the type used in the current research project. Fisher's LDA for two classes can be defined by Equation 2, where $\bar{x}_1$ and $\bar{x}_2$ are the data mean vectors for the two groups, and S_P is the pooled covariance matrix (sum of the group covariance matrices), as defined in Equation 3 (Varmuza and Filzmoser, 2009).

$$b_{FISHER} = S_P^{-1}(\bar{x}_1 - \bar{x}_2) \quad (2)$$

$$S_P = \frac{(n_1-1)S_1+\cdots+(n_k-1)S_k}{n_1+\cdots+n_k-k} \quad (3)$$

Using Equations 2 and 3, a discriminant score for a sample can be calculated, which is then used to assign the sample to a specific class. For example, for a sample, x_i, the sample's discriminant score, y_i would be found by:

$$y_i = b_{FISHER}^T x_i \quad (4)$$

In order to classify the sample, the discriminant score (y_i) will then be compared against a classification threshold, y_0 (calculated using Equation 5) (Varmuza and Filzmoser, 2009). If the sample's discriminant score is less than the classification threshold, it will be assigned to Group 1; whereas, if it is greater than the classification threshold, it will be assigned to Group 2.

$$y_0 = \frac{b_{FISHER}^T \bar{x}_1 + b_{FISHER}^T \bar{x}_2}{2} \quad (5)$$

If the data does not have equal covariances across the groups being analyzed, but is still normally distributed, it may be appropriate to use quadratic discriminant analysis (QDA). In QDA, samples are assigned to categories using a quadratic surface as the separating mechanism between the groups, rather than the unidirectional linear surfaces used in Fisher LDA (Silva and Stam, 1995). In order to assign samples to a class, the Mahalanobis distances are calculated for each sample with respect to each class center, and then samples are assigned to the class with the smallest Mahalanobis distance (closest class) (Wehrens, 2011), as described by Equation 6:

$$Mahalanobis\ distance = d\ or\ d^2(x,i) = (x-\mu_i)^T \Sigma_i^{-1}(x-\mu_i) \qquad (6)$$

Both LDA and QDA are hard classifiers, meaning that samples subjected to either analysis must be assigned to a class or category, and failure to assign to a class is not an option (Silva and Stam, 1995).

Hierarchical Cluster Analysis

Cluster analysis is used to find similarities or patterns within a set of data and group the data according to these similarities (Varmuza and Filzmoser, 2009). Cluster analysis is an unsupervised method, as the analysis determines the groups without any prior knowledge of group membership, including the number of groups that may be found (Varmuza and Filzmoser, 2009). This is different from LDA and QDA, where the methods rely on known groups for comparison; as such, LDA and QDA are called supervised methods (Varmuza and Filzmoser, 2009).

Hierarchical cluster analysis (HCA) is specific in that the groups or clusters found in the data are represented in the form of a dendrogram, which distinctly shows the data clusters and the "hierarchical relations between different groups" (Varmuza and Filzmoser, 2009:251). While the distance measure between groups or clusters can be varied to obtain optimal clustering results, the preferred measure of distance for cluster analysis is the Euclidean distance (Varmuza and Filzmoser, 2009). Additionally, the linkage between clusters can be varied to obtain optimal clustering results. The most frequently used methods for determining linkage are summarized in Table 5.

Table 5: Summary of methods for determining linkage in hierarchical cluster analysis (Varmuza and Filzmoser, 2009)

Linkage	Equation Using Euclidean Distance	Definition
Complete Linkage	$max_i \left\| x_i^{(j)} - x_i^{(l)} \right\|$	Uses the maximum of all pairwise distances between data in two clusters
Single Linkage	$min_i \left\| x_i^{(j)} - x_i^{(l)} \right\|$	Uses the minimum of all pairwise distances between data in two clusters
Average Linkage	$average_i \left\| x_i^{(j)} - x_i^{(l)} \right\|$	Computes the average distance between all pairs of data in the two clusters and uses this number as the distance
Centroid Method	$\left\| c_i - c_j \right\|$	Uses the distance between the cluster centroids
Ward's Method	$\left\| c_i - c_j \right\| \cdot \frac{\sqrt{2 n_j n_l}}{\sqrt{n_j + n_l}}$	Uses the distance between the cluster centroids with a correction factor for minimum variance

Summary

The background provided above on PCA, LDA/QDA and hierarchical cluster analysis is not meant to be comprehensive, but rather is intended to provide the reader with enough information to understand the methods used in this study. Information on the application of these methods will be discussed in the following chapter regarding data analysis.

CHAPTER FOUR: MATERIALS AND METHODS

In this chapter, the materials and methods used in the study will be discussed. The materials included both the samples in the dataset, as well as analytical equipment used for sampling. The methods of this research include two types: (1) methods for data collection, and (2) methods for data analysis.

Materials

Sample

The sample was comprised of five main groups of materials that were derived from previous studies (Ubelaker et al., 2002; Christensen et al., 2012) and expanded to include additional items. The five groups included: (1) an assortment of human bone and teeth, (2) nonhuman bone, (3) non-biological materials, (4) other types of biological materials, and (5) taphonomically modified materials. The human and nonhuman bone samples used in the analysis were acquired from the University of Central Florida Teaching Collection. Data recorded for each bone specimen consisted of sample type (human or nonhuman), bone element, approximate biological age of specimen (juvenile or adult), time period (modern or ancient), taphonomic modifications (burned or weathered), file name, and specimen notes (Appendix B). Other biological materials and non-biological materials were collected from the environment, from colleagues and purchased for use in the study. Data recorded for non-bone elements (other biological and non-biological materials) consisted of sample type (other biological or non-biological), material, taphonomic modifications, file name, and specimen notes (Appendix C).

Human bone samples (Table 6, Figure 3) were chosen to represent the different bone types present in the skeleton (long, flat and irregular), and were also chosen based on those examined in previous studies (Ubelaker et al., 2002; Christensen et al., 2012). Human teeth were also included in the study, as teeth are similar in chemical composition to bone since they contain calcium and phosphorus in a similar elemental concentration to bone. The types of human teeth chosen for the study were based on those analyzed in previous studies (Ubelaker et al., 2002; Christensen et al., 2012).

Table 6: Human skeletal elements examined in the study.

Human Elements			
Bone		**Tooth**	
Cranium*+	parietal, zygomatic	Molar+	upper, enamel and dentin/cementum
Humerus+		Premolar+	lower, enamel and dentin/cementum
Femur+		Canine+	upper, enamel and dentin/cementum
Rib+			
Fibula+			
Foot phalanx+	proximal pedal phalanx		
Metacarpal	right 3rd metacarpal		

* Examined by Ubelaker et al., 2002

\+ Examined by Christensen et al., 2012

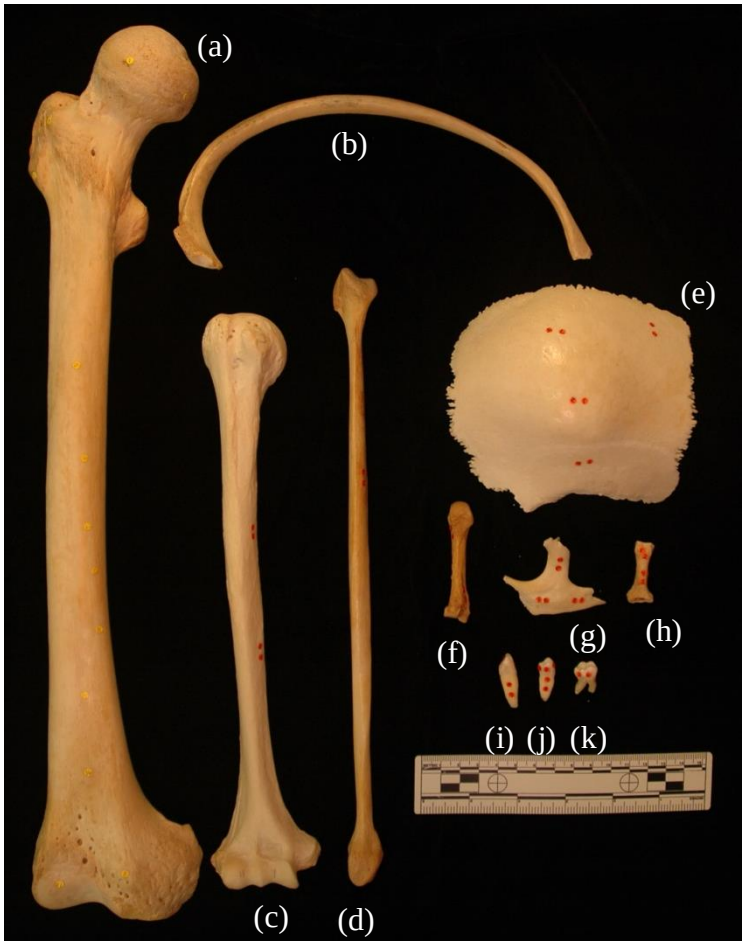

Figure 3: Human elements examined in the study: (a) femur, (b) rib, (c) humerus, (d) fibula, (e) parietal, (f) metacarpal, (g) zygomatic, (h) pedal phalanx, (i) canine, (j) premolar and (k) molar. The stickers on the specimens denote data collection sites.

Nonhuman bone samples (Table 7, Figure 4) were chosen to represent the species commonly encountered by forensic anthropologists in Central Florida and also reflect those examined by researchers in previous studies (Ubelaker et al., 2002; Christensen et al., 2012). In order to standardize this aspect of the study, only femora from the nonhuman species were analyzed, and all femora were analyzed in approximately the same locations for each species. There were a few exceptions to this, however. A turkey tarsometatarsus was substituted for a

turkey humerus, a sample of deer antler was included to compare to the deer humerus and other bone samples, and turtle shell was included to reflect the nonhuman sample analyzed by Christensen et al. (2012).

Table 7: Nonhuman species and skeletal elements examined in the study.

Nonhuman Samples		
Common Name	**Species Name**	**Element Examined**
Pig[+]	*Sus scrofa*	Femur
Turtle[+]	*Species example*	Femur
Turtle shell[+]	*Species example*	Shell
Dog*[+]	*Canis lupus familiaris*	Femur
Deer	*Odocoileus virginianus*	Femur, antler
Gator	*Alligator mississippiensis*	Femur
Bird	*Example species*	Femur
Armadillo	*Dasypus novemcinctus*	Femur
Raccoon	*Procyon lotor*	Femur
Turkey	*Meleagris gallopavo osceola*	Tarsometatarsus

* Examined by Ubelaker et al., 2002

\+ Examined by Christensen et al., 2012

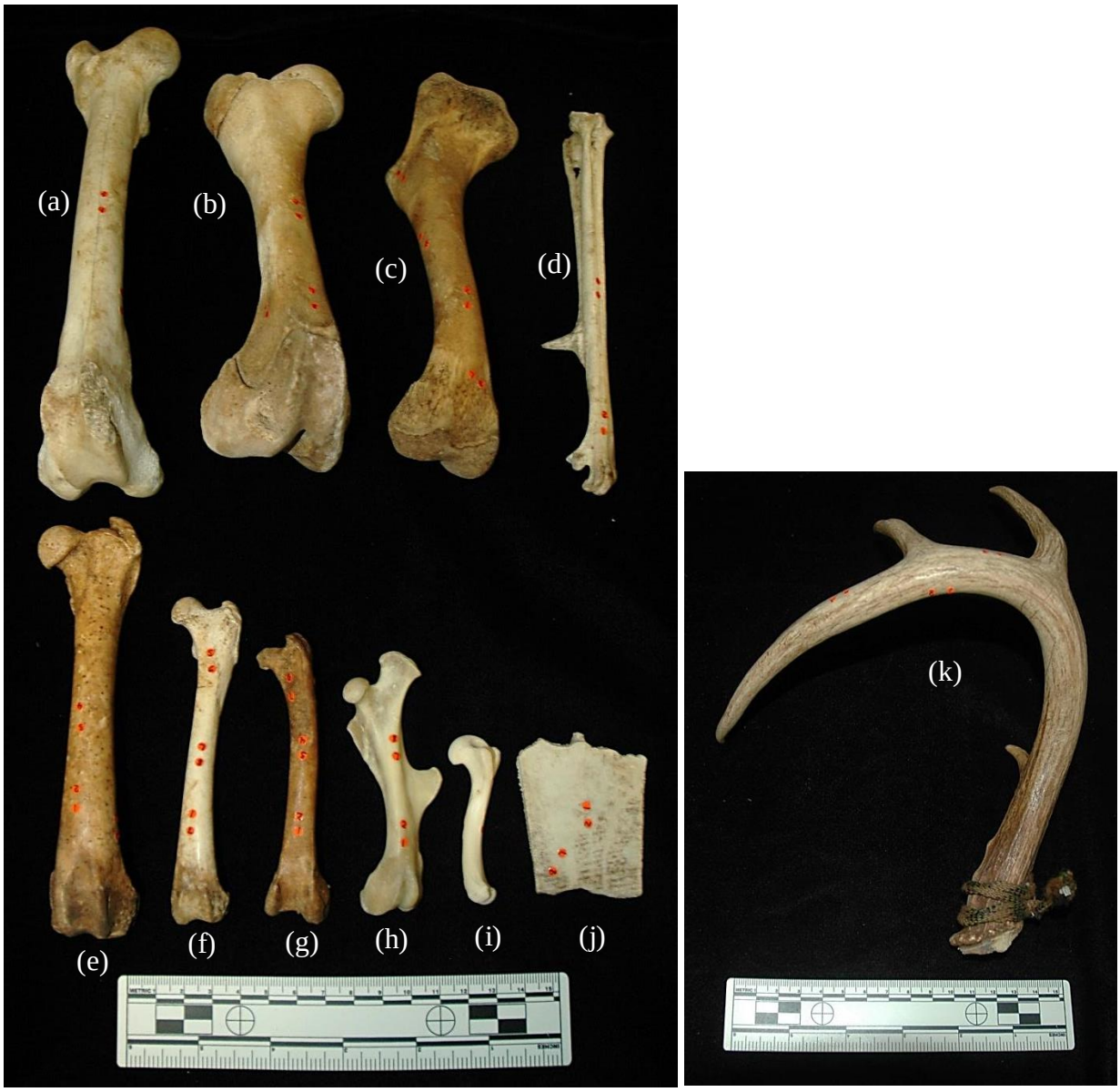

Figure 4: Nonhuman elements examined in the study: (a) deer femur, (b) pig femur, (c) alligator femur, (d) turkey tarsometatarsus, (e) dog femur, (f) raccoon femur, (g) bird femur, (h) armadillo femur, (i) turtle femur, (j) turtle shell and (k) deer antler. The stickers on the specimens denote data collection sites.

The non-biological samples (Table 8, Figure 5) were chosen to represent elements commonly encountered by forensic anthropologists in Central Florida that could be mistaken for bone in certain forensic contexts, such as plant material that may be mistaken for fragmentary or juvenile bone that has undergone various taphonomic processes. Additional elements were selected based on those examined in previous studies (Ubelaker et al., 2002; Christensen et al., 2012) and were added based on availability of the material.

Table 8: Non-bone materials examined in the study.

Sample Type	Material
Plant	twig[+]
	bark
	root
	seeds
Glass	float glass[+]
	beer bottle
Lime	limestone[+]
Synthetic hydroxyapatite	synthetic hydroxyapatite[*]
Rock	rock apatite[*+]
	rock phosphate

* Examined by Ubelaker et al., 2002

\+ Examined by Christensen et al., 2012

Figure 5: Non-biological materials examined in the study: (a) rock apatite, (b) limestone, (c) float glass, (d) beer bottle, (e) plant root, (f) twig, (g) bark, (h) seed, (i) synthetic hydroxyapatite and (j) rock phosphate. The stickers on the specimens denote data collection sites.

The other types of biological samples, termed "Other Biological" (Table 9, Figure 6), were selected based on those examined in previous studies (Ubelaker et al., 2002; Christensen et al., 2012) and were included in the study due to their similar chemical composition to bone in terms of their Ca/P ratio, as noted by previous researchers (Ubelaker et al., 2002; Christensen et al., 2012). These materials were chosen by the researchers to represent elements that may be encountered by forensic anthropologists and that could be mistaken for bone under certain circumstances.

Table 9: Other biological materials examined in the study.

Category	Common Name	Species Name(s)
Shell	Atlantic Bay scallop+	*Argopecten irradians*
	Clam	*Macrocallista nimbosa*
	Oyster	*Not known*
Sand dollar+	Common sand dollar	*Echinarachnius parma*
Octocoral	Green Florida and Haitian Ricordea	*Octocoralia ricordea*
Coral (processed/cleaned)	Not known	*Not known*
Ivory*	Legal vintage example	*Not known*
Starfish	Representative species	*Not known*

* Examined by Ubelaker et al., 2002

\+ Examined by Christensen et al., 2012

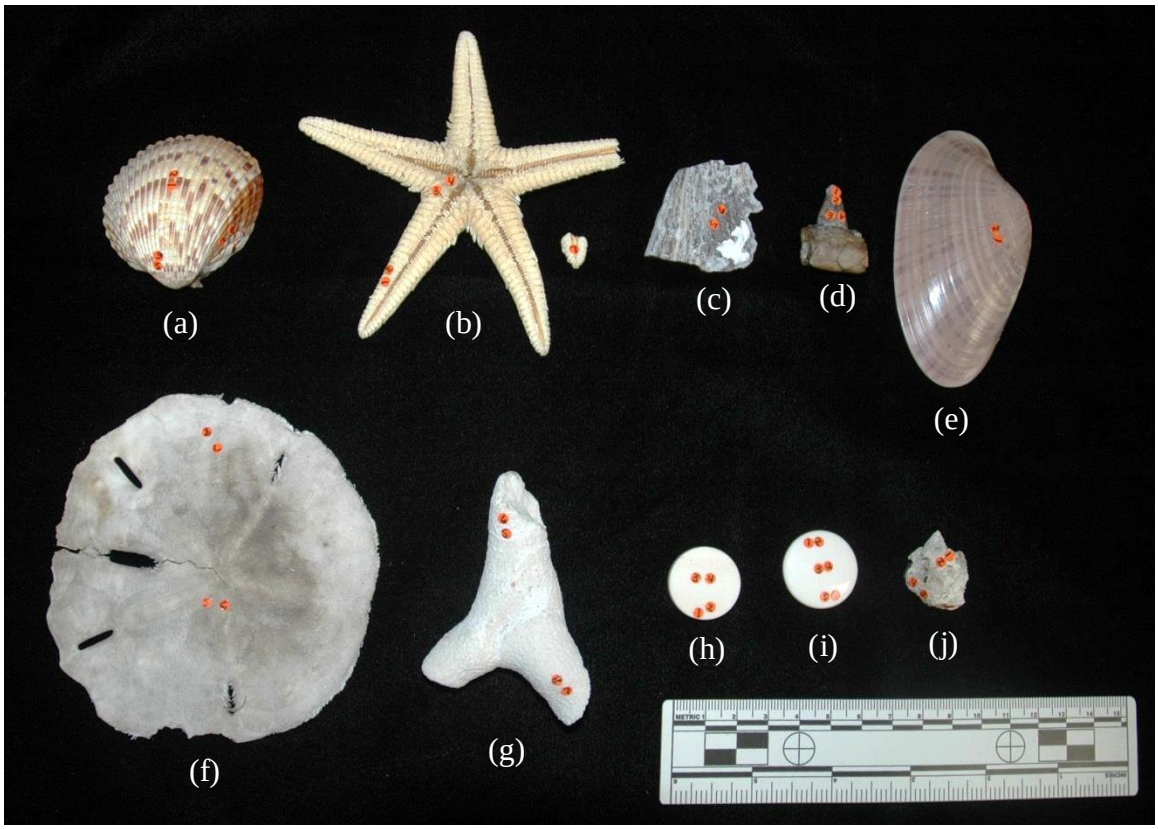

Figure 6: Other biological materials examined in the study: (a) scallop shell, (b) starfish, (c) oyster shell, (d) spur, (e) clam shell, (f) sand dollar, (g) coral, (h) ivory round, (i) ivory flat and (j) octocoral. The stickers on the specimens denote data collection sites.

Additional materials were analyzed that had been subjected to different taphonomic processes (Table 10, Figure 7). These included burned human bone and teeth, burned wood and plastic, weathered human bone, and archaeological human bone. These materials were included in the study in order to examine the effects of taphonomy on the elemental composition (if any) and the ability of the HHXRF to detect these changes.

Table 10: Taphonomically-modified materials examined the study.

Sample Type	**Taphonomic Condition**
Human fibula	Burned (calcined)
Human molars (2)	Burned (charred)
Human femur (fetal)	Archaeological
Human metacarpal	Weathered (sunbleaching, exfoliation)
Plastic	Burned
Wood	Burned

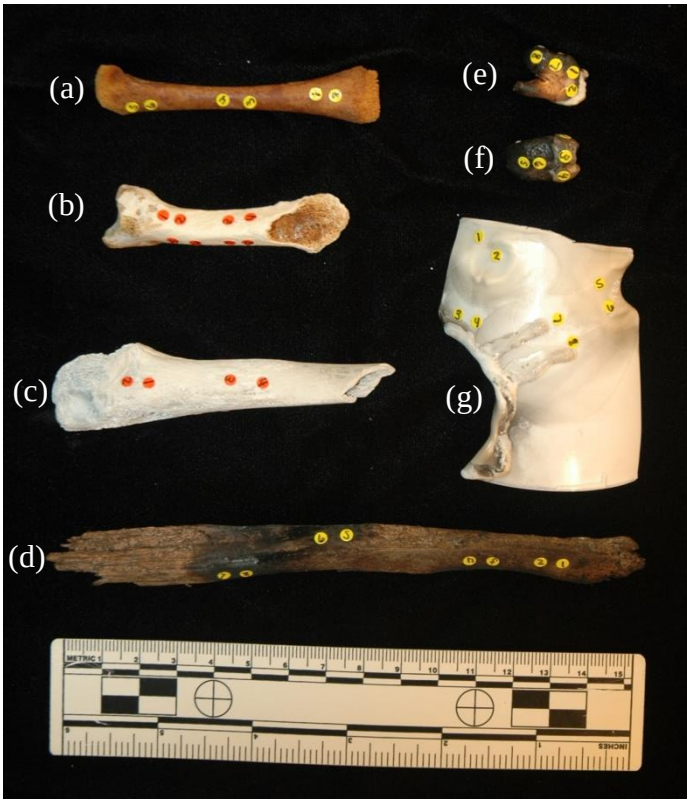

Figure 7: Taphonomically-modified materials examined the study: (a) human fetal femur (archaeological), (b) human metacarpal (burned), (c) human fibula (burned), (d) wood (burned), (e) human molar (burned), (f) human molar (burned) and (g) plastic (burned). The stickers on the specimens denote data collection sites.

Equipment

The instrument used for the analysis was a Bruker Elemental S1 Turbo-SDR HHXRF unit (Figure 8). The unit included upgraded analytical software, S1PXRF, which was provided by the manufacturer on an accompanied laptop computer (Figure 9). According to the manufacturer, the software allowed for the detection of low-mass elements (as low as Magnesium, 24.305 g/mol). For analysis, the HHXRF was mounted on a vertical stand, and a stationary analysis was performed. The HHXRF was connected to the laptop and the S1PXRF

software was used to collect the data. All data was collected using the 15 keV/Filter 2 setting on the instrument. This setting is known as "Lab Rat Mode" in which Filter 2 acts as a default setting (a lack of filter), and allows the instrument to detect the maximum amount of elements present. The analysis time was also controlled using the S1PXRF software, and was set to 60 seconds for each sample.

Figure 8: Bruker Elemental S1 Turbo-SDR HHXRF unit shown mounted on a vertical stand for stationary analysis.

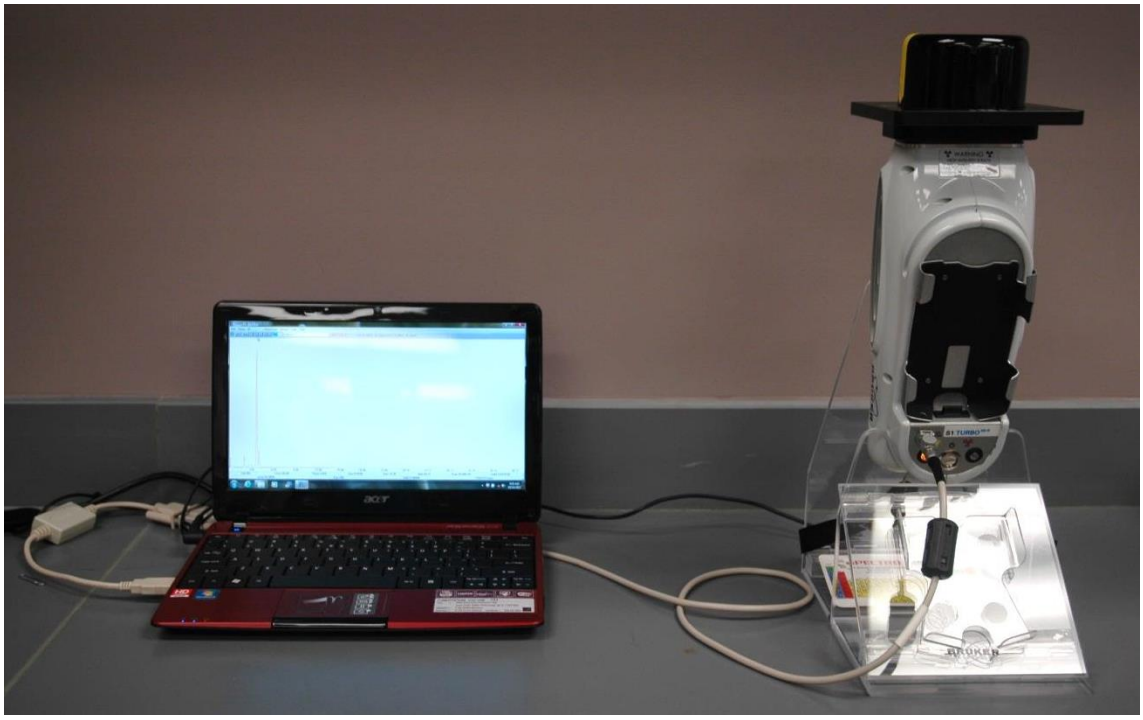

Figure 9: Accompanying laptop computer provided by the manufacturer connected to the HHXRF via the white cable in the photo. The laptop came with upgraded analytical software, S1PXRF, which was used for all data collection events and allowed for the detection of low-mass elements.

Samples were placed directly onto the examination window for analysis (Figure 10), in order to reduce the distance between the detector and the object being analyzed. This helped to increase the detection of low-mass elements, such as P, without the use of a vacuum with the instrument. The use of a vacuum increases the detection of light elements by reducing the interference from air (Shackley, 2011). Christensen et al. (2012) suggests that handheld or portable XRF instruments that do not use a vacuum may not be suitable for analyzing bone specimens, as P is considered a light or low mass element and would not be detected. While a vacuum does not typically accompany standard handheld or portable XRF instruments, as these are designed to identify metal alloys in settings such as restricted materials screening (i.e.,

screening of toys for lead), soil contamination analysis, repatriating cultural artifacts (by pigment matching), and sorting scrap metal (©Bruker Corporation, 2013), there are models available that are designed to provide trace element analysis. Current examples sold by the ©Bruker Corporation include the Tracer III – V+/III-SD models, which when used with accompanying S1PXRF software, allow for trace element analysis (©Bruker Corporation, 2013). The instrument used in the analysis is not a Tracer model and does not include a vacuum adapter or option, however, the S1PXRF software was used, which should allow for trace element analysis. In order to test the ability of the HHXRF to reliably detect Ca and P (without the use of a vacuum), a controlled experiment was performed, as discussed in the following chapter.

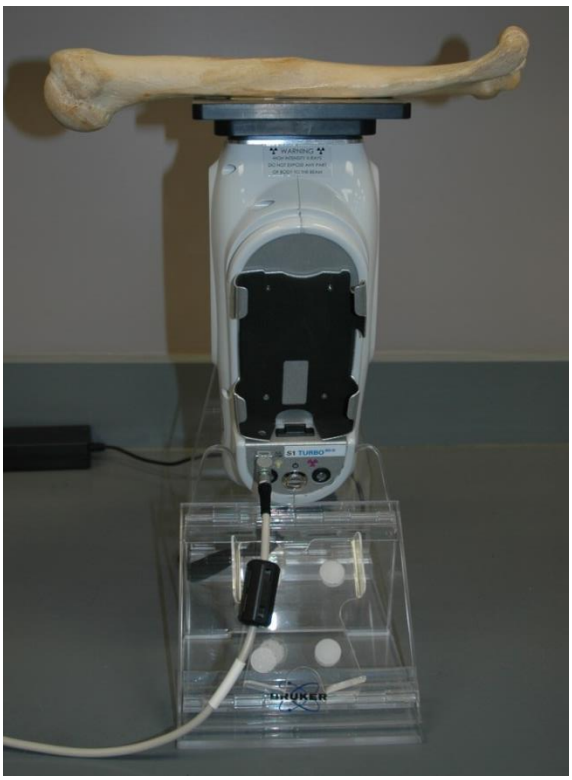

Figure 10: HHXRF shown in data collection position with human humerus on the examination window.

Methods

For the purposes of this research, methods were devised both for data collection and data analysis. The study was separated into three parts, each of which had its own set of methods for data collection and data analysis: (1) Reliability Test, (2) Accuracy Test, and (3) Ca/P Detection Test. First, data collection methods for each of the three tests will be discussed, followed by the methods used for data analysis for each of the three tests.

Data Collection

Reliability Test

Previous studies have suggested that bone is not homogeneous in terms of elemental composition, and that cortical bone is less variable than cancellous bone (Vass et al., 2005; Castro et al., 2010; Rusak et al., 2011). Additionally, previous research has suggested that XRF spectrometry performed on "flat, polished surface[s]" of bone yield the most valuable results in terms of quantitative data (Christensen et al., 2012:48). However, since fragmentary and taphonomically modified bone may not always allow for the analysis of ideal material consisting of cortical bone with flat surfaces, it was necessary to test the reliability of the HHXRF in detecting elements consistently throughout all surfaces of a single bone. Therefore, the first component of the project consisted of a Reliability Test, in which data was collected from one femur systematically using the HHXRF in the benchtop setting, as discussed previously. Thirty locations representing the entire length and all surfaces of the femur (anterior, posterior, medial, and lateral) were analyzed. Data were sequentially collected from each of these locations a total of five times, resulting in 150 total spectra. After each data collection event, a numbered

marker/sticker was placed on the bone to mark the location of the data collection for reference purposes, and the number on the sticker corresponds to the sample filename (Figure 11). All spectra were compiled into a single Excel spreadsheet for data analysis.

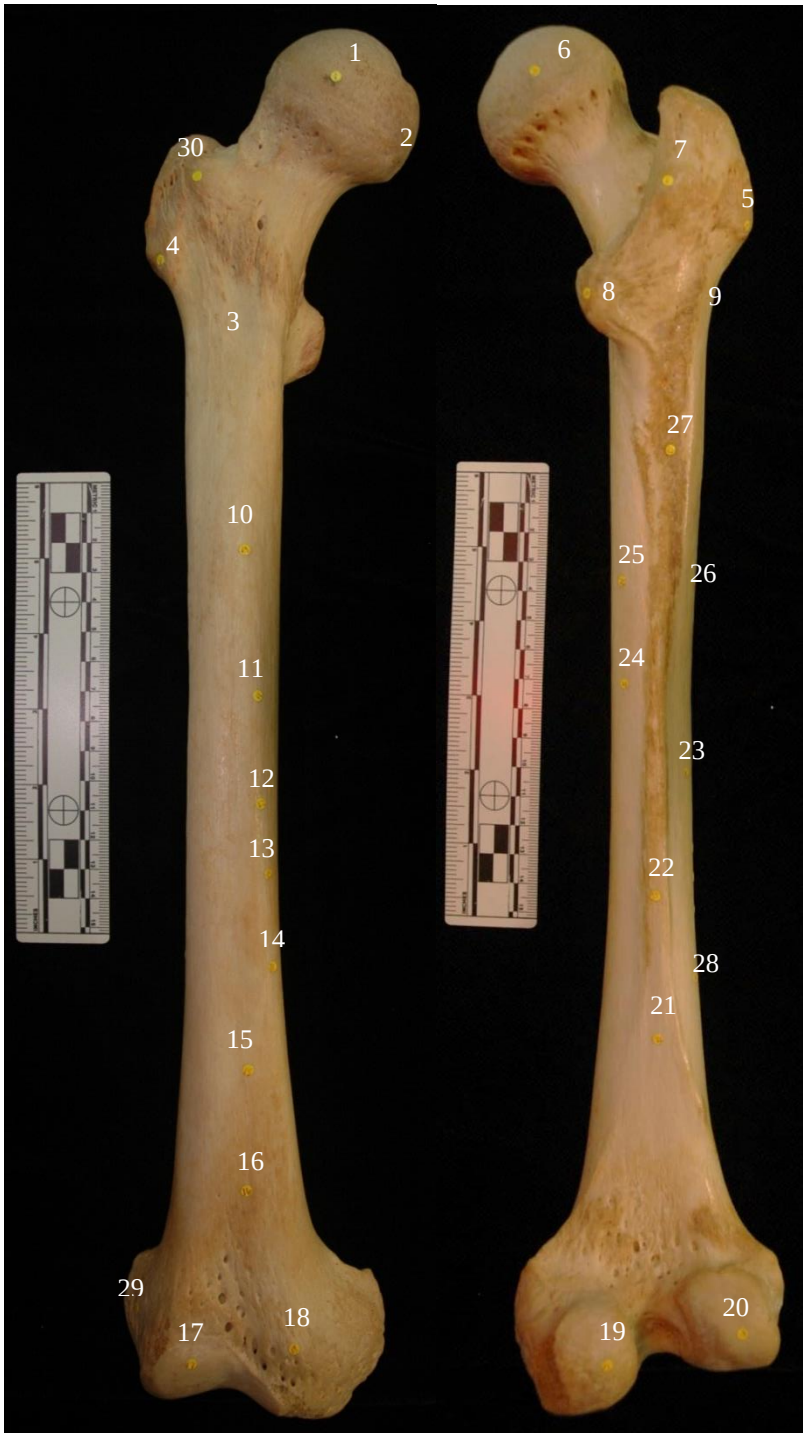

Figure 11:Femur analyzed during the reliability test (Left: anterior view, Right: posterior view). The yellow stickers are labeled with their corresponding location number (1-30) and denote areas where data was collected.

Accuracy Test

In the second component of the project, several samples were analyzed to test the accuracy of the technique in discriminating bone and non-bone materials. Data were collected on each specimen a total of eight times from four separate locations on the specimen, with the data being collected in groupings of two at each of the four locations. This systematic technique was used for several reasons: (1) eight spectra per sample ensured that the chemical properties of the bone were well-represented; (2) the groupings of two at each location allowed for a continuance of the reliability test on the samples (examination of consistency in the data collection and within the chemical composition of the sample); and (3) the four sampling locations per sample ensured that several areas of the sample could be represented in the spectra while still avoiding areas determined to be problematic in the Reliability Test. After each data collection event, a numbered marker/sticker was placed on the bone to denote the location of the data collection for reference purposes, and the number on the sticker corresponds to the sample filename. All spectra were compiled into a single Excel spreadsheet for data analysis.

Ca/P Detection Test

Due to reports in the literature that handheld or portable XRF may not be suitable for the analysis of bone due to the inability of the instrument to detect light or low mass elements (Christensen et al., 2012), it was necessary to test the ability of the HHXRF unit used in the study to detect Ca and P. This was accomplished by measuring the ratio of the Ca K_{β} band at 4.013 keV (the non-dominant of the two Ca peaks detected in bone/teeth) and P K_{α} band at 2.014 keV for a series of prepared samples with molar ratios of Ca/P ranging from 1.67 to 3.36. The

prepared samples were comprised of synthetic hydroxyapatite and combinations of synthetic hydroxyapatite and calcium carbonate at known molar ratios (determined by controlling the measurements of the substances used). These prepared standards consisted of powdered mixtures of weighed portions of synthetic hydroxyapatite and calcium carbonate, which were packed into pellets for analysis with the HHXRF.

Data Analysis

Part I: Reliability Test

Several quantitative methods were used to test the reproducibility of the technique. The purpose of this aspect of the study was (1) to determine how reliable the instrument was in detecting elements over a single bone (within site reliability), and (2) to determine whether a single bone was homogeneous in terms of the elements the HHXRF was able to detect when several surfaces were randomly sampled (between site reliability). To test the within site reliability, each site chosen for data collection was analyzed five times sequentially in order to further test the reliability of the instrument.

Within Site Reliability

In order to examine the within site variance, a series of channels (10 total, corresponding to all measurements of that channel within a site) were chosen both corresponding to known elements, and at random, and examined using the reliability function in IBM SPSS 20.0. This provided a Cronbach's alpha value for each of the 10 channels, which could be examined for consistency. Cronbach's alpha values describe the level of consistency within a variable, and are

considered a coefficient of reliability (Silva and Stam, 1995). For the reliability test, a select group of channels were chosen, with four corresponding to known elemental peaks (P:105, S:120, Ar: 134, Ca:200), and the other six being chosen at random (165, 319, 375, 429, 493, 559), but also corresponding to peaks in the spectra. The average intensity value and the standard deviation for each chosen channel were used as variables for the reliability analysis, and then the Cronbach's alpha values were compared. A Cronbach's alpha value that approaches 1 indicates consistency or reliability within measurements (Silva and Stam, 1995), which in this case were the selected channels.

The spectral data was also examined using principal components analysis (PCA) and scatterplot analysis, shown in previous studies to be a reliable technique for analyzing correlation between variables in spectral data (Shimoyama et al., 1997; Brody et al., 2001; Shimoyama et al., 2004; Edwards et al., 2006; Castro et al., 2010; McLaughlin and Lednev, 2012). Before PCA, the data was pretreated, which involved post-processing of the raw spectral data in order to remove specific areas and standardize the data for use in PCA. The areas removed from the spectra included background noise and the dominating Ca K_α peak at 3.9 keV; the removal of these areas was necessary in order to emphasize the trace elements during PCA. Post-processing of the data from both data collection events involved: (1) removing background noise (channels 0-10), (2) removing the Ca K_α peak at 3.9 keV (channels 170-193), and (3) normalizing the remaining trace elements to the Ca K_β peak at 4.0 keV. PCA was then performed on the compiled and post-processed data. The PCA was performed in the statistical program MatLab version 2012b by Mathworks.

The principal component's scores obtained from the femur spectral data representing a significant amount of the variance in the data were used for the analysis, which corresponded to principal components 1-4. All of the principal component scores for each site were plotted on a 3D scatter in order to visually examine the within site variance and compare the results to those obtained in the Cronbach's alpha analysis. This was accomplished by examining and comparing 3D scatterplots of both principal components 1-3 and 2-4.

Between Site Reliability

The PC scatterplots were also examined for the relationship between the 30 sites (between-site variance). This was accomplished visually by examining the relative distances between the points corresponding to data collection sites. Sites that were visually determined as outliers were considered to have a high degree of between site variance relative to the within site variance and were further examined in ARTAX, a computer program provided by ©Bruker Corporation (2013) for spectral examinations related to the HHXRF. For the sites exhibiting a higher degree of between site variance than others, spectrum A from each of the sites were overlaid with a "normal" site spectrum A in order to determine how individual spectra differed from one another. In this case, "spectrum A" refers to the first spectra collected at each of the 30 locations on the femur, and a "normal" site spectrum A is one that lies within the group of closely associated sites on the principal component plot(s).

Additionally, in order to examine how spectra collected from different locations on the bone varied from one another, spectra A from all 30 sites were plotted on a single graph. Due to the amount of overlay on this graph, another graph was constructed based on the average

spectrum A values from all 30 sites resulting in an average spectrum for the sample. Error bars were added to this graph at select channels that correspond to the standard deviation of the values of that channel. These graphs provide information as to why some of the sites on the same bone have a higher variance than other sites.

Part II: Accuracy Test

Data analysis involved post-processing of the compiled raw spectral data collected from the different samples in order to remove specific areas and standardize the data for use in PCA, followed by scatterplots analysis and multivariate statistical analyses. The areas removed from the spectra included background noise and the dominating Ca K_α peak at 3.9 keV; the removal of these areas was necessary in order to emphasize the trace elements during PCA. Post-processing of the data involved: (1) identifying the spectra as Ca-Dominated (Figure 12a) or Non Ca-Dominated (based on Ca K_α peak at 3.9 keV) (Figure 12b), (2) sorting the spectra by Ca-Dominated and Non Ca-Dominated, (3) removing the Non Ca-Dominated spectra from the compiled data, (4) removing background noise (channels 0-10) (Figure 13a), (5) removing the Ca K_α peak at 3.9 keV (channels 170-193) (Figure 13b), and (6) normalizing the remaining trace elements to the Ca K_β peak at 4.0 keV (Figure 13c). Since bone is composed of a combination of hydroxyapatite and phosphate in a predictable elemental ratio/composition ($Ca_5(PO_4)_3OH$) in which Ca is the dominant element, it was assumed that any Non Ca-Dominated spectra were representative of non-bone materials. Thus, these Non Ca-Dominated spectra were removed from the compiled data and not included in subsequent analyses. Principal components analysis

was performed on the post-processed compiled data. The PCA was performed with the statistical program R i386 2.15.1.

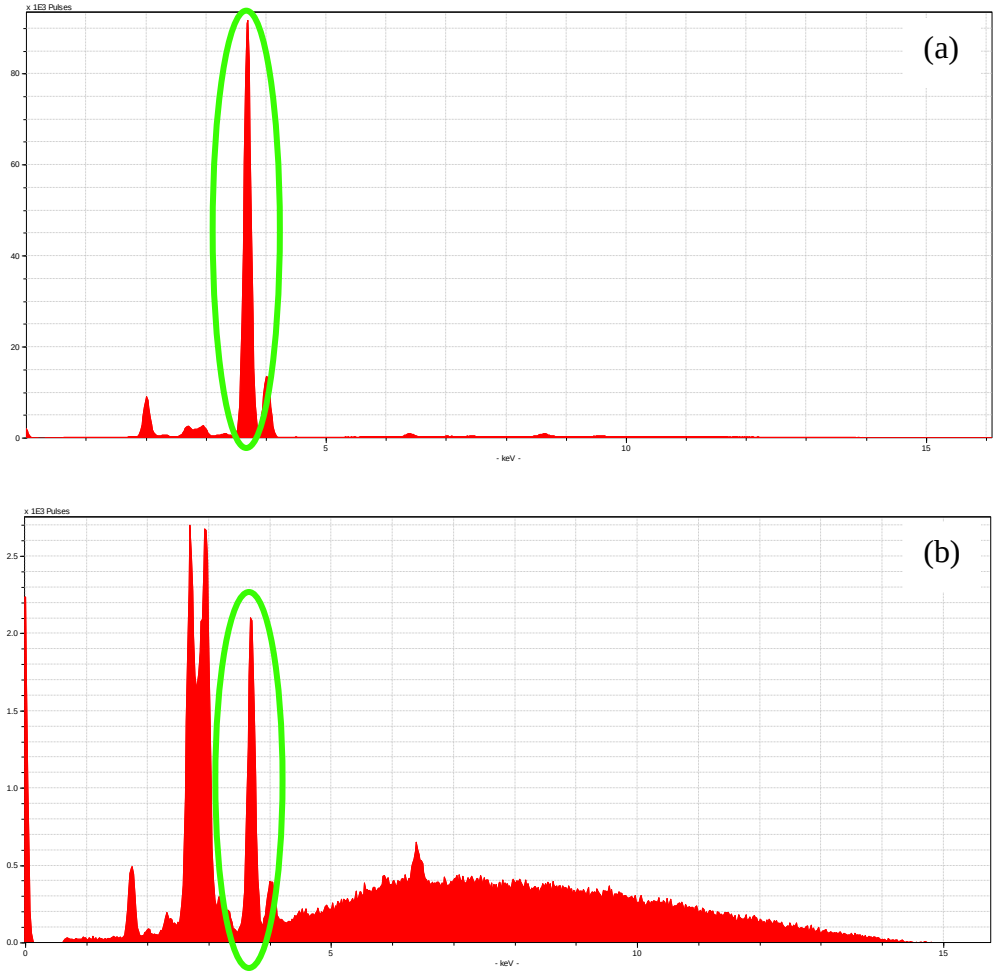

Figure 12: Example HHXRF spectra with Ca peak highlighted in green. (a) Spectrum identified as Ca-Dominated. (b) Spectrum identified as Non Ca-Dominated.

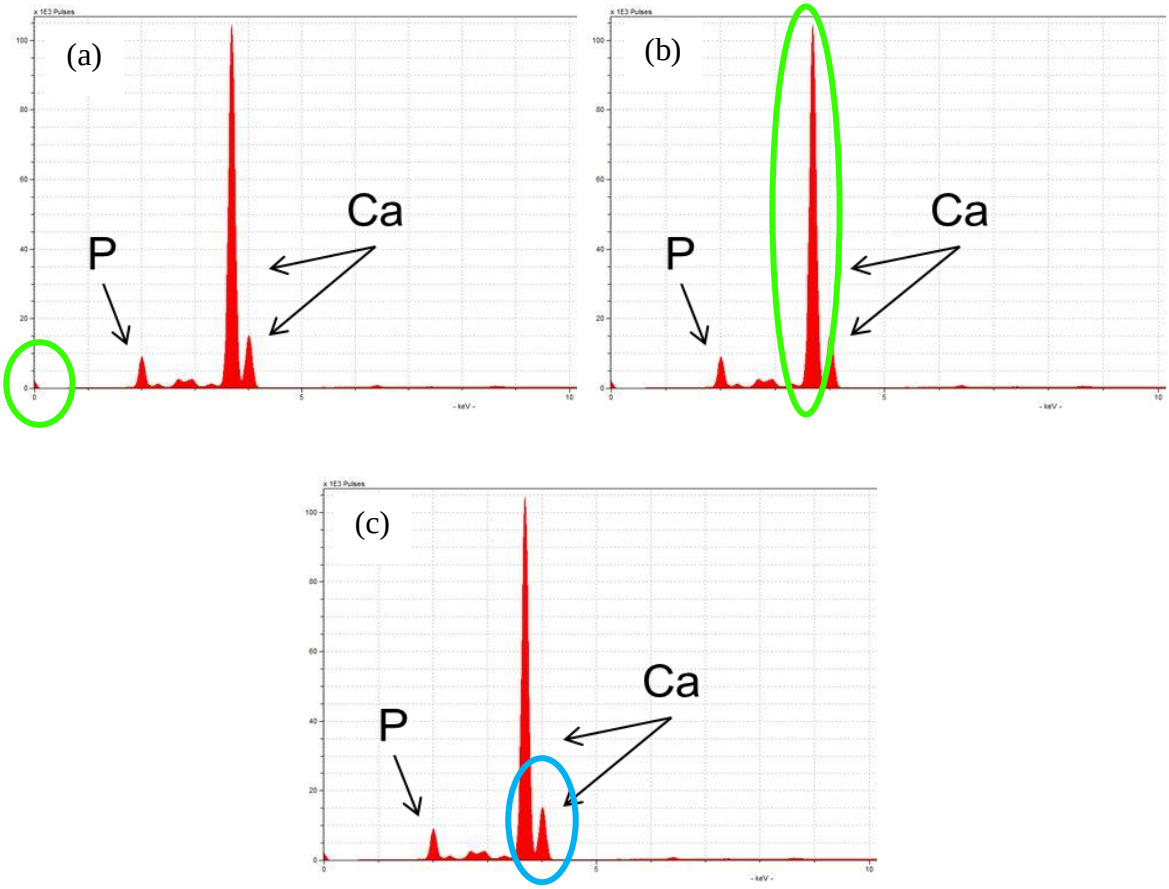

Figure 13: Example HHXRF bone spectra. (a) The area highlighted in green denotes the area determined to be background noise (channels 0-10) that was removed from all Ca-Dominated spectra. (b) The area highlighted in green denotes the Ca K_α peak (channels 170-193) that was removed from all Ca-Dominated spectra. (c) The area highlighted in blue denotes the Ca K_β peak; the remaining data was normalized to this peak.

For the data collected using the larger dataset (Accuracy Test), principal components representing a significant amount of the variance in the data (97%) were used as variables for additional analyses as determined using a scree plot. Scatterplots of the principal component scores were analyzed to see how the bone and non-bone spectra separate, as well as how bone samples separate from several groups of non-bone materials. The scatterplots were also used to

examine how similar the bone and non-bone materials were in terms of their chemical composition (as represented by the principal component scores).

The principal component scores were used as variables in LDA and QDA, in order to determine if the technique can accurately classify materials as "Bone" or "Non-bone". These analyses provide correct classification percentages for each category and overall correct classification, both of which will be used to assess the validity of the technique. For both LDA and QDA, the prior probabilities were set equal for each group, assuming that the number of variables in each class was relatively equal and the probability of assignment to each class should reflect this assumption. Scores from the first three principal components were also used for hierarchical clustering analysis using Euclidean distance and average linkage. The corresponding heat map was produced using R software. The dendrogram and associated heat map were used to assess the similarity and differences between groups.

Ca/P Detection Test

The Ca/P ratios detected by the HHXRF were plotted against the molar ratios of the prepared materials in order to determine if the spectral ratio was proportional to the molar ratio. A linear instrumental response would indicate that the instrument is reliably detecting both Ca and P and would allow the analytical determination of Ca/P ratios in samples.

CHAPTER FIVE: RESULTS

Part I: Reliability Test

Within Site Reliability

The results of the reliability analysis can be found in Table 11, which shows the selected channels, the variables used (averages intensity values and standard deviations for each channel) and the Cronbach's alpha values yielded from the analysis. The Cronbach's alpha values indicate that there is a significant amount of reliability in the measurements. This is indicated by the individual Cronbach's alpha values for each channel, as well as the average Cronbach's alpha value for the sample. Recall that a Cronbach's alpha of 1 indicates that each measurement is consistent with the initial measurement, and since the value obtained in the analysis is close to 1, the data is showing consistency in the measurements in each case, as well as overall. This indicates that there is little within site variance present in the sample. If it is assumed that this sample is an accurate representation of the larger sample, then it can be assumed that the dataset, as a whole, is reliable within each measurement site.

Table 11: Results of the Cronbach's alpha analysis used to examine the reliability within the 30 sites examined on the femur.

Channel	Average Intensity Value for Channel	Std. Dev. For Channel	Cronbach's Alpha	Corresponding Element (if applicable)
100	11844	3978.336	0.999	Phosphorus
120	400	95.65637	0.993	Sulfur
134	3032	504.3036	0.998	Argon
165	1448	501.2475	0.999	
200	16968	4738.235	1.000	Calcium
319	2940	1509.335	1.000	
375	418	92.30533	0.989	
429	1188	743.9264	1.000	
493	412	90.64828	0.989	
559	349	78.93668	0.988	
Average Cronbach's Alpha			0.996	

A 3D scatterplot of principal component scores 1, 2, and 3 for each of the 30 sample sites and the five sample measurements from each site can be found in Figure 14. This graph plots all three of the principal components against one another, which allows for the examination of close associations between the points at each site (and between the sites). The sample number was determined by grouping together the samples belonging to each of the 30 sites. For example, femur1a60s, femur1b60s, femur1c60s, femur1d60s, and femur1e60s are all samples that were grouped together and called "Site 1". Therefore, in the figure, all five PC scores are plotted for each site, but they are grouped by site number. The scatterplot indicates that there is minimal variation within the measurements taken at each of the 30 sites. This is demonstrated by the alignment of the five symbols at each of the 30 locations on the graph, the extent of which is so great that they appear to be single points upon first glance.

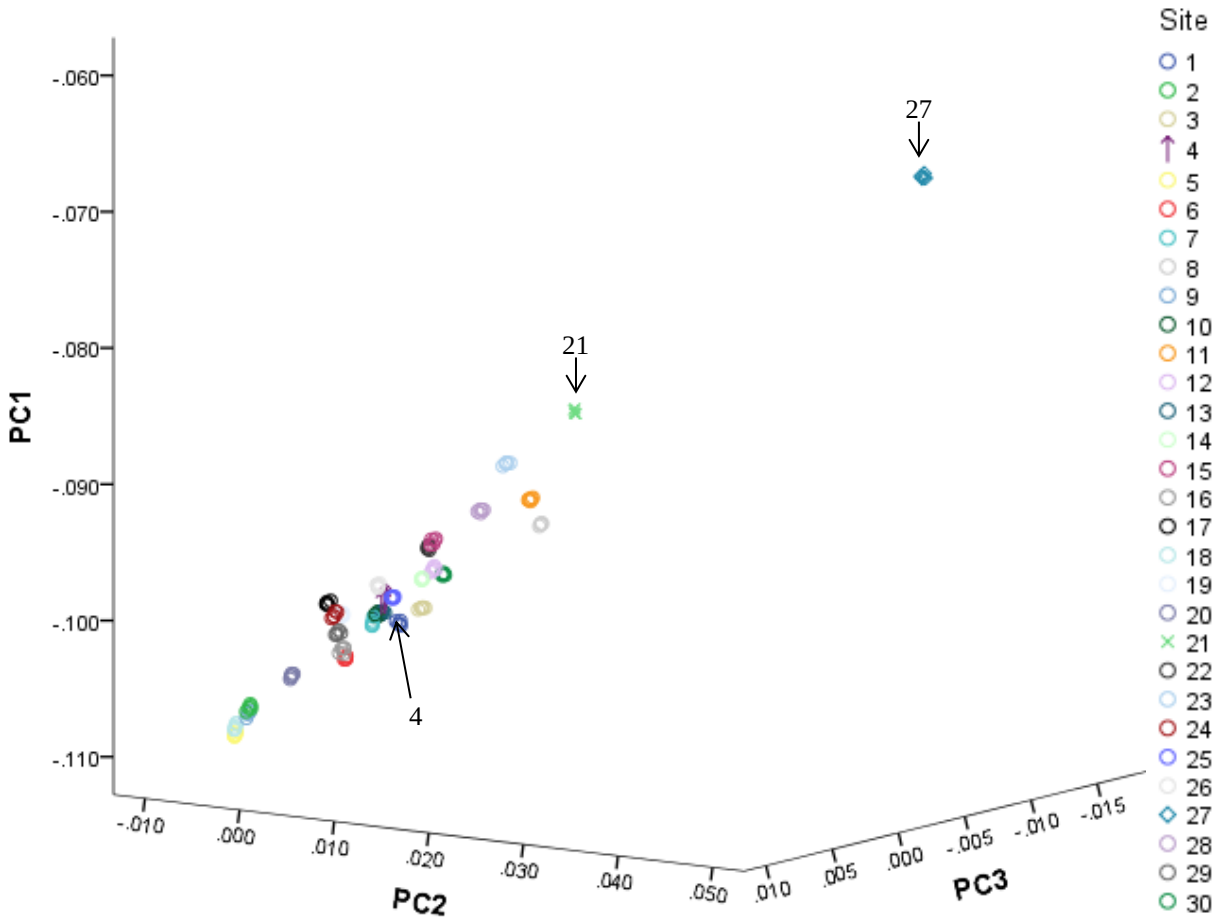

Figure 14: Graph of the scores of principal components 1-3. Each of the 30 sites is plotted (as indicated 1-30 and by the different colors in the key), as well as each of the 5 repetitions collected for each site. Sites 27 and 21 were classified as outliers; Site 4 indicates a site within the range considered to be normal.

The plot in Figure 14 shows a possible linear relationship between the PCs, which is atypical. In order to conclude if there was a linear relationship between the PCs, plots of the scores of PCs 1-2 (Figure 15) and PCs 2-3 (Figure 16) were created. The plot of the scores of PCs 2-3 showed a normal or nonlinear distribution of the data. The plot of the scores of PCs 1-2

showed a linear relationship between the data; the linearity was statistically significant with a correlation coefficient of 0.917.

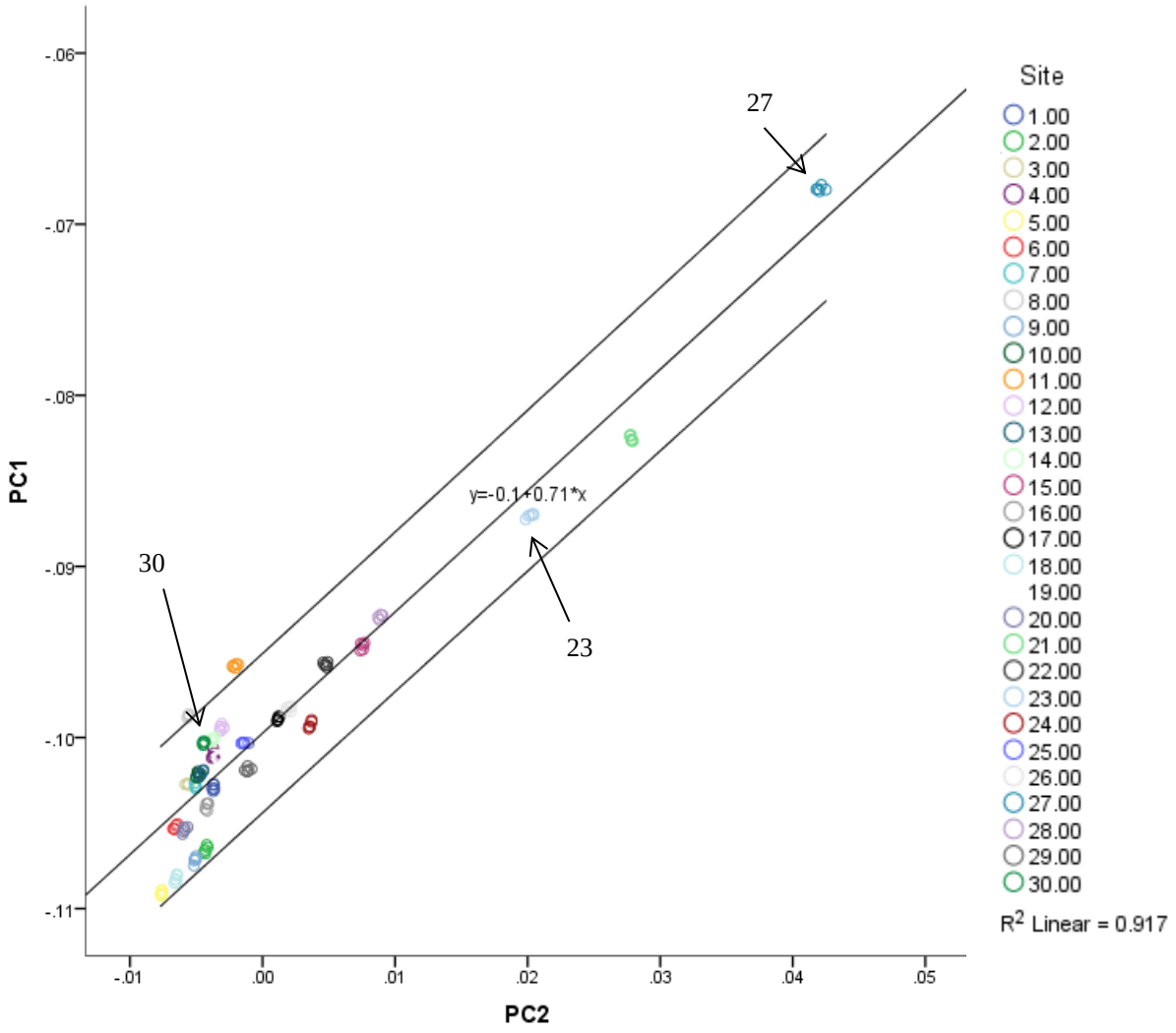

Figure 15: Graph of the scores of principal components 1-2. Each of the 30 sites is plotted (as indicated 1-30 and by the different colors in the key), as well as each of the 5 repetitions collected for each site. The plot shows a linear relationship between the PCs. A line of best fit and 95% confidence interval lines are provided.

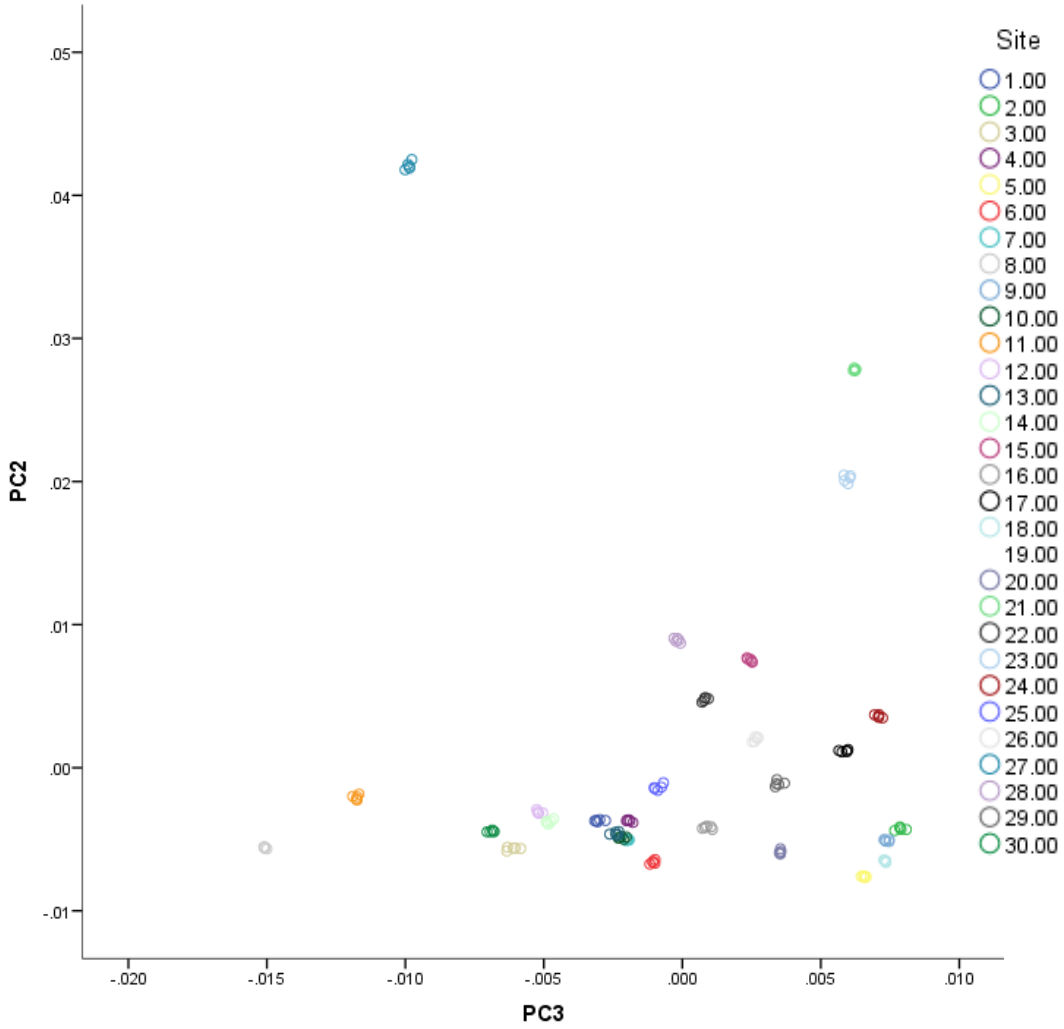

Figure 16: Graph of the scores of principal components 2-3. Each of the 30 sites is plotted (as indicated 1-30 and by the different colors in the key), as well as each of the 5 repetitions collected for each site. The plot shows a normal (nonlinear) distribution of the data between the PCs.

In order to determine the possible cause of the linearity in the PC 1-2 scores plot, eigenvector loading spectra of PCs 1 and 2 were produced (Figure 17). This graph shows that most of the variance in the components (as described by the eigenvectors) is a result of the peak(s) labeled as "unassigned" in Figure 17, and there are only minor differences in intensity at the other four main peaks: (1) P K_{α}, (2) Ca K_{β}, (3) Fe, and (4) Zn. The peak(s) was/were considered "unassigned" as no single element could be matched either to the peak using the ARTAX software. A list of possible elements was compiled based on the accepted photon energies of the X-ray emission lines (Bearden, 1967) (Table 12) in order to determine which element was most likely being represented by the peak(s), which was occurring between 2.5 and 3.1 keV. The $K_{\alpha 1}$, $K_{\alpha 2}$ and $K_{\beta 1}$ values for the five elements (S, Cl, Ar, K and Ca) indicate that the unknown peak is most likely a Cl emission, due the K_{α} and K_{β} values for this element being the most similar to the unknown.

Table 12: X-ray atomic energy levels (Bearden, 1967)

Element	**$K_{\alpha 1}$**	**$K_{\alpha 2}$**	**$K_{\beta 1}$**
S	2.30784	2.30664	2.46404
Cl	2.62239	2.62078	2.8156
Ar	2.95770	2.95563	3.1905
K	3.3138	3.3111	3.5896
Ca	3.69168	3.68809	4.0127

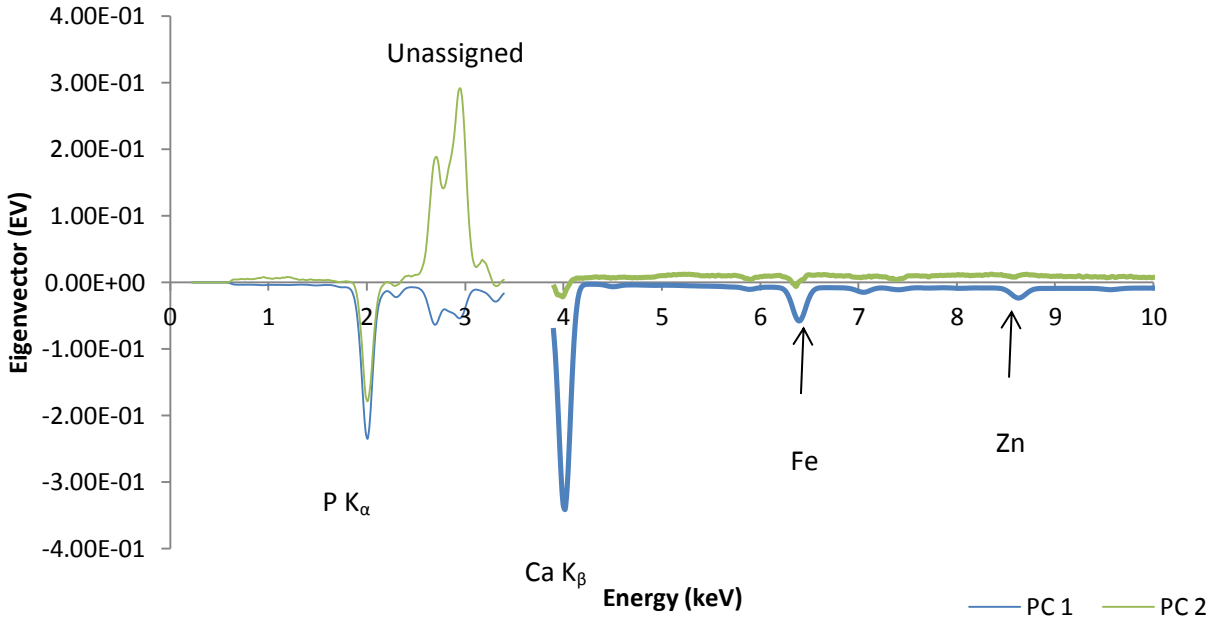

Figure 17: Eigenvectors of PCs 1-2 plotted (PC1 in blue, PC2 in green) showing the factor loadings of the components. The gap in the graph indicates data that was removed (Ca K_α peak) during post-processing.

It should also be noted that the Ca/P ratio of the sites change along the line that results from plotting the scores of PC1 and 2 (Figure 15). Specifically, sites occurring at the lower end of the line, near Site 30 (marked in Figure 15), have a lower Ca/P ratio than those occurring near Site 27. This is due to a decreased influence from the unassigned peak in regards to PC1, as shown in Figure 17 (the EV values for the unknown for PC1 are negative, while those for PC2 are positive). However, as the Ca/P ratio increases, so does the influence from the unassigned band(s), as the influence from PC2 is greater. This can be demonstrated by plotting example spectra from three sites found at different intervals along the line in the PC 1-2 scores plot

(Figure 18). The graph shows the changes in the Ca/P ratio and corresponding changes to the unassigned peak(s) as the sites move positively on the linear graph (from Figure 15), from Site 30 to Site 15 to Site 27.

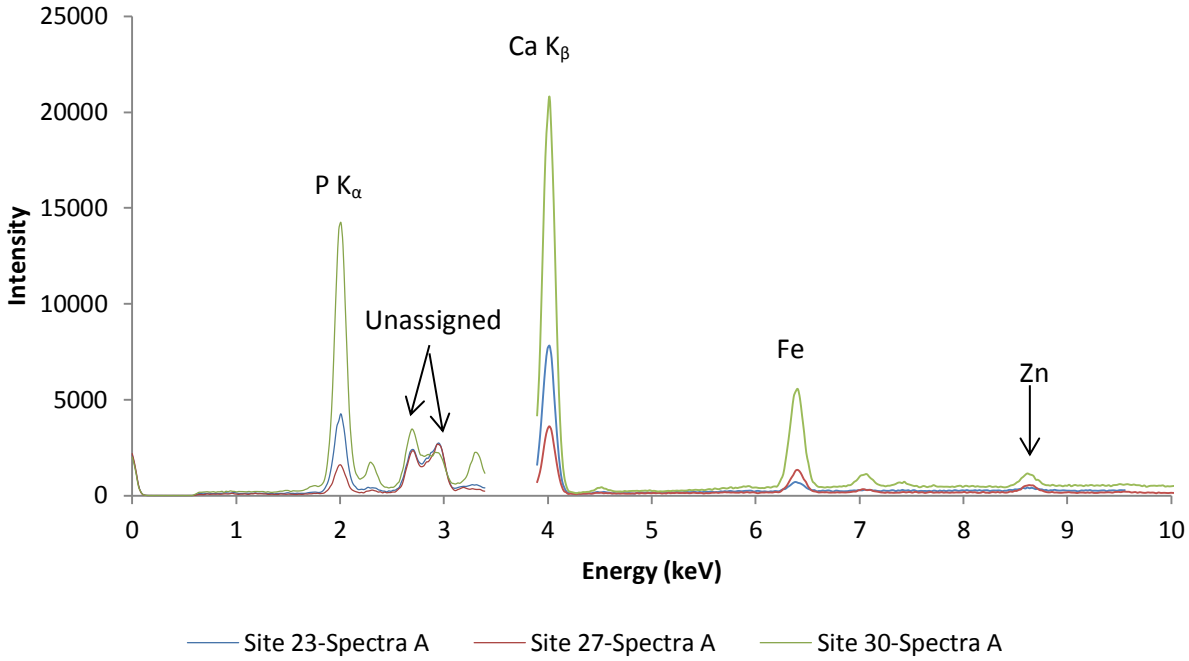

Figure 18: Example spectra (Spectra A) from three sites (23, 27 and 30) found at different intervals along the line that forms in the data when the scores of PCs 1-2 are plotted. The graph shows the changes in the Ca/P ratio and corresponding changes to the unassigned peak(s) as the sites move positively on the linear graph, from Site 30 to Site 23 to Site 27.

A 3D scatterplot of principal component scores 2, 3, and 4 for each of the 30 sample sites and the five sample measurements from each site can be found in Figure 19. This scatterplot is identical to the previous one, except that PC1 has been replaced with PC4, which resulted in a different formation of the data points. The PC 2-4 scores plot shows a nonlinear relationship between the data points, indicating that PC1 encourages linearity in the data. Despite the

difference in the way the data plotted on the graph (in comparison to the PC 1-3 plot), the scatterplot again indicates that there is minimal variation within the measurements taken at each of the 30 sites. However, this graph does show more within site variation than the one constructed using principal components 1-3, since the data points from each site do not align as well at some sites as they did in the PC 1-3 scores plot (Figure 14).

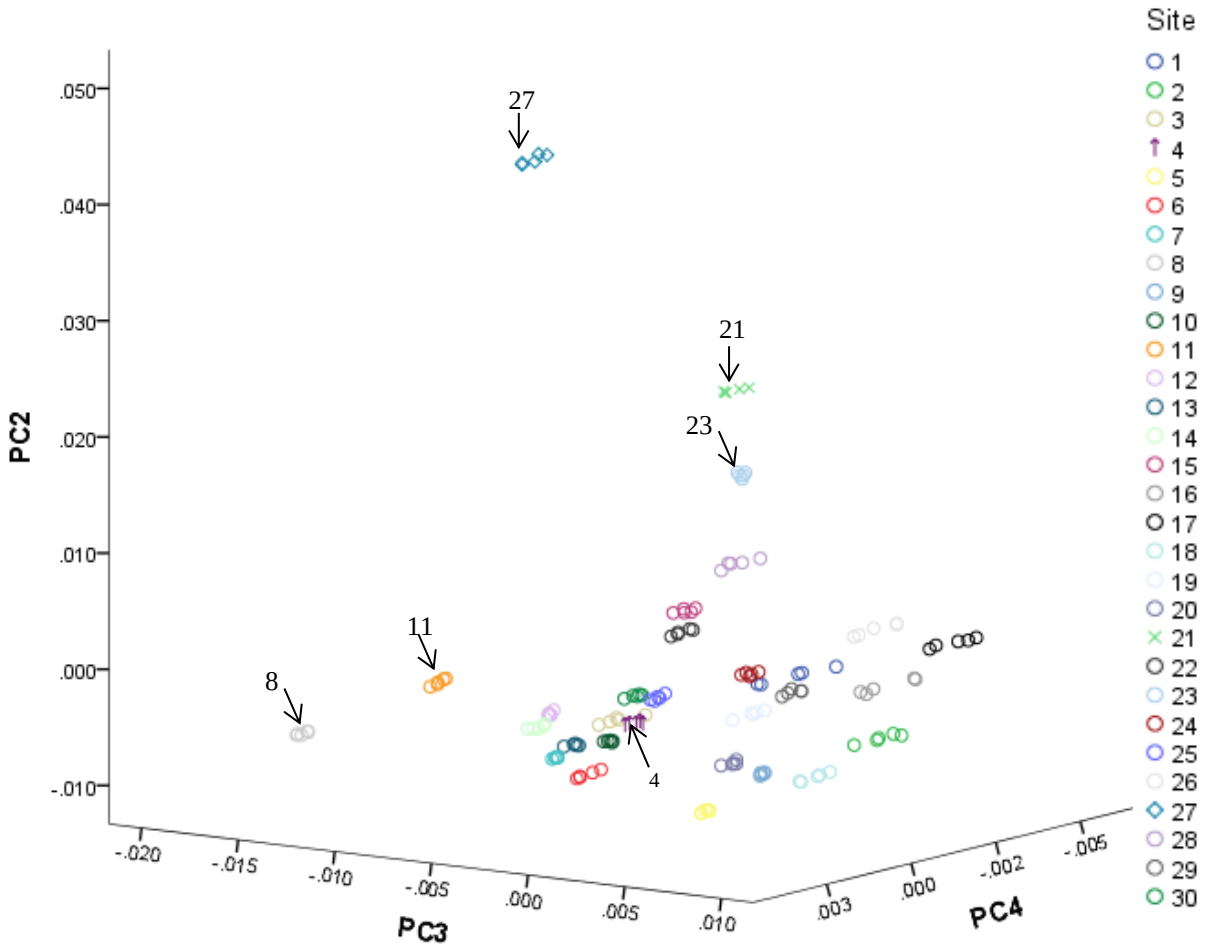

Figure 19: Graph of scores of principal components 2-4. Each of the 30 sites is plotted (as indicated 1-30 and by the different colors in the key), as well as the 5 repetitions recorded for each site. Sites 27, 21, 23, 11, and 8 were classified as outliers; Site 4 indicates a site within the range considered to be normal.

Between Site Reliability

The scatterplots of PC 1-3 and PC 2-4 were also used to examine between site reliability (Figures 14 and 19). This can be examined by comparing the distribution of the data points on the graphs corresponding to sites in terms of proximity to the other data points. This type of analysis identifies visual outliers or sites that exhibit a high degree of variance from the other sites. An examination of both scatterplots shows that there is higher variation between the 30 sites than within the five repetitions recorded at each site. This is demonstrated by the distribution of the colors that represent the 30 sites, as compared to the closer proximity of points of the same color representing data collected at a single site. Additionally, the distribution of the 30 sites shows that some sites are significantly different from other sites. Sites 27, 21 and 23 were selected as possible outliers from the plots in Figures 14-15, as they appeared to be separate from the main group of data points representing the other sites. Additionally, using the graph in Figure 15, and the information discussed previously regarding the change in Ca/P ratio along the best-fit line in this graph, it was assumed that an increased Ca/P ratio (relative to the other sites) caused sites 27, 21 and 23 to be outliers. Sites 11 and 8 were also classified as potential outliers based on visual analysis of the plots in Figures 16 and 19, as they also appeared to be separate from the main group of data points representing the other sites, but only when PC1 was not included in the scatterplot analysis.

The sites visually classified as outliers were examined in ARTAX, a spectral analysis software, for signs of major differences between these spectra and a spectra determined to fall within the "normal" range; site 4 was selected to represent "normal". Spectra A from each site was used as a representation of all data collected from the site. These results can be found in

Figure 20. For the purposes of this analysis, a classification of normal was determined based on a point's close proximity to most other points, resulting in not being classified as a visual outlier. The analysis showed that the differences in the spectra were the result of differences in relative intensity, or in the amount of each of element at each sampling location, rather than from differences in the types of elements detected at each site. These differences in intensity are greatest at the Ca K_{α}, Ca K_{β}, and P K_{α} peaks, which are considered the major elements in each spectrum.

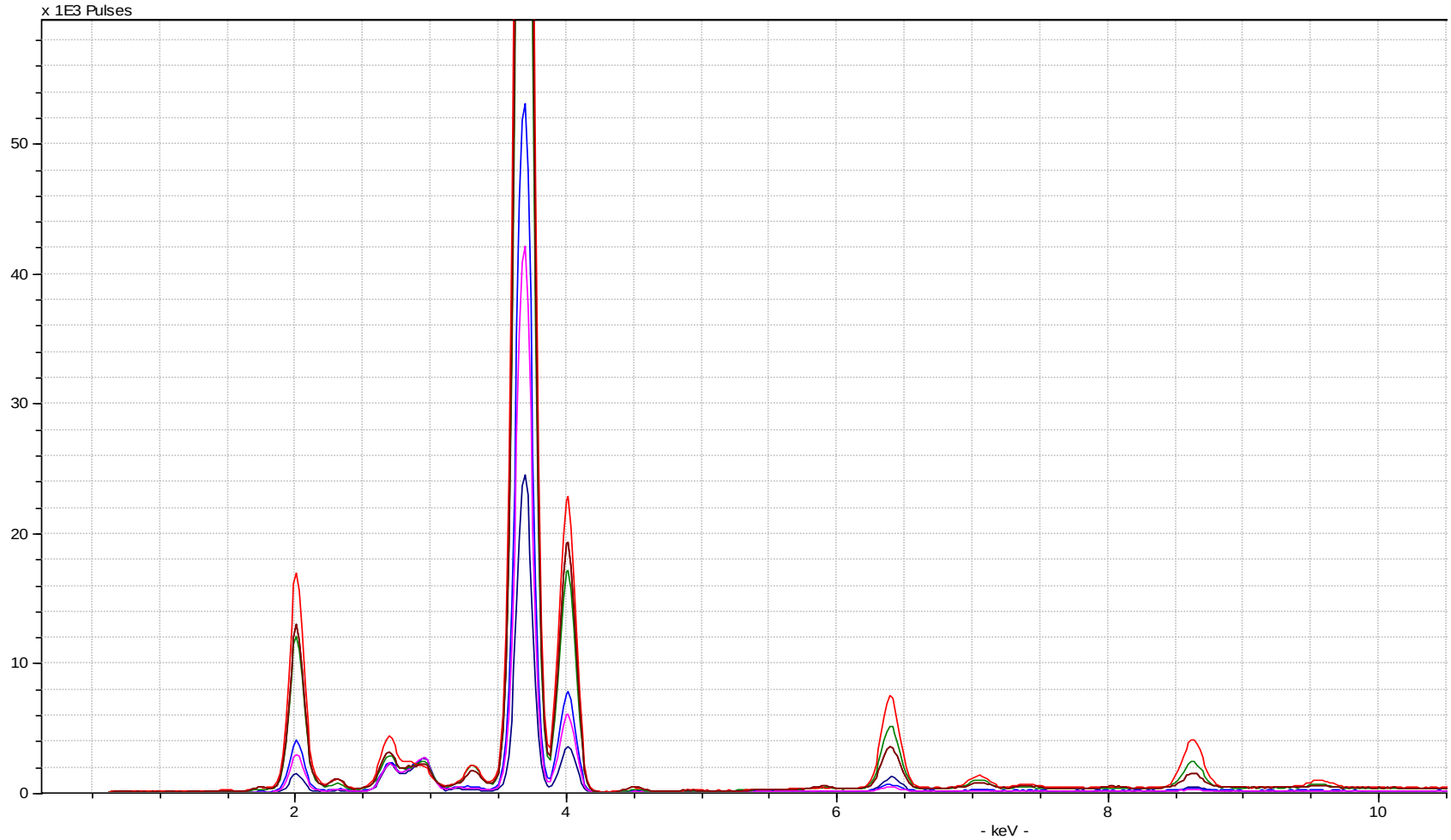

Figure 20: Spectral overlays from ARTAX for sites shown to be outliers: 27 (shown in dark blue), 21 (shown in pink), 23 (shown in light blue), 11 (shown in green), 8 (shown in red), and one site that fell within the normal range: 4 (shown in brown). Spectra A from each site is shown in the overlay.

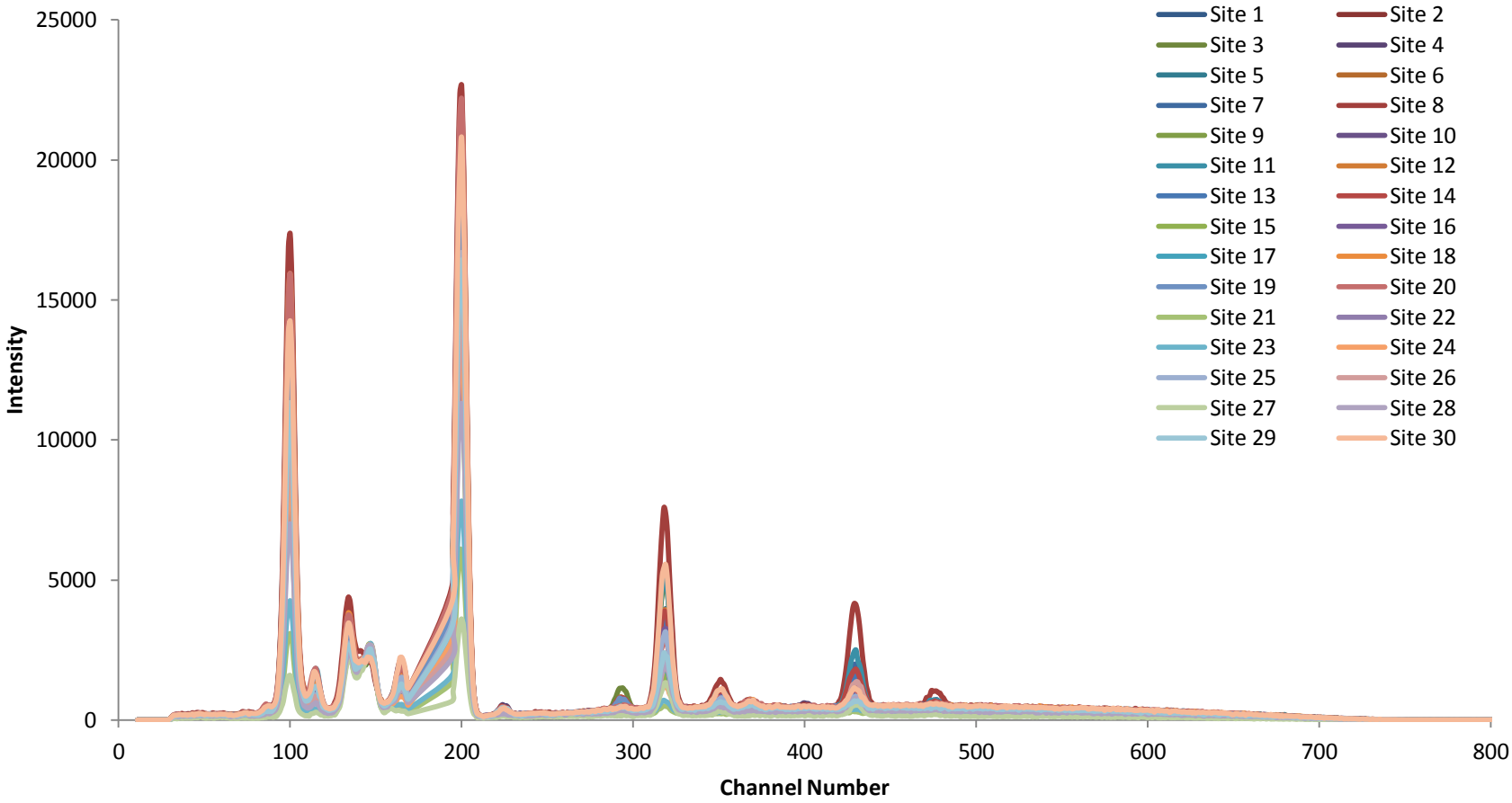

Figure 21: Spectra A from all 30 sites graphed on a single diagram. This is too difficult to interpret in terms of specifics, but it appears that most, if not all, of the variation lies in the differences in intensity between the spectra.

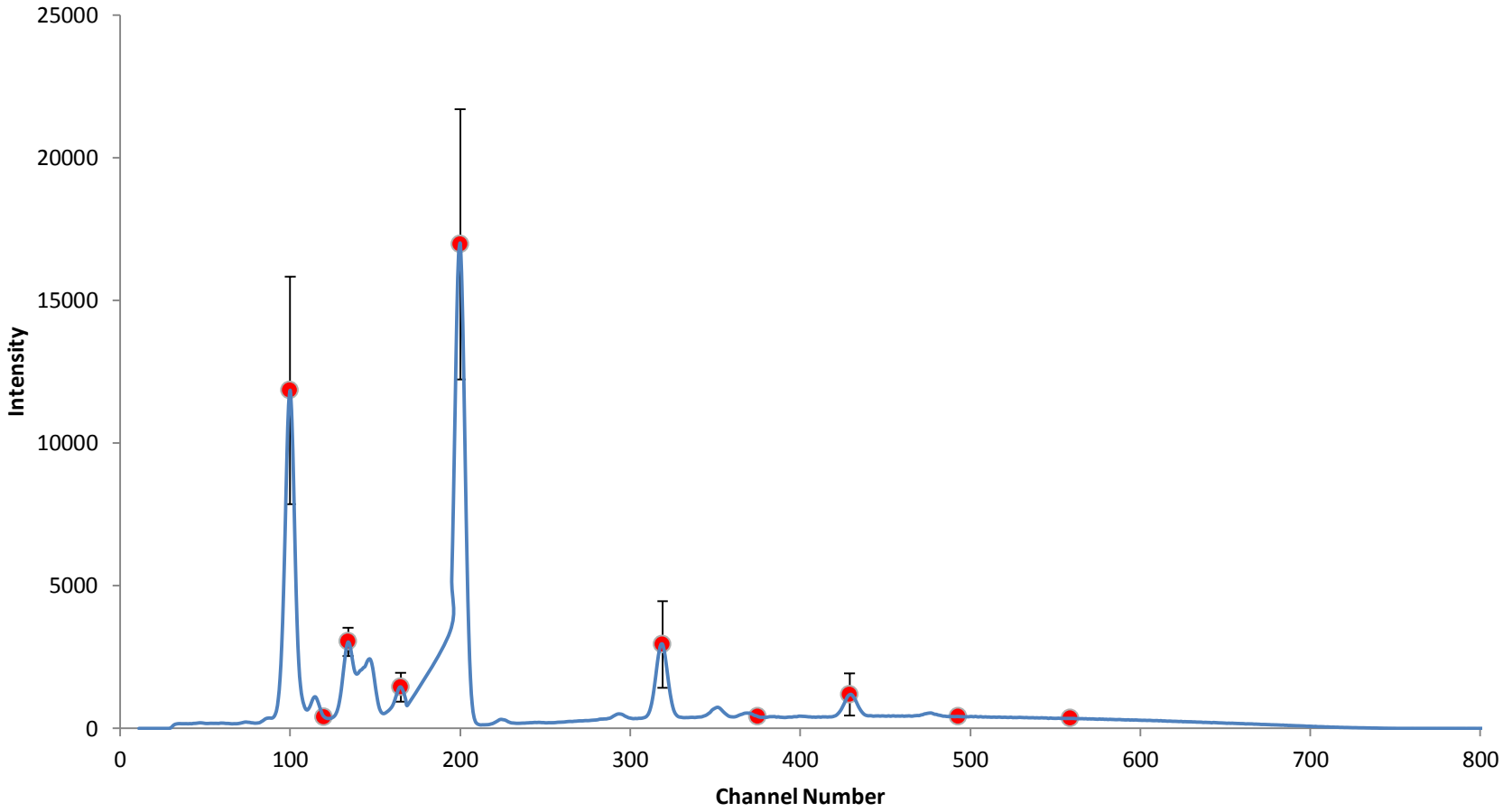

Figure 22: Averages of all spectra A channels plotted on single graph with error bars included at select channels (same channels as those used in the Cronbach's alpha analysis). (*the points showing no error bars have standard deviation less than 100, which inhibited error bar presentation due to the x-axis scale)*

The graph showing spectrum A from all 30 sites can be found in Figure 21. Limited results can be drawn from this graph since the 30 spectra show a high degree of overlap. However, there are noticeable differences in the intensity values for some channels, most of which occur at elemental peaks. There do not appear to be any instances of peaks occurring in some spectra and not in others. However, there are some cases in which several spectra have much higher intensity values for a given channel.

The graph representing the average spectrum for the sample, constructed using the average spectrum A values from all 30 sites, can be found in Figure 22. The error bars on the graph are located at the same channels examined in the Cronbach's alpha analysis (for standardization purposes), and use the mean and standard deviation values found in Table 11, which correspond to the mean and standard deviation for all collected data at those channels. The graph shows that the highest error occurs at the strongest peaks, which correspond to Ca K_{β} and P K_{α}, with most of the other points analyzed having relatively low error (the points showing no error bars have standard deviation less than 100, which inhibited error bar presentation). This error can be related back to the differences in elemental detection or intensity discussed previously, and supplements the idea that a large amount of the between-site variance corresponds to differences in the spectral intensities of the detected elements.

Summary

Overall, the results of the reliability test using the single human femur indicate that the between site variance is greater than the within site variance, as determined using reliability analysis (Cronbach's alpha) and scatterplot comparisons. Sites 8, 11, 21, 23 and 27, were

visually determined to be outliers, and these sites all represent rough areas of the bone or areas of the epiphyses. Both rough areas and epiphyses are not recommended for data collection due to the non-flat surface of the bone, which causes scattering of the light rays and inhibits proper analysis (Christensen et al. 2012). Christensen et al. (2012:48) recommend collecting data only on "flat, polished surface[s]" to obtain quantitative results of value. While other sites were also located on non-flat surfaces and did not seem to have problems, in terms of differences in intensity, this suggests that data collection should be standardized, when possible, and thus limited to "flat, polished surfaces" of the bone (i.e., the diaphysis, excluding muscle attachments).

Part II: Accuracy Test

The results of the Accuracy Test involved outcomes from several separate, yet related, tests, which will be discussed separately. These tests were used to differentiate human and nonhuman bone and teeth from non-bone material.

Ca-Dominated Spectra

The compiled spectral data were identified as being Ca-Dominated or Non Ca-Dominated based on the Ca K_α peak at 3.9 keV, and then sorted by this identification. The spectra identified as being Ca-Dominated were retained for subsequent analyses, while any spectra identified as Non Ca-Dominated were removed from the compiled data and excluded from any subsequent analysis of the data. The spectra identified as Non Ca-Dominated were: acorn seed (4), twig (1), spur (8), and burned plastic (8), with the number indicating the number of spectra. This simple analysis of the data acted as the first comparison step in the exclusion of non-bone materials, as

spectra that do not have the Ca K_{α} peak at 3.9 keV as the dominant peak cannot be bone. This is due to the chemical composition of bone, as discussed previously.

Principal Components Analysis (PCA)

All Ca-Dominated spectra were subjected to PCA using R i386 2.15.1 and R-code written by Sigman (2013) (Appendix E). A scree plot was used to determine the number of components to include in subsequent analyses (Figure 23). According to Cattell (1966), breaks or drops in the graph indicate components that should be retained. The break in the graph at the third component in the plot (designated by an arrow) indicates that three principal components should be retained for later analyses.

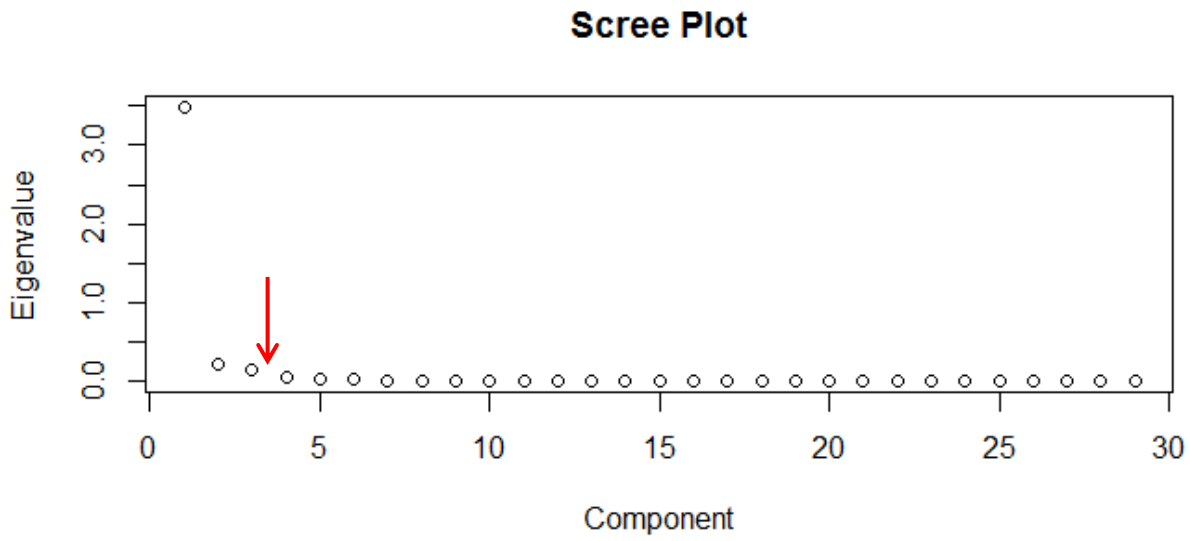

Figure 23: Scree plot to determine the number of principal components to use in subsequent statistical analyses.

Similar to in the Reliability Test, the eigenvectors corresponding to PCs 1-3 were plotted in order to examine the component loadings (Figure 24). The graph shows that a significant amount of the variance in P occurs in PC 2, while PC 3 contains a significant amount of variance in regards to Ca and Fe. This indicates that PCs 2-3 may be more helpful in discriminating the samples than PC 1.

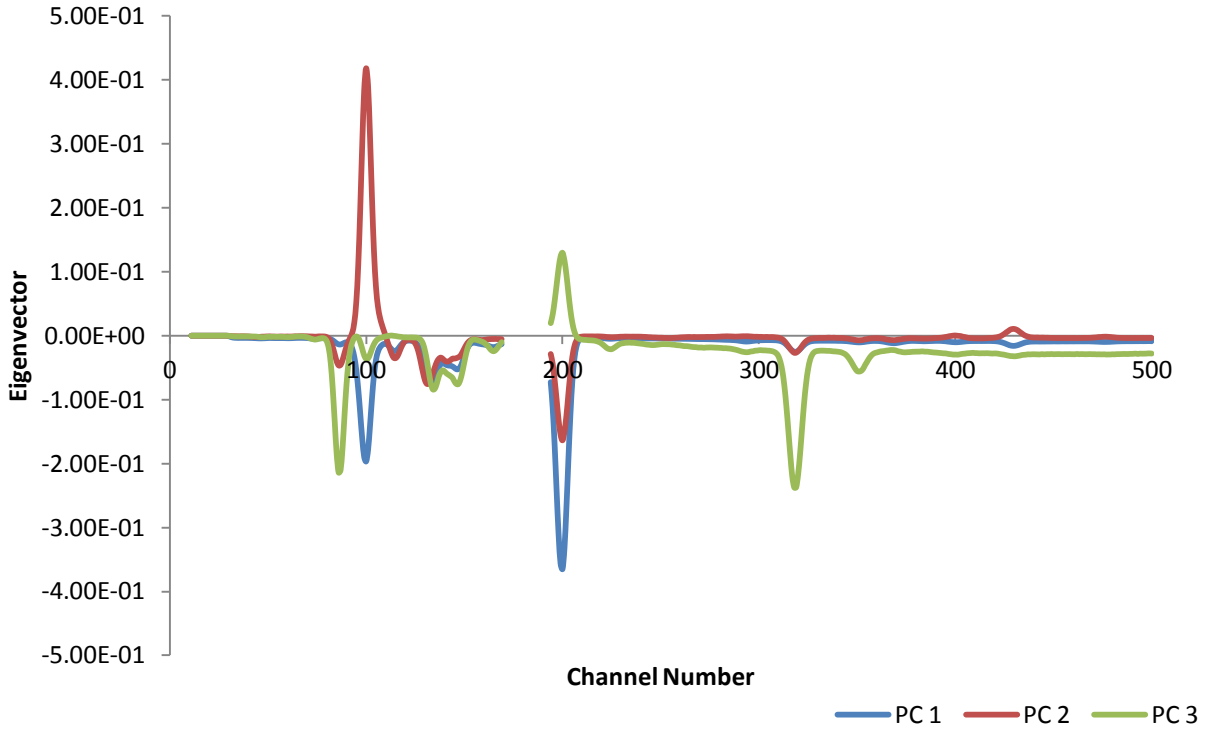

Figure 24: Eigenvectors of PCs 1-3 plotted (PC1 in blue, PC2 in red, PC3 in green) showing the factor loadings of the principal components. The gap in the graph indicates data that was removed (Ca K_α peak) during post-processing.

Discriminant Analysis

The scores from the first three principal components were modeled using linear and quadratic discriminant analysis (LDA and QDA), which allowed for classification of the spectra as "Bone" or "Non-Bone". The results of LDA and QDA are provided in Table 13 in the form of a confusion matrix, with the first column indicating the known class (B: Bone, NB: Non-Bone), and the column headings indicating the assigned class, total spectra, and percent correct classification (class and total). While the results for both LDA and QDA are offered, it was determined that since the covariances were unequal between the known classes (B and NB), QDA was a more reliable statistical test, as equal covariances are required for the use of LDA. Therefore, the QDA results of 94% are deemed more reliable than the LDA results.

Table 13: Confusion matrix showing results from LDA and QDA based on scores from three principal components.

	LDA				**QDA**			
	B	**NB**	**Total**	**% Correct**	**B**	**NB**	**Total**	**% Correct**
B	195	13	208	93.8	199	9	208	95.7
NB	28	126	154	81.8	12	142	154	92.2
Total	231	131	362	88.7	211	151	362	94.2

The results of QDA show high correct classification rates for both classes and overall. However, there are cases of misclassification for both groups, with bone spectra misclassifying approximately 4% of the time and non-bone misclassifying approximately 8% of the time. The misclassifications between the groups was determined by analyzing the Mahalanobis distances for the spectra following QDA. Mahalanobis distances are similar to the Euclidean distance (discussed previously), except it is dependent on the correlation between variables and

independent of the scale of the variables (Vamuza and Filzmoser, 2009). Using the Mahalanobis distances provided information regarding which spectra misclassified during the analysis. The Mahalanobis distances indicated that the non-bone spectra that misclassified during QDA were from synthetic hydroxyapatite (8) and rock apatite (4), while the bone spectra that misclassified were all human and consisted of: molar (2), premolar (2), canine (1), rib (2), burned fibula (1), and weathered metacarpal (1).

Scatterplot Matrices

Scatterplot matrices (SPLOMs) were used to visualize the discrimination between the different samples. The spectra were all plotted separately on the SPLOMs in order to identify outliers in the data, if necessary, and scores from the first three principal components were used for each plot. The data was first analyzed by grouping the spectra into bone and non-bone classes (Figure 25).

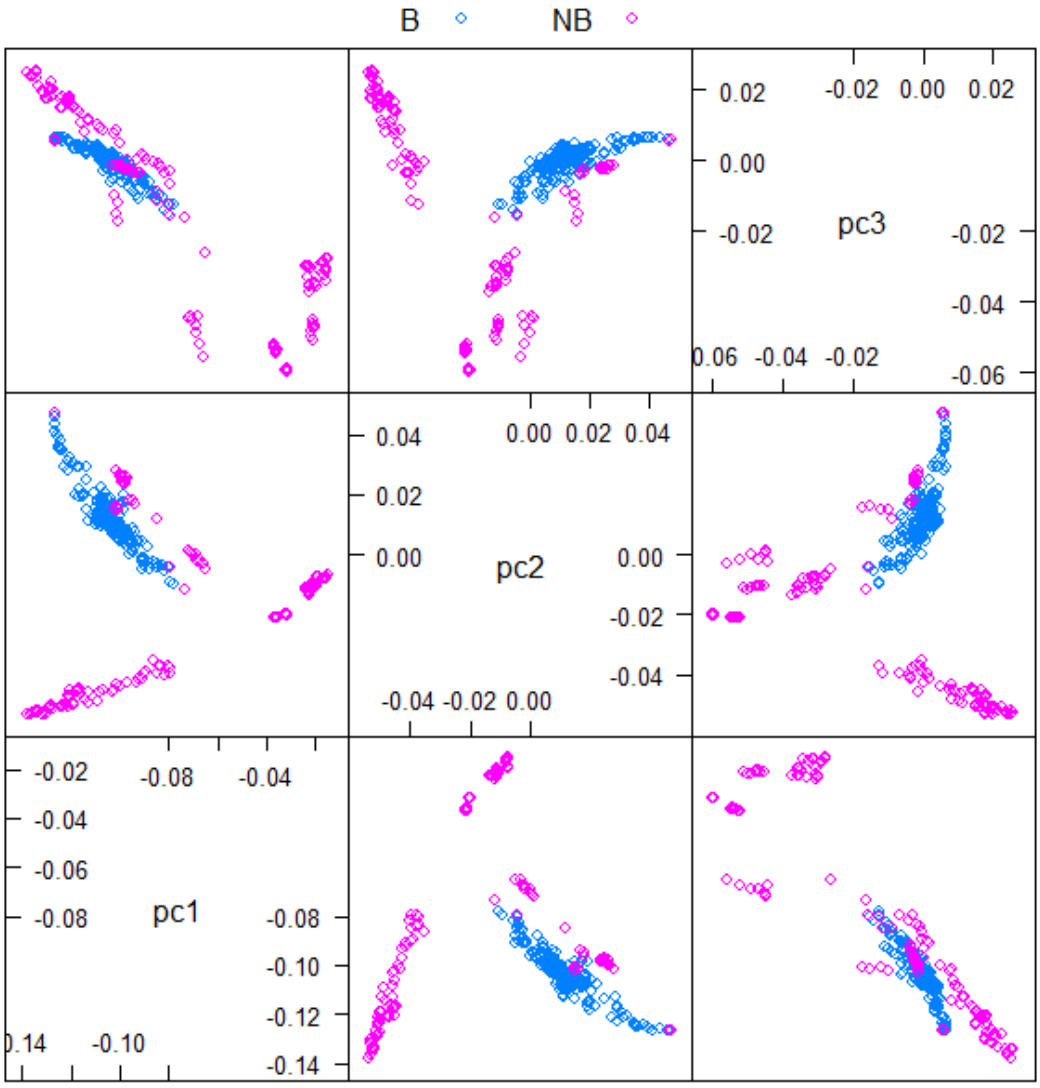

Figure 25: SPLOM of scores from the first three principal components with spectra separated into groups of bone (B) and non-bone (NB). The plots show distinct sample groups of B and NB, with some overlap between the spectra.

The SPLOM shows distinct groups of bone and non-bone in the plots, with some overlap between the spectra in each. This is expected as some materials included in the analysis, such as rock apatite, ivory, octocoral and synthetic hydroxyapatite, have a chemical composition more similar to bone than others. There are also distinct groups of non-bone samples within the larger

group, some of which are more similar to bone than others. In order to further analyze the non-bone groups and their overlap with the bone spectra, the non-bone group was split into several smaller groups (Figure 26). This SPLOM showed overlap between bone and rock apatite, bone and ivory, and bone and synthetic hydroxyapatite.

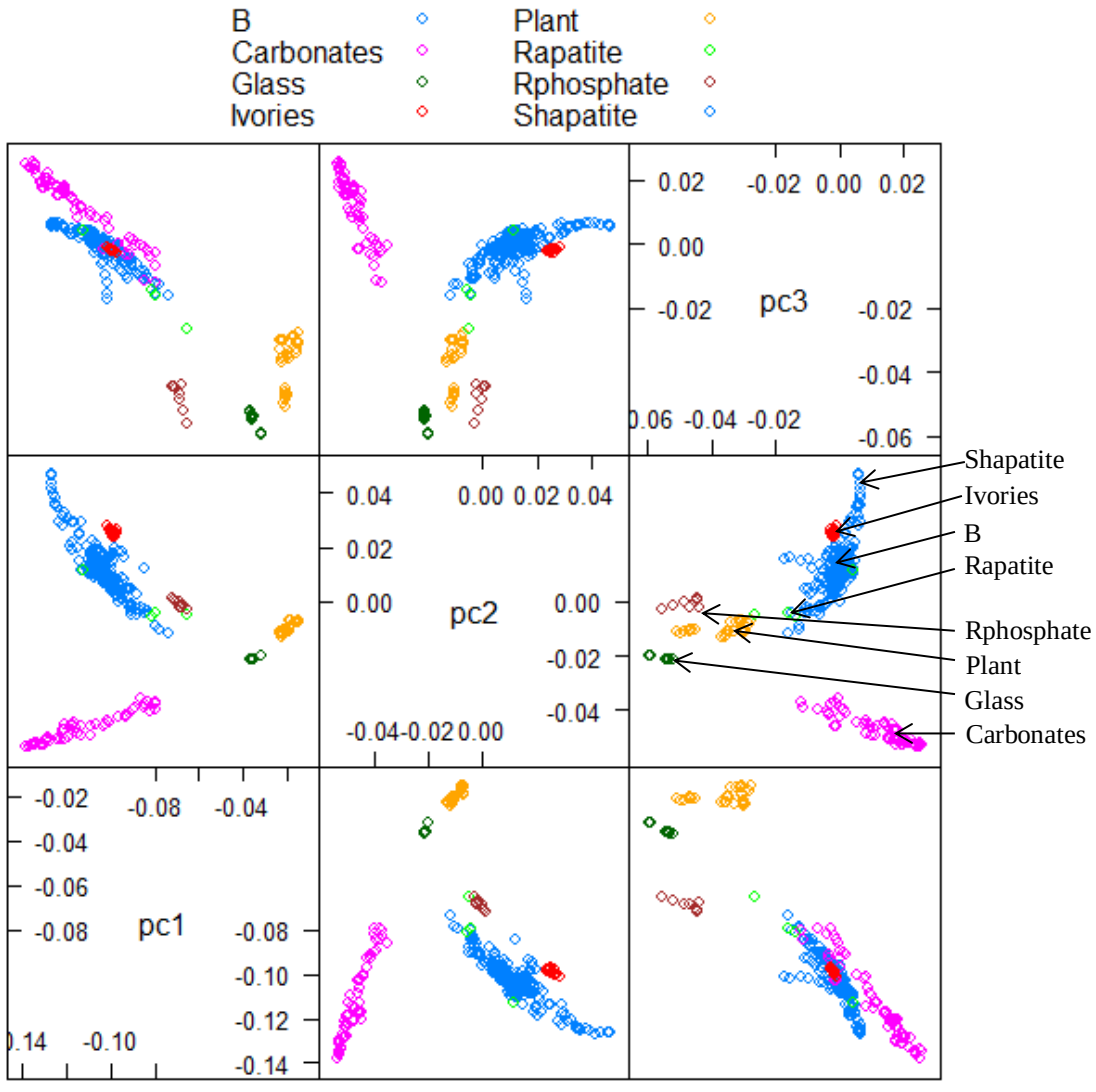

Figure 26: Scatterplot matrix of scores from the first three principal components showing overlap between bone and rock apatite, bone and ivory, and bone and synthetic hydroxyapatite.

In order examine the overlap between the bone spectra and the spectra of ivory, synthetic hydroxyapatite and rock apatite, the bone group was separated into human and nonhuman (Figure 27). This allowed for visualization of the overlap in terms of whether these materials were more similar to human or nonhuman bone. The SPLOM shows that these materials are more similar to human bone than nonhuman bone, as indicated by the overlap with human spectra in the plots.

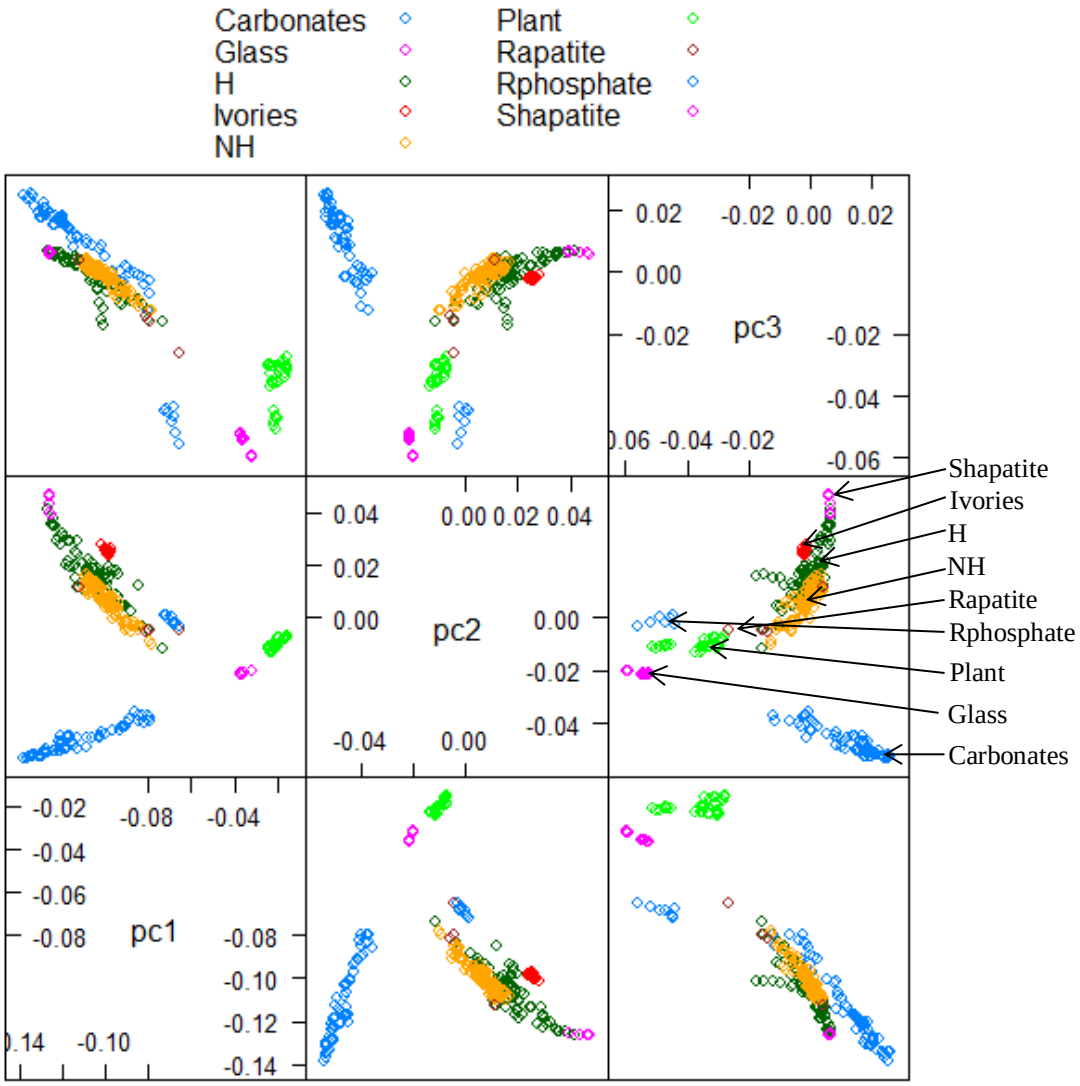

Figure 27: Scatterplot matrix of scores from the first three principal components showing overlap between human (H) and nonhuman (NH) bone spectra and spectra from ivory, synthetic hydroxyapatite (Shapatite) and rock apatite (Rapatite).

The groupings of the spectra were further modified in order to examine the overlap between the taphonomically modified bone and non-bone materials and the other groups (Figure 28). The SPLOM shows that burned, weathered and juvenile/archaeological human bone groups with human bone, and burned teeth group with burned human bone. Additionally, the SPLOM shows that burned plant matter groups with non-bone material. This indicates that taphonomy does not alter the elemental composition of the material as detected by the HHXRF, thus allowing for discrimination even when it has been subjected to taphonomic alteration(s).

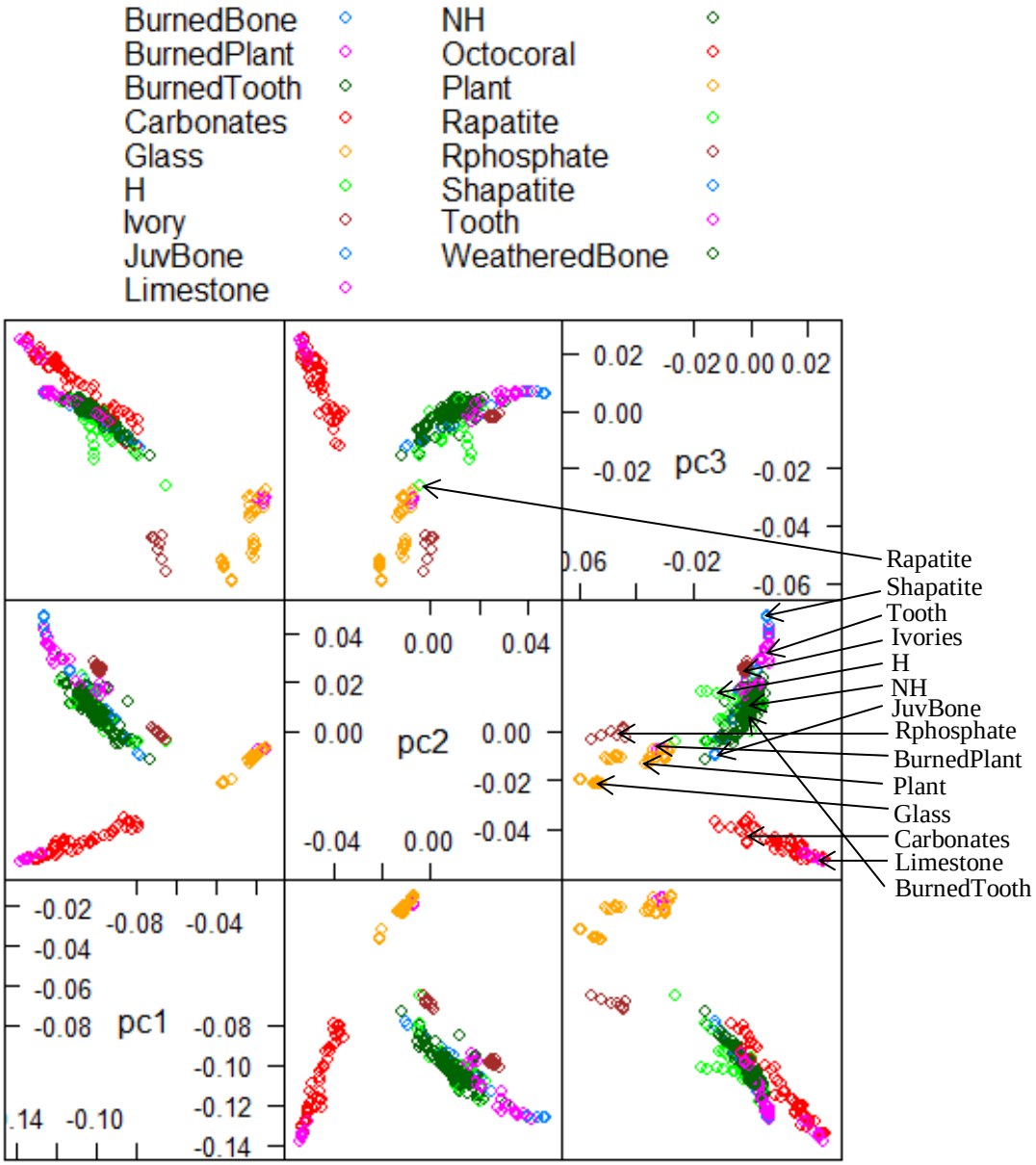

Figure 28: Scatterplot matrix of scores from the first three principal components examining overlap of taphonomically modified specimens. The plots show that burned, weathered and juvenile/archaeological human bone (JuvBone) groups with human bone; burned teeth group with human bone; and burned plant matter groups with non-bone material, specifically with other plant material.

It is also necessary to examine the location of tooth spectra in relation to bone and non-bone specimens since 5 tooth spectra misclassified during QDA (2 molar, 2 premolar, and 1 canine). The same SPLOM examined previously was re-categorized to emphasize the location of tooth spectra (Figure 29). The SPLOM shows overlap between human tooth spectra and spectra from other groups of specimens. Specifically, the plots show that human tooth overlaps with nonhuman bone, human bone, burned human tooth, and synthetic hydroxyapatite. Additionally, the plots show that the tooth spectra are in close proximity to ivory spectra, but do not appear to overlap in any plots. This indicates that the tooth spectra that misclassified may have been those located closest to the ivory spectra, as ivory was considered (and correctly classified as) a non-bone specimen. It is unclear from the analysis whether the spectra that misclassified were collected from the enamel, dentin or cementum area of the tooth, as the spectra were analyzed collectively from each tooth rather than differentiated by location of data collection on the tooth.

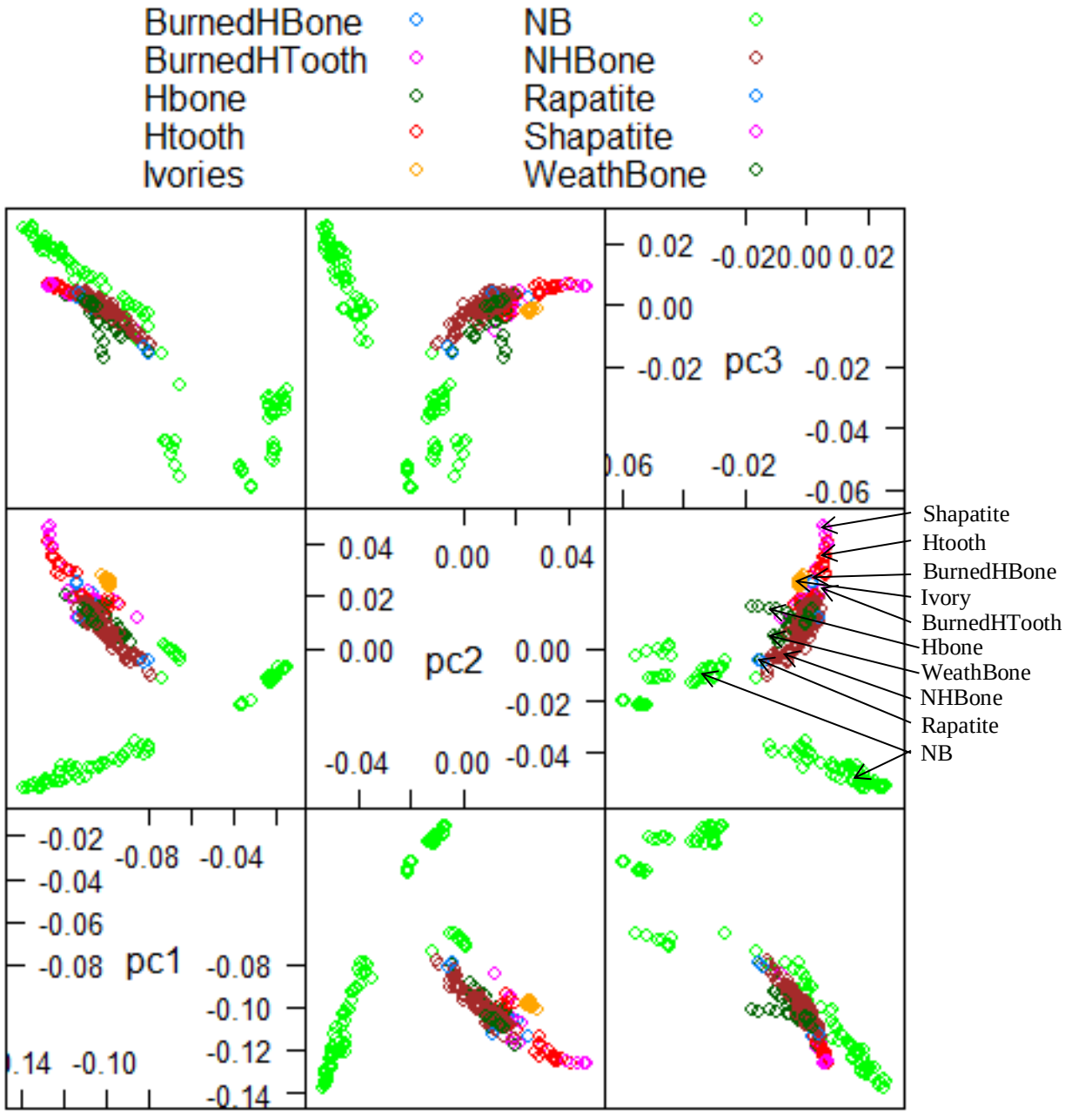

Figure 29: Scatterplot matrix of scores from the first three principal components examining overlap between human tooth spectra and spectra from all other specimens. The plots show that human tooth (Htooth, shown in light red) overlaps with nonhuman bone (NHBone, dark red), human bone (Hbone, dark green), burned human tooth (BurnedHTooth, pink), and synthetic hydroxyapatite (Shapatite, pink).

Ca/P Detection Test

The prepared synthetic hydroxyapatite and calcium carbonate samples were analyzed using the HHXRF to test the reliability of the instrument in detecting Ca and P without the use of a vacuum attachment. The information of specific interest was the ratio of the Ca K_β band at 4.013 keV to the P K_α band at 2.014 keV for these samples (Table 14). The molar ratio of Ca/P for these prepared materials is also shown in Table 14, and ranges from 1.67 to 3.36. A plot of the ratios as detected by the HHXRF against the molar ratios of the prepared materials shows that they are directly proportional (Figure 30). This indicates that the HHXRF unit is reliably detecting low mass elements.

Table 14: Molar and experimental ratios of Ca and P used to analyze the ability of the HHXRF to reliably detect low mass elements.

Molar Ratio	**Peak Height**		**Experimental Ratio**
Ca/P	**Ca K_β (4.013 keV)**	**P K_α (2.014 keV)**	**Ca K_β/ P K_α**
1.67	26460	27922	0.948
1.67b	25051	26497	0.945
1.67c	26447	27755	0.953
2.18	26263	17645	1.488
2.18b	26011	17647	1.474
2.18c	25758	17413	1.479
3.36	25348	11192	2.265
3.36b	25649	11493	2.232
3.36c	25920	11354	2.283

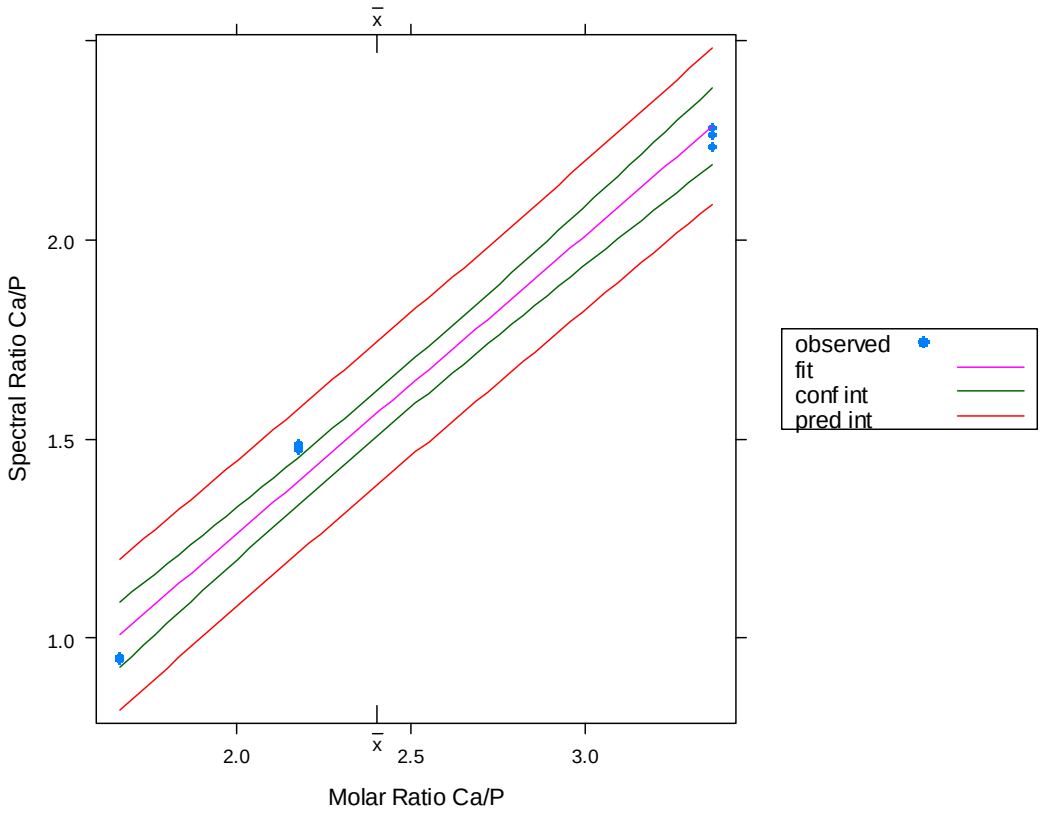

Figure 30: The ratio of the spectral intensity of the Ca K_β peak at 4.013 keV and P K_α peak at 2.014 keV (as measured by the HHXRF) plotted against the molar ratio of Ca/P of prepared materials. The 95% confidence (green) and prediction (red) intervals are provided.

A line of best fit for the graph provides the following equation (Equation 7), which can be used to calculate the average Ca K_β/P K_α ratio for the four major groups of samples analyzed during the Accuracy Test (the samples from the "Taphonomically Modified" group were placed in their respective groups; for example, burned plant matter grouped with the non-biological samples) (Table 15).

$$y = 0.1969x + 0.5784 \quad (7)$$

The average molar ratios obtained for the four classes using Equation 7 show between-class variation, most notably between the bone (H and NH) and non-bone (OB and NB) groups. The average molar ratios for the H and NH groups are relatively dissimilar considering the low spectral ratio standard deviation for both groups. In contrast, the OB and NB groups have distinct differences in their average molar ratios accompanied by large a spectral ratio standard deviation for both groups.

Table 15: Average spectral and molar ratios (Ca K_β/P K_α) for the four main classes of samples analyzed in the Accuracy Test

Class	Average Spectral Ratio Ca K_β/P K_α	Spectral Ratio Std. Dev.	Average Molar Ratio Ca K_β/P K_α*
NB	9.276692	7.919829	44.17619
OB	16.27738	8.675949	79.73075
H	1.362912	0.200728	3.984319
NH	1.555545	0.203278	4.962644

*Calculated using Equation 7

Cluster Analysis

Hierarchical clustering of the scores from the first three principal components using Euclidean distance and average linkage resulted in the dendrogram and associated heat map in Figure 31. The four clusters created by cutting the dendrograms on the red dashed line are composed of: (1) plant material (lower left); (2) glass (smallest cluster); (3) rock phosphate, rock apatite, bone (including teeth), ivory, and synthetic hydroxyapatite; (4) shells, coral, limestone. Cutting the dendrogram on the blue dashed line results in an additional sub-cluster comprised of synthetic hydroxyapatite and teeth. Cluster 4 is split into two sub-clusters, one comprised of assorted shells and coral and the second comprised of shells and limestone.

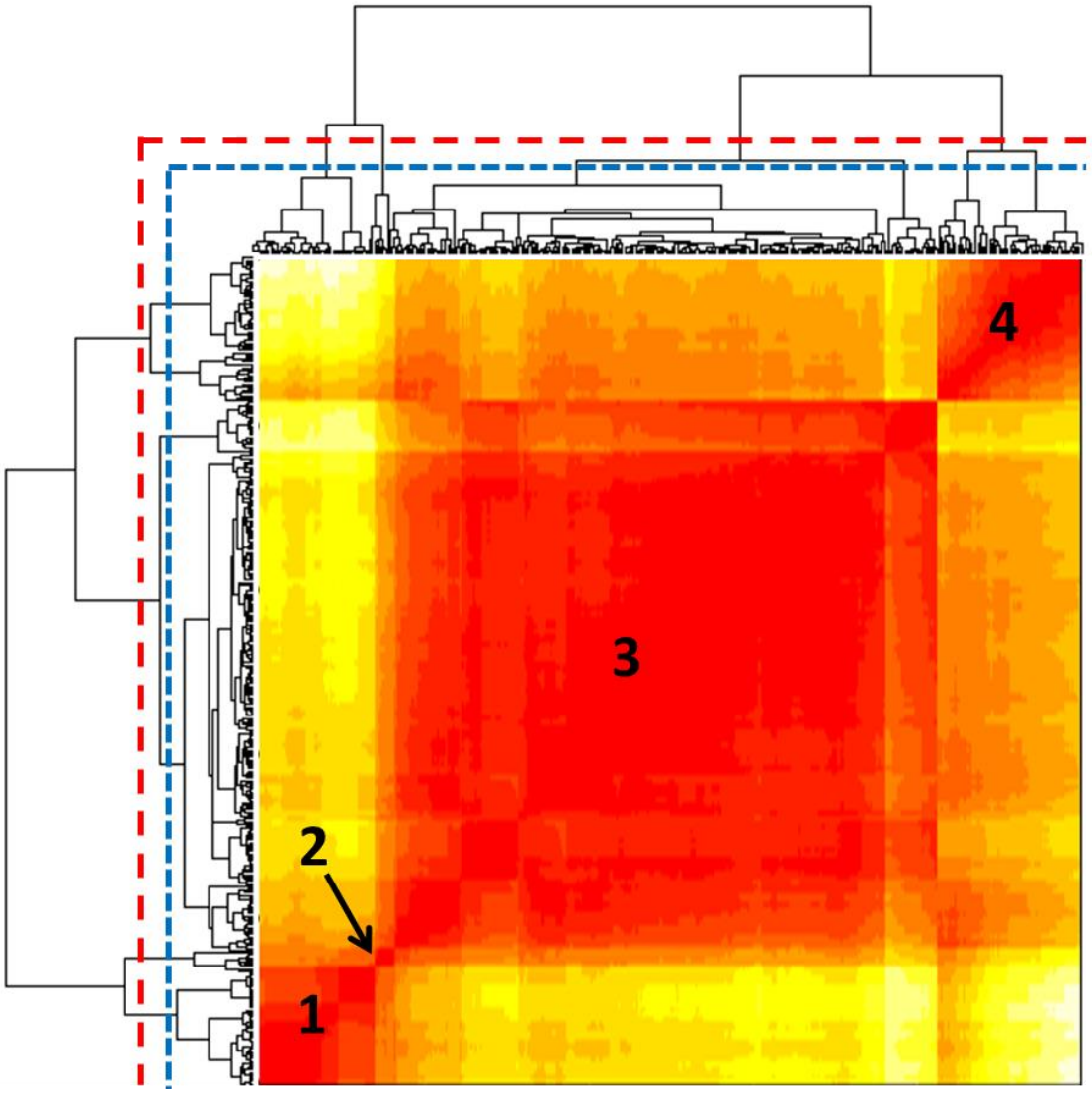

Figure 31: Dendrogram and associated heat map resulting from hierarchical cluster analysis using scores from the first three principal components.(1) plant material; (2) glass; (3) rock phosphate, rock apatite, bone (including teeth), ivory, synthetic hydroxyapatite; (4) shells, coral, limestone.

Summary

Results of the QDA (Table 13) showed 94% average discrimination between bone and non-bone samples when scores from three principal components were used; 4% of bone spectra misclassified as non-bone and 8% of non-bone misclassified as bone. The non-bone spectra that misclassified during QDA were from synthetic hydroxyapatite and rock apatite, both groups that show overlap in the scatterplots in Figures 25-29. While ivory shows overlap in some scatterplots, it is still discriminated from bone samples during QDA. The results also show that taphonomy does not influence the method. The bone spectra that misclassified were 2 molar, 2 premolar, 1 canine, 2 rib, 1 burned fibula, and 1 weathered metacarpal, indicating that these samples required further examination before exclusion. Since eight spectra were analyzed separately from each sample, it is possible that the spectra that misclassified represented outliers from the represented samples, which is why further analysis of the represented samples is necessary.

CHAPTER SIX: DISCUSSION

The use of elemental analysis in forensic anthropology is limited, and while several techniques have been proposed for different aspects of forensic anthropological analysis (sorting bone and non-bone material, distinguishing human bone/teeth from nonhuman remains, etc.), they have failed to gain enough momentum to become standard methods in the field. This is unfortunate, as there are many benefits to the elemental analytical techniques that have been proposed (XRF, Raman spectroscopy, LIBS), including little to no sample destruction and little to no sample preparation. Many of the elemental analytical techniques that have been proposed for use in forensic anthropology (for example, those using Raman spectroscopy and XRF spectrometry) also rely on statistical methods. This is especially useful for standardizing these techniques for use in court, as they have the ability to provide error rates as required under the Daubert standard (*Daubert v. Merrell Dow Pharmaceuticals, Inc.*, 1993). This emphasizes the need for further study of elemental analysis in forensic anthropology, most notably in the establishment of a standardized method for data collection and analysis, which is the purpose of this research, specifically in regards to using elemental analysis to distinguish bone and teeth from non-bone materials.

Recently, Christensen et al. (2012) proposed a successful method regarding the use of XRF as an analytical tool for distinguishing human bone fragments from non-bone material in forensic anthropology. However, to date, no methods have been proposed using HHXRF for fragment discrimination in forensic anthropology, despite the low-cost and ease of use of this instrument. Due to these benefits, HHXRF was chosen for this research, and methods were

devised to apply the technique to forensic anthropology using the study by Christensen et al. (2012) as a model. The devised method involved two phases, prompting the research to be conducted in phases. The first phase of the research tested the reliability of the HHXRF and involved sampling a single human femur in several locations along the bone with multiple replications of each site. The second phase of the research tested the accuracy of the method in distinguishing bone/teeth from non-bone material. This involved sampling a large dataset consisting of human bone/teeth, nonhuman bone, other biological materials and non-biological materials and using multivariate statistical analyses to sort the materials.

The results of the reliability test indicate that the HHXRF can reliably detect the elements found on the surface of a single human long bone. The results also show that some areas of a human long bone are more problematic than others for data collection (Figures 14 and 19), specifically roughened areas of the bone where muscles attach (Figure 11). This is consistent with the findings by Christensen et al. (2012:48) recommending that "flat, polished surface[s]" of the bone are the most appropriate for data collection using XRF spectrometry. This also indicates that, whenever possible, these areas should be avoided when collecting spectral data using the HHXRF.

The results of the accuracy test indicate that osseous and dental tissue can be distinguished from non-bone material of similar chemical composition with a high degree of accuracy when data is collected from several locations on a sample and analyzed separately during statistical analyses. This method cannot currently distinguish all non-bone materials from bone with a similar Ca/P ratio, as in the case of synthetic hydroxyapatite and rock apatite.

However, bone was distinguished from other materials of similar chemical composition including ivory and octocoral, which other methods focusing on the use of Ca/P had difficulty discriminating from bone (Ubelaker et al., 2002; Christensen et al., 2012). Synthetic hydroxyapatite or synthetic bone is a material manufactured for implantation in the human body, either for adhering larger implantation devices (such as knee or hip implants) (Cook et al., 1988) or acting as the implanted device (such as in cases of plastic surgery) (Jordan et al., 1998). For this reason, synthetic hydroxyapatite has a chemical composition similar to bone, even down to the trace elements found in bone, indicating that this material would be very difficult to distinguish from bone using elemental analysis. However, as suggested by Christensen et al. (2012) it is not likely that this material would be found in isolation and require sorting from bone/teeth in a forensic setting. Additionally, if it were found in a forensic setting, it is likely that it would be associated with human remains in the context of implanted material.

The results of the Accuracy Test (Table 13) also showed high (96%) correct classification specifically for bone, which is necessary to prevent false exclusion of bone material. It is important to note that while 96% of bone spectra classified correctly during QDA, a small percentage of bone spectra (4%) misclassified as non-bone material, possibly due to surface contamination or collecting the spectra on an irregular surface. Additionally, while not as problematic as bone misclassifying as non-bone material, it also important to note that 8% of non-bone spectra misclassified as bone during QDA. The samples corresponding to the spectra that misclassified in both cases were subjected to individual examination in order to avoid false exclusion (of bone material) and false inclusion (of non-bone material). Individual examination of the misclassifying bone spectra showed that in each case, only 1-2 out of the 8 total spectra

collected for each sample had misclassified, indicating that a majority of the spectra had classified correctly. It was determined that the misclassifying spectra were likely outliers in these cases, and not representative of the majority of spectra collected from the sample. Subsequently, the samples were classified into the category ("Bone" or "Non-Bone") to which the majority of the spectra classified. Individual examination of the misclassifying non-bone spectra showed that the discrimination of synthetic hydroxyapatite from bone/teeth spectra was not likely even with further analysis, due to all spectra from the sample misclassifying as bone. Individual examination of the rock apatite spectra, from which 4 out of the 8 total spectra had misclassified as bone indicated that further data collection from the sample was necessary for discrimination.

Based on the procedure above, the method was expanded into a two-step approach; this is recommended in order to ensure maximum correct classification of materials and avoid false exclusion of materials. In this two-step approach, the first step involves following the methods as outlined in detail in the Methods chapter, including collecting spectra from several locations and analyzing spectra separately during statistical analyses. The second step involves individually analyzing the samples that had misclassifying spectra during QDA, and classifying these based on the class to which the majority of the spectra from the sample classified, or analyzing the sample further if this is not possible.

The Accuracy Test results were also positive in demonstrating that taphonomic modifications do not inhibit correct classification of materials (Figure 28). This indicates that the taphonomic factors included in this study (weathering, burning, and antiquity) do not

compromise the chemical composition of the bone, tooth, or other material. Regarding the burned bone/teeth included in this research, it is important to note that burning did not alter the chemical composition of the bone/teeth to the point where they grouped with non-bone materials, for example, rock phosphate or the carbonates included in the study. Rather, these specimens maintained a chemical composition consistent with the other bones and teeth examined in the study. This is relevant to studies regarding cremains, in which researchers are often attempting to determine the authenticity of the cremains in terms of whether or not the remains represent skeletal material. For example, a variety of analytical methods have been successfully used to sort legitimate cremains from those of questionable origin using elemental analysis (Kravchenko et al., 2001; Warren et al., 2002; Brooks et al., 2006; Schultz et al., 2008). The results of this study indicate that the use of HHXRF may be appropriate for assessing the legitimacy of cremains.

As demonstrated, the results, overall, were very positive, indicating that HHXRF can reliably detect the elements found on the surface of a single human long bone, and that elements detected in bone/teeth could be used to reliably discriminate non-bone materials due to their differing elemental composition. However, it was not possible to further discriminate the bone/teeth group into groups of human and nonhuman using the elements detected. Research has indicated that elemental analysis coupled with multivariate statistical analysis allows for discrimination of human and nonhuman bone (McLaughlin and Lednev, 2012), and further discrimination of the nonhuman bone into separate species (McLaughlin and Lednev, 2012; Brody et al., 2001; Edwards et al., 2006; Shimoyama et al., 1997; Vass et al., 2005) due to differences in chemical composition at the trace element level. However, there was significant

overlap in the bone spectra examined this study (Figures 25-29), preventing additional discrimination of the bone group into human and nonhuman classes.

There are some limitations to this research, in terms of sample size and the specimens chosen for analysis. While the sample size is adequate (for all sample types) it could always be expanded. For example, other bones from the human skeleton could be added, such as vertebrae, carpals/tarsals, and additional cranial bones (sphenoid, ethmoid, maxilla), as these were not presented in the dataset examined in this study. Additionally, other nonhuman bones should be examined since only femora were the focus of this study; it would be most beneficial to examine all comparative elements from the nonhuman skeleton relative to the human elements examined in the study. Furthermore, any other non-bone materials that forensic anthropologists have encountered in their work and found themselves unable to distinguish from human bone should be added, such as the brachiopod shells mentioned by Christensen et al. (2012). Additionally, while this analysis includes burned materials in the dataset, the focus is not on distinguishing burned bone and dental material from other burned materials, and thus is likely to not be comprehensive in this aspect (especially in terms of fragmentary analysis). The dataset is also limited in terms of its analysis of juvenile remains, which can be problematic for forensic anthropologists; the sample could be expanded to include additional juvenile elements, namely unfused epiphyses.

CHAPTER SEVEN: CONCLUSIONS AND FUTURE WORK

The combination of an HHXRF analysis with multivariate statistical analysis shows promise for discriminating fragmentary osseous and dental tissue from other types of biologic and non-biologic material. This method focuses on the major and trace elements detected in the spectrum rather than limiting the analysis to a comparison of the Ca/P ratio, which was the method undertaken in earlier studies (Ubelaker et al., 2002; Christensen et al., 2012). The trace element analysis is accomplished by removing the dominating Ca peak from the spectra (Ca K_{α} peak), normalizing the remaining data, and performing PCA. Discriminant analysis using the scores of the PCA is then used to distinguish bone from non-bone samples. Furthermore, while existing chemical methods have had difficulty distinguishing non-bone with similar chemical composition to bone as reflected in a similar Ca/P ratio (Ubelaker et al., 2002; Christensen et al., 2012), this method could distinguish bone from ivory and octocoral.

The laboratory techniques typically used in forensic anthropology to identify questionable remains as (1) bone, and as (2) human or nonhuman bone, include histology (Chamberlain, 1994; Ubelaker, 1989; Mulhern and Ubelaker, 2001; Cattaneo et al., 1999; Urbanova and Novotny, 2005) and protein analysis (Lowenstein, 1980); Cattaneo et al., 1992a, 1992b, 1994, 1995; Ubelaker et al., 2004). Analytical techniques have also been proposed for the purposes of discriminating bone/teeth from non-bone material (Ubelaker et al., 2002; Christensen et al., 2012) and human from nonhuman skeletal material (McLaughlin and Lednev, 2012; Brody et al., 2001; Edwards et al., 2006; Shimoyama et al., 1997; Vass et al., 2005), however, elemental analysis is not typically available in forensic anthropology labs, as most

cases only require gross or microscopic examination of the bone. This is likely why forensic anthropologists tend to rely on histological techniques – the instruments needed (microscopes) are already available. Nevertheless, the main advantage to developing a technique using HHXRF is the feasibility for integration of this method into a forensic anthropology lab due to the relatively low cost of the instrument compared to other analytical instruments, as well as the device's relative ease of use.

In addition to being used for identifying fragments of forensic significance (as proposed by this research), HHXRF can be integrated into other aspects of the forensic analysis. For example, research was recently presented regarding the use of portable XRF to detect transfer metal (copper) on cut bone in dismemberment cases (Williams, 2012). In a controlled research experiment, portable XRF detected trace amounts of copper on cut bone samples 77.4% of the time, and 0% of the time in uncut samples (control). Based on detection percentages, the researchers determined copper was directly transferred to the bone in high enough trace amounts that the portable XRF was able to clearly detect it in the sample (Williams, 2012), supporting the notion that elemental analysis, namely portable or HHXRF, is becoming more commonplace in forensic anthropology, and is likely to increase in use in the future.

Additionally, the research proposed here has broader implications, most specifically to the application of this method to other areas of anthropology. As previously mentioned, handheld or portable XRF is already used in other areas of anthropology, such as archaeology, in the sourcing or provenancing of ceramics (Liritzis et al. 2002, 2007; Liritzis 2005; Mantzourani and Liritzis, 2006; Papadopoulou et al., 2006; Papageorgiou and Liritzis, 2007), metals (Ferretti

et al., 1997; Ferretti and Moioli, 1998) and lithics (Williams-Thorpe, 1995; Williams-Thorpe et al., 1999; Pappalardo et al., 2003; De Francesco et al., 2007; Phillips and Speakman, 2009; Frahm et al., 2013). Additionally, HHXRF was used in bioarchaeology in the analysis of bog bodies, natural mummies that formed in peat bogs under limited oxygen supply, in order to understand how burial practice may have aided in the preservation of these individuals (Granite, 2012). While HHXRF has only been narrowly used in bioarchaeology/physical anthropology thus far, other types of elemental analysis (laser induced breakdown spectroscopy (LIBS), inductively coupled plasma mass spectrometry (ICP-MS), laser ablation (LA-ICP-MS), and XRF) have been proposed for use in studying diet and lifestyle of passed populations of individuals (Samek et al., 2001; Kasem et al., 2011; Alvira et al., 2010; Djingova et al., 2004; Castro et al., 2010; Webb et al., 2005; Wessen et al., 1978; Mantler & Schreiner, 2000; Carvalho et al., 2004). This indicates that HHXRF may be applicable for use in bioarchaeology as a replacement for these other elemental analytical techniques since HHXRF is a nondestructive, less expensive alternative that can also be used in the field. The field portability of this instrument would also allow for collaboration during archaeological field work between archaeologists, physical anthropologists and bioarchaeologists. A single HHXRF could be used by all researchers to quickly collect data on ceramics, lithics, metals, bone, burial artifacts and other items, allowing the artifacts to stay and be curated in the country in which the research is being conducted.

Further refinement of this research may lead to an initial sorting method for the forensic anthropologist when implemented as a two-step approach for discriminating fragments of unknown composition from dental and osseous material. In this two-step approach, the first step

includes collecting and analyzing the spectra using the methods detailed previously (spectra collected from several locations and analyzed separately during statistical analyses). In the second step, samples that had misclassifying spectra should be analyzed individually before exclusion, to check that misclassifications were not the results outlier spectra; this ensures that a single spectrum does not determine the outcome of an entire sample. It is recommended that spectra from a single specimen that classify into two different groups be classified into the group to which the majority of the spectra classify. For example, if 1-2 spectra from a bone sample misclassify as non-bone, but 6 or more classify as bone, the sample should be considered a bone specimen, and the misclassifying spectra should be treated as outliers.

This technique can be particularly useful as an initial sorting method (human bone and teeth from non-bone material) involving mass fatalities when human remains have undergone extreme fragmentation. For example, mass disasters such as airline crashes, the September 2001 terrorist attacks and Hurricane Katrina, may result in fragmentary human remains that have been subjected to any number or taphonomic processes that include burning, animal scavenging and weathering (Sledzik et al., 2009; Dirkmaat, 2012). This results in skeletal material that is difficult to identify as bone, especially in the case of the World Trade Center attacks, as the skeletal material was significantly burned, highly fragmented, and resembled the building debris (Sledzik et al., 2009). In these cases, this technique would be useful as the initial step in quickly identifying questionable material as bone or non-bone. Once questionable material is identified as bone, it can be further analyzed using histological or biochemical methods (i.e., DNA) to determine if the bone is human, and to make an identification if DNA is present.

Future work should explore the application of this method to fragmentary and cremation analysis. The sample size should also be expanded to incorporate additional bones from the human skeleton, bones from additional nonhuman species, bones subjected to different taphonomic processes, and other non-bone materials that forensic anthropologists may encounter. Additionally, work should include blind testing focusing on fragmentary remains and non-bone materials.

APPENDIX A: PERIODIC TABLE OF THE ELEMENTS

Number	Atomic Weight	Name	Symbol	Group (by column)
1	1.0079	Hydrogen	H	1
2	4.0026	Helium	He	18
3	6.941	Lithium	Li	1
4	9.0122	Beryllium	Be	2
5	10.811	Boron	B	13
6	12.0107	Carbon	C	14
7	14.0067	Nitrogen	N	15
8	15.9994	Oxygen	O	16
9	18.9984	Fluorine	F	17
10	20.1797	Neon	Ne	18
11	22.9897	Sodium	Na	1
12	24.305	Magnesium	Mg	2
13	26.9815	Aluminum	Al	13
14	28.0855	Silicon	Si	14
15	30.9738	Phosphorus	P	15
16	32.065	Sulfur	S	16
17	35.453	Chlorine	Cl	17
18	39.948	Argon	Ar	18
19	39.0983	Potassium	K	1
20	40.078	Calcium	Ca	2
21	44.9559	Scandium	Sc	3
22	47.867	Titanium	Ti	4
23	50.9415	Vanadium	V	5
24	51.9961	Chromium	Cr	6
25	54.938	Manganese	Mn	7
26	55.845	Iron	Fe	8
27	58.9332	Cobalt	Co	9
28	58.6934	Nickel	Ni	10
29	63.546	Copper	Cu	11
30	65.39	Zinc	Zn	12
31	69.723	Gallium	Ga	13
32	72.64	Germanium	Ge	14
33	74.9216	Arsenic	As	15
34	78.96	Selenium	Se	16
35	79.904	Bromine	Br	17
36	83.8	Krypton	Kr	18
37	85.4678	Rubidium	Rb	1
38	87.62	Strontium	Sr	2

Number	Atomic Weight	Name	Symbol	Group (by column)
39	88.9059	Yttrium	Y	3
40	91.224	Zirconium	Zr	4
41	92.9064	Niobium	Nb	5
42	95.94	Molybdenum	Mo	6
43	98	Technetium	Tc	7
44	101.07	Ruthenium	Ru	8
45	102.9055	Rhodium	Rh	9
46	106.42	Palladium	Pd	10
47	107.8682	Silver	Ag	11
48	112.411	Cadmium	Cd	12
49	114.818	Indium	In	13
50	118.71	Tin	Sn	14
51	121.76	Antimony	Sb	15
52	127.6	Tellurium	Te	16
53	126.9045	Iodine	I	17
54	131.293	Xenon	Xe	18
55	132.9055	Cesium	Cs	1
56	137.327	Barium	Ba	2
57	138.9055	Lanthanum	La	3
58	140.116	Cerium	Ce	101
59	140.9077	Praseodymium	Pr	101
60	144.24	Neodymium	Nd	101
61	145	Promethium	Pm	101
62	150.36	Samarium	Sm	101
63	151.964	Europium	Eu	101
64	157.25	Gadolinium	Gd	101
65	158.9253	Terbium	Tb	101
66	162.5	Dysprosium	Dy	101
67	164.9303	Holmium	Ho	101
68	167.259	Erbium	Er	101
69	168.9342	Thulium	Tm	101
70	173.04	Ytterbium	Yb	101
71	174.967	Lutetium	Lu	101
72	178.49	Hafnium	Hf	4
73	180.9479	Tantalum	Ta	5
74	183.84	Tungsten	W	6
75	186.207	Rhenium	Re	7
76	190.23	Osmium	Os	8

Number	Atomic Weight	Name	Symbol	Group (by column)
77	192.217	Iridium	Ir	9
78	195.078	Platinum	Pt	10
79	196.9665	Gold	Au	11
80	200.59	Mercury	Hg	12
81	204.3833	Thallium	Tl	13
82	207.2	Lead	Pb	14
83	208.9804	Bismuth	Bi	15
84	209	Polonium	Po	16
85	210	Astatine	At	17
86	222	Radon	Rn	18
87	223	Francium	Fr	1
88	226	Radium	Ra	2
89	227	Actinium	Ac	3
90	232.0381	Thorium	Th	102
91	231.0359	Protactinium	Pa	102
92	238.0289	Uranium	U	102
93	237	Neptunium	Np	102
94	244	Plutonium	Pu	102
95	243	Americium	Am	102
96	247	Curium	Cm	102
97	247	Berkelium	Bk	102
98	251	Californium	Cf	102
99	252	Einsteinium	Es	102
100	257	Fermium	Fm	102
101	258	Mendelevium	Md	102
102	259	Nobelium	No	102
103	262	Lawrencium	Lr	102
104	261	Rutherfordium	Rf	4
105	262	Dubnium	Db	5
106	266	Seaborgium	Sg	6
107	264	Bohrium	Bh	7
108	277	Hassium	Hs	8
109	268	Meitnerium	Mt	9

APPENDIX B: RECORDED DATA OF BONE SPECIMENS

File Location: _NCFS → 10012012 →60s_____

XRF Settings: Voltage: 15.00 kV Anode Current: 39.20 μA Pulse Length: 200 Filter: 2

Sample Type	Bone Element	Biological Age	Time Period	Taphonomic Modifications (if any)	File Name/ Sample Name	Specimen Notes
deer	antler	adult	modern	none	antler[1-8]-60sNH	Flat baseline
armadillo	femur	adult	modern	none	armadillo[1-8]-60sNH	Flat baseline
bird	femur	adult	modern	none	bird[1-8]-60sNH	Flat baseline
deer	femur	adult	modern	none	deer[1-8]-60sNH	Flat baseline
dog	femur	adult	modern	none	dog[1-8]-60sNH	Flat baseline
gator	femur	adult	modern	none	gator[1-8]-60sNH	Flat baseline
pig	femur	juvenile	modern	none	pig[1-8]-60sNH	Flat baseline
raccoon	femur	adult	modern	none	raccoon[1-8]-60sNH	Flat baseline
turkey	tarsometatarsus	adult	modern	none	turkey[1-8]-60sNH	Flat baseline
turtle	femur	adult	modern	none	turtle[1-8]-60sNH	Flat baseline
turtle	shell	adult	modern	none	turtleshell[1-8]-60sNH	Flat baseline
human	fibula	adult	modern	none	fibula[1-8]-60sH	Flat baseline
human	humerus	adult	modern	none	humerus[1-8]-60sH	Flat baseline
human	metacarpal	adult	modern	none	metacarpal[1-8]-60sH	Flat baseline
human	parietal	adult	modern	none	parietal[1-8]-60sH	Flat baseline
human	pedal phalanx	adult	modern	none	pedalphalanx[1-8]-60sH	Flat baseline
human	rib	adult	modern	none	rib[1-8]-60sH	Flat baseline
human	zygomatic	adult	modern	none	zygomatic[1-8]-60sH	Flat baseline

Sample Type	Bone Element	Biological Age	Time Period	Taphonomic Modifications (if any)	File Name/ Sample Name	Specimen Notes
human	canine	adult	modern	none	canine[1-8]-60sH	Flat baseline; 1-4 enamel, 5-8 dentine
human	premolar	adult	modern	none	premolar[1-8]-60sH	Flat baseline; 1-4 enamel, 5-8 dentine
human	molar	adult	modern	none	molar[1-8]-60sH	Flat baseline; 1-4 enamel, 5-8 dentine
human	fibula	adult	modern	burned	burnedfibula[1-8]-60sH	Flat baseline
human	femur	juvenile	ancient	ancient, dating to AD 50-450, from the Dakhleh Oasis, Egypt	juvfemur[1-8]-60sH	Flat baseline
human	metacarpal	adult	modern	weathered	weatheredMC[1-8]-60sH	Flat baseline
human	molar, lower	adult	modern	burned	burnedmolarL[1-8]-60sH	Flat baseline; 1-4 enamel, 5-8 dentine
human	molar, upper	adult	modern	burned	burnedmolarU[1-8]-60sH	Flat baseline; 1-4 enamel, 5-8 dentine

Other comments:

-All specimens analyzed for 60 seconds

-No specimens stood out as inconsistent

APPENDIX C: RECORDED DATA OF NON-BONE SPECIMENS

File Location: _NCFS → 10012012 →60s_____

XRF Settings: Voltage: 15.00 kV Anode Current: 39.20 μA Pulse Length: 200 Filter: 2

Sample Type	Material	Taphonomic Modifications (if any)	File Name/ Sample Name	Specimen Notes
Plant	stick	none	stick[1-8]-60sNB	Very irregular baseline (not flat)
Plant	bark	none	bark[1-8]-60sNB	Very irregular baseline
Plant	root	none	root[1-8]-60sNB	Irregular baseline (but better than stick and bark)
Glass	float glass	none	floatglass[1-8]-60sNB	Irregular baseline but better
Glass	beer bottle	none	beerbottle[1-8]-60sNB	Irregular baseline
Plant	seeds	none	acornseed[1-8]-60sNB	Erratic baseline
Limestone	limestone	none	limestone[1-8]-60sNB	Flat baseline
Synthetic hydroxyapatite	synthetic hydroxyapatite	none	synhydapatite[1-8]-60sNB	Flat baseline
Rock apatite	rock apatite	none	rockapatite[1-8]-60sNB	Flat baseline
Rock phosphate	rock phosphate	none	rockphosphate[1-8]-60sNB	Flat baseline
Shell	scallop	none	scallopshell[1-8]-60sOB	Flat baseline
Shell	clam	none	clamshell[1-8]-60sOB	Flat baseline
Shell	oyster	none	oystershell[1-8]-60sOB	Flat baseline
Shell	sand dollar	none	sanddollar[1-8]-60sOB	Flat baseline
Shell	starfish	none	starfish[1-8]-60sOB	Flat baseline
Coral	coral	none	coral[1-8]-60sOB	Flat baseline
Coral	octocoral	none	octocoral[1-8]-60sOB	Flat baseline
Spur	spur	none	spur[1-8]-60sOB	Very irregular baseline
Ivory	rounded ivory	none	ivoryround[1-8]-60sOB	Flat baseline

Sample Type	Material	Taphonomic Modifications (if any)	File Name/ Sample Name	Specimen Notes
Ivory	flat ivory	none	ivoryflat[1-8]-60sOB	Flat baseline
Plant	wood	burned	burnedwood[1-8]-60sNB	Erratic baseline
Plastic	plastic	burned	burnedplastic[1-8]-60sNB	Irregular baseline but better than burned wood

Other comments:

-All specimens analyzed for 60 seconds

-Plant materials stood out as inconsistent (irregular baselines) possibly due to soil present on specimens

APPENDIX D: REPRESENTATIVE SPECTRA

Human Spectra: shown below is the first spectrum collected from each human bone sample. The spectrum is shown with the elements identified (autoidentified using ARTAX software).

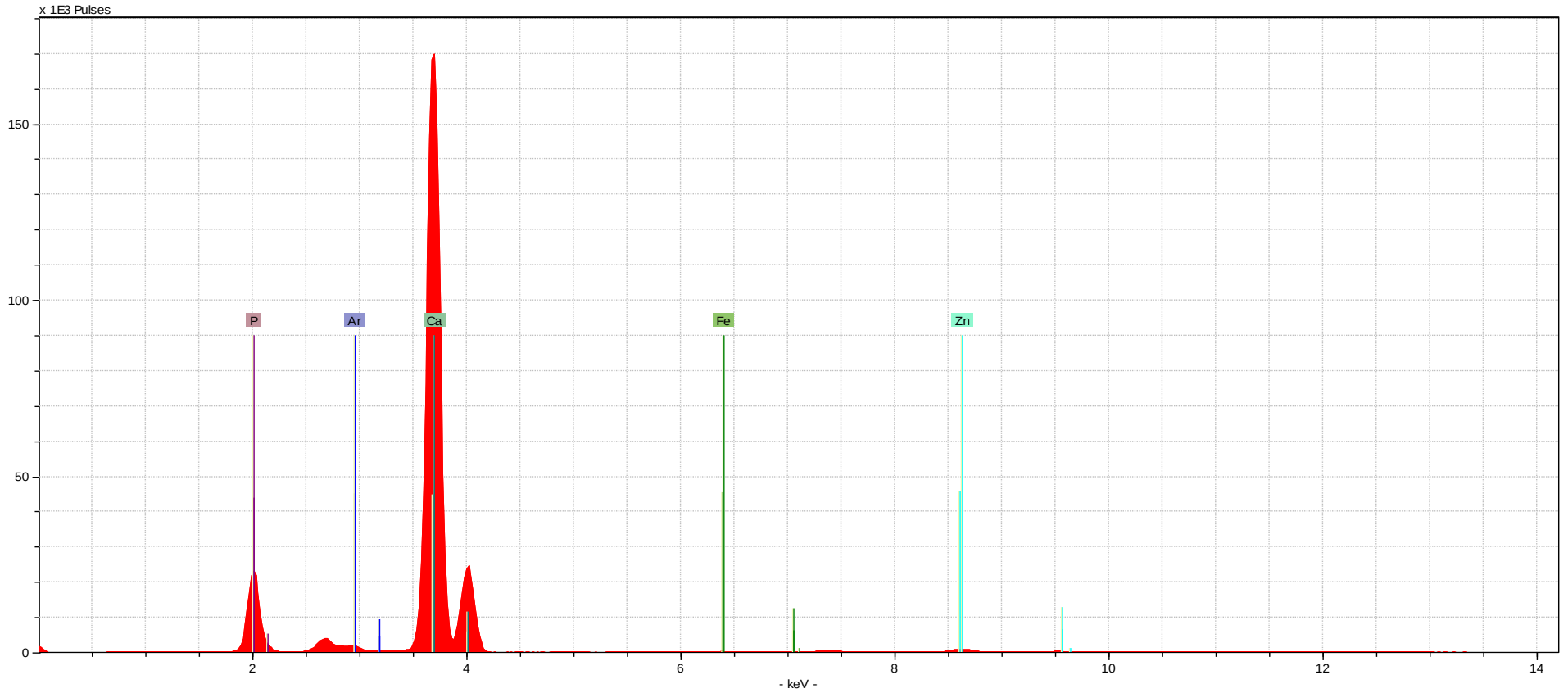

Bone Element	Biological Age	Time Period	Taphonomic Modifications	File Name/ Sample Name	Identified Elements (in order from L to R)
canine	adult	modern	none	canine1-60sH	P, Ar, Ca, Fe, Zn

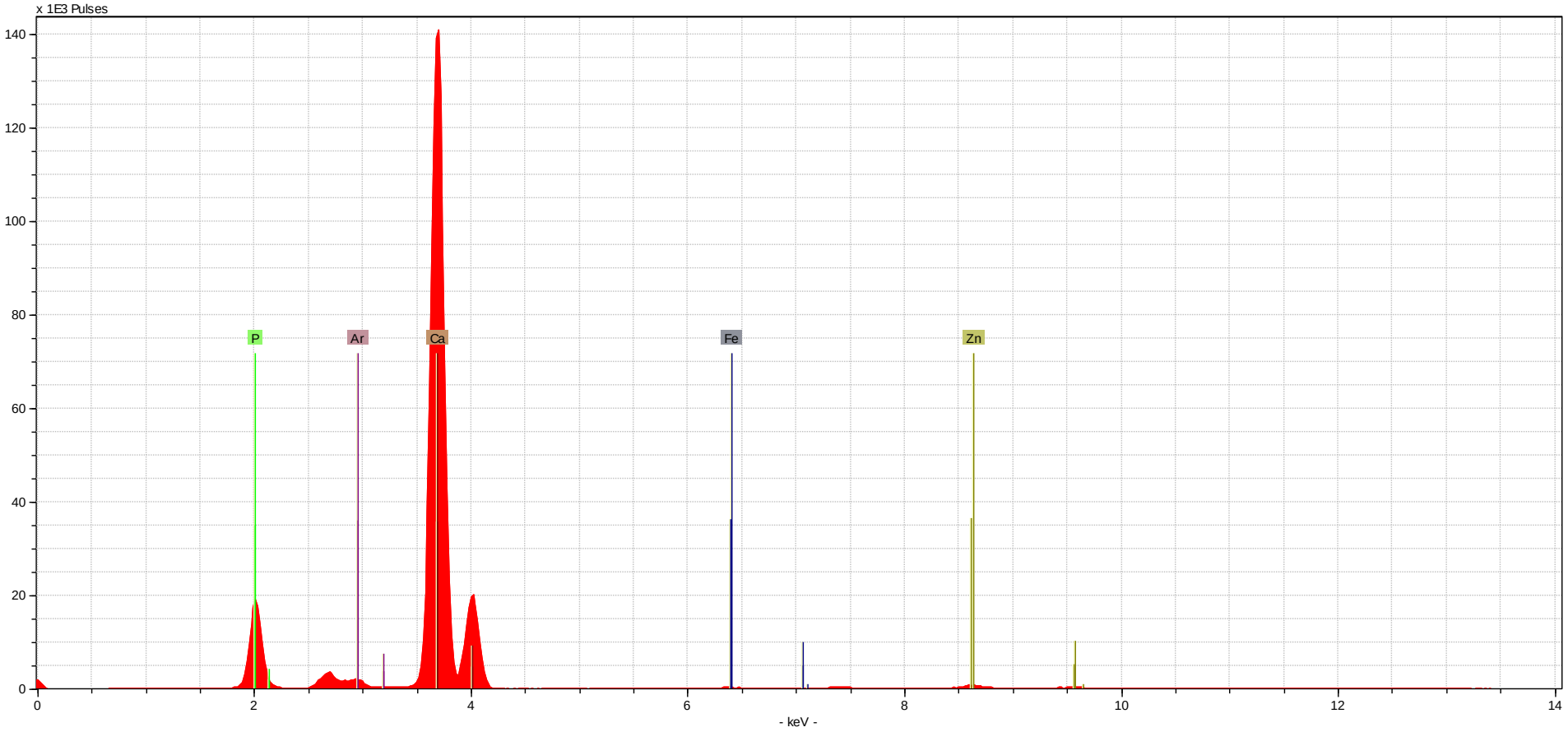

Bone Element	Biological Age	Time Period	Taphonomic Modifications	File Name/ Sample Name	Identified Elements (in order from L to R)
premolar	adult	modern	none	premolar1-60sH	P, Ar, Ca, Fe, Zn

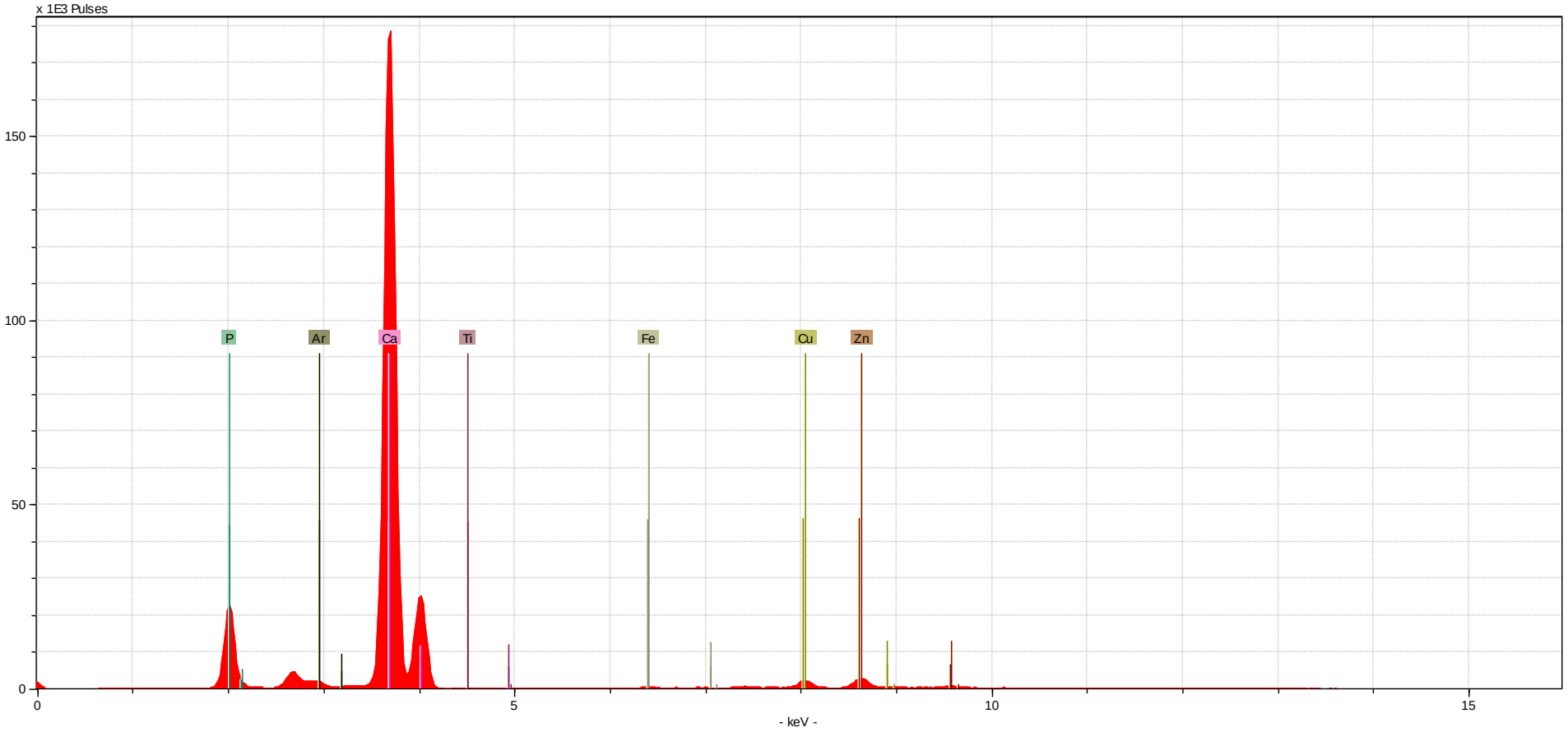

Bone Element	Biological Age	Time Period	Taphonomic Modifications	File Name/ Sample Name	Identified Elements (in order from L to R)
molar	adult	modern	none	molar1-60sH	P, Ar, Ca, Ti, Fe, Cu, Zn

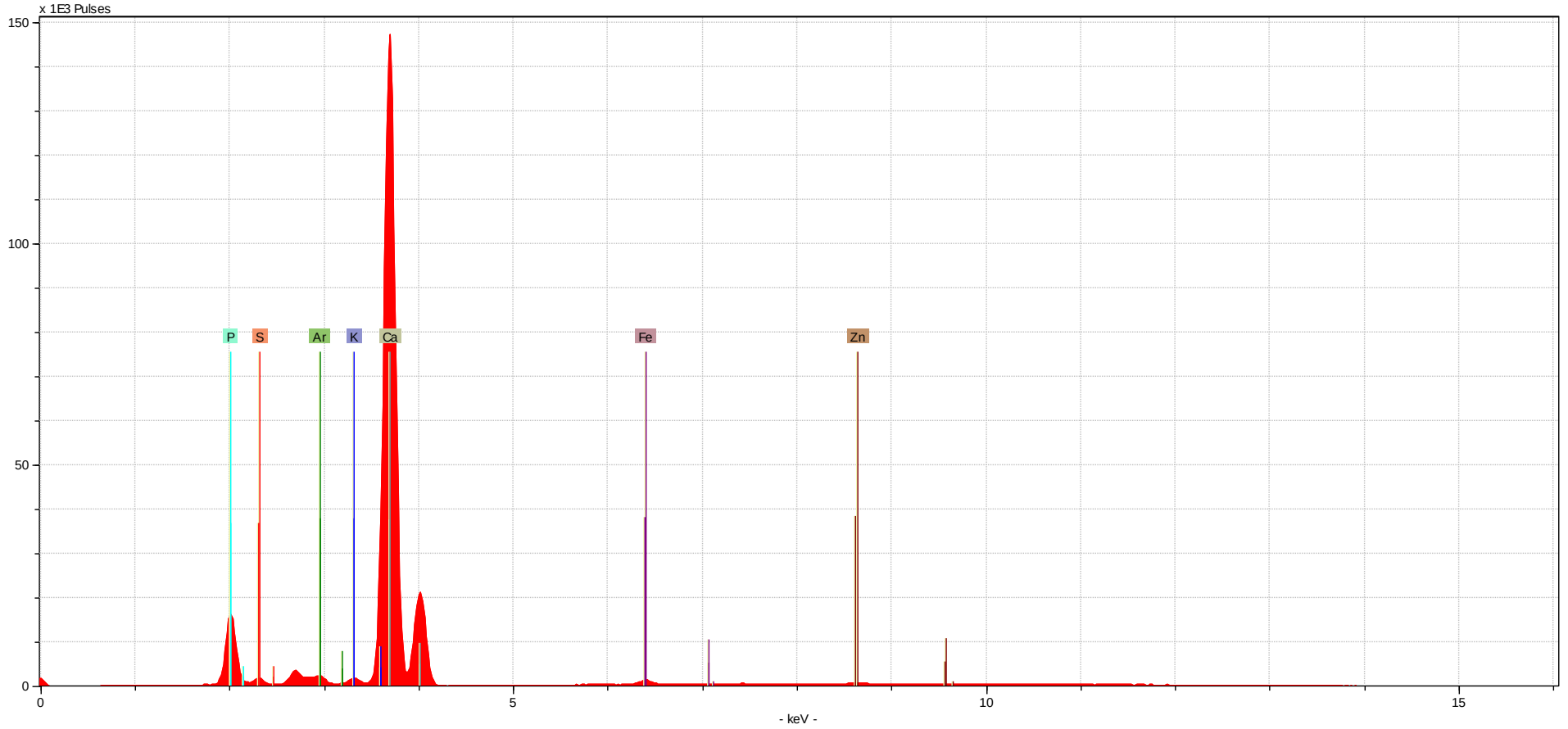

Bone Element	Biological Age	Time Period	Taphonomic Modifications	File Name/ Sample Name	Identified Elements (in order from L to R)
parietal	adult	modern	none	parietal1-60sH	P, S, Ar, K, Ca, Fe, Zn

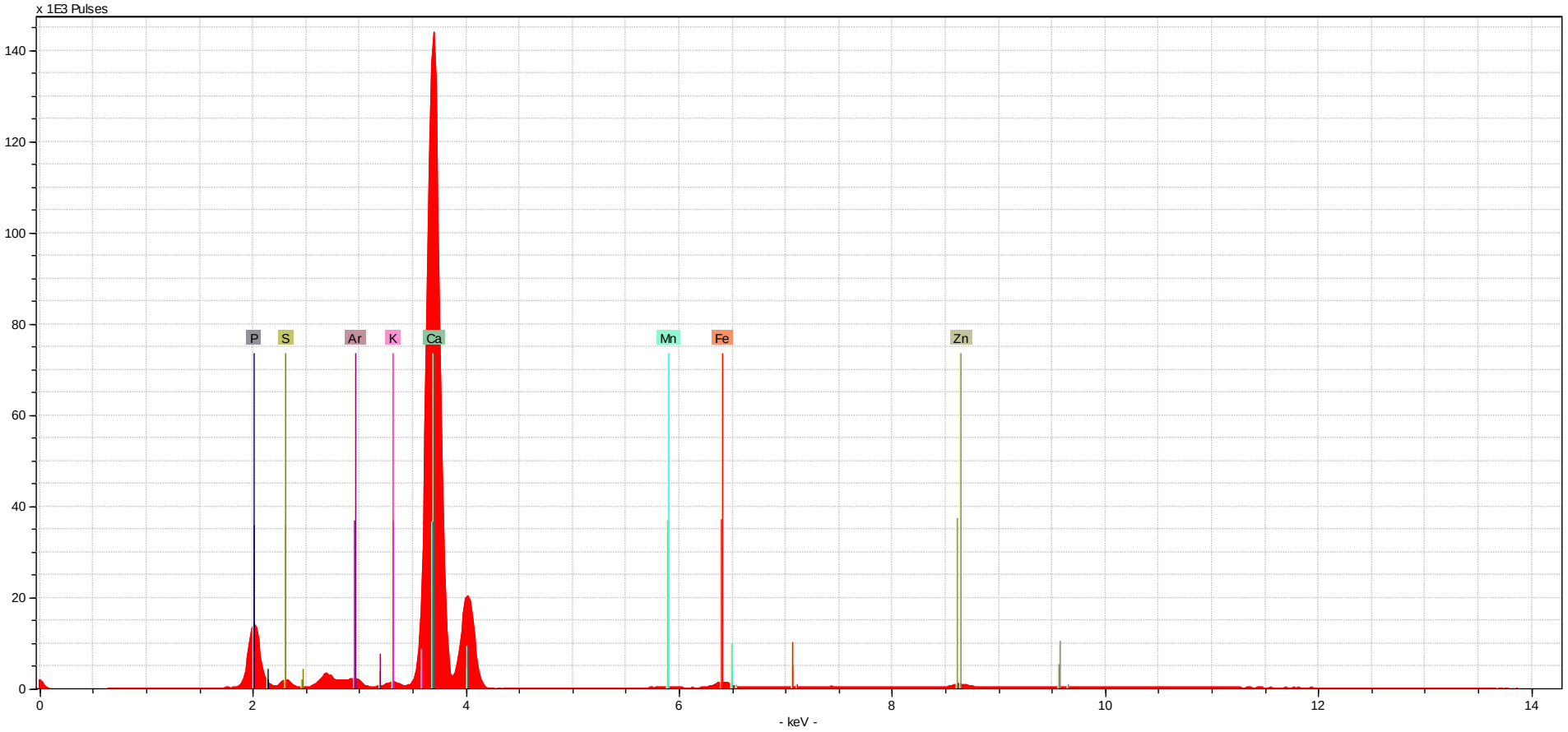

Bone Element	Biological Age	Time Period	Taphonomic Modifications	File Name/ Sample Name	Identified Elements (in order from L to R)
zygomatic	adult	modern	none	zygomatic1-60sH	P, S, Ar, K, Ca, Mn, Fe, Zn

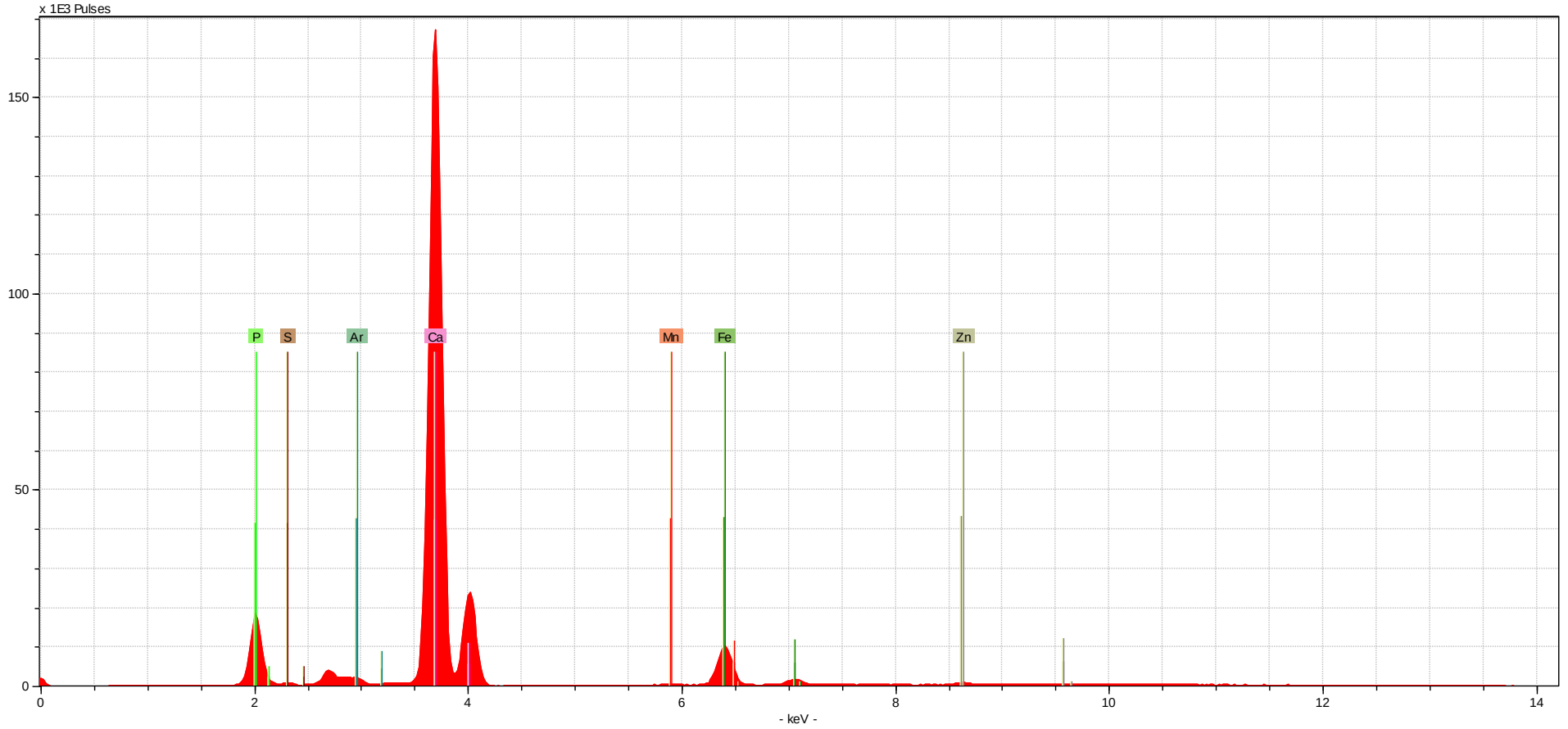

Bone Element	Biological Age	Time Period	Taphonomic Modifications	File Name/ Sample Name	Identified Elements (in order from L to R)
rib	adult	modern	none	rib1-60sH	P, S, Ar, Ca, Mn, Fe, Zn

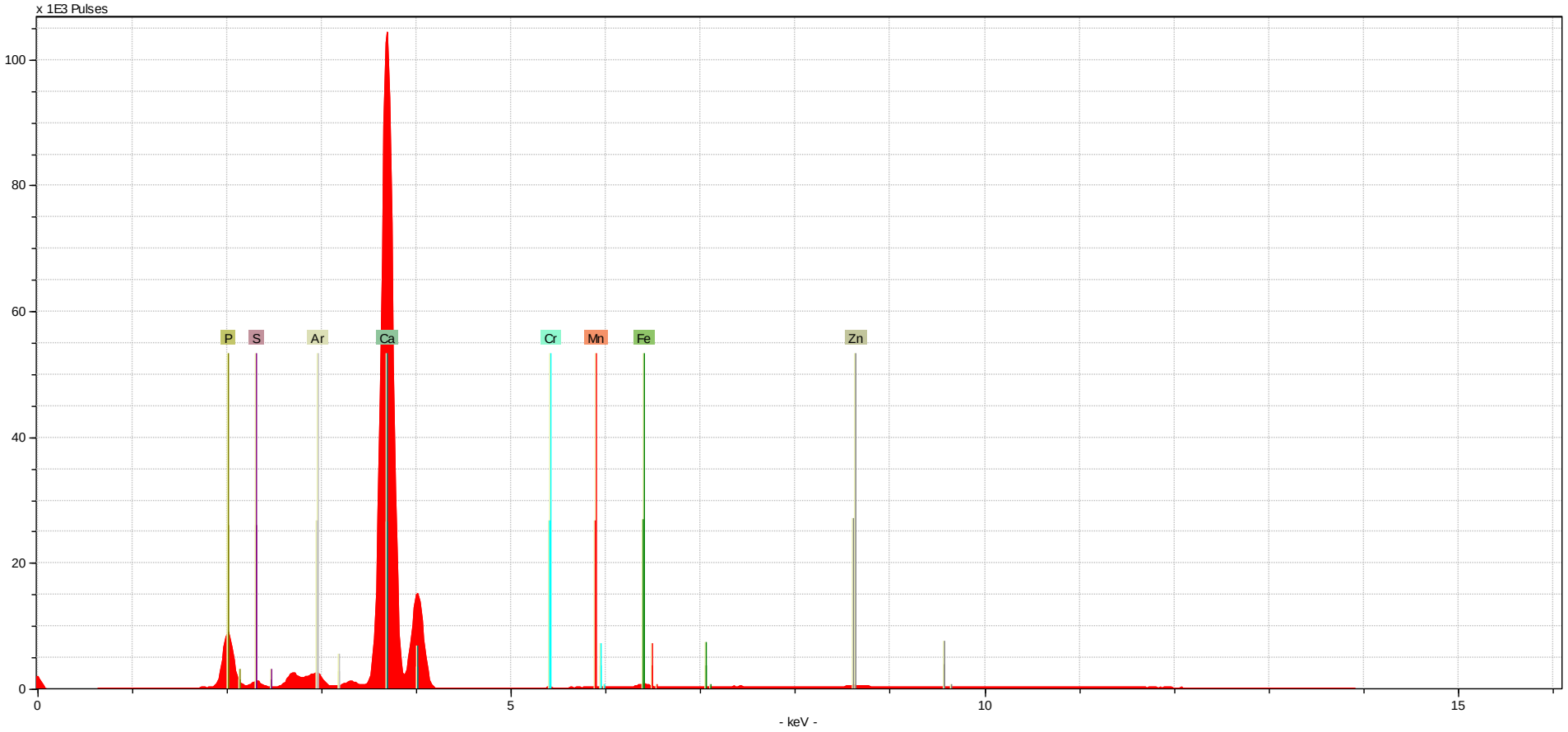

Bone Element	Biological Age	Time Period	Taphonomic Modifications	File Name/ Sample Name	Identified Elements (in order from L to R)
humerus	adult	modern	none	humerus1-60sH	P, S, Ar, Ca, Cr, Mn, Fe, Zn

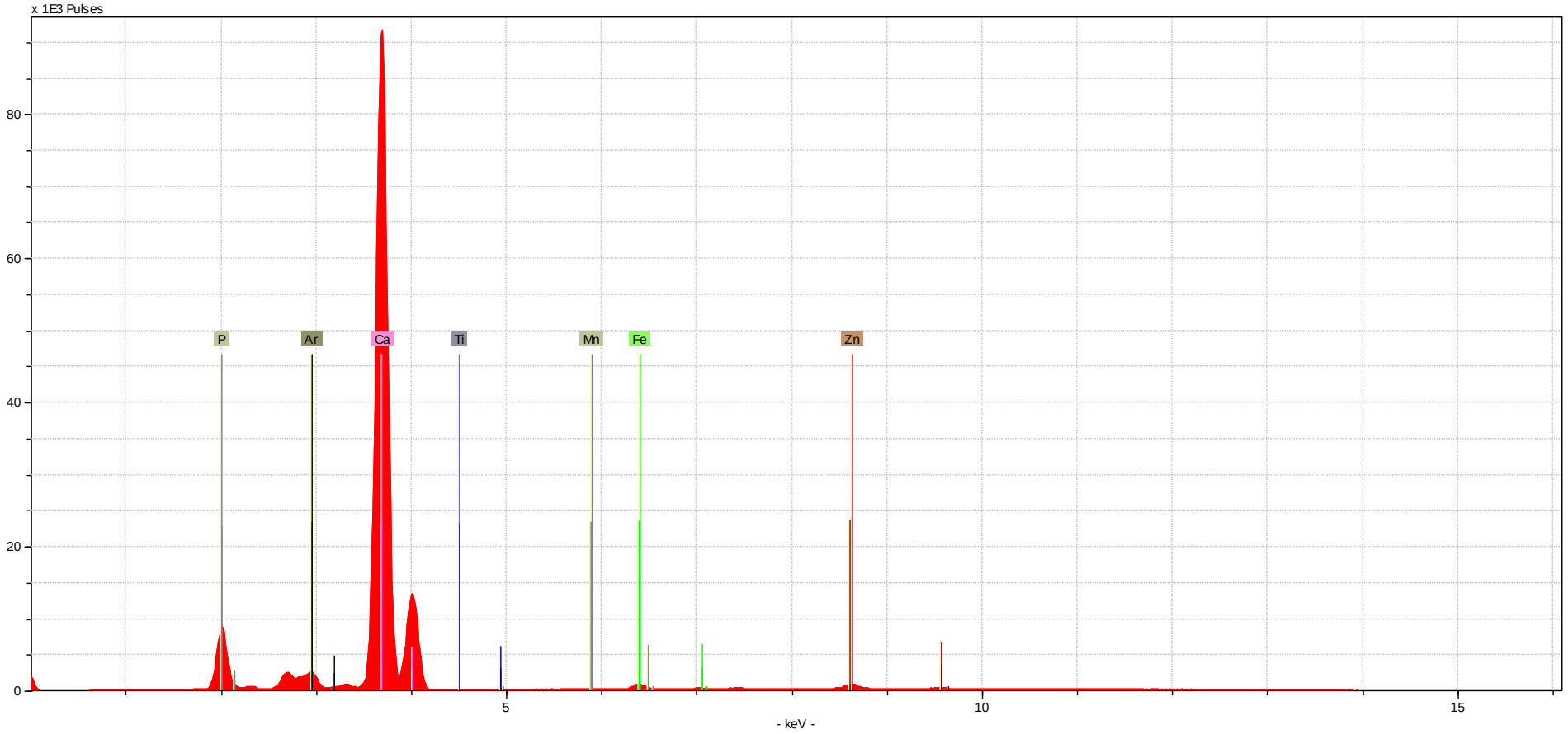

Bone Element	Biological Age	Time Period	Taphonomic Modifications	File Name/ Sample Name	Identified Elements (in order from L to R)
fibula	adult	modern	none	fibula1-60sH	P, Ar, Ca, Ti, Mn, Fe, Zn

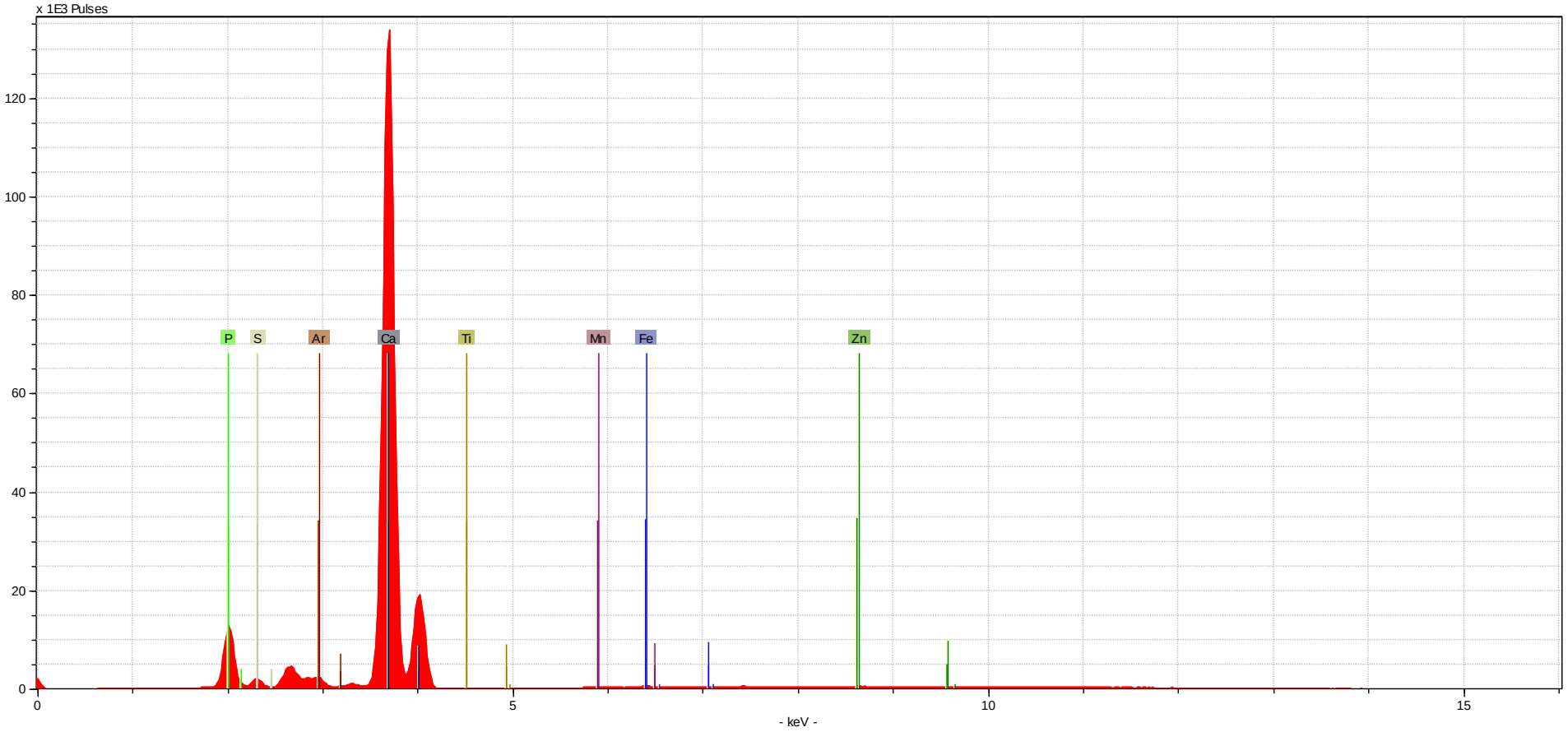

Bone Element	Biological Age	Time Period	Taphonomic Modifications	File Name/ Sample Name	Identified Elements (in order from L to R)
metacarpal	adult	modern	none	metacarpal1-60sH	P, S, Ar, Ca, Ti, Mn, Fe, Zn

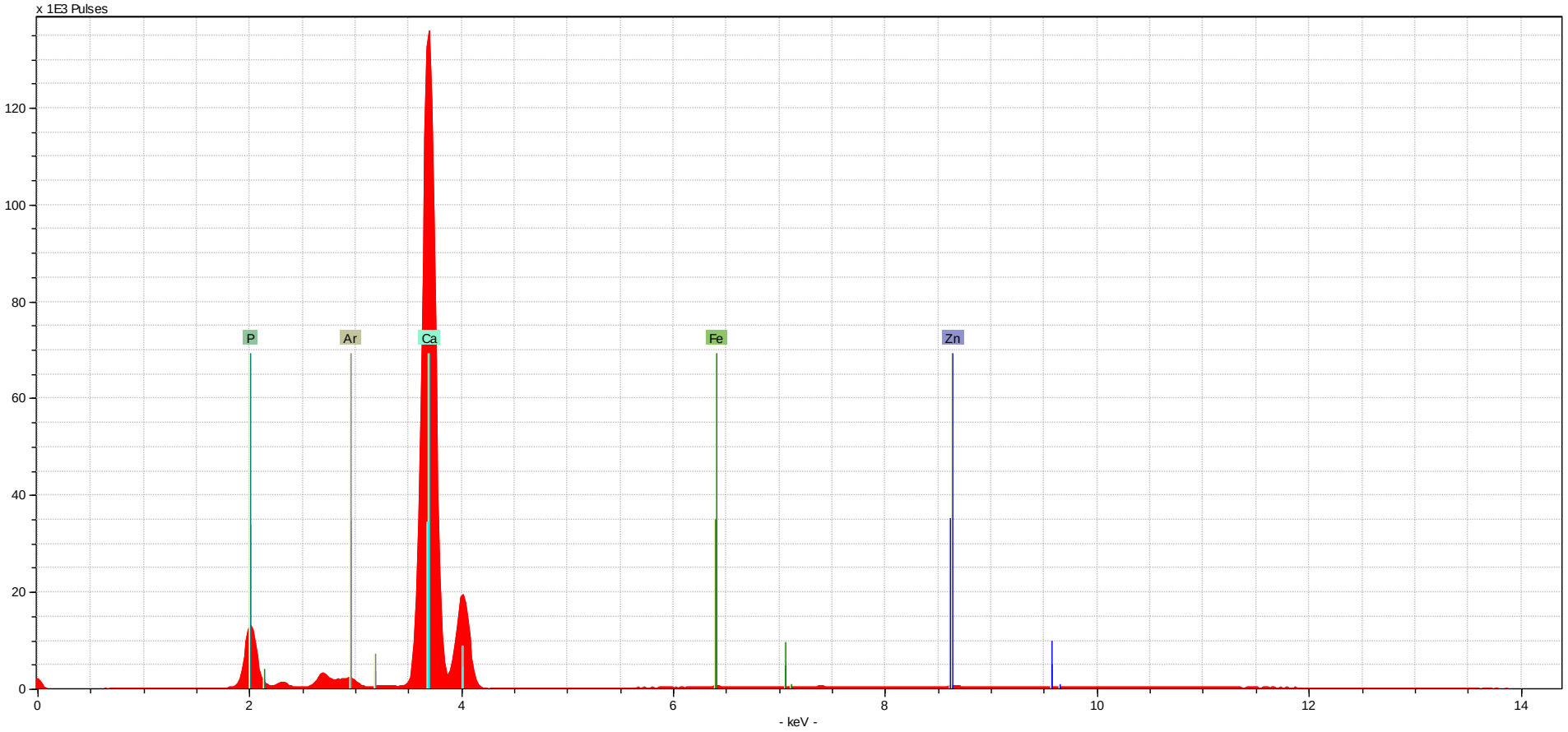

Bone Element	Biological Age	Time Period	Taphonomic Modifications	File Name/ Sample Name	Identified Elements (in order from L to R)
pedal phalanx	adult	modern	none	pedalphalanx1-60sH	P, Ar, Ca, Fe, Zn

<u>Nonhuman Spectra:</u> shown below is the first spectrum collected from each nonhuman bone sample. The spectrum is shown with the elements identified (autoidentified using ARTAX software).

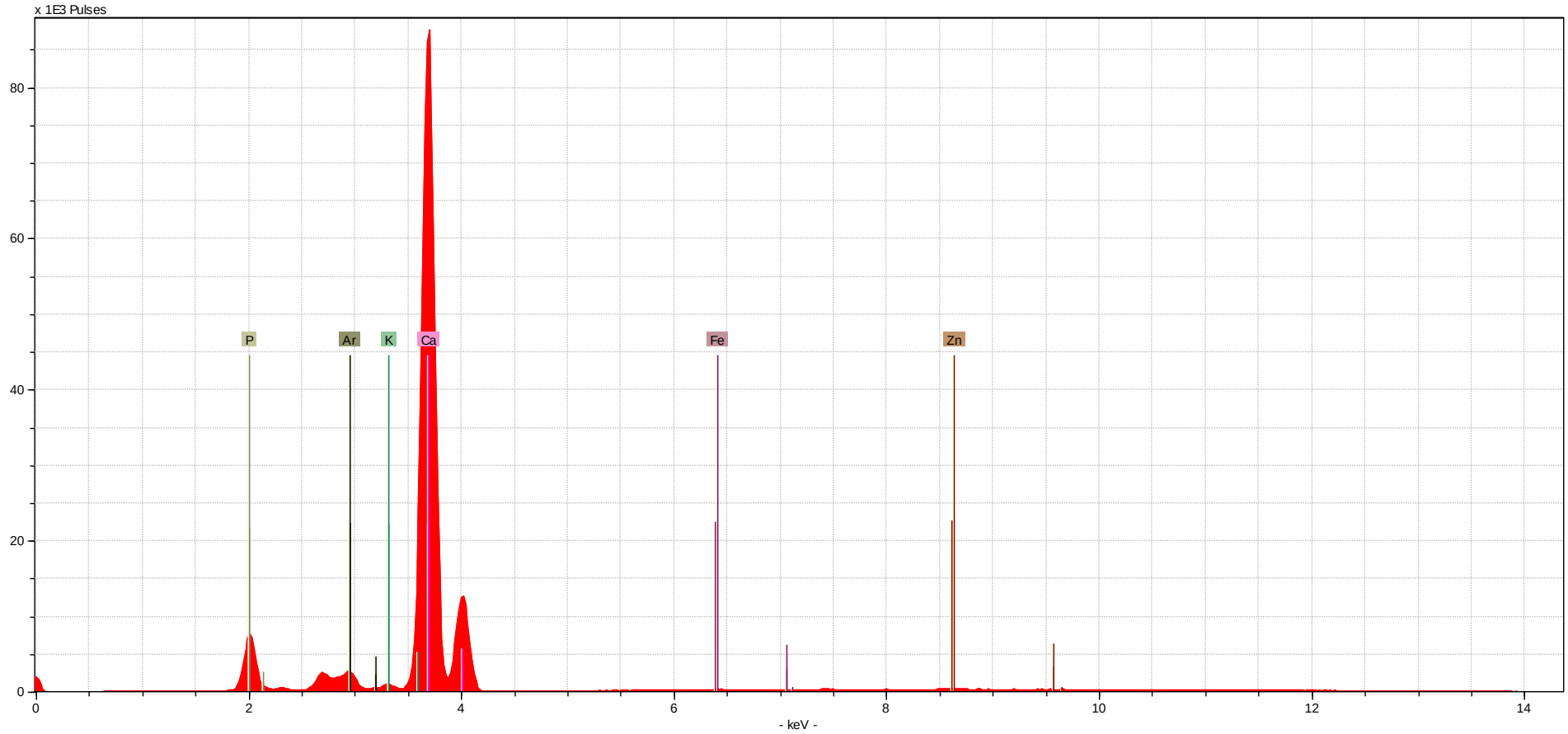

Sample Type	Bone Element	Biological Age	Time Period	Taphonomic Modifications	File Name/ Sample Name	Identified Elements (in order from L to R)
armadillo	femur	adult	modern	none	armadillo1-60sNH	P, Ar, K, Ca, Fe, Zn

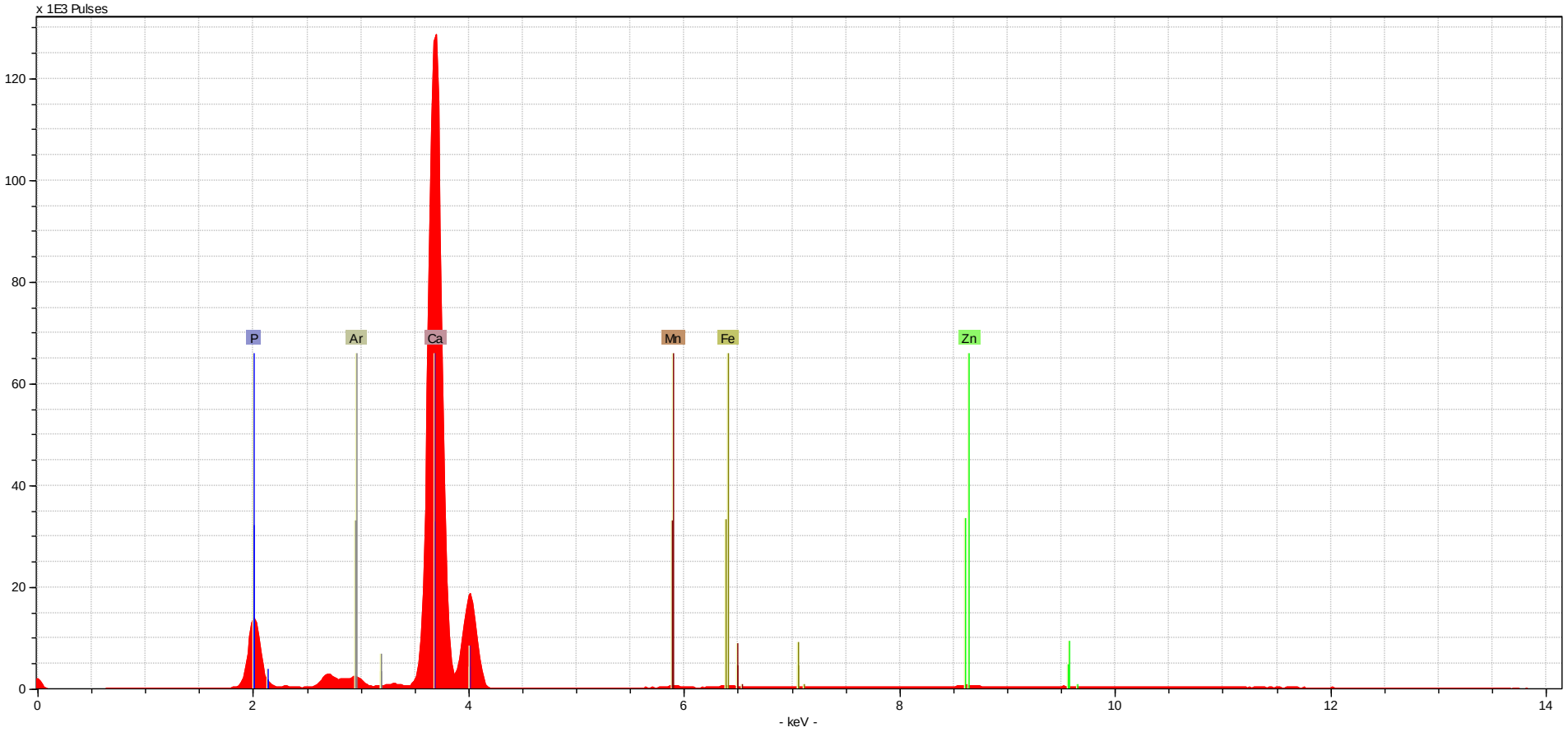

Sample Type	Bone Element	Biological Age	Time Period	Taphonomic Modifications	File Name/ Sample Name	Identified Elements (in order from L to R)
raccoon	femur	adult	modern	none	raccoon1-60sNH	P, Ar, Ca, Mn, Fe, Zn

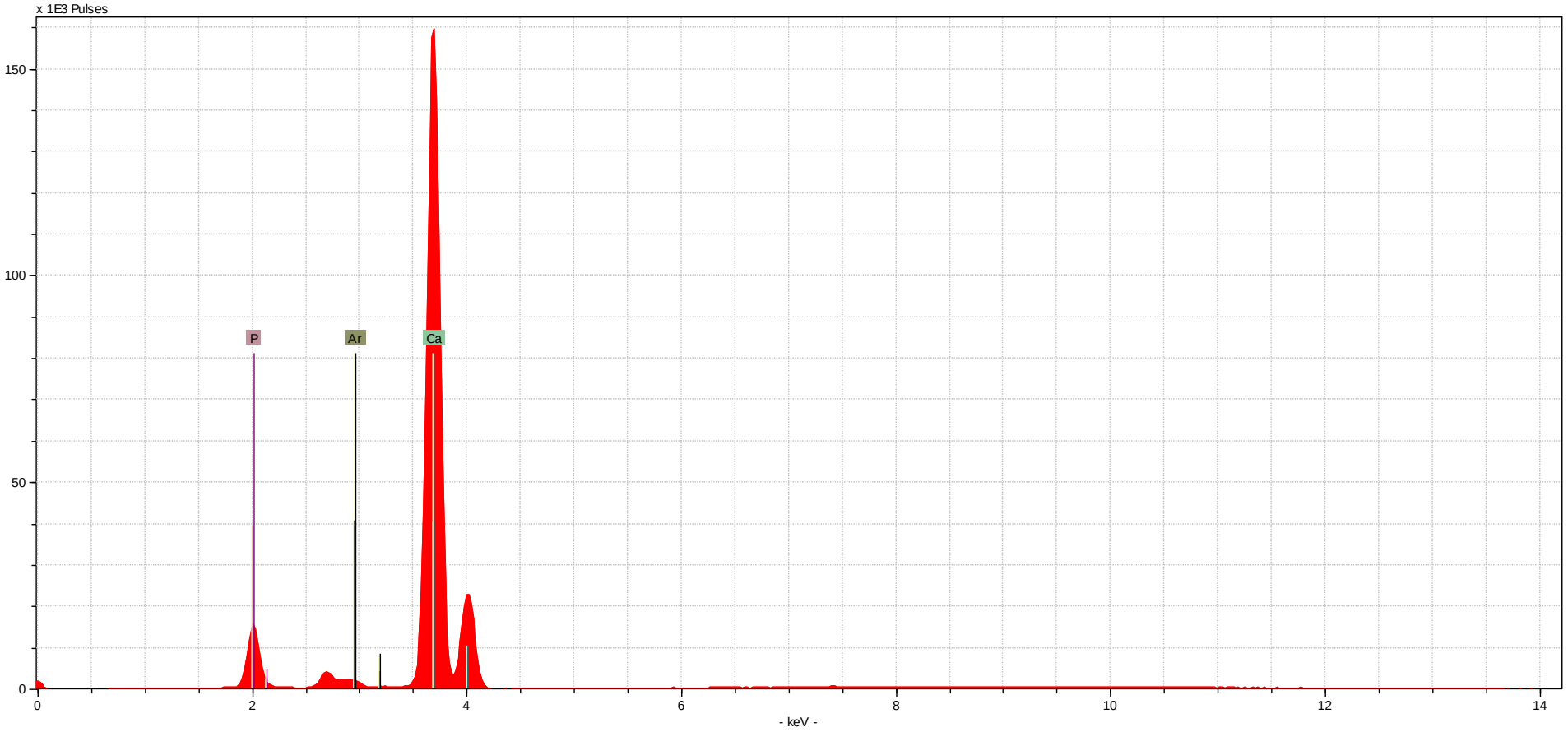

Sample Type	Bone Element	Biological Age	Time Period	Taphonomic Modifications	File Name/ Sample Name	Identified Elements (in order from L to R)
turtle	femur	adult	modern	none	turtle1-60sNH	P, Ar, Ca

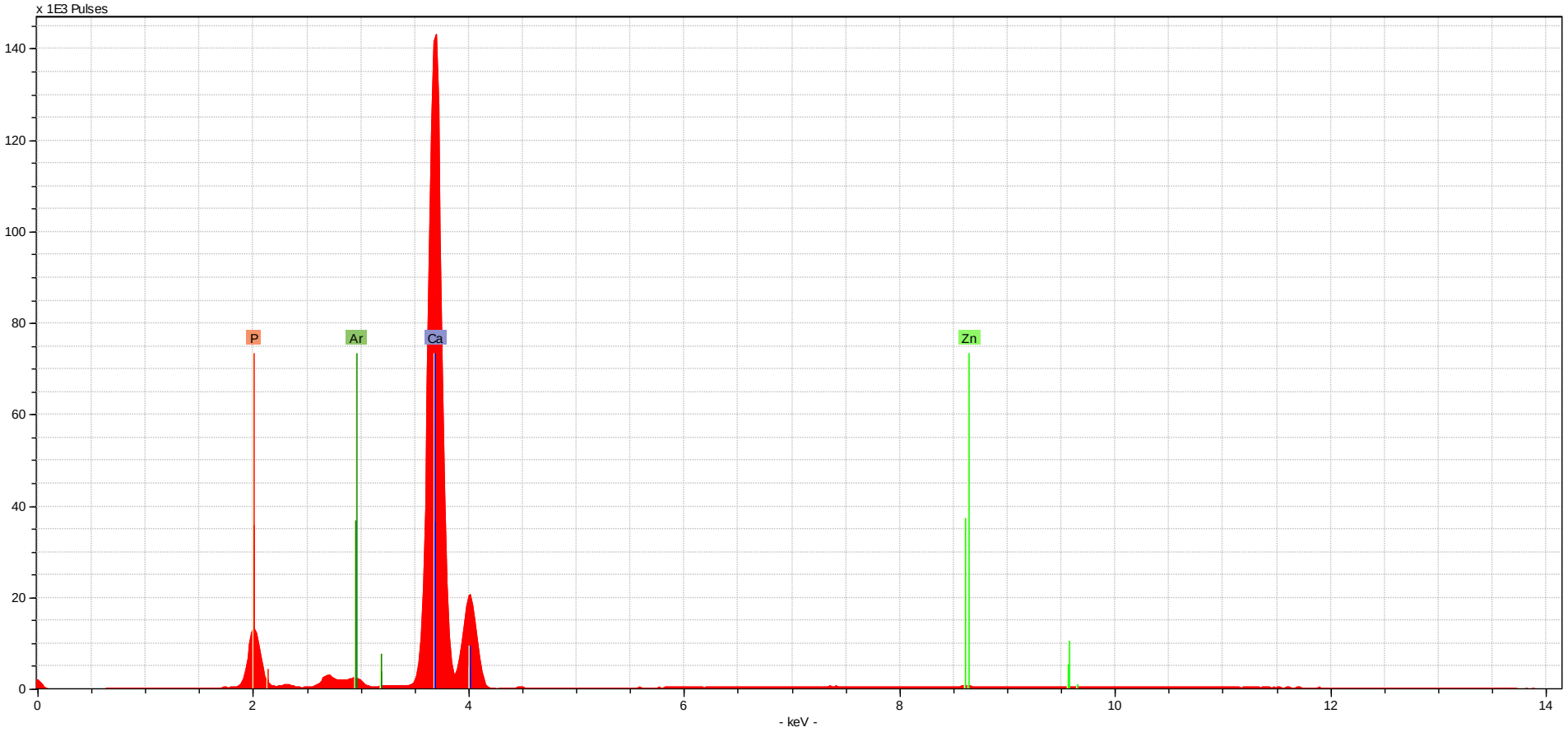

Sample Type	Bone Element	Biological Age	Time Period	Taphonomic Modifications	File Name/ Sample Name	Identified Elements (in order from L to R)
turtle	shell	adult	modern	none	turtleshell1-60sNH	P, Ar, Ca, Zn

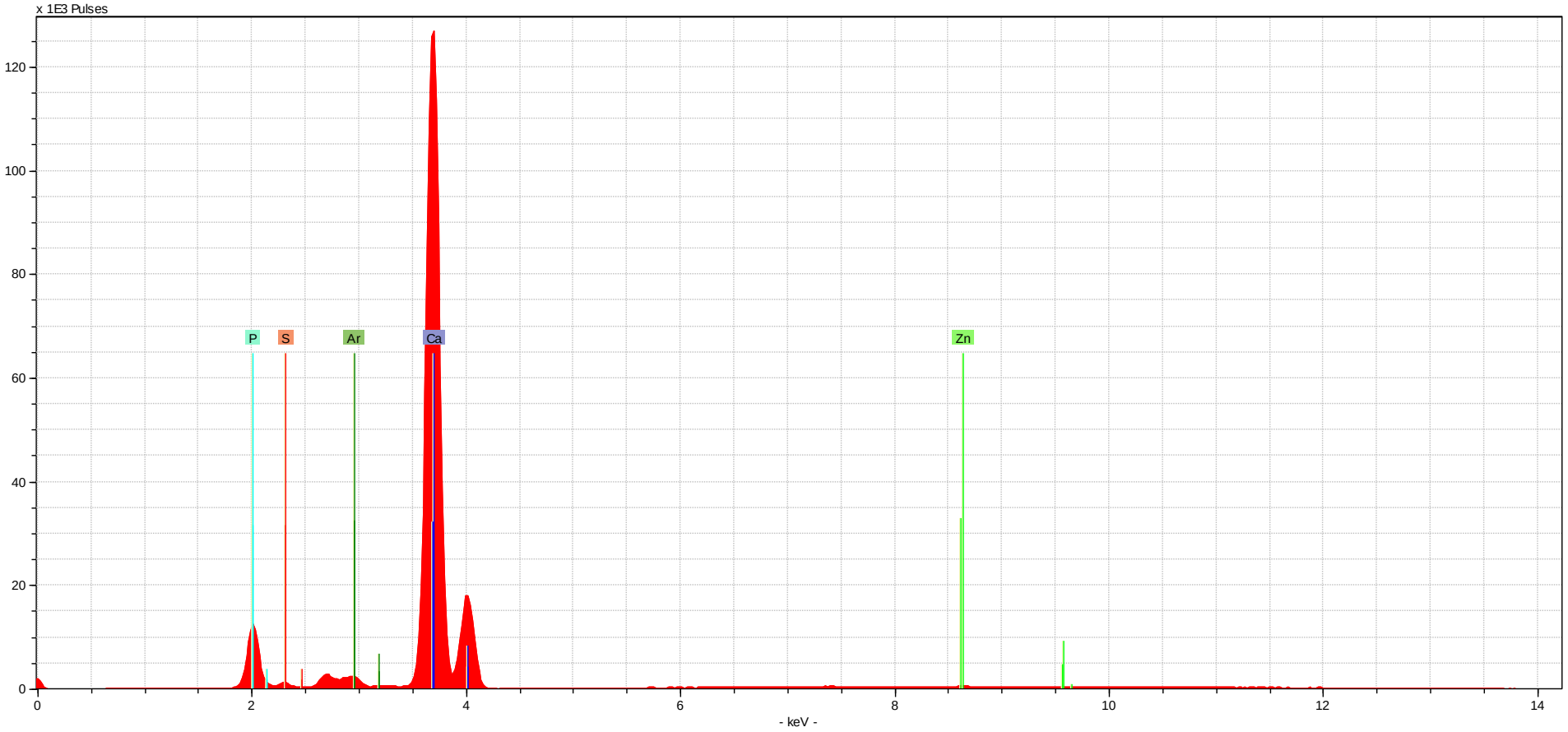

Sample Type	Bone Element	Biological Age	Time Period	Taphonomic Modifications	File Name/ Sample Name	Identified Elements (in order from L to R)
bird	femur	adult	modern	none	bird1-60sNH	P, S, Ar, Ca, Zn

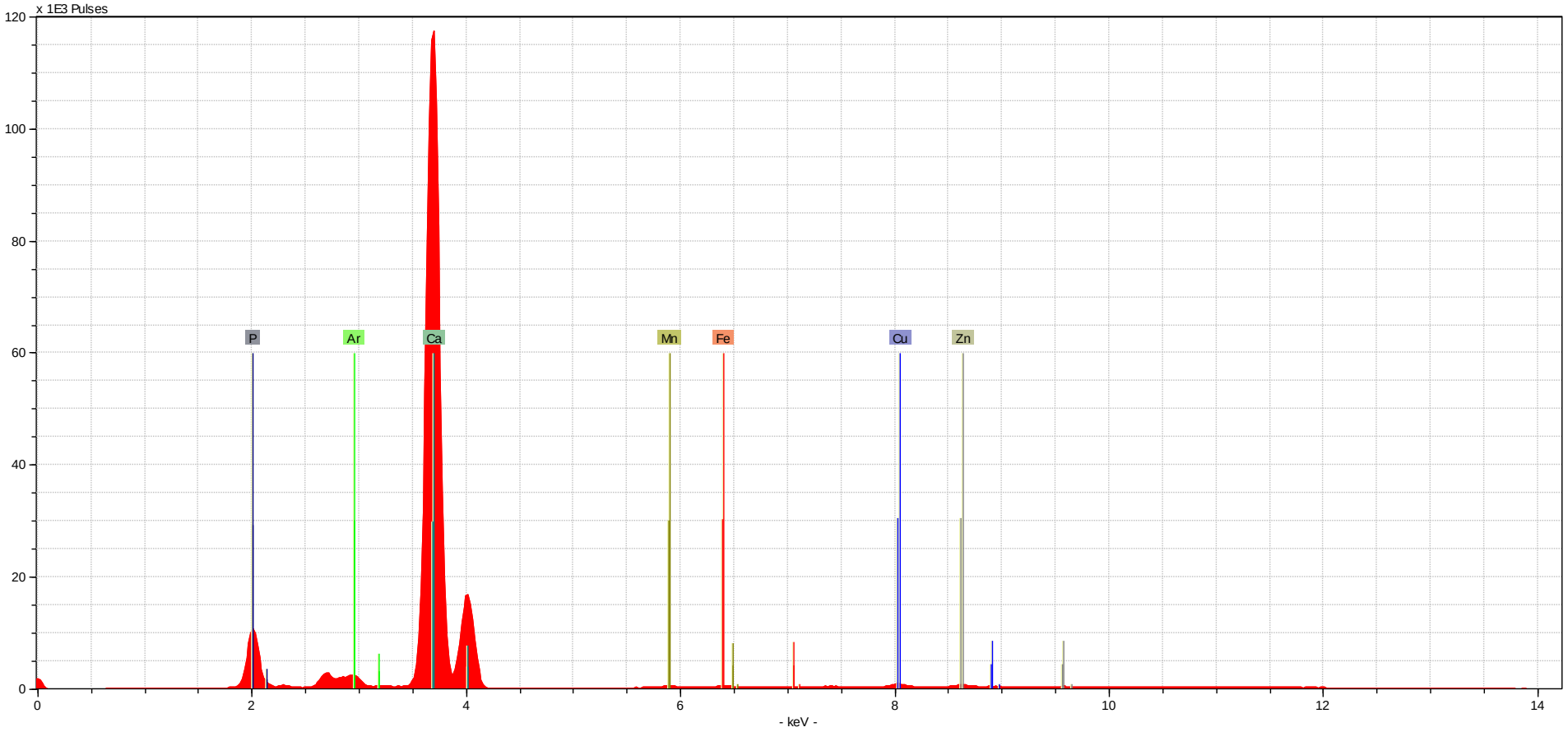

Sample Type	Bone Element	Biological Age	Time Period	Taphonomic Modifications	File Name/ Sample Name	Identified Elements (in order from L to R)
turkey	tarsometatarsus	adult	modern	none	turkey1-60sNH	P, Ar, Ca, Mn, Fe, Cu, Zn

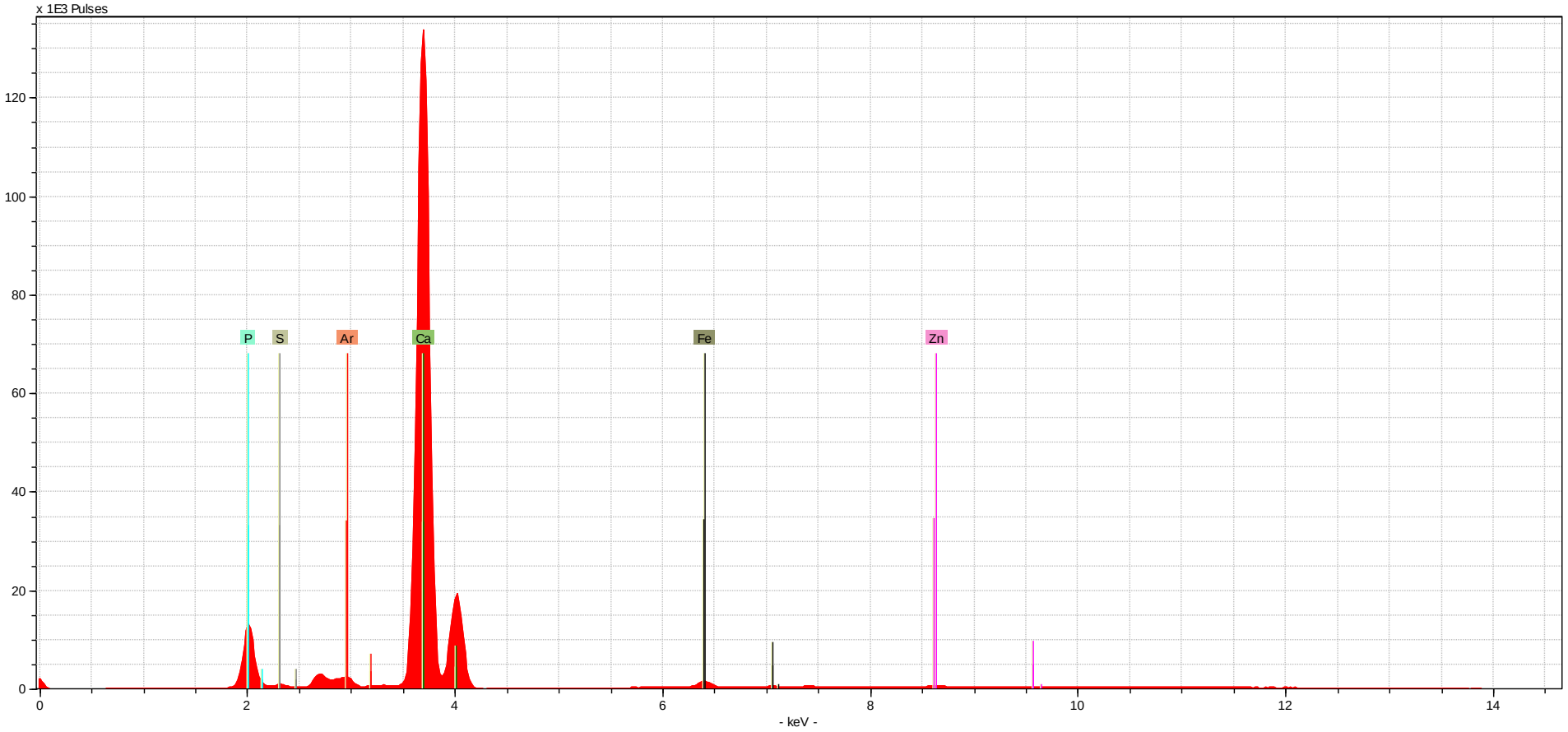

Sample Type	Bone Element	Biological Age	Time Period	Taphonomic Modifications	File Name/ Sample Name	Identified Elements (in order from L to R)
gator	femur	adult	modern	none	gator1-60sNH	P, S, Ar, Ca, Fe, Zn

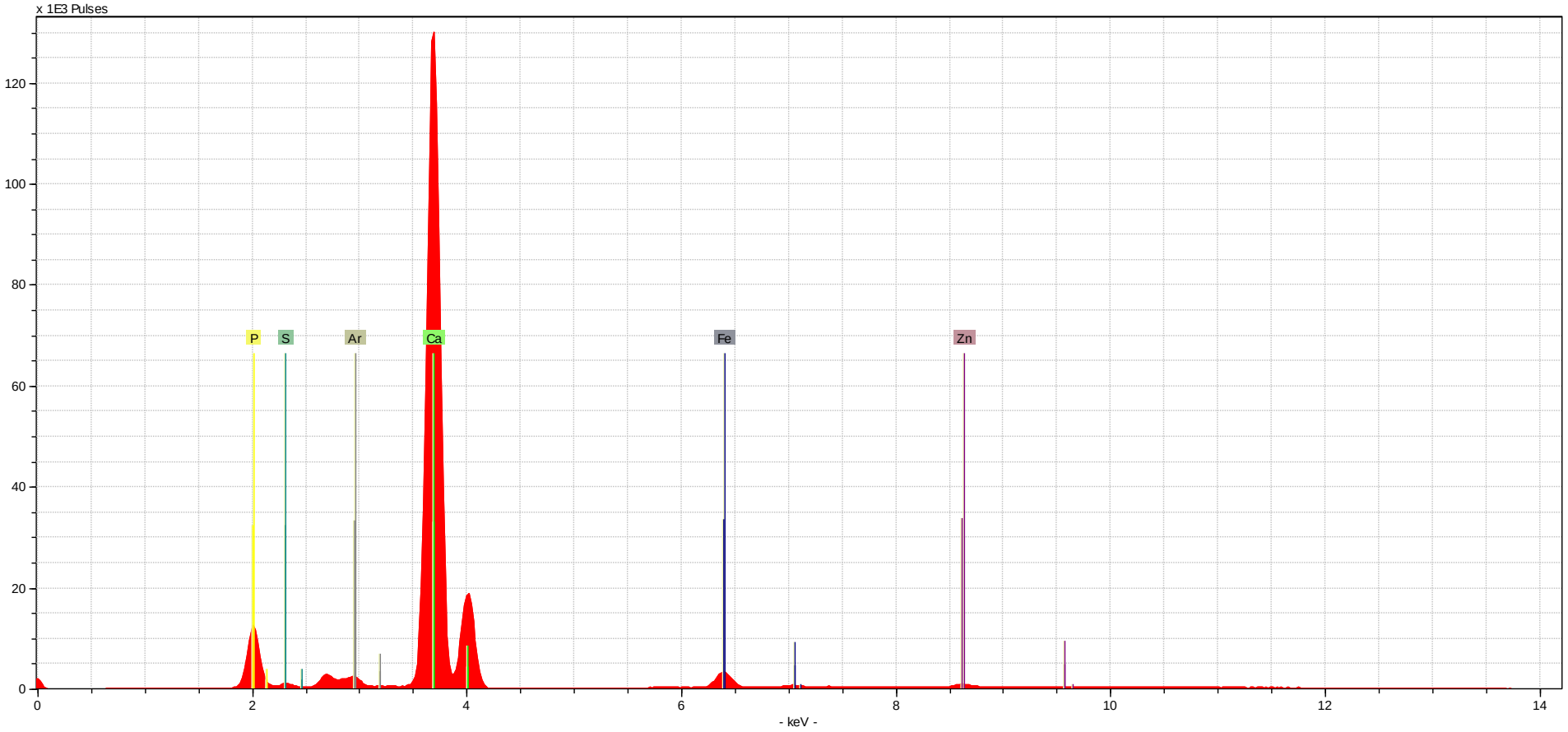

Sample Type	Bone Element	Biological Age	Time Period	Taphonomic Modifications	File Name/ Sample Name	Identified Elements (in order from L to R)
dog	femur	adult	modern	none	dog1-60sNH	P, S, Ar, Ca, Fe, Zn

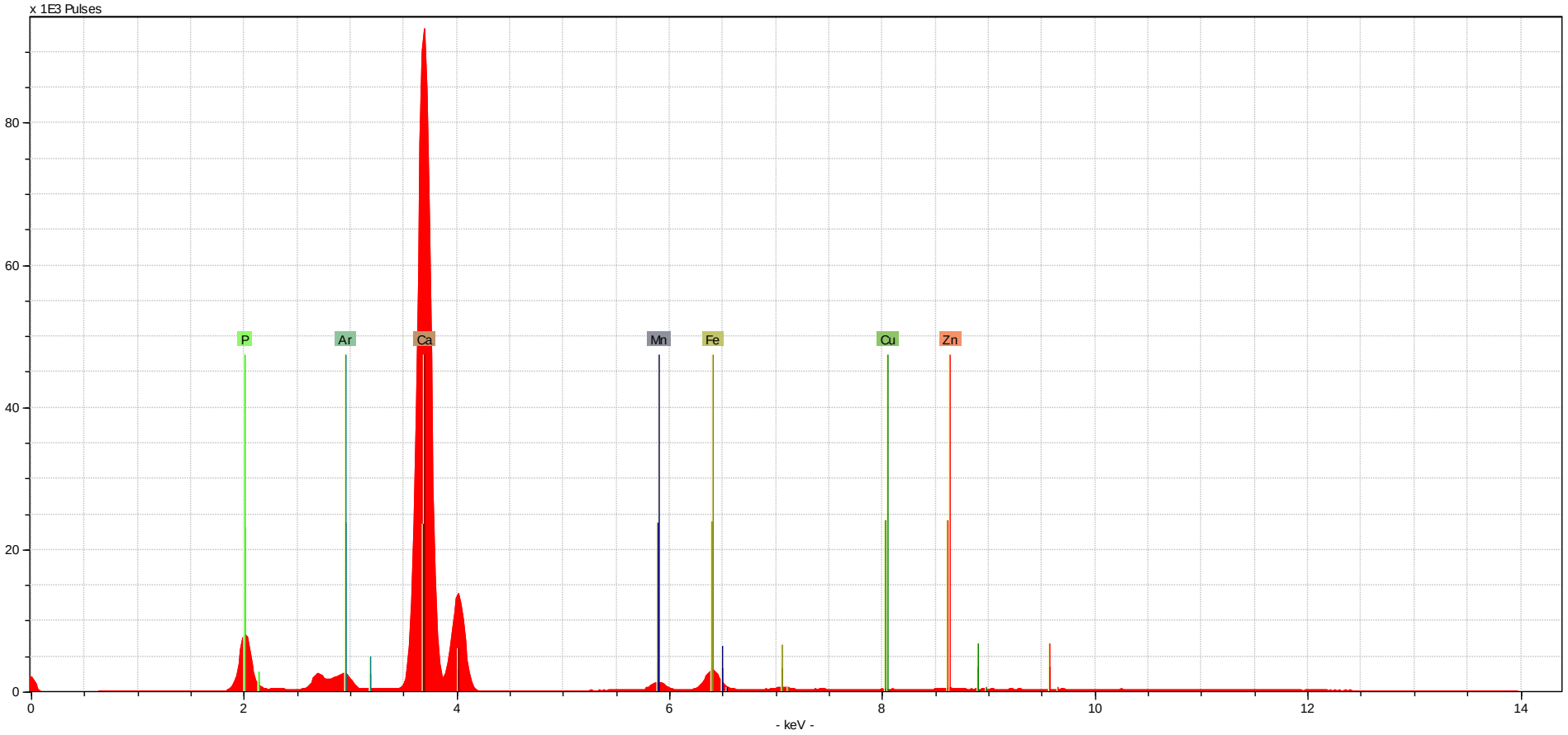

Sample Type	Bone Element	Biological Age	Time Period	Taphonomic Modifications	File Name/ Sample Name	Identified Elements (in order from L to R)
pig	femur	juvenile	modern	none	pig1-60sNH	P, Ar, Ca, Mn, Fe, Cu, Zn

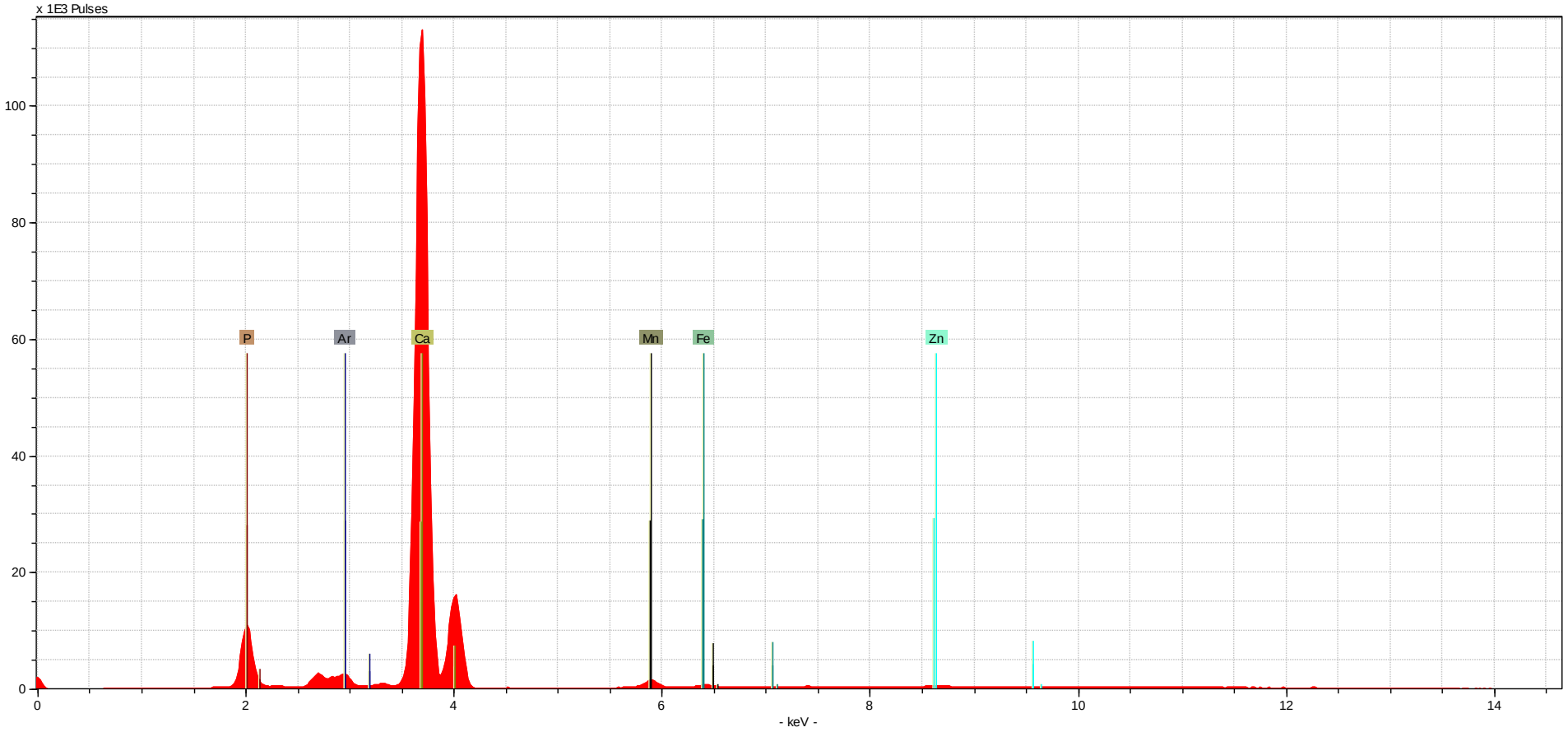

Sample Type	Bone Element	Biological Age	Time Period	Taphonomic Modifications	File Name/ Sample Name	Identified Elements (in order from L to R)
deer	femur	adult	modern	none	deer1-60sNH	P, Ar, Ca, Mn, Fe, Zn

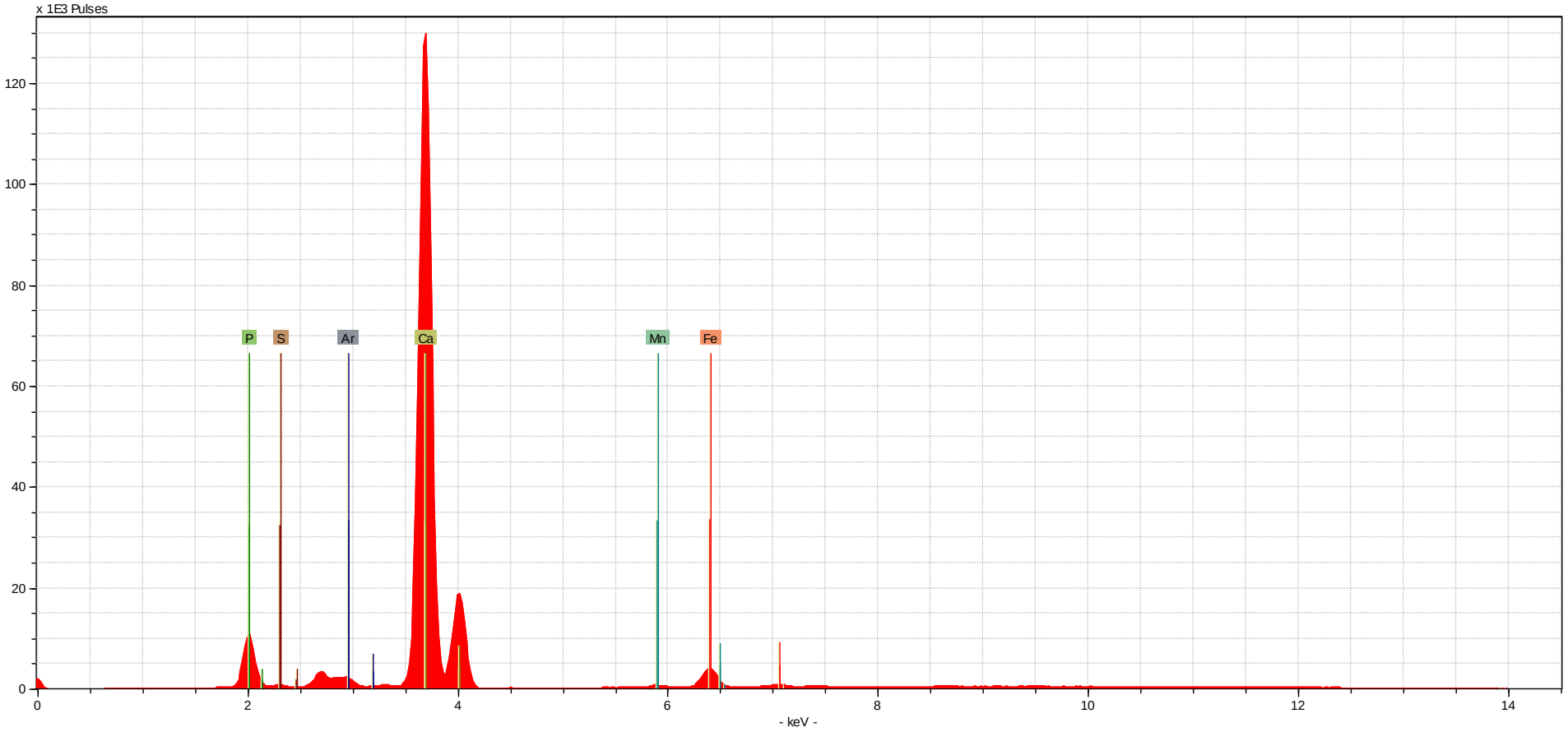

Sample Type	Bone Element	Biological Age	Time Period	Taphonomic Modifications	File Name/ Sample Name	Identified Elements (in order from L to R)
deer	antler	adult	modern	none	antler1-60sNH	P, S, Ar, Ca, Mn, Fe

Other Biological Specimens Spectra: shown below is the first spectrum collected from each of the specimens from the other biological group. The spectrum is shown with the elements identified (autoidentified using ARTAX software).

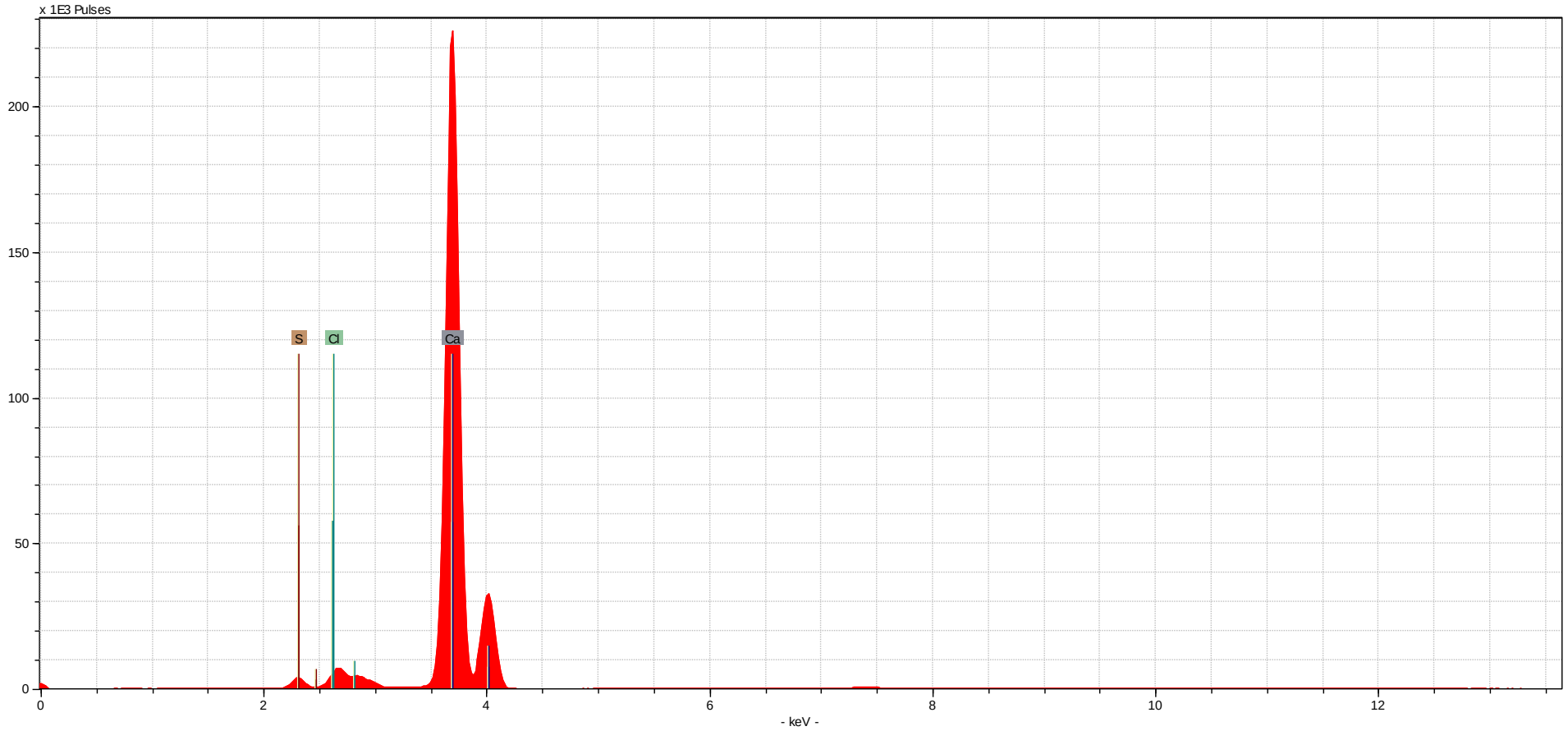

Sample Type	Material	Taphonomic Modifications	File Name/ Sample Name	Identified Elements (in order from L to R)
shell	clam	none	clamshell1-60sOB	S, Cl, Ca

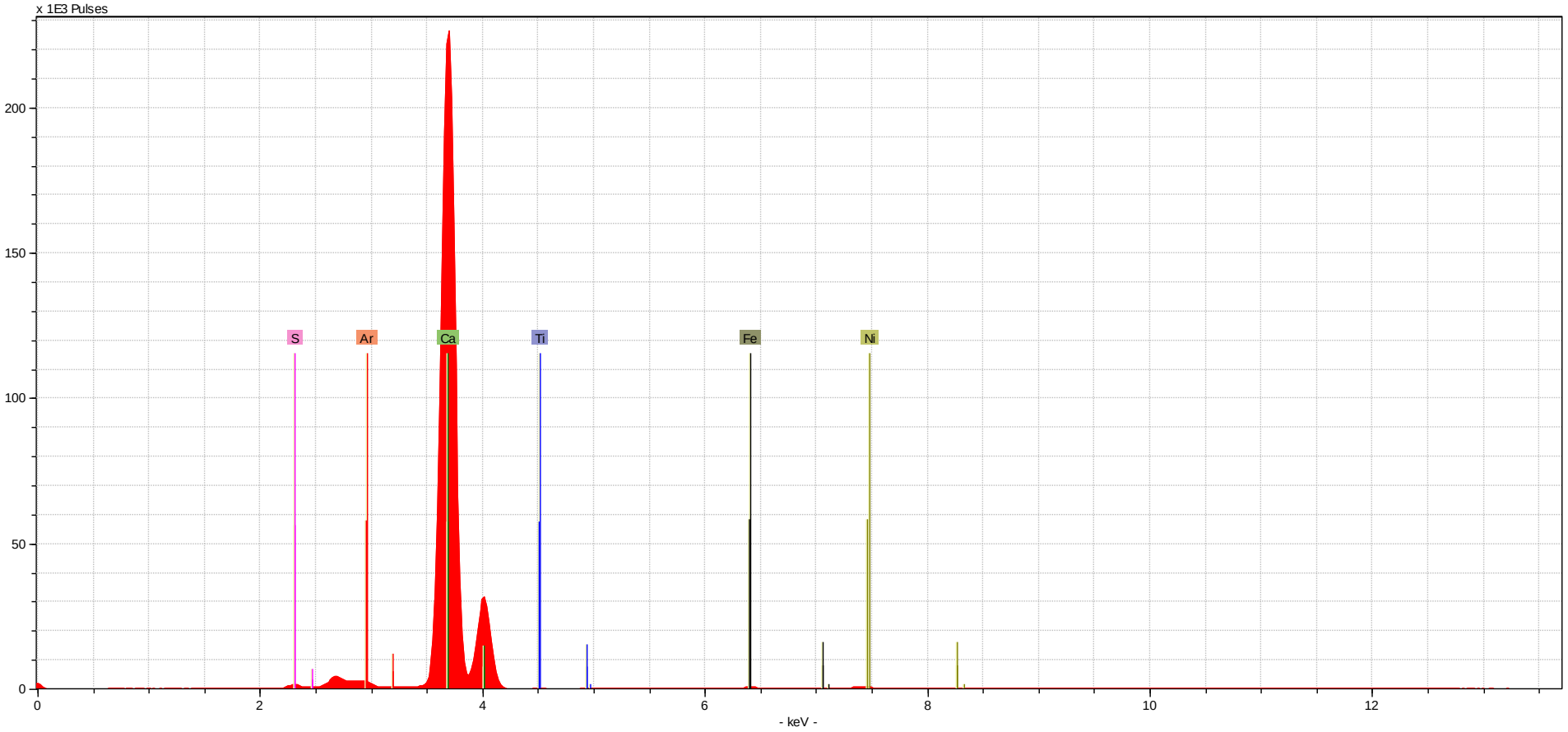

Sample Type	Material	Taphonomic Modifications	File Name/ Sample Name	Identified Elements (in order from L to R)
shell	oyster	none	oystershell1-60sOB	S, Ar, Ca, Ti, Fe, Ni

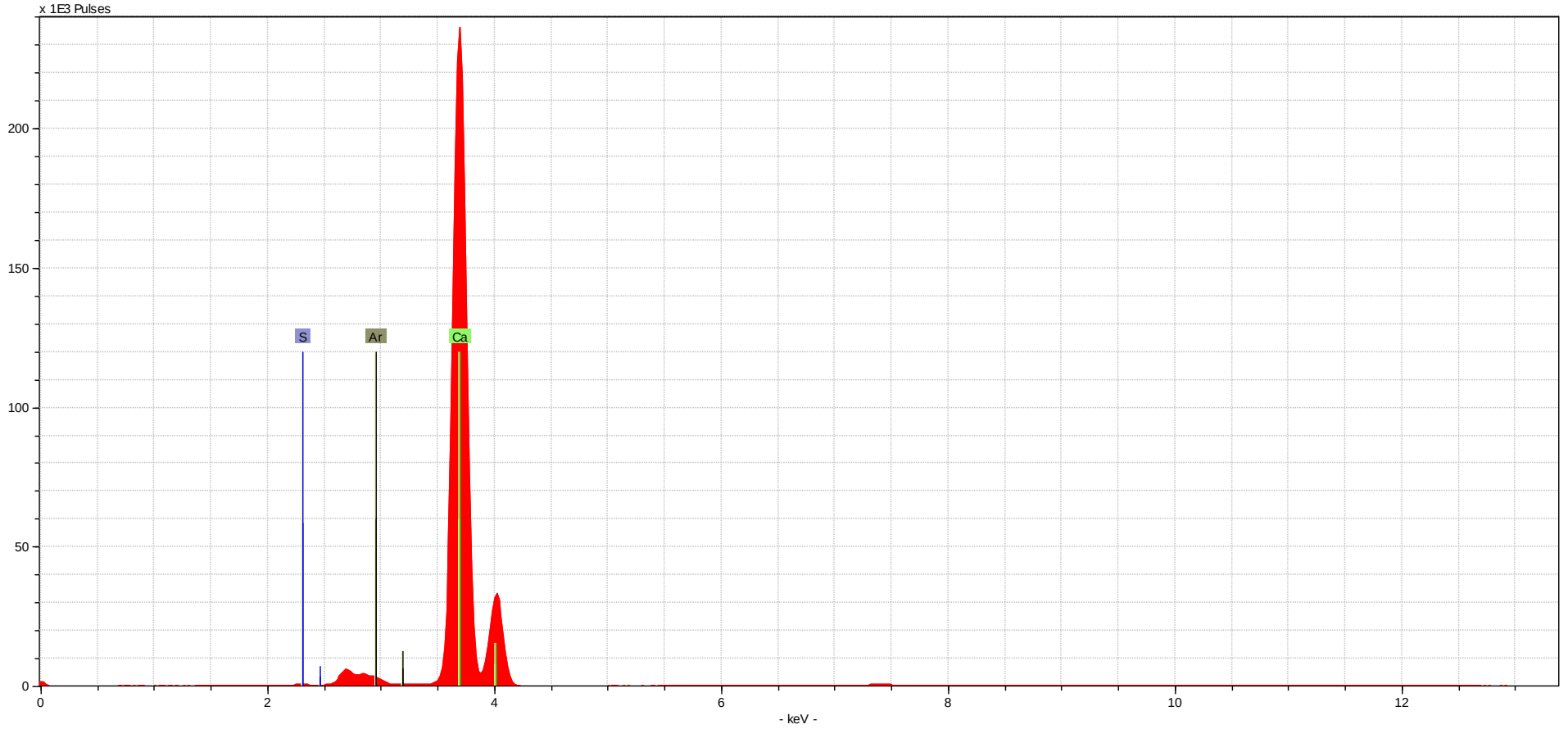

Sample Type	Material	Taphonomic Modifications	File Name/ Sample Name	Identified Elements (in order from L to R)
shell	scallop	none	scallopshell1-60sOB	S, Ar, Ca

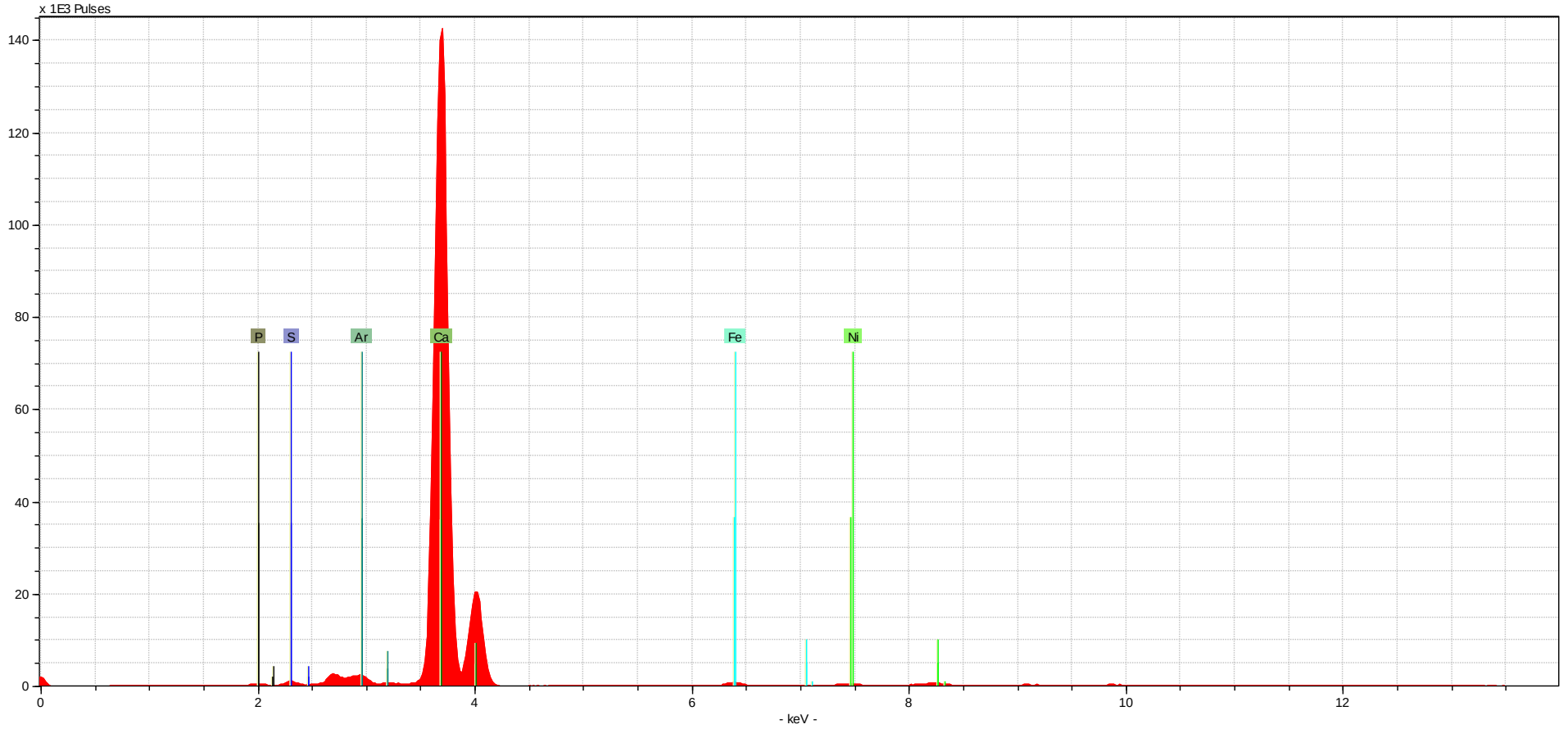

Sample Type	Material	Taphonomic Modifications	File Name/ Sample Name	Identified Elements (in order from L to R)
shell	sand dollar	none	sanddollar1-60sOB	P, S, Ar, Ca, Fe, N

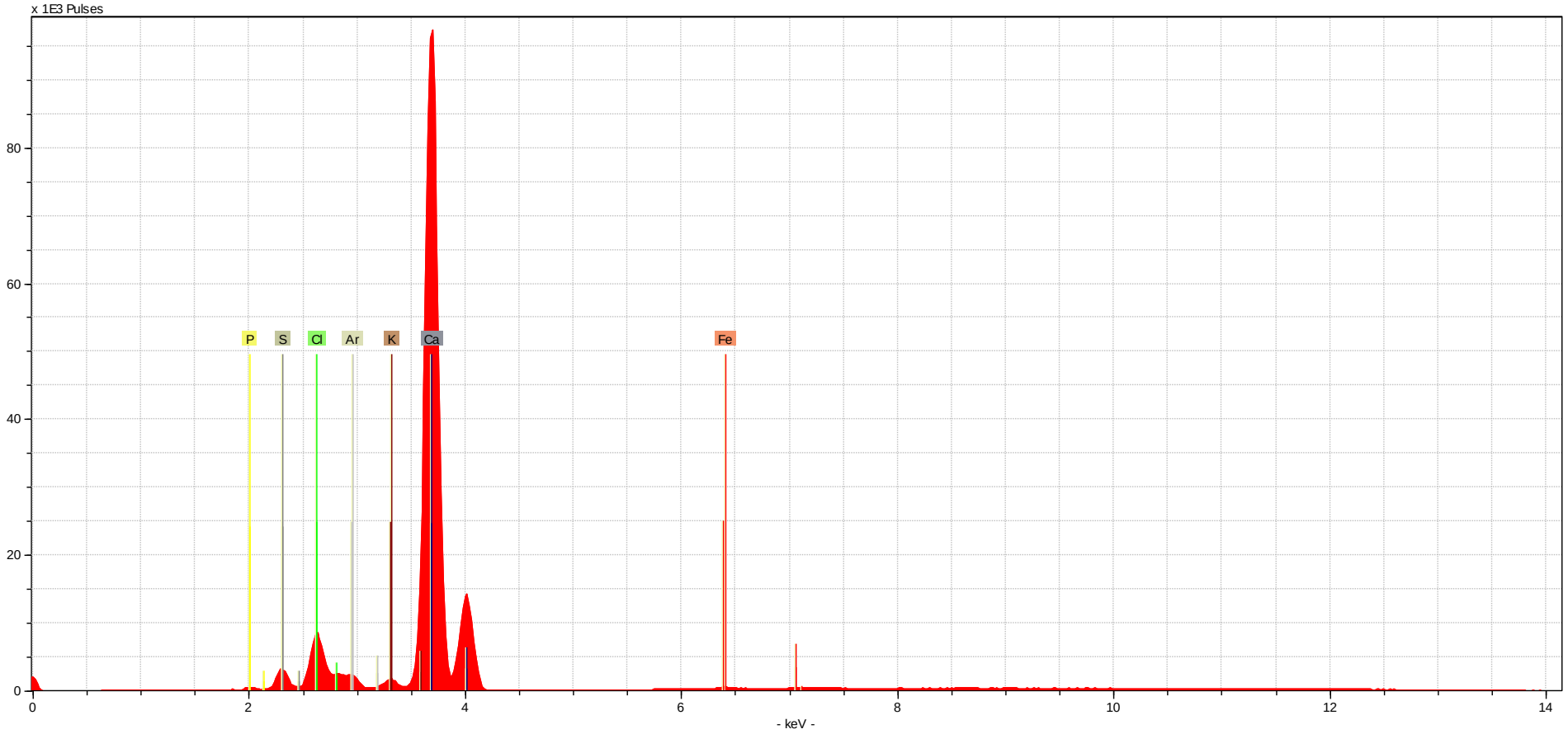

Sample Type	Material	Taphonomic Modifications	File Name/ Sample Name	Identified Elements (in order from L to R)
shell	starfish	none	starfish1-60sOB	P, S, Cl, Ar, K, Ca, Fe

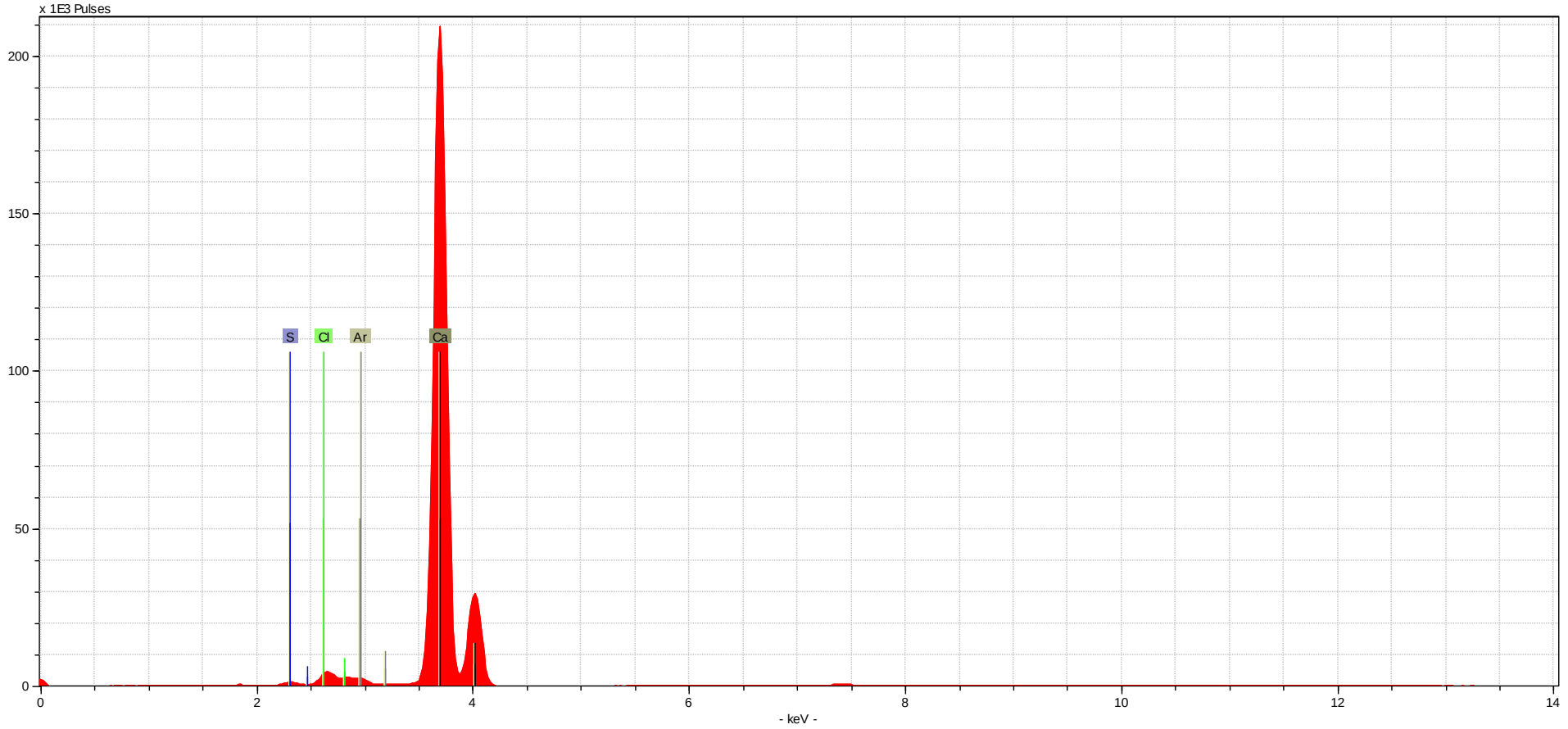

Sample Type	Material	Taphonomic Modifications	File Name/ Sample Name	Identified Elements (in order from L to R)
coral	coral	none	coral1-60sOB	S, Cl, Ar, Ca

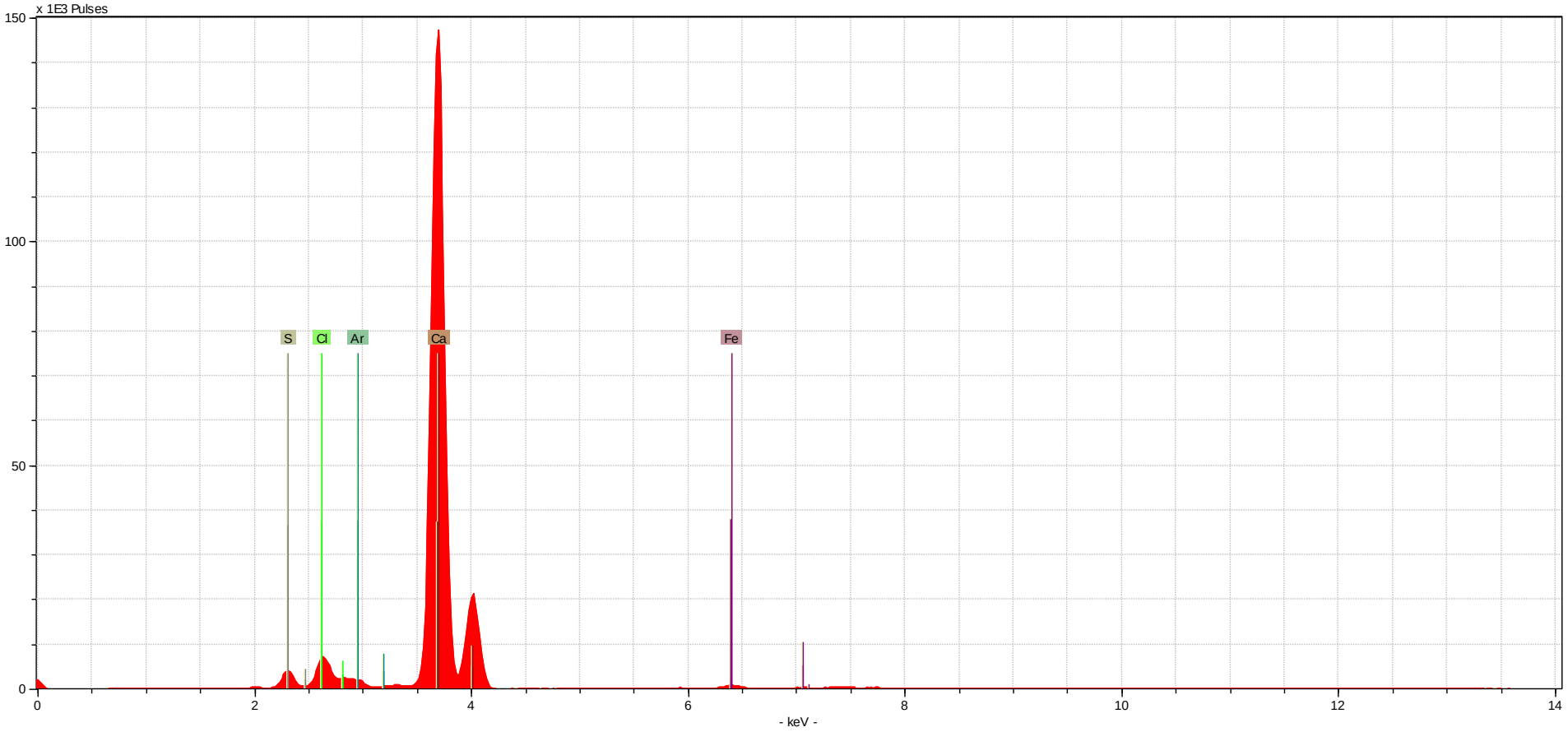

Sample Type	Material	Taphonomic Modifications	File Name/ Sample Name	Identified Elements (in order from L to R)
coral	octocoral	none	octocoral1-60sOB	S, Cl, Ar, Ca, Fe

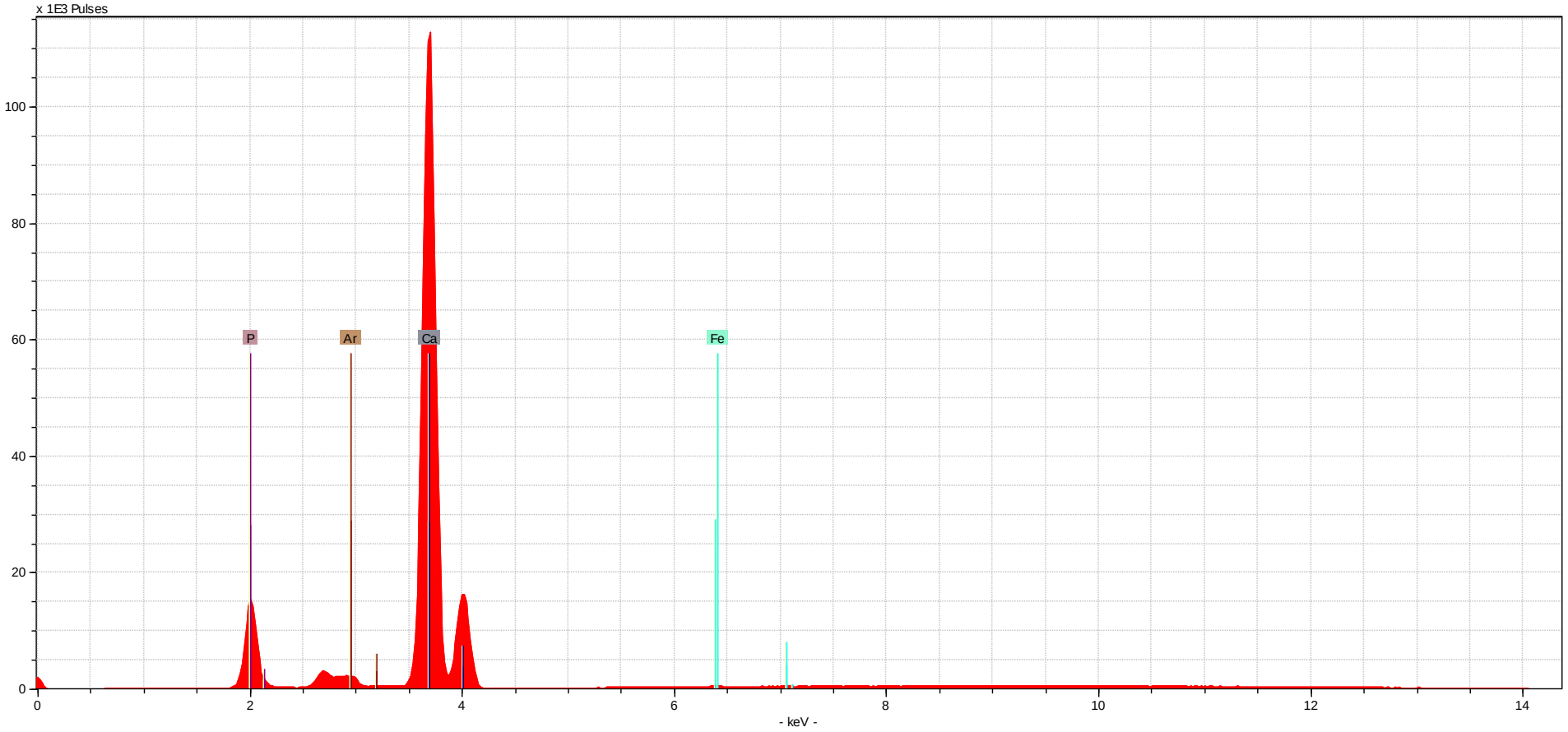

Sample Type	Material	Taphonomic Modifications	File Name/ Sample Name	Identified Elements (in order from L to R)
ivory	flat ivory	none	ivoryflat1-60sOB	P, Ar, Ca, Fe

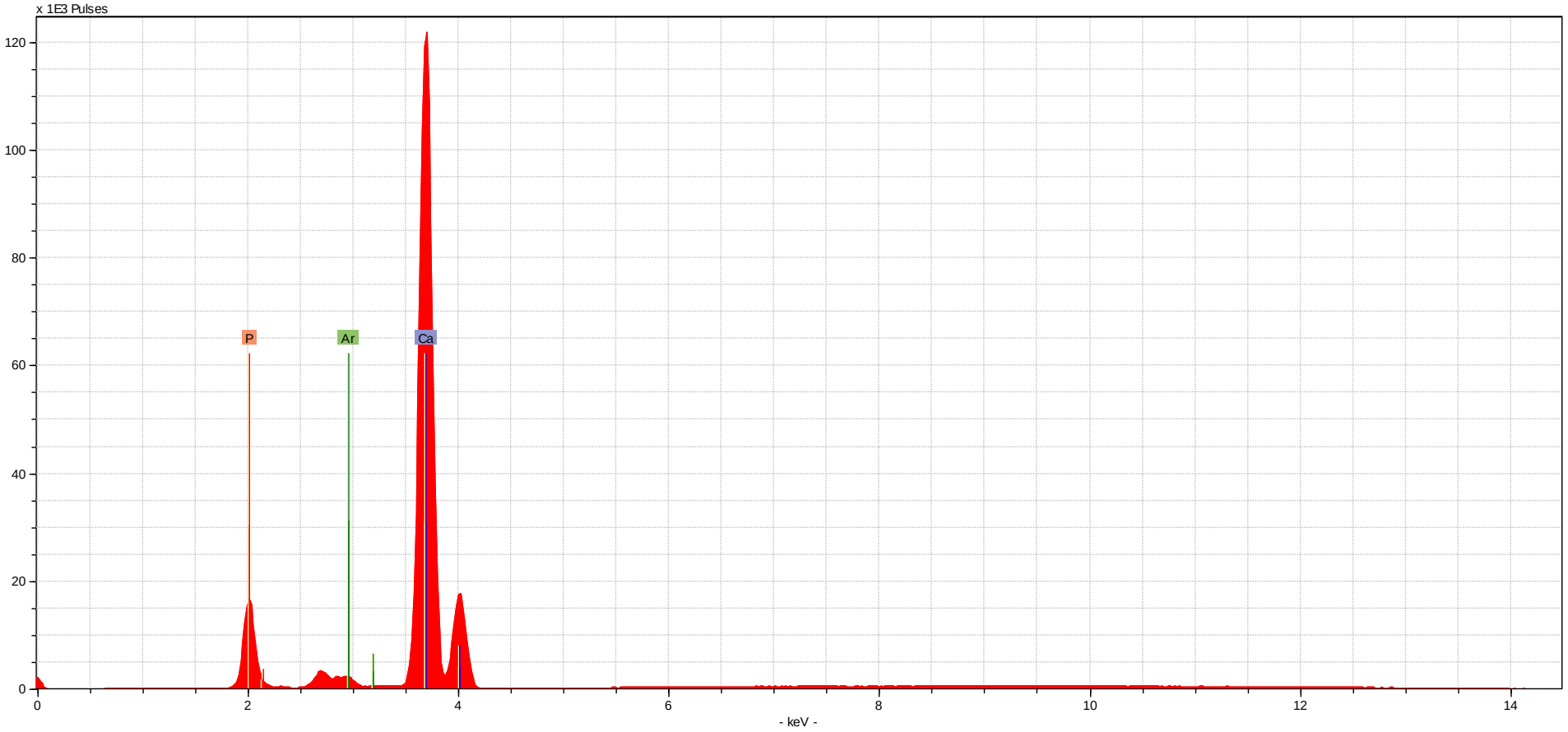

Sample Type	Material	Taphonomic Modifications	File Name/ Sample Name	Identified Elements (in order from L to R)
ivory	rounded ivory	none	ivoryround1-60sOB	P, Ar, Ca

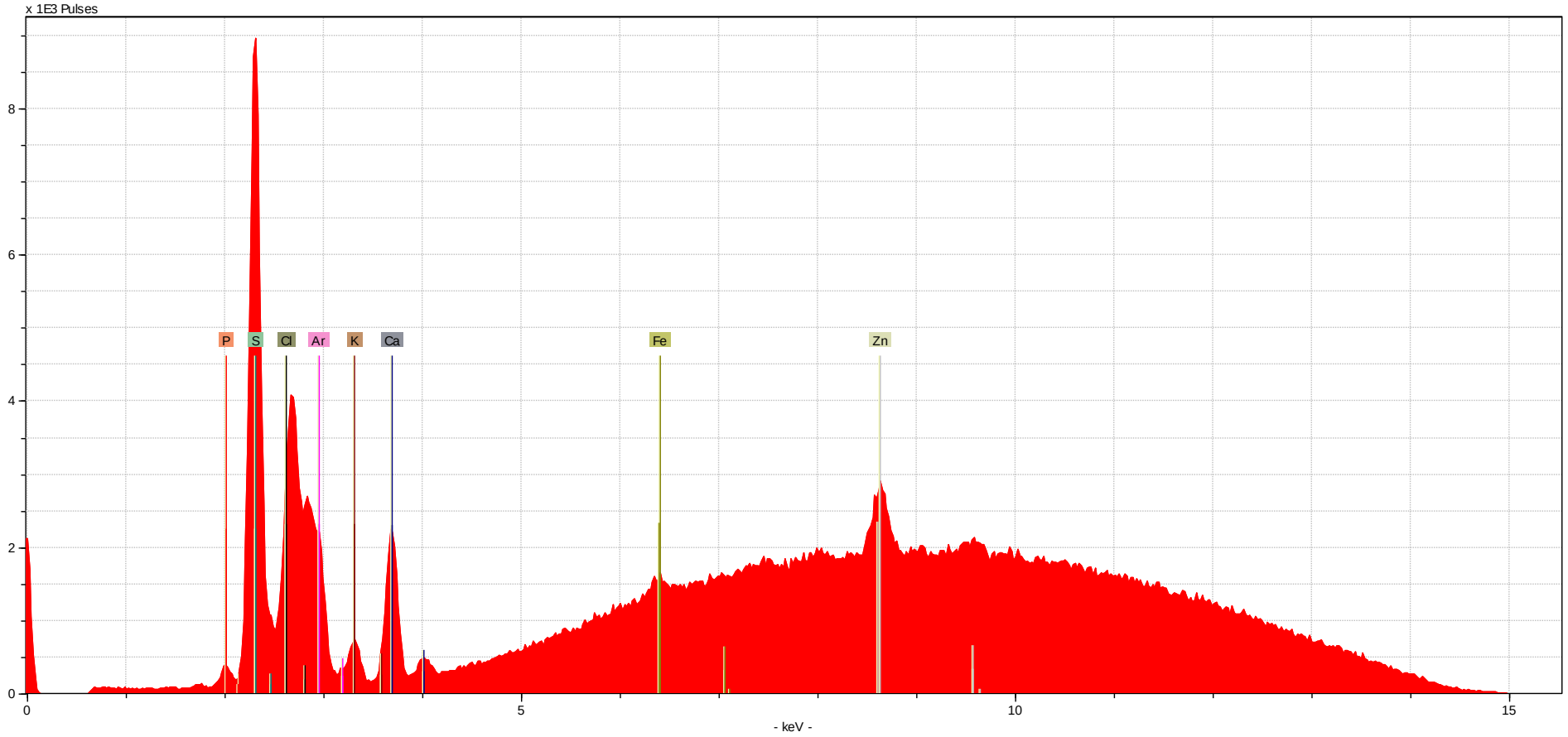

Sample Type	Material	Taphonomic Modifications	File Name/ Sample Name	Identified Elements (in order from L to R)
spur*	spur	none	spur1-60sOB	P, S, Cl, Ar, K, Ca, Fe, Zn

*Note: all spectra collected from this specimen were sorted out during initial processing, as they were found to be "Non Ca-Dominated"

Non-biological Specimens Spectra: shown below is the first spectrum collected from each non-biological sample. The spectrum is shown with the elements identified (autoidentified using ARTAX software).

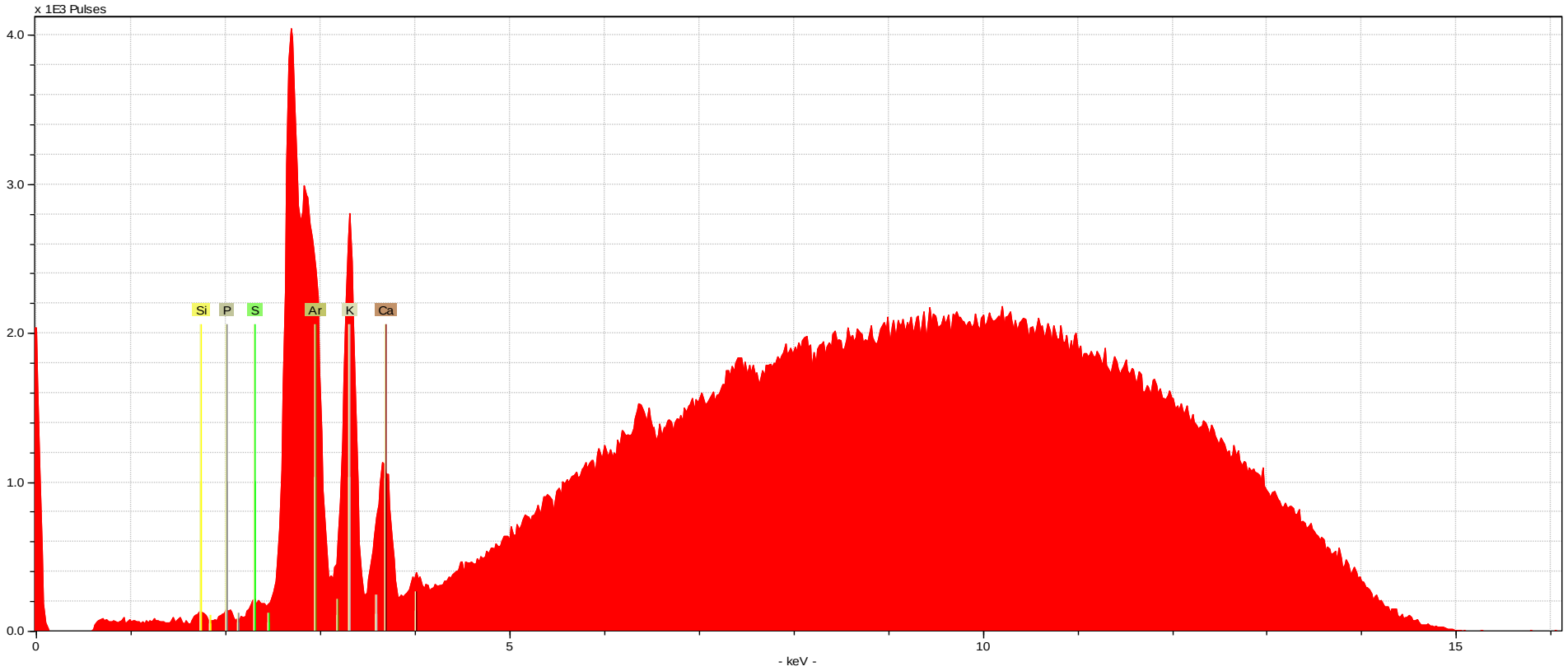

Sample Type	Material	Taphonomic Modifications	File Name/ Sample Name	Identified Elements (in order from L to R)
plant	seeds*	none	acornseed3-60sNB	Si, P, S, Ar, K, Ca

*Note: 4 out of the 8 spectra collected from this specimen were sorted out during initial processing, as they were found to be "Non Ca-Dominated"

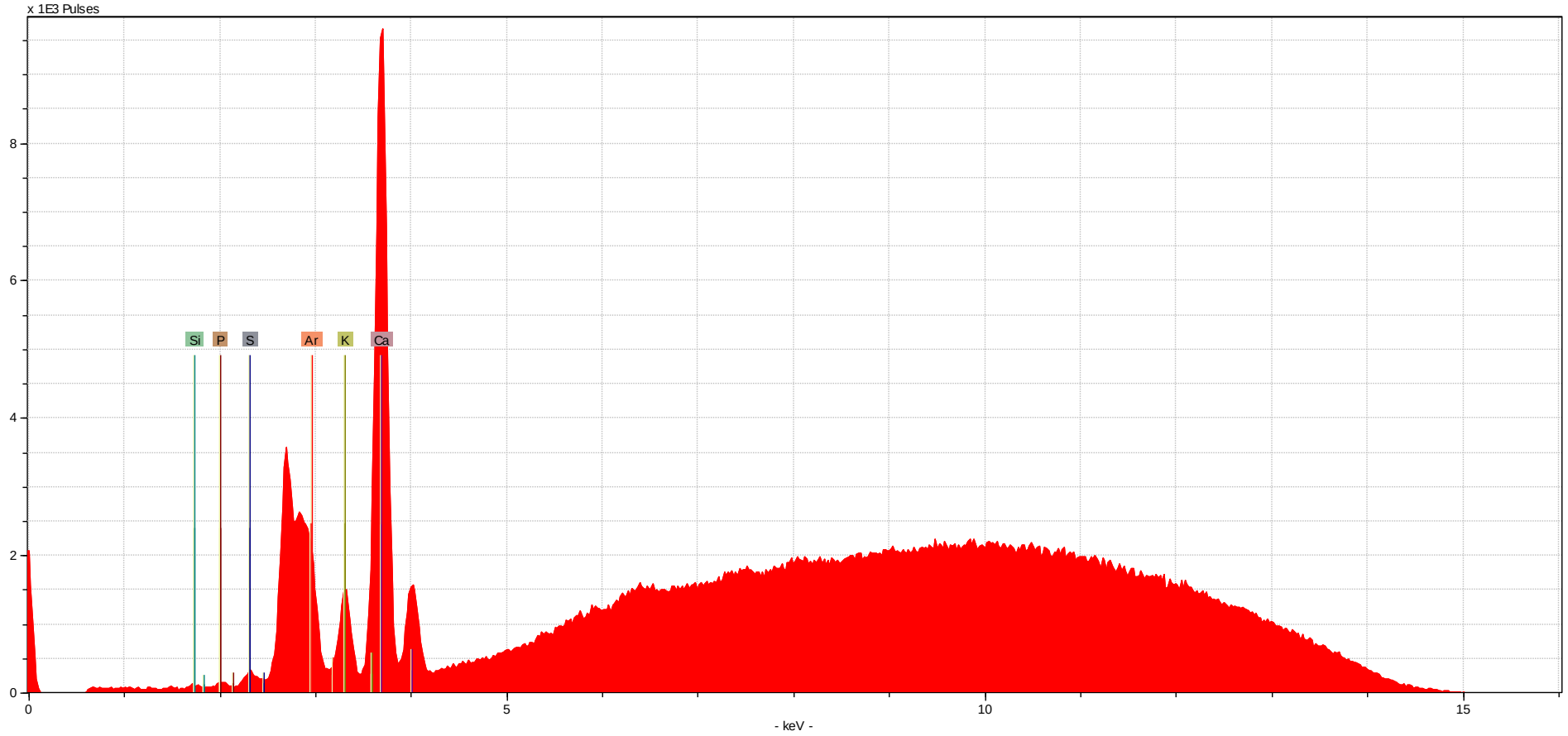

Sample Type	Material	Taphonomic Modifications	File Name/ Sample Name	Identified Elements (in order from L to R)
plant	seeds	none	acornseed1-60sNB	Si, P, S, Ar, K, Ca

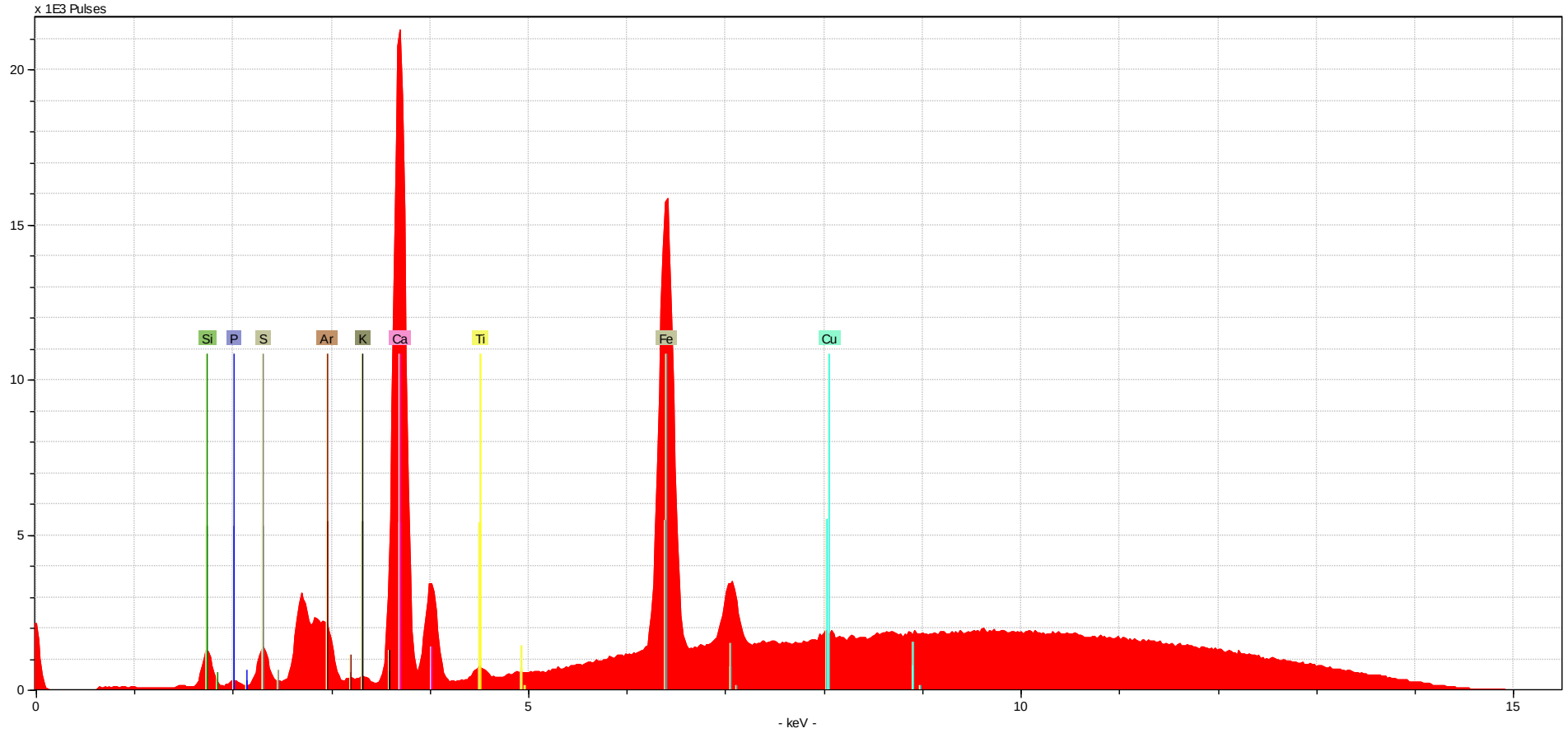

Sample Type	Material	Taphonomic Modifications	File Name/ Sample Name	Identified Elements (in order from L to R)
plant	bark	none	bark1-60sNB	Si, P, S, Ar, K, Ca, Ti, Fe, Cu

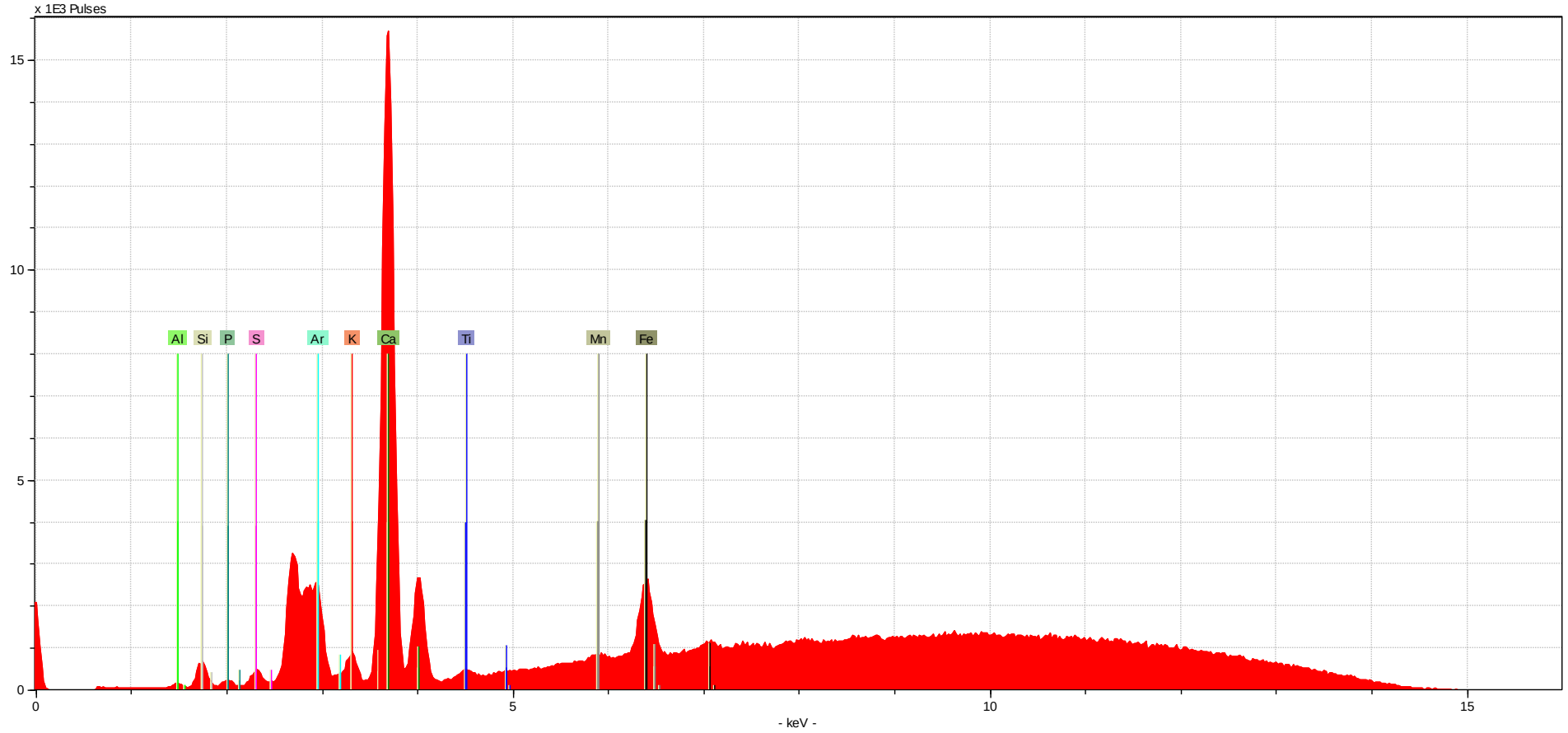

Sample Type	Material	Taphonomic Modifications	File Name/ Sample Name	Identified Elements (in order from L to R)
plant	root	none	root1-60sNB	Al, Si, P, S, Ar, K, Ca, Ti, Mn, Fe

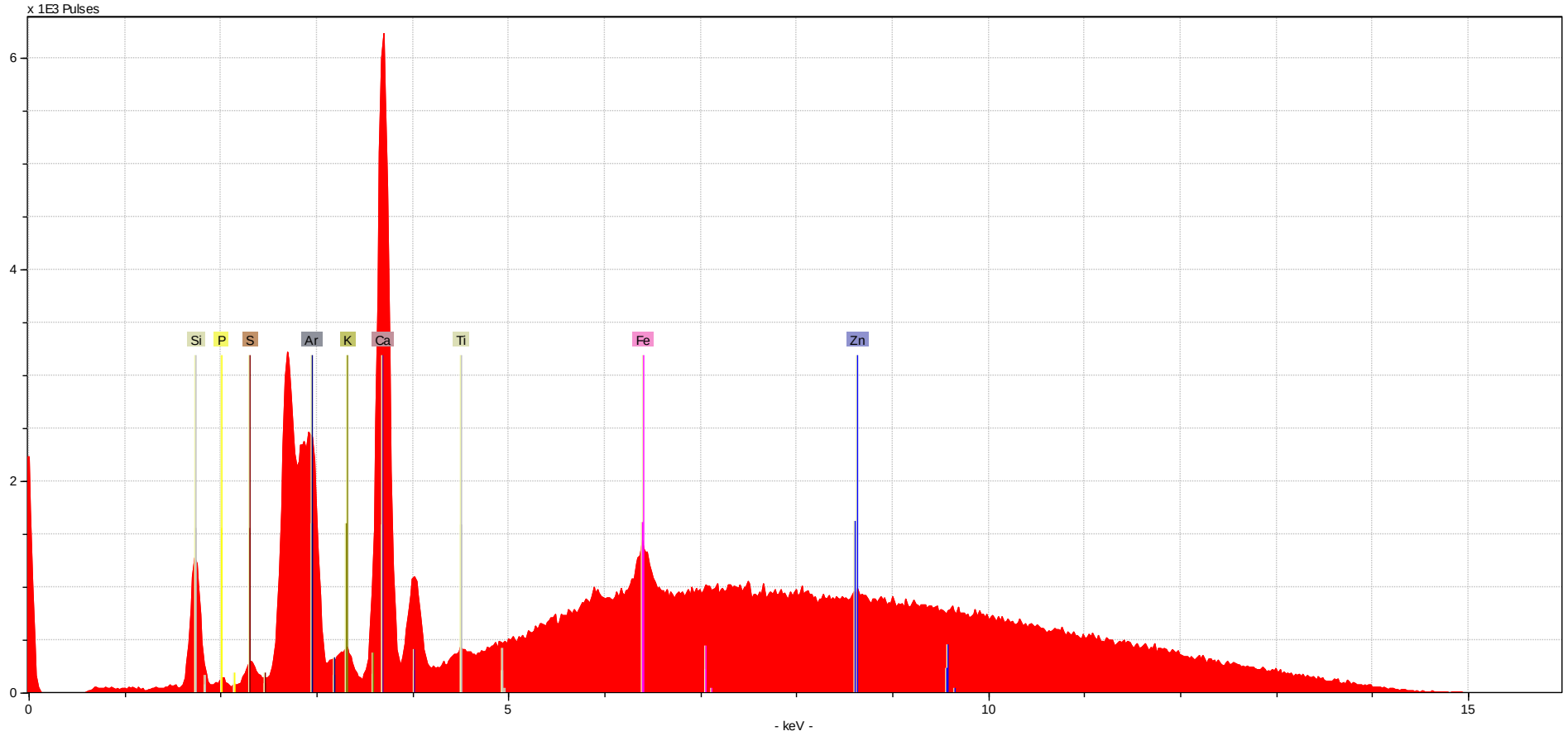

Sample Type	Material	Taphonomic Modifications	File Name/ Sample Name	Identified Elements (in order from L to R)
plant	twig	none	stick1-60sNB	Si, P, S, Ar, K, Ca, Ti, Fe, Zn

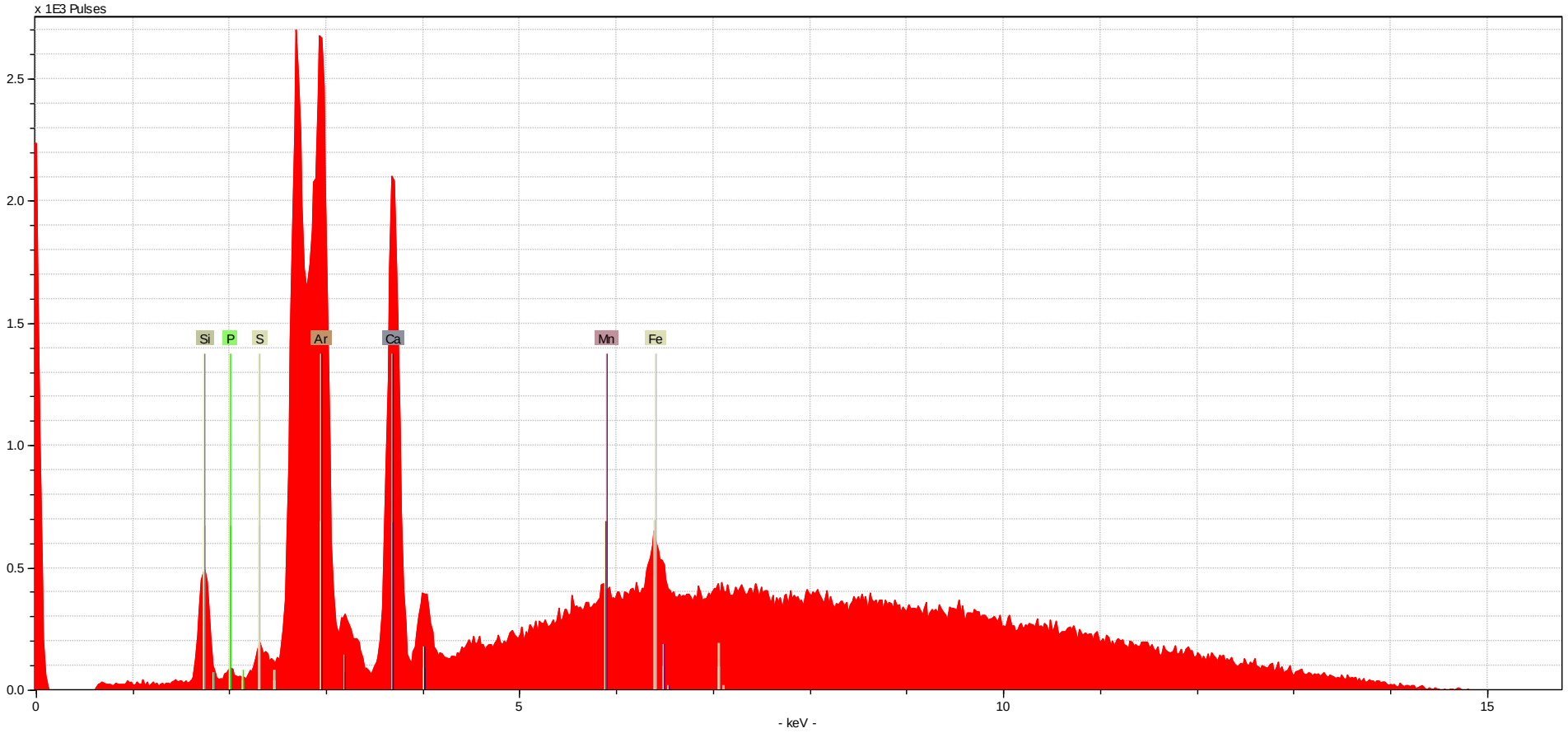

Sample Type	Material	Taphonomic Modifications	File Name/ Sample Name	Identified Elements (in order from L to R)
plant	twig	none	stick4-60sNB*	Si, P, S, Ar, Ca, Mn, Fe

*Note: A single spectra collected from the twig specimen (shown here) was sorted out during initial processing, as it was found to be "Non Ca-Dominated"

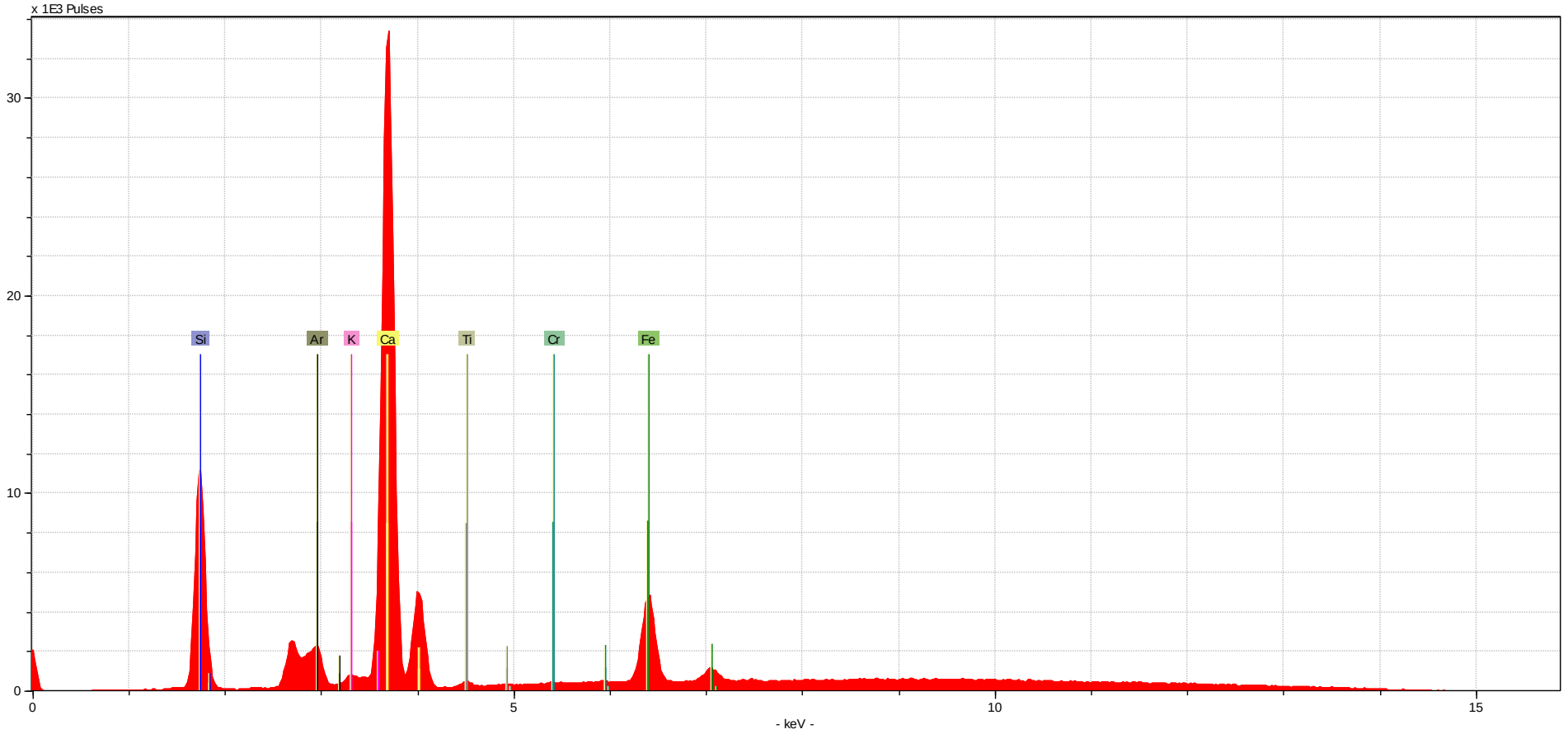

Sample Type	Material	Taphonomic Modifications	File Name/ Sample Name	Identified Elements (in order from L to R)
glass	beer bottle	none	beerbottle1-60sNB	Si, Ar, K, Ca, Ti, Cr, Fe

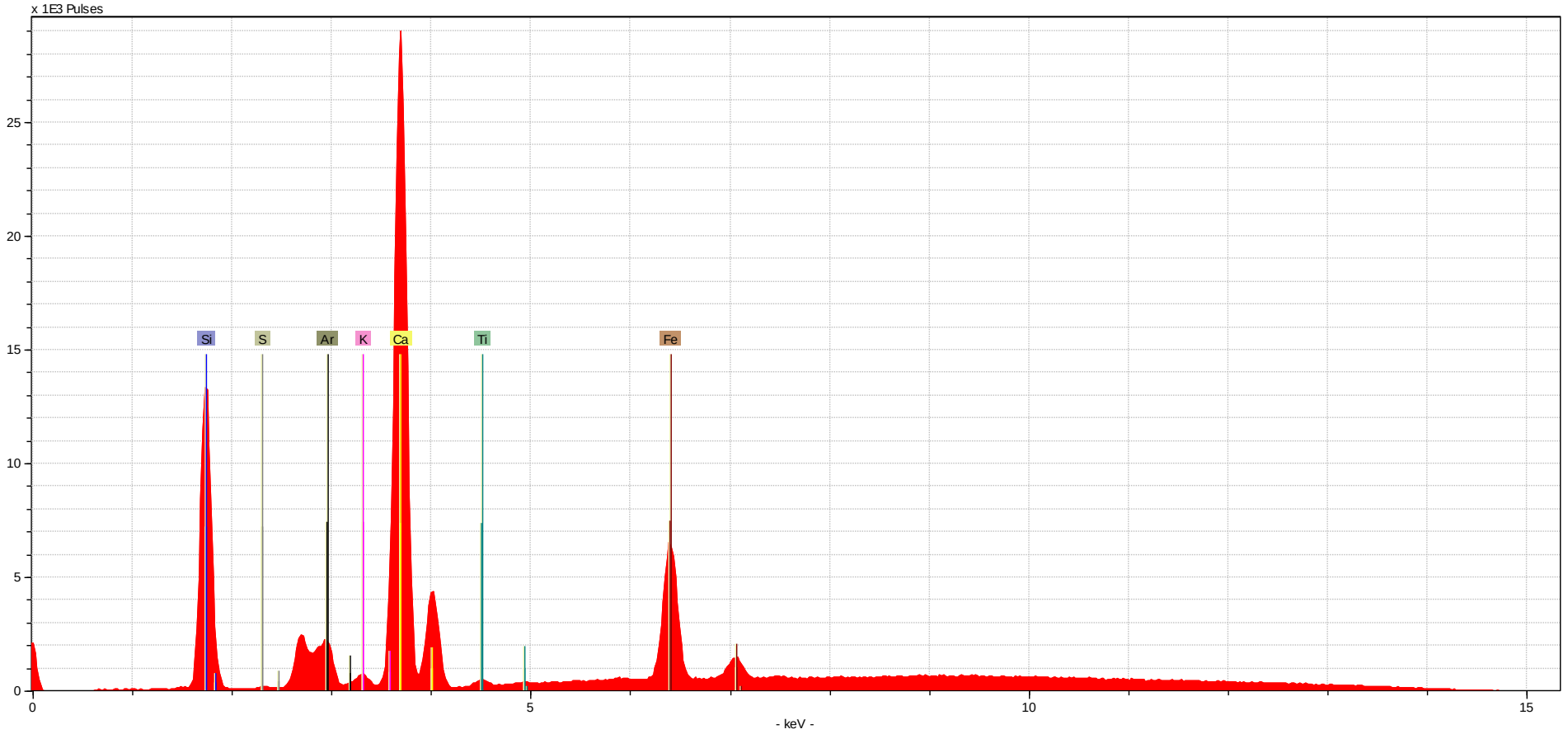

Sample Type	Material	Taphonomic Modifications	File Name/ Sample Name	Identified Elements (in order from L to R)
glass	float glass	none	floatglass1-60sNB	Si, S, Ar, K, Ca, Ti, Fe

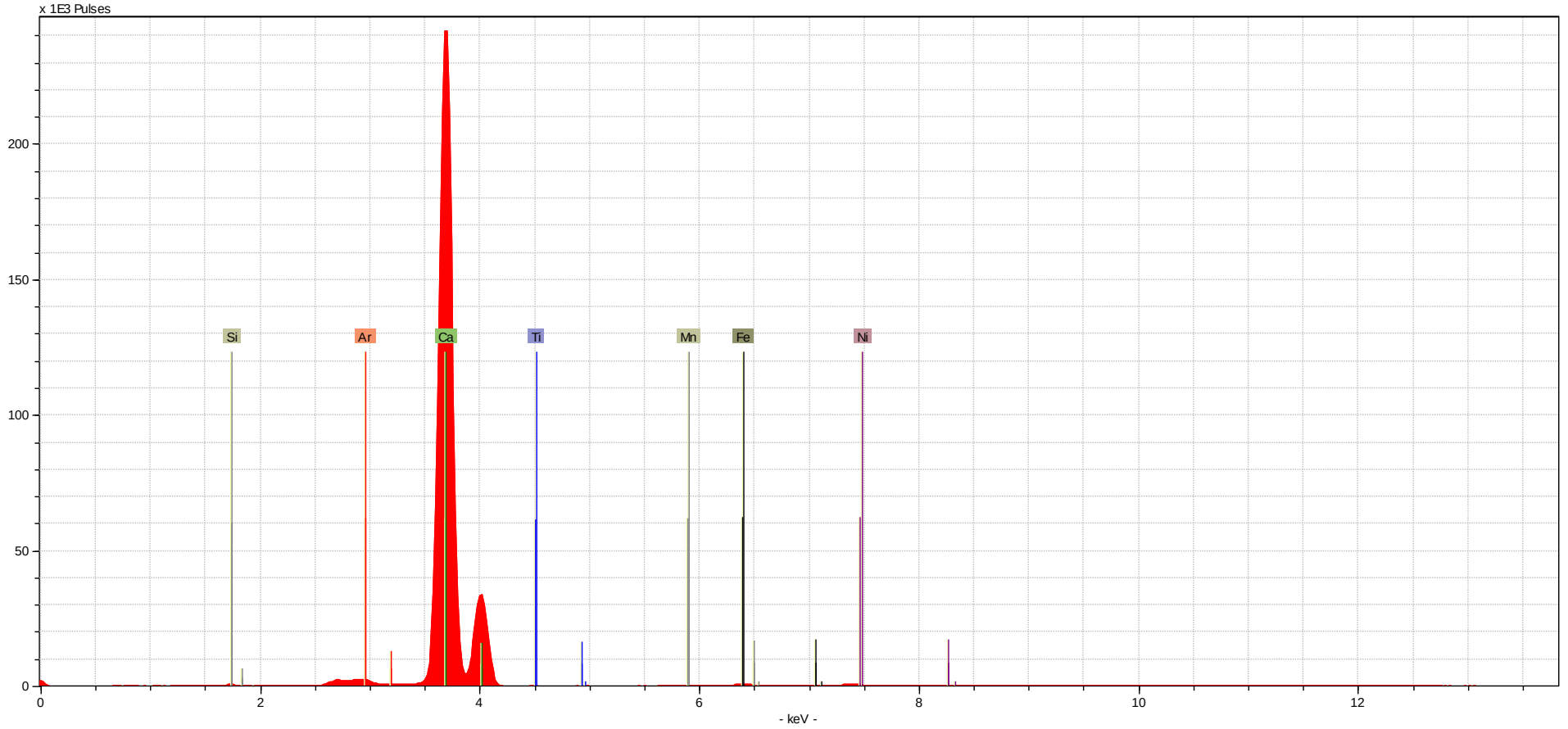

Sample Type	Material	Taphonomic Modifications	File Name/ Sample Name	Identified Elements (in order from L to R)
limestone	limestone	none	limestone1-60sNB	Si, Ar, Ca, Ti, Mn, Fe, Ni

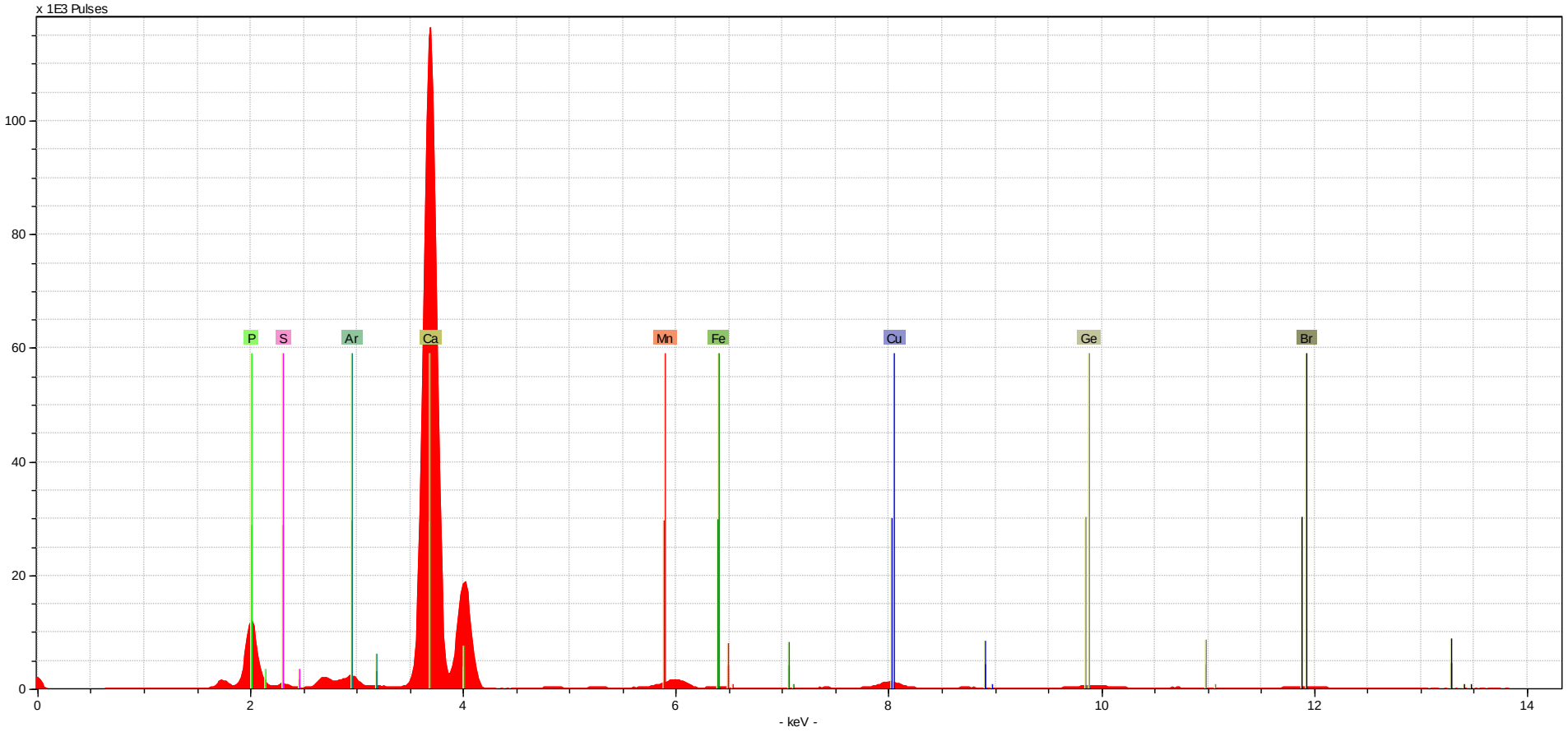

Sample Type	Material	Taphonomic Modifications	File Name/ Sample Name	Identified Elements (in order from L to R)
rock apatite	rock apatite	none	rockapatite1-60sNB	P, S, Ar, Ca, Mn, Fe, Cu, Ge, Br

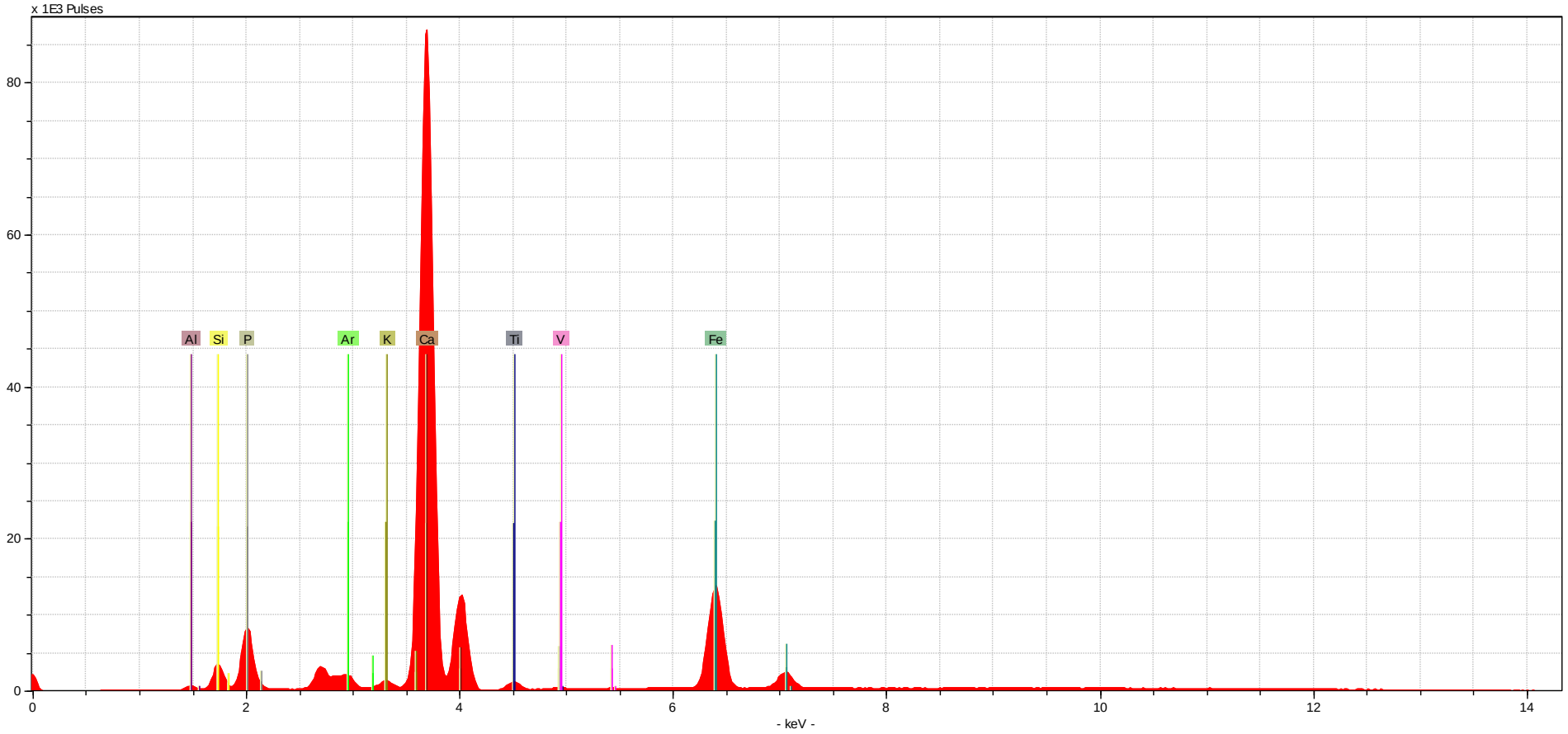

Sample Type	Material	Taphonomic Modifications	File Name/ Sample Name	Identified Elements (in order from L to R)
rock phosphate	rock phosphate	none	rockphosphate1-60sNB	Al, Si, P, Ar, K, Ca, Ti, V, Fe

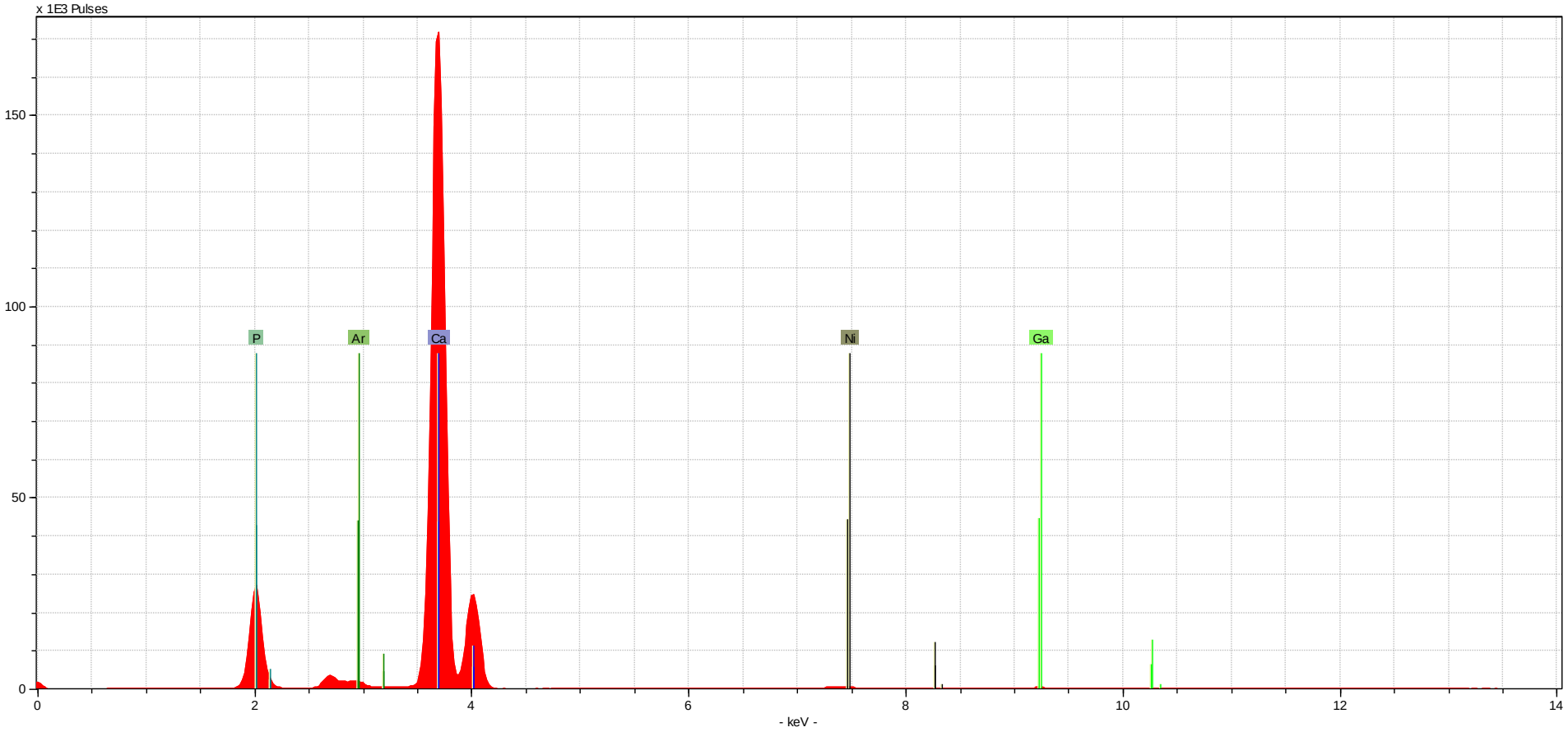

Sample Type	Material	Taphonomic Modifications	File Name/ Sample Name	Identified Elements (in order from L to R)
synthetic hydroxyapatite	synthetic hydroxyapatite	none	synhydapatite1-60sNB	P, Ar, Ca, Ni, Ga

Spectra from Taphonomically Altered Materials: shown below is the first spectrum collected from each sample. The spectrum is shown with the elements identified (autoidentified using ARTAX software).

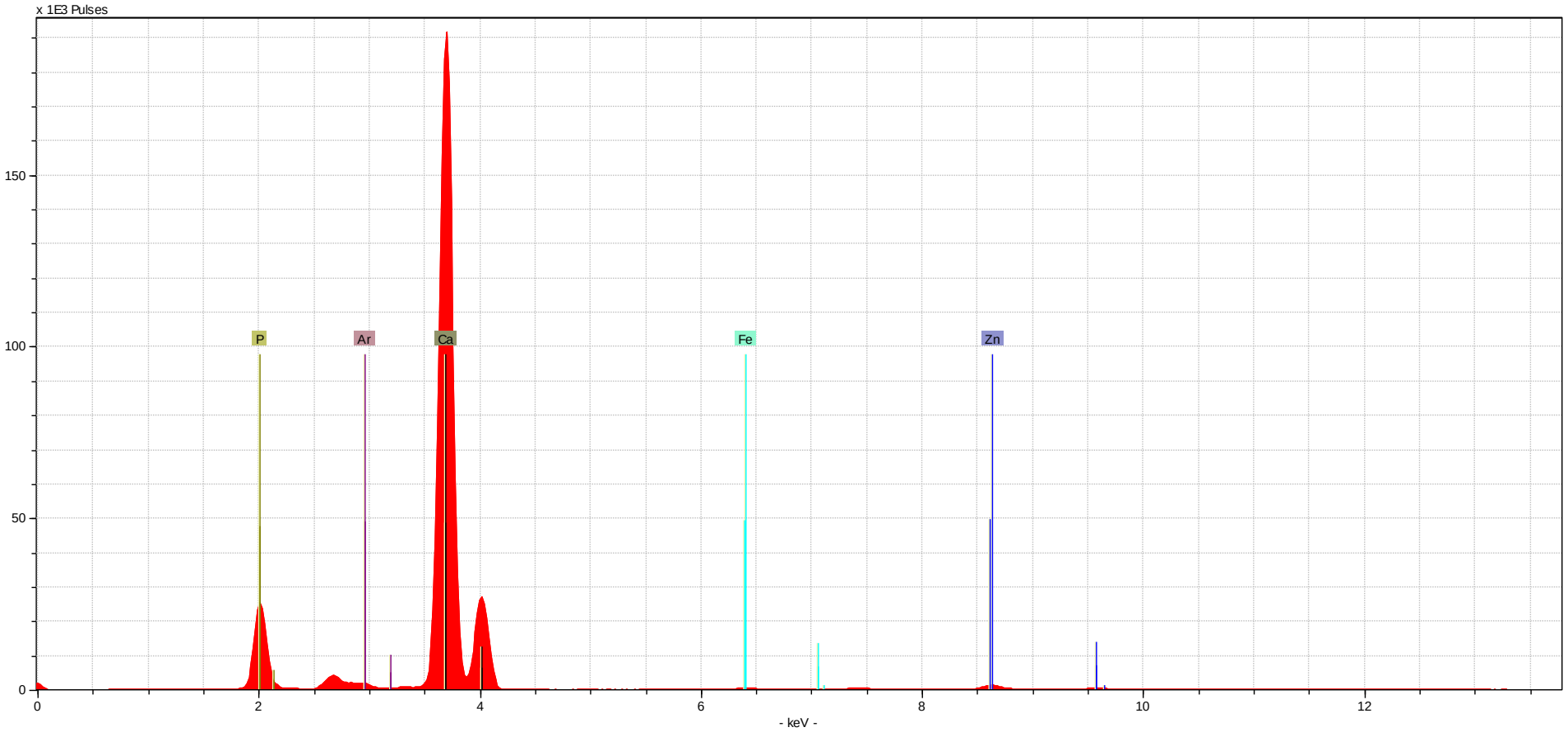

Sample Type	Bone Element	Biological Age	Time Period	Taphonomic Modifications	File Name/ Sample Name	Identified Elements (in order from L to R)
human	molar, lower	adult	modern	burned	burnedmolarL1-60sH	P, Ar, Ca, Fe, Zn

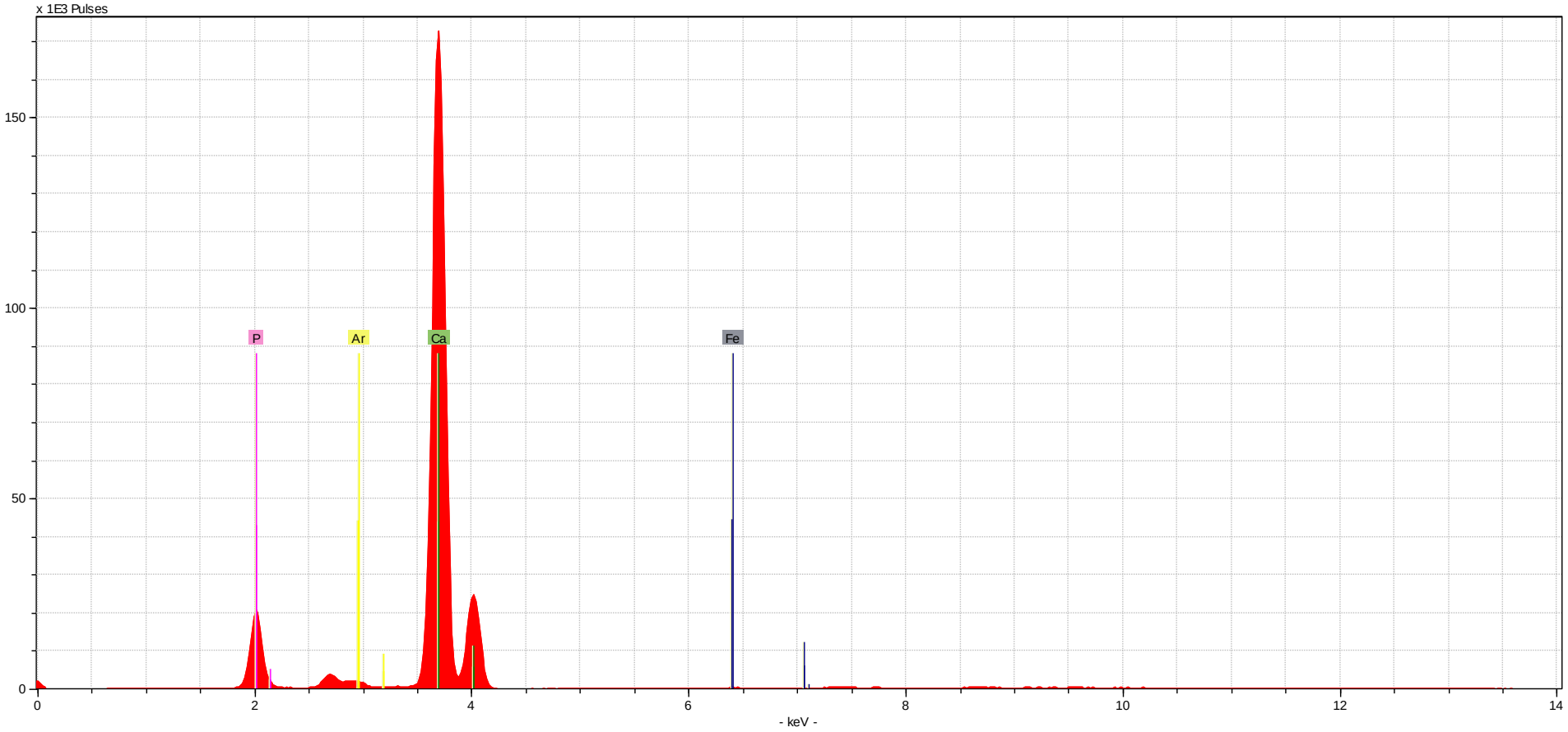

Sample Type	Bone Element	Biological Age	Time Period	Taphonomic Modifications	File Name/ Sample Name	Identified Elements (in order from L to R)
human	molar, upper	adult	modern	burned	burnedmolarU1-60sH	P, Ar, Ca, Fe

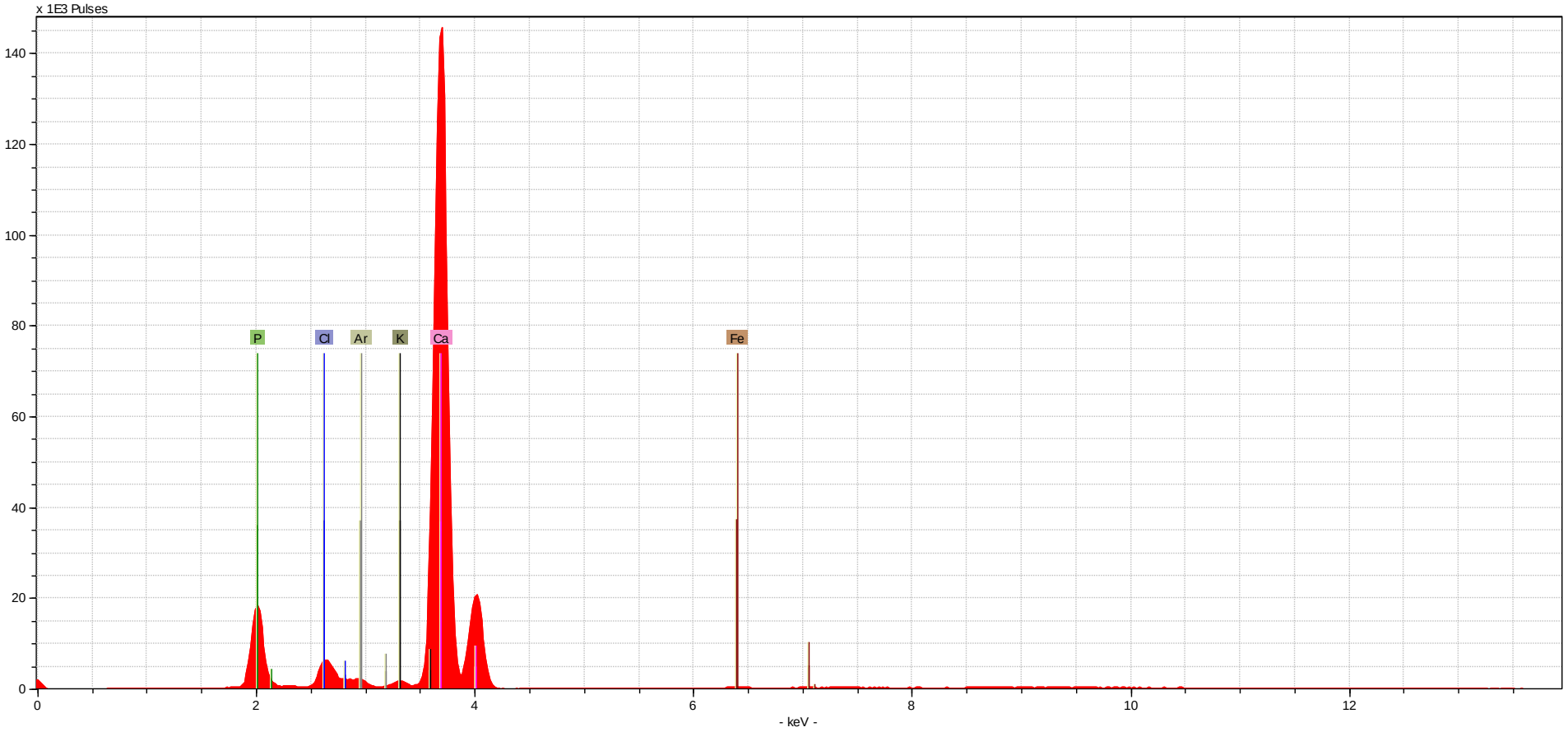

Sample Type	Bone Element	Biological Age	Time Period	Taphonomic Modifications	File Name/ Sample Name	Identified Elements (in order from L to R)
human	fibula	adult	modern	burned	burnedfibula1-60sH	P, Cl, Ar, K, Ca, Fe

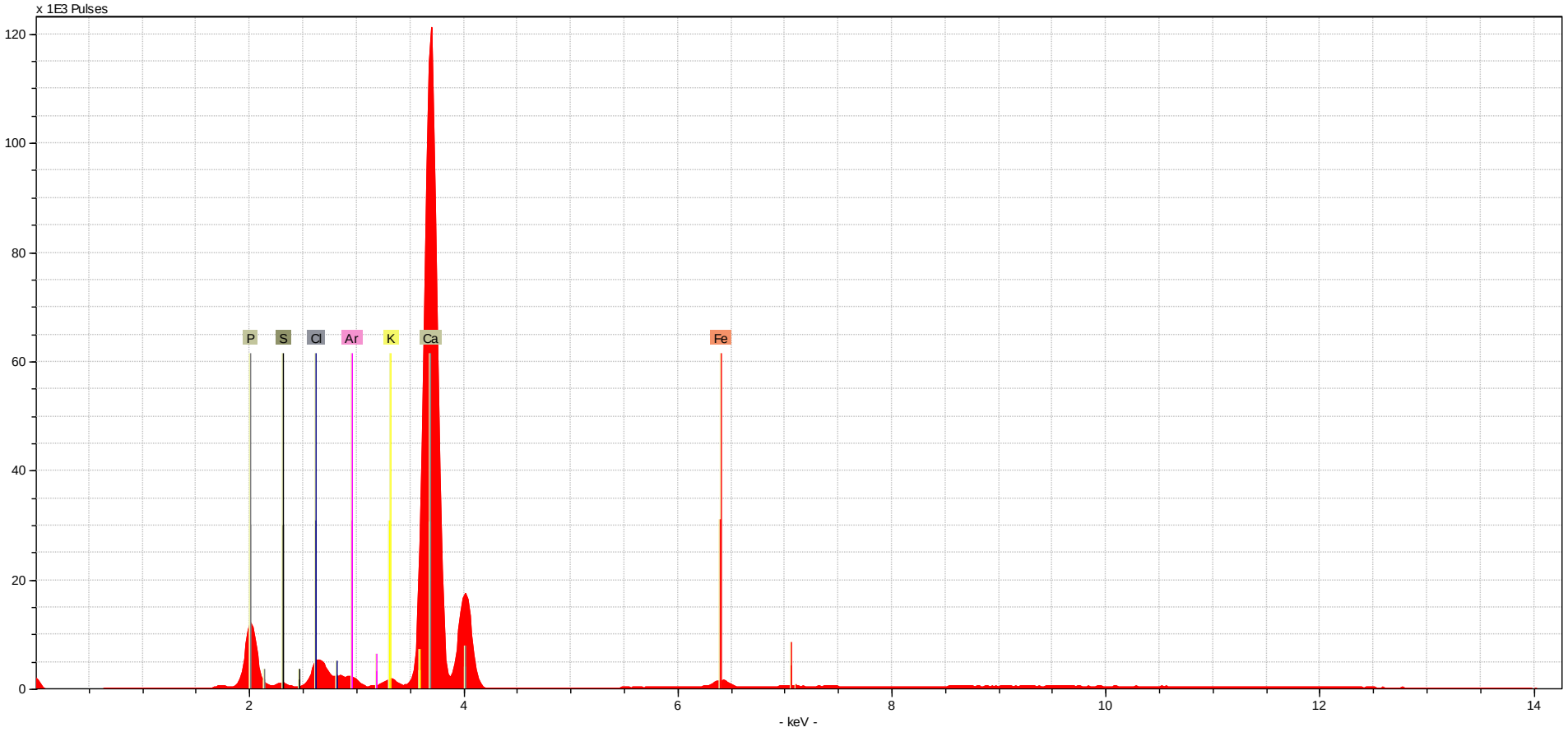

Sample Type	Bone Element	Biological Age	Time Period	Taphonomic Modifications	File Name/ Sample Name	Identified Elements (in order from L to R)
human	femur	juvenile	ancient	ancient, dating to AD 50-450, from the Dakhleh Oasis, Egypt	juvfemur1-60sH	P, S, Cl, Ar, K, Ca, Fe

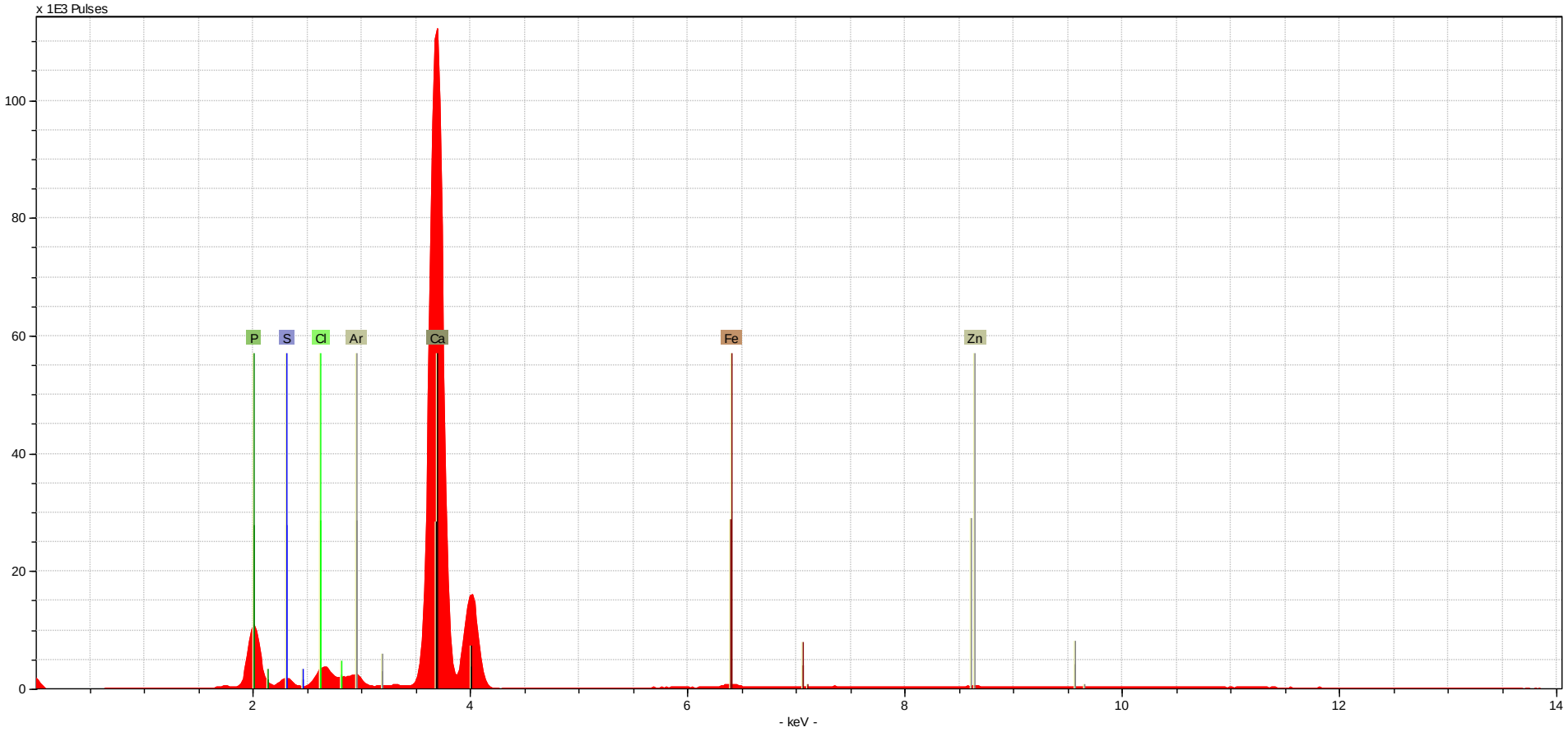

Sample Type	Bone Element	Biological Age	Time Period	Taphonomic Modifications	File Name/ Sample Name	Identified Elements (in order from L to R)
human	metacarpal	adult	modern	weathered	weatheredMC1-60sH	P, S, Cl, Ar, Ca, Fe, Zn

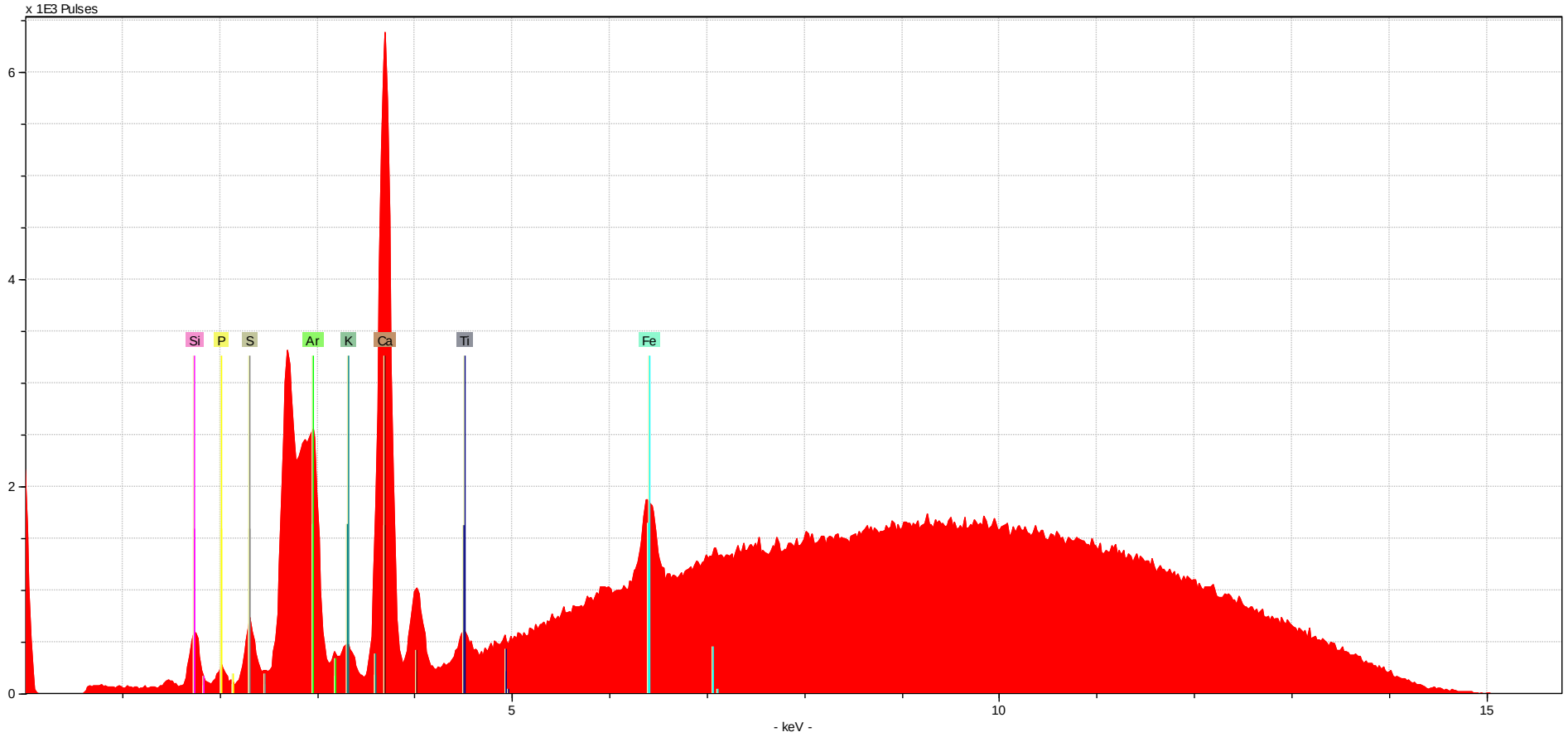

Sample Type	Material	Taphonomic Modifications	File Name/ Sample Name	Identified Elements (in order from L to R)
plant	wood	burned	burnedwood1-60sNB	Si, P, S, Ar, K, Ca, Ti, Fe

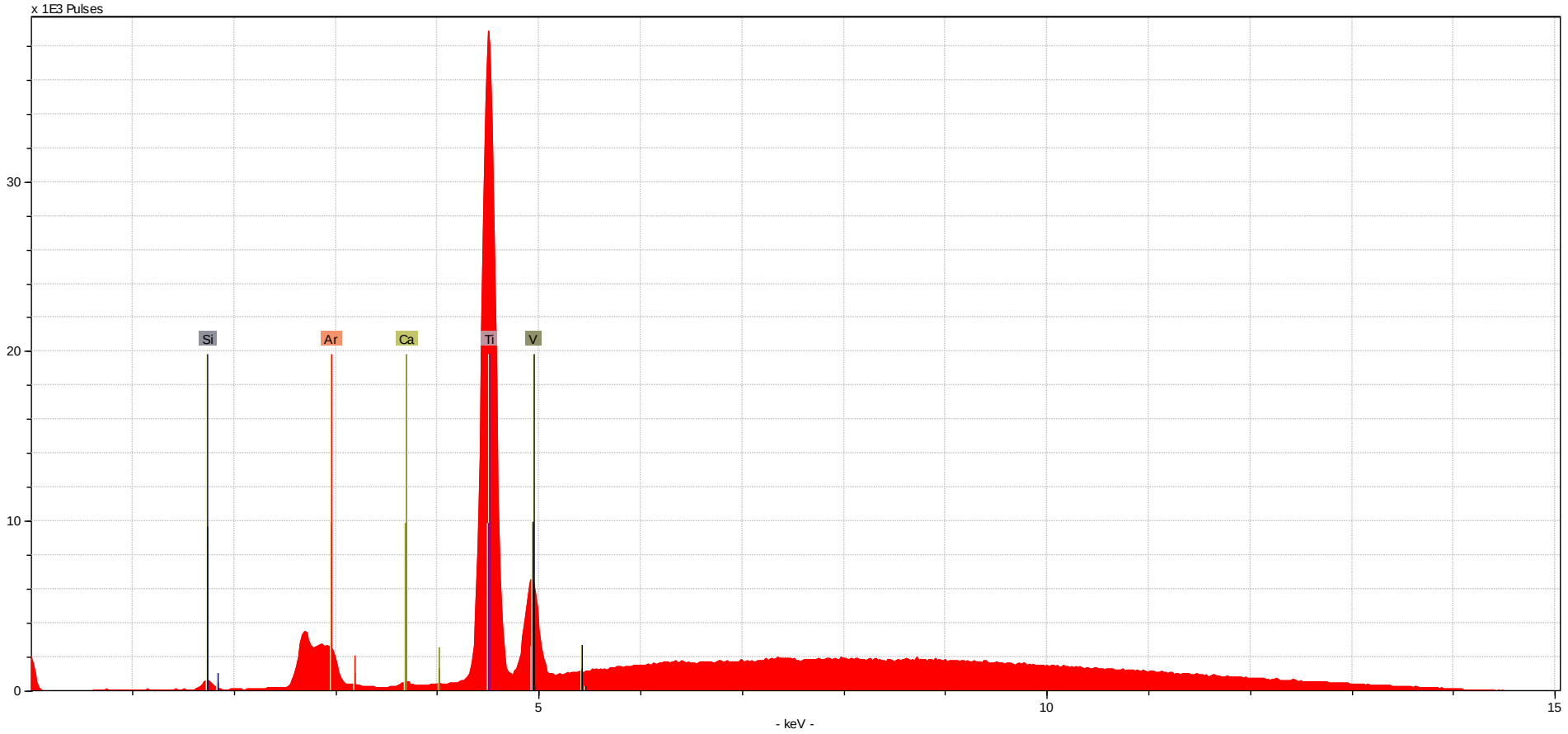

Sample Type	Material	Taphonomic Modifications	File Name/ Sample Name	Identified Elements (in order from L to R)
plastic	plastic*	burned	burnedplastic1-60sNB	Si, Ar, Ca, Ti, V

*Note: all spectra collected from this specimen were sorted out during initial processing, as they were found to be “Non Ca-Dominated”

APPENDIX E: R CODE

DATA SETUP, LDA, QDA, HCA:

#The dataset ("d") was saved as a .csv file under the heading "final dataset for Rv3.csv" in which multiple classes were established as separate columns
#Class 1: B and NB categories
#Class 2: B, Plant, Glass, Rapatite, Rphosphate, Shapatite, Carbonates, Ivories
#Class 3: H, NH, Plant, Glass, Rapatite, Rphosphate, Shapatite, Carbonates, Ivories
#Class 4: B, Tooth, Burned Bone, JuvBone, WeatheredBone, Plant, Glass, Rapatite, Rphosphate, Shapatite, Carbonates, Ivory, Octocoral, BurnedPlant, Limestone
#Class 5: H, NH, Tooth, Burned Bone, JuvBone, WeatheredBone, Plant, Glass, Rapatite, Rphosphate, Shapatite, Carbonates, Ivory, Octocoral, BurnedPlant, Limestone
#The following R code provides steps for PCA, LDA and QDA
#PCA provides # of factors using DRMAD and scree plot
#LDA and QDA are based on 3 PCs but can be modified for any number of PCs (6 PC LDA is provided as example)

```
d <- read.table("final dataset for Rv2.csv", sep=",", header=T)
dd <- dim(d)
 source("myPCAv2.r")
myPCA(d[,4:dd[2]], NM="s")

library(lattice)
library(MASS)
```

#LDA

```
#LDA for Class 1
Rlda <- data.frame(class=factor(d$Class.1), pc1=RR[,1],pc2=RR[,2],pc3=RR[,3])
Rlda
pri <- array(1/length(levels(factor(Rlda$class))),length(levels(factor(Rlda$class))))
fit <- lda(class ~.,Rlda, CV = TRUE, na.action = "na.omit", prior=pri)
ct <- table(Rlda$class, fit$class)
ct
diag(prop.table(ct, 1))

# total percent correct
sum(diag(prop.table(ct)))

#Scatterplot matrix of PCs1-3 for Class 1
splom(Rlda[,c(2,3,4)], groups=Rlda$class,panel=panel.superpose, key = simpleKey(columns =
2, title="Source", levels(Rlda$class) ))

#LDA Class Boundaries for Class 1
library(klaR)
```

```
par(mfrow=c(2,2))
partimat(class~pc1+pc2+pc3,data=Rlda,method="lda",nplots.hor=2,nplots.vert=2)
```

```
#6 PC LDA for Class 1
Rlda.6pc <- data.frame(class=factor(d$Class.1),
pc1=RR[,1],pc2=RR[,2],pc3=RR[,3],pc4=RR[,4],pc5=RR[,5],pc6=RR[,6])
pri <- array(1/length(levels(factor(Rlda$Class.1))),length(levels(factor(Rlda$Class.1))))
fit <- lda(class ~.,Rlda.6pc, CV = TRUE, na.action = "na.omit", prior=pri)
ct <- table(Rlda.6pc$class, fit$class)
ct
diag(prop.table(ct, 1))

# total percent correct
sum(diag(prop.table(ct)))

#Scatterplot matrix of PCs1-6 for Class 1
splom(Rlda.6pc[,c(2,3,4)], groups=Rlda.6pc$class,panel=panel.superpose, key =
simpleKey(columns = 2, title="Source", levels(Rlda.6pc$class) ))

#LDA Class Boundaries for Class 1 (6PCs)
library(klaR)
par(mfrow=c(2,2))
partimat(class~pc1+pc2+pc3+pc4+pc5+pc6,data=Rlda.6pc,method="lda",nplots.hor=2,nplots.ve
rt=2)
```

```
#LDA for Class 2
Rlda2 <- data.frame(class=factor(d$Class.2), pc1=RR[,1],pc2=RR[,2],pc3=RR[,3])
Rlda2
pri2 <- array(1/length(levels(factor(Rlda2$class))),length(levels(factor(Rlda2$class))))
fit2 <- lda(class ~.,Rlda2, CV = TRUE, na.action = "na.omit", prior=pri2)
ct <- table(Rlda2$class, fit2$class)
ct
diag(prop.table(ct, 1))
# total percent correct
sum(diag(prop.table(ct)))
splom(Rlda2[,c(2,3,4)], groups=Rlda2$class,panel=panel.superpose, key = simpleKey(columns
= 2, title="Source", levels(Rlda2$class) ))
library(klaR)
par(mfrow=c(2,2))
partimat(class~pc1+pc2+pc3,data=Rlda2,method="lda",nplots.hor=2,nplots.vert=2)
```

```
#LDA for Class 3
Rlda3 <- data.frame(class=factor(d$Class.3), pc1=RR[,1],pc2=RR[,2],pc3=RR[,3])
Rlda3
```

```
pri3 <- array(1/length(levels(factor(Rlda3$class))),length(levels(factor(Rlda3$class))))
fit3 <- lda(class ~.,Rlda3, CV = TRUE, na.action = "na.omit", prior=pri3)
ct <- table(Rlda3$class, fit3$class)
ct
diag(prop.table(ct, 1))

# total percent correct
sum(diag(prop.table(ct)))

#Scatterplot matrix of PCs1-3 for Class 3
splom(Rlda3[,c(2,3,4)], groups=Rlda3$class,panel=panel.superpose, key = simpleKey(columns
= 2, title="Source", levels(Rlda3$class) ))

#LDA Class Boundaries for Class 3
library(klaR)
par(mfrow=c(2,2))
partimat(class~pc1+pc2+pc3,data=Rlda3,method="lda",nplots.hor=2,nplots.vert=2)
```

```
#LDA for Class 4
Rlda4 <- data.frame(class=factor(d$Class.4), pc1=RR[,1],pc2=RR[,2],pc3=RR[,3])
Rlda4
pri4 <- array(1/length(levels(factor(Rlda4$class))),length(levels(factor(Rlda4$class))))
fit4 <- lda(class ~.,Rlda4, CV = TRUE, na.action = "na.omit", prior=pri4)
ct <- table(Rlda4$class, fit4$class)
ct
diag(prop.table(ct, 1))

# total percent correct
sum(diag(prop.table(ct)))

#Scatterplot matrix of PCs1-3 for Class 4
splom(Rlda4[,c(2,3,4)], groups=Rlda4$class,panel=panel.superpose, key = simpleKey(columns
= 2, title="Source", levels(Rlda4$class) ))

#LDA Class Boundaries for Class 4
library(klaR)
par(mfrow=c(2,2))
partimat(class~pc1+pc2+pc3,data=Rlda4,method="lda",nplots.hor=2,nplots.vert=2)
```

```
#LDA for Class 5
Rlda5 <- data.frame(class=factor(d$Class.5), pc1=RR[,1],pc2=RR[,2],pc3=RR[,3])
Rlda5
pri5 <- array(1/length(levels(factor(Rlda5$class))),length(levels(factor(Rlda5$class))))
fit5 <- lda(class ~.,Rlda5, CV = TRUE, na.action = "na.omit", prior=pri5)
```

```
ct <- table(Rlda5$class, fit5$class)
ct
diag(prop.table(ct, 1))

# total percent correct
sum(diag(prop.table(ct)))

#Scatterplot matrix of PCs1-3 for Class 5
splom(Rlda5[,c(2,3,4)], groups=Rlda5$class,panel=panel.superpose, key = simpleKey(columns
= 2, title="Source", levels(Rlda5$class) ))

#LDA Class Boundaries for Class 5
library(klaR)
par(mfrow=c(2,2))
partimat(class~pc1+pc2+pc3,data=Rlda5,method="lda",nplots.hor=2,nplots.vert=2)
```

#QDA

```
#QDA for Class 1
fitq <- qda(class ~.,Rlda, CV = TRUE, na.action = "na.omit", prior=pri)
ct <- table(Rlda$class, fitq$class)
ct
diag(prop.table(ct, 1))

# total percent correct
sum(diag(prop.table(ct)))

#Scatterplot matrix of PCs1-3 for Class 1
splom(Rlda[,c(2,3,4)], groups=fitq$class,panel=panel.superpose, key = simpleKey(columns = 2,
title="Source", levels(fitq$class) ))

#QDA Class Boundaries for Class1
library(klaR)
par(mfrow=c(2,2))
partimat(class~pc1+pc2+pc3,data=Rlda,method="qda",nplots.hor=2,nplots.vert=2)
```

```
#QDA for Class 2
fitq2 <- qda(class ~.,Rlda2, CV = TRUE, na.action = "na.omit", prior=pri2)
ct <- table(Rlda2$class, fitq2$class)
ct
diag(prop.table(ct, 1))
```

```
# total percent correct
sum(diag(prop.table(ct)))

#Scatterplot matrix of PCs1-3 for Class 2
splom(Rlda2[,c(2,3,4)], groups=fitq2$class,panel=panel.superpose, key = simpleKey(columns =
2, title="Source", levels(fitq2$class) ))

#QDA Class Boundaries for Class2
library(klaR)
par(mfrow=c(2,2))
partimat(class~pc1+pc2+pc3,data=Rlda2,method="qda",nplots.hor=2,nplots.vert=2)
```

```
#QDA for Class 3
fitq3 <- qda(class ~.,Rlda3, CV = TRUE, na.action = "na.omit", prior=pri3)
ct <- table(Rlda3$class, fitq3$class)
ct
diag(prop.table(ct, 1))

# total percent correct
sum(diag(prop.table(ct)))

#Scatterplot matrix of PCs1-3 for Class 3
splom(Rlda3[,c(2,3,4)], groups=fitq3$class,panel=panel.superpose, key = simpleKey(columns =
2, title="Source", levels(fitq3$class) ))

#QDA Class Boundaries for Class3
library(klaR)
par(mfrow=c(2,2))
partimat(class~pc1+pc2+pc3,data=Rlda3,method="qda",nplots.hor=2,nplots.vert=2)
```

```
#QDA for Class 4
fitq4 <- qda(class ~.,Rlda4, CV = TRUE, na.action = "na.omit", prior=pri4)
ct <- table(Rlda4$class, fitq4$class)
ct
diag(prop.table(ct, 1))

# total percent correct
sum(diag(prop.table(ct)))

#Scatterplot matrix of PCs1-3 for Class 4
splom(Rlda4[,c(2,3,4)], groups=fitq4$class,panel=panel.superpose, key = simpleKey(columns =
2, title="Source", levels(fitq4$class) ))
```

```
#QDA Class Boundaries for Class4
library(klaR)
par(mfrow=c(2,2))
partimat(class~pc1+pc2+pc3,data=Rlda4,method="qda",nplots.hor=2,nplots.vert=2)
```

```
#QDA for Class 5
fitq5 <- qda(class ~.,Rlda5, CV = TRUE, na.action = "na.omit", prior=pri5)
ct <- table(Rlda5$class, fitq5$class)
ct
diag(prop.table(ct, 1))

# total percent correct
sum(diag(prop.table(ct)))

#Scatterplot matrix of PCs1-3 for Class 5
splom(Rlda5[,c(2,3,4)], groups=fitq5$class,panel=panel.superpose, key = simpleKey(columns =
2, title="Source", levels(fitq5$class) ))

#QDA Class Boundaries for Class5
library(klaR)
par(mfrow=c(2,2))
partimat(class~pc1+pc2+pc3,data=Rlda5,method="qda",nplots.hor=2,nplots.vert=2)
```

```
#HCA
```

```
## Cluster Rlda for Class 1
#  Packages to install and load:  "amap" and "cba" (both found in CRAN US (CA 1)
library(amap)
library(cba)
data1<-as.matrix(Rlda[,2:7])
d <- dist(data1, method = "euclidean", diag = TRUE, upper = TRUE)
hc<-hclust(d, method="centroid")
d2<-cophenetic(hc)
coph<-cor(d,d2)
co<-order.optimal(d, hc$merge)
ho <- hc
ho$merge <- co$merge
ho$order <- co$order
op <- par(mfrow=c(2,2))
plot(hc, main="hclust", hang = -1)
plot(ho, main="optimal", hang = -1)
image(as.matrix(d[[hc$order]]), main="hclust")
image(as.matrix(d[[co$order]]), main="optimal")
diff = order.length(d, hc$order)-order.length(d, co$order)
```

```
cat("Compare:  Hierarchical clustering order length (", order.length(d, hc$order), ") and Optimal Leaf Order length (", order.length(d, co$order), ").  The difference is ", diff, ".", "\n")
cat("The cophenetic correlation coefficient is ", coph, ".", "\n")
```

Cluster Rlda2 for Class 2

```
#  Packages to install and load:  "amap" and "cba" (both found in CRAN US (CA 1) and "stats"
library(amap)
library(cba)
data1<-as.matrix(Rlda2[,2:4])
d <- dist(data1, method = "euclidean", diag = TRUE, upper = TRUE)
hc<-hclust(d, method="centroid")
d2<-cophenetic(hc)
coph<-cor(d,d2)
co<-order.optimal(d, hc$merge)
ho <- hc
ho$merge <- co$merge
ho$order <- co$order
op <- par(mfrow=c(2,2))
plot(hc, main="hclust", hang = -1)
plot(ho, main="optimal", hang = -1)
image(as.matrix(d[[hc$order]]), main="hclust")
image(as.matrix(d[[co$order]]), main="optimal")
diff = order.length(d, hc$order)-order.length(d, co$order)
cat("Compare:  Hierarchical clustering order length (", order.length(d, hc$order), ") and Optimal Leaf Order length (", order.length(d, co$order), ").  The difference is ", diff, ".", "\n")
cat("The cophenetic correlation coefficient is ", coph, ".", "\n")
```

PCA:

```
#myPCAv2 (Sigman, 2013)
##############################################
# myPCA
##############################################
# Receives a data matrix x arranged with variables
# in columns and samples in rows. Matrix x may be
# extracted from a data.frame (i.e. X[,4:200])
# Also receives a single character variable NM.
# NM is the normalization mode and must correspond to:
# "s" = sum all values in each row to 1
# "m" = make maximum value in each row 1
# "v" = normalize each row to a unit length vector
# "n" = no normalization.
# Variables created include: [RR] the scores matrix
# [CC] the eigenvectors matrix, EV the eigenvalues,
# EVpct the percent variance in each eigenvector,
# CumEVpct the cumulative percent variance in the
# eigenvectors. myPCA uses singular value decomposition.
# The number of principal components is determined by
# DRMAD (Malinowski - Ref.) and the number returned
# to the user. A scree plot and plot of CumEVpct are
# generated at the end of the routine.
# M. Sigman 2013
##############################################
myPCA <- function(x, NM = "s"){
# check x to ensure intensitite in each row sum to one
  dx <- dim(x);
  rr <- dx[1];
  cc <- dx[2];
  sm <- rr;
  if (rr < cc){
    sm <- rr;
  }else{
    sm <- cc;
  }
    # normalize data to sum to one for each case
  if ( NM == "s"){
    for (i in 1:rr){
      x[i,] <- x[i,]/sum(x[i,]);
    }
  } else if ( NM == "m") {
    for (i in 1:rr){
```

```
    x[i,] <- x[i,]/max(x[i,]);
   }
  } else if ( NM == "v") {
   for (i in 1:rr){
      s2<-0;
    for (j in 1:dx[2]){
     s2 <- s2 + x[i,j]^2
    }
    x[i,] <- x[i,]/sqrt(s2);
   }
  }


# perform pca on x
  x.svd <- svd(x);
  x.R <- x.svd$u %*% diag(x.svd$d);
  x.C <- t(x.svd$v);
  x.EV <- x.svd$d * x.svd$d
  x.EVpct <- x.EV/sum(x.EV);
  x.EV <- x.EV[1:sm];
  x.EVpct <- x.EVpct[1:sm];
  x.CumEVpct <- x.EVpct;
  for (i in 2:sm){
   x.CumEVpct[i] = x.CumEVpct[i-1]+x.EVpct[i];
  }

# calculate the number of principal factors based on DRMAD

  sev <- 0; #initialize sev
  for (i in 1:sm){
   sev[i] <- sum(x.EV[i:sm]);
  }
  rsd <- 0;
  ev <- 0;
  for (i in 1:sm){
   rsd[i] <- sqrt(sev[i]/((rr-i+1)*(cc-i+1)));
  }
  rsd <- c(rsd, NA);
  ev <- c(NA, x.EV[1:sm]);
  # perform MAD test
  test <- 0;
  for (i in 1:(sm-1)){
   test[i] <- MADtest(rsd[i:sm]);
  }
```

```
princf <- 0;
for (i in 1:sm){
  if(test[i] == 0){
    princf <- princf +1;
  }else{
    break; #breaks out of for loop at first test[i]=1
  }
}

print("***Number of principal factors by DRMAD***");
print(princf);
RR <<- 0;
CC <<-0;
EV <<- 0;
EVpct <<- 0;
RR <<- x.R[,1:sm];
CC <<- x.C[1:sm,];
EV <<- x.EV;
EVpct <<- x.EVpct;
CumEVpct <<- x.CumEVpct;
par(mfrow=c(2,1))
plot(EV[1:(princf+10)], type="p", xlab="Component", ylab="Eigenvalue", main="Scree Plot");
plot(CumEVpct[1:(princf+10)], type="p", xlab="Component", ylab="Percent Variance")
#r <- c(x.R, x.C, x.EV, x.EVpct);
#return(r);
```

REFERENCES

Aerssens J, Boonen S, Lowet G, Dequeker J. 1998. Interspecies differences in bone composition, density, and quality: potential implications for *in vivo* bone research. Endo 139(2):663-670.

Alvira FC, Ramirez Rozzi F, Bilmes GM. 2010. Laser-induced breakdown spectroscopy microanalysis of trace elements in Homo sapiens teeth. Appl Spectrosc 64(3):313-319.

Bearden JA. 1967. X-ray wavelengths. Rev Mod Phys 39:86-99.

Beckett S, Rogers K, Clement JG. 2011. Inter-species variation in bone mineral behavior upon heating. J Forensic Sci 56(3):571-579.

Biltz RM, Pellegrino ED. 1969. The chemical anatomy of bone: a comparative study of bone composition in sixteen vertebrates. J Bone Joint Surg 31A:456-466.

Bratter P, Gawlik D, Lausch J, Rosick U. 1977. On the distribution of trace elements in human skeleton. J Radioanal Chem 37:393-403.

Braz VS. 2001. Study of the taphonomic processes in skeletal remains of the Moa and Beirada shell mounts, Saqurema–RJ (Brazil) [M.Sc. thesis]. Rio de Janeiro: Department of Anatomy, Federal University of Rio de Janeiro.

Bridge CM, Powell J, Steele KL, Sigman ME. 2007. Forensic comparative glass analysis by laser-induced breakdown spectroscopy. Spectrochim Acta B 62:1419-1425.

Brody RH, Edwards HGM, Pollard AM. 2001. Chemometric methods applied to the differentiation of Fourier-transform Raman spectra of ivories. Analytica Chimica Acta 427:223-232.

Brooks TR, Bodkin TE, Potts GE, Smullen SE. 2006. Elemental analysis of human cremains using ICP-OES to classify legitimate and contaminated cremains. J Forensic Sci 51(5):967-973.

©Bruker Corporation. 2013. Handheld XRF spectrometry. < http://www.bruker.com/products/x-ray-diffraction-and-elemental-analysis/handheld-xrf.html>. Accessed 21 May 2013.

Bryant FB, Yarnold PR. 2010. Principal-components analysis and exploratory and confirmatory factor analysis. Washington, DC: American Psychological Association. p 99-136.

Bush MA, Miller RG, Norrlander AL, Bush PJ. 2008. Analytical survey of restorative resins by SEM/EDS and XRF: database for forensic purposes. J Forensic Sci 53(2):419-425.

Carvalho ML, Marquesa AF, Lima MT, Reuse U. 2004. Trace elements distribution and post-mortem intake in human bones from Middle Age by total reflection X-ray fluorescence. Spectrochim Acta B 59:1251-1257.

Castro W, Hoogewerff J, Latkoczy C, Almirall JR. 2010. Application of laser ablation (LA-ICP-SF-MS) for the elemental analysis of bone and teeth samples for discrimination purposes. Forensic Sci Int 195:17-27.

Cattaneo C. 2007. Forensic anthropology: developments of a classical discipline in the new millennium. Forensic Sci Int 165:185-193.

Cattaneo C, DiMartino S, Scali S, Craig OE, Grandi M, Sokol RJ. 1999. Determining the human origin of fragments of burnt bone: a comparative study of histological, immunological and DNA techniques. Forensic Sci Int 102:181-191.

Cattaneo C, Gelsthorpe K, Phillips P, Sokol RJ.1992a. Detection of blood proteins in ancient human bone using ELISA: a comparative study of the survival of IgG and albumin. Int J Osteoarchaeology 2:103–107.

Cattaneo C, Gelsthorpe K, Phillips P, Sokol RJ. 1992b. Reliable identification of human albumin in ancient bone using ELISA and monoclonal antibodies. Am J Phys Anthropol 87(3):365–372.

Cattaneo C, Gelsthorpe K, Sokol RJ. 1994. Immunological detection of albumin in ancient human cremations using ELISA and monoclonal antibodies. J Archaeological Sci 21:565–571.

Cattaneo C, Gelsthorpe K, Phillips P, Sokol RJ. 1995. Differential survival of albumin in ancient bone. J Archaeological Sci 22:271–276.

Cattaneo C, Porta D, Gibelli D, Gamba C. 2009. Histological determination of the human origin of bone fragments. J Forensic Sci 54(3):531-533.

Cattell RB. 1966. The scree test for the number of factors. Multivariate Behav Res 1(2):245-276.

Chamberlain A. 1994. Identifying human bone. In: Human remains, (Vol. 7). Berkeley: University of California Press. p 7-12.

Christensen AM, Crowder CM. 2009. Evidentiary standards for forensic anthropology. J Forensic Sci 54(6):1211-1216.

Christensen AM, Smith MA, Thomas RM. 2012. Validation of X-ray fluorescence spectrometry for determining osseous or dental origin of unknown material. J Forensic Sci 57(1):47-51.

Cook SD, Thomas KA, Kay JF, Jarcho M. 1988. Hydroxyapatite-coated titanium for orthopedic implant applications. Clin Orthop Relat R 232:225-243.

Daubert v. Merrell Dow Pharmaceuticals, Inc., 509 US 579. (1993).

De Fransesco AM, Crisci GM, Bocci M. 2007. Non destructive analytical method using XRF for determination of provenance of archaeological obsidian from the Mediterranean area: a comparison with traditional XRF method. Archaeometry 50(2):337–350.

Dirkmaat DC. 2012. Forensic anthropology at the mass fatality incident (commercial airliner) crash scene. In: Dirkmaat DC, editor. A companion to forensic anthropology. Malden: Wiley-Blackwell. p 136-156.

Djingova R, Zlateva B, Kuleff I. 2004. On the possibilities of inductively coupled plasma mass spectrometry for analysis of archaeological bones for reconstruction of paleodiet. Talanta 63:785-789.

Edwards HGM, Hassan NF, Arya N. 2006. Evaluation of Raman spectroscopy and application of chemometric methods for the differentiation of contemporary ivory specimens I: elephant and mammalian species. J Raman Spectrosc 37:353-360.

Ferretti M, Moioli P. 1998. The use of portable XRF systems for preliminary compositional surveys on large bronze objects. A critical review after some years' experience. In: Mourey W and Robiola L, editors. Proceedings of the International Conference Metal, Draguignan, May 1998. p 39-44.

Ferretti M, Miazzo L, Moioli P. 1997. The application of a nondestructive XRF method to identify different alloys in the bronze statue of the Capitoline Horse. Studies in Conservation 42:241–246.

Frahm E, Doonon R, Kilikoglou V. 2013. Handheld portable X-ray fluorescence of Aegean obsidians. Archaeometry doi: 10.1111/arcm.12012

Glascock MD. Comparison and contrast between XRF and NAA: used for characterization of obsidian sources in Central Mexico. In: Shackley MS, editor. X-ray fluorescence spectrometry (XRF) in geoarchaeology. New York: Springer. p 161-192.

Gonzalez-Rodriguez J, Fowler G. 2013. A study on the discrimination of human skeletons using X-ray fluorescence and chemometric tools in chemical anthropology. Forensic Sci Int http://dx.doi.org/10.1016/j.for-sciint.2013.04.035

Granite GE. 2012. Portable X-ray fluorescence spectroscopy and its research applications to Northern European bog bodies. [PhD dissertation] State University of New York at Buffalo.

Grivas CR, Komar DA. 2008. *Kumho, Daubert,* and the nature of scientific inquiry: implications for forensic anthropology. J Forensic Sci 53(4):771-776.

Hagelberg E, Gray IC, Jeffreys AJ. 1991. Identification of the skeletal remains of a murder victim by DNA analysis. Nature 352:427-429.

Jarvis KE, Gray AL, Houk RS. 1992. Handbook of inductively coupled plasma mass spectrometry. Oakland: Blackie Academic and Professional.

Jordan DR, Munro SM, Brownstein S, Gilberg SM, Grahovav SZ. 1998. A synthetic hydroxyapatite implant: the so-called counterfeit implant. Ophthal Plast Recons 14(4):244-249.

Kaiser J, Galiova M, Novotny K, Cervenka R, Reale L, Novotny J, Liska M, Samek O, Kanicky V, Hrdlicka A, Stejskal K, Adam V, Kizek R. 2009. Mapping of lead, magnesium and copper accumulation in plant tissues by laser-induced breakdown spectroscopy and laser-ablation inductively coupled plasma mass spectrometry. Spectrochim Acta B At Spectrosc 64:67-73.

Kasem MA, Russo RE, Harith MA. 2011. Influence of biological degradation and environmental effects on the interpretation of archaeological bone samples with laser-induced breakdown spectroscopy. J Anal At Spectrom 26:1733-1739.

Kravchenko II, Dunnam FE, Van Rinsvelt HA, Warren MW, Falsetti AB. 2001. A forensic application of PIXE analysis. In: Duggan JL, Morgan IL, editors. Application of Accelerators in Research and Industry - Sixteenth Int'l Conference. American Institute of Physics.

Liritzis I. 2005. Ulucak (Smyrna, Turkey): chemical analysis with clustering of ceramics and soils and obsidian hydration dating. Mediterr Archaeol Archaeometry 5(3):33– 45.

Liritzis I, Drakonaki S, Vafiadou A, Sampson A, Boutsika T. 2002. Destructive and nondestructive analysis of ceramics, artefacts and sediments of Neolithic Ftelia (Mykonos) by portable EDXRF spectrometer: first results. In: Sampson A, editor. The Neolithic settlement at Ftelia, Mykonos. Rhodes: University of the Aegean, Department of Mediterranean Studies. p 251–272.

Liritzis I, Sideris C, Vafiadou A, Mitsis J. 2007. Mineralogical petrological and radioactivity aspects of some building material from Egyptian Old Kingdom monuments. J Cult Herit 9:1–13.

Lowenstein JM. 1980. Species-specific proteins in fossils. Naturwissenschaften 67:343-346.

Mantler M, Schreiner M. 2000. X-ray fluorescence spectrometry in art and archaeology. X-ray Spectrom 29:3-17.

Mantzourani H, Liritzis I. 2006. Chemical analysis of pottery samples from Kantou Kouphovounos and Sotira Tepes (Cyprus): a comparative approach. Reports of the Department of Antiquities, Cyprus, 63–76.

Marieb EN, Hoehn K. 2007. The digestive system. In: Human anatomy and physiology (7th ed.). San Francisco: Pearson Education, Inc. p 882-941.

McLaughlin G, Lednev IK. 2012. Spectroscopic discrimination of bone samples from various species. Am J Anal Chem 3:161-167.

Migliori A, Bonanni P, Carraresi L, Grassi N, Mando PA. 2011. A novel portable XRF spectrometer with range of detection extended to low-Z elements. X-Ray Spectrom 40:107-112.

Mulhern DM, Ubelaker DH. 2001. Differences in osteon banding between human and non-human bone. J Forensic Sci 46(2):220–222.

Mulhern DM, Ubelaker DH. 2012. Differentiating human and nonhuman bone microstructure. In: Crowder C, Stout S, editors. Bone histology: an archaeological perspective. Boca Raton: CRC Press. p 109-134.

Papadopoulou DN, Zachariadis GA, Anthemidis AN, Tsirliganis NC, Stratis JA. 2006. Development and optimisation of a portable microXRF method for in situ multielement analysis of ancient ceramics. Talanta 68(5):1692–1699.

Papageorgiou I, Liritzis I. 2007. Multivariate mixture of normals with unknown number of components. An application to cluster Neolithic ceramics from the Aegean and Asia Minor. Archaeometry 49(4):795–813.

Pappalardo G, Karydas AG, La Rosa V, Militello P, Pappalardo L, Rizzo F, Romana FP. 2003. Provenance of obsidian artefacts from different archaeological layers of Phaistos and Hagia Triada. Creta Antica 4:287–300.

Phillips SC, Speakman RJ. 2009. Initial source evaluation of archaeological obsidian from the Kuril Islands of the Russian Far East using portable XRF. J Archaeol Sci 36:1256-1263.

Pietrzyk DJ, Frank CW. 1979. Analytical chemistry, 2nd ed. New York: Academic Press.

Rautray TR, Mishra S, Patnaik SK, Vijayan V, Panigrahi S. 2007. Analysis of human bone and teeth. Indian J Phys 81(1):99-102.

Rusak DA, Marsico RM, Taroli BL. 2011. Using laser-induced breakdown spectroscopy to assess preservation quality of archaeological bones by measurement of calcium-to fluorine ratios. App Spectr 65(10):1193-1196.

Samek O, Beddows DCS, Telle HH, Kaiser J, Liska M, Caceres JO, Gonzales Urena A. 2001. Quantitative laser-induced breakdown spectroscopy analysis of calcified tissue samples. Spectrochim Acta B At Spectrosc 56:865-875.

Schultz JJ, Warren MW, Krigbaum JS. 2008. Analysis of human cremains: gross and chemical methods. In: Schmidt CW, Symes SA. The analysis of burned human remains. San Diego: Academic Press. p 75-94.

Shackley MS. 2011. An introduction to X-ray fluorescence (XRF) analysis in archaeology. In: X-ray fluorescence spectrometry (XRF) in geoarchaeology. New York: Springer Science + Business Media, LLC.

Shimoyama M, Maeda H, Sato H, Ninomiya Y, Ozaki Y. 1997. Nondestructive discrimination of biological materials by near-infrared Fourier transform Raman spectroscopy and chemometrics: discrimination among hard and soft ivories of African elephants and mammoth tusks and prediction of specific gravity of the ivories. Appl Spectrosc 51(8):1154-1158.

Shimoyama M, Morimoto S, Ozaki Y. 2004. Non-destructive analysis of the two sub-species of African elephants, mammoth, hippopotamus, and sperm whale ivories by visible and short-wave near infrared spectroscopy and chemometrics. Analyst 129:559-563.

Sigman ME. 2010. Application of laser-induced breakdown spectroscopy to forensic science: analysis of paint and glass samples. Final Technical Report, US Department of Justice.

Silva APD, Stam A. 1995. Discriminant analysis. In: Grimm LG, Yarnold PR, editors. Reading and understanding multivariate statistics. Washington, DC: American Psychological Association. p 277-318.

Sledzik PS, Dirkmaat DC, Mann RW, Holland TD, Mundorf AZ, Adams BJ, Crowder CM, DePaolo F. 2009. Disaster victim recovery and identification: forensic anthropology in the aftermath of September 11. In: Steadman DW, editor. Hard evidence: case studies in forensic anthropology (2nd ed.). Upper Saddle River: Prentice Hall. p 289-302.

Ubelaker DH. 1989. Human skeletal remains: excavation, analysis, interpretation (2nd ed.). Washington: Taraxacum.

Ubelaker DH, Ward DC, Braz VS, Stewart J. 2002. The use of SEM/EDS analysis to distinguish dental and osseus tissue from other materials. J Forensic Sci 47(5):1-4.

Ubelaker DH, Lowenstein JM, Hood DG. 2004. Use of solid-phase double-antibody radioimmunoassay to identify species from small skeletal fragments. J Forensic Sci 49(5):1-6.

Ubanova P, Navotny V. 2005. Distinguishing between human and non-human bones: histometric method for forensic anthropology. Anthropologie 43(1):77-85.

Varmuza K, Filzmoser P. 2009. Introduction to multivariate statistical analysis in chemometrics. Boca Raton: CRC Press.

Vass AA, Madhavi M, Synstelien J, Collins K. 2005. Elemental characterization of skeletal remains using laser-induced breakdown spectroscopy (LIBS). Proceedings of the American Academy of Forensic Sciences 11:307-308.

Vij DR. 2006. Handbook of applied solid state spectroscopy. New York: Springer.

Ward DC, Colby J. 2008. SLICE, a database approach to EDS. Micosc Microanal 14:1258-1259.

Warren MW, Falsetti AB, Kravchenko II, Dunnamb FE,Van Rinsveltb HA, Maples WR. 2002. Elemental analysis of bone: proton-induced X-ray emission testing in forensic cases. Forensic Sci Int 125:37–41.

Webb E, Amarasiriwardena D, Tauch S, Green EF, Jones J, Goodman AH. 2005. Inductively coupled plasma-mass (ICPMS) and atomic emission spectrometry (ICP-AES): versatile analytical techniques to identify the archived elemental information in human teeth. Microchem J 81:201-208.

Wehrens R. 2011. Chemometrics with R: multivariate data analysis in the natural sciences and life sciences. Heidelberg: Springer.

Wessen G, Ruddy FH, Gustafson CE, Irwin H. 1978. Trace element analysis in the characterization of archaeological bone. Adv Chem Ser 171:99-108.

Williams JA. 2012. Using a portable XRF to detect the transfer of material from the prior use of a saw in cutting bone. Proceedings of the American Academy of Forensic Sciences 18:379-380.

Williams-Thorpe O. 1995. Obsidian in the Mediterranean and Near East: a provenancing success story. Archaeometry 37:217–248.

Williams-Thorpe O, Potts PJ, Webb PC. 1999. Field portable non destructive analysis of lithic archaeological samples by X ray fluorescence instrumentation using a mercury iodide detector: comparison with wavelength – dispersive XRF and a case study in British stone Axe provenancing. J Archaeol Sci 26(2):215–237.